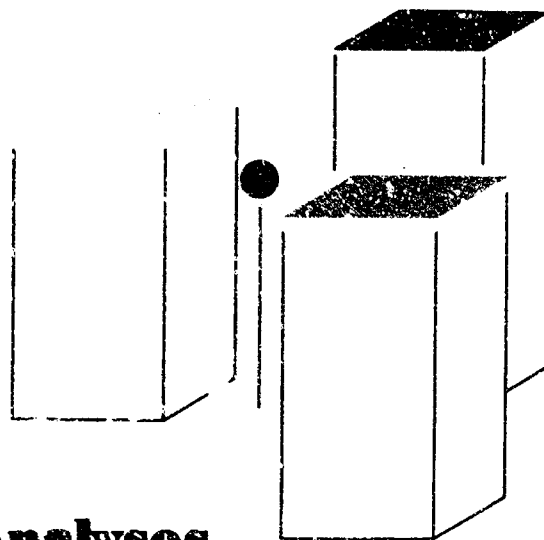


FINAL REPORT***Radiological Recovery Requirements, Structures,
and Operations Research*****Volume II, Development of****Analytical, Computer, and****Systems Models in****Support of Decontamination Analyses**

CLEARINGHOUSE
FOR FEDERAL SCIENTIFIC AND
TECHNICAL INFORMATION

Hardcopy

Microfilm

\$ 5.00

\$ 1.00

175

PP

by **J. T. Ryan and T. Johnson**

PREPARED FOR THE
OFFICE OF CIVIL DEFENSE
DEPARTMENT OF THE ARMY
WASHINGTON, D. C. 20310
OCD WORK UNIT NO. 3233B

1 **ARCHIVE COPY**

UNDER

TECHNICAL MANAGEMENT OFFICE
U. S. NAVAL RADIOLOGICAL DEFENSE LABORATORY
SAN FRANCISCO, CALIFORNIA 94135
CONTRACT N228 (62470)-48153
RTI PROJECT OU-214

6 June 1966

RESEARCH TRIANGLE INSTITUTE • DURHAM, NORTH CAROLINA

AD 635822

R
T
I

FINAL REPORT: VOLUME II, Development of
Analytical, Computer, and Systems Models in
Support of Decontamination Analysis

Radiological Recovery Requirements, Structures, and
Operations Research

Prepared for the
Office of Civil Defense
Department of the Army
Washington, D. C. 20310
OCD Work Unit No. 3233B
under
Technical Management Office
U. S. Naval Radiological Defense Laboratory
San Francisco, California 94135
Contract N228(62479)-68153
RTI Project OU-214

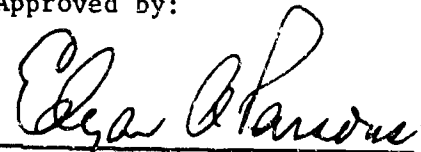
by

J. T. Ryan

T. Johnson

THE RESEARCH TRIANGLE INSTITUTE
Operations Research and Economics Division
Post Office Box 490
Durham, North Carolina

Approved by:



Edgar A. Parsons
Director



Robert S. Titchen
Deputy Director

6 June 1966

PREFACE

The conclusions given in this report are based upon the "Engineering Manual (PM100-1)" method for calculation of "protection factors". Since an error analysis is not presently available, the conclusions should be regarded as tentative, pending the development of such an analysis. In addition, a redistribution of fallout and/or changes in the γ -ray spectrum emitted by the fallout may introduce further uncertainties into these conclusions.

ACKNOWLEDGMENTS

The authors are pleased to acknowledge W. R. Davis and M. K. Moss of North Carolina State of the University of North Carolina and A. J. Benjamin of Research Triangle Institute for their help in establishing the theoretical basis upon which the analytical models of detector response to gamma radiation were based.

Appreciation is also extended to A. A. Qadeer, K. E. Willis, R. O. Lyday, P. B. McGill, C. N. Dillard, P. Rasberry, and A. M. Fuller for their assistance during the course of the project.

ABSTRACT

This is Volume II of four separately bound volumes that report the research completed in fulfillment of Office of Civil Defense Work Unit No. 3233B, "Radio-logical Recovery Requirements, Structures, and Operations Research." This describes six supporting studies all previously reported to the Office of Civil Defense in research memoranda. Volume I describes the general aspects of the investigations and presents the conclusions and recommendations. The abstract for each of the volumes is presented on the following pages.

ABSTRACT FOR VOLUME I

This study examines the application of decontamination strategies to extensive urban areas. Urban areas of various sizes (from a few acres to an interconnected system involving hundreds of acres) are examined with regard to decontaminating vital sections and their connecting links. Feasible creation of decontaminated "islands" or marshalling areas is determined. The nature and scope of command and control system elements required for conducting effective decontamination in practical situations are defined together with the preattack and postattack data required by such a system. Several models of detector response to gamma radiation developed during the course of the project are briefly discussed.

ABSTRACT FOR VOLUME II

Volume II contains six supporting studies. Described are a number of models for determining the cost and effectiveness of decontaminating municipal areas. One study examines the system components of a command and control system for municipal decontamination. These studies cover the following subjects:

1. A Feasibility Study of the Application of Analog Computers to the Analysis of Decontamination: This study describes the research completed on the application of analog computers to the analysis of decontamination. A simplified analog model of the effect of a single decontamination effort on a single plane of contamination is explained and described. Sample analog records of output from a prototype of this model are presented. The design of a more elaborate model requiring substantially more analog equipment is described, and applications are indicated.

2. A Circular Model for Approximating Gamma Ray Intensity at a Single Detector Location: An approximate procedure for determining the gamma ray intensity at a point, due to fallout radiation, is investigated. A reasonably accurate model using circular annulus geometry was developed which includes the effects of gamma ray attenuation, build-up, backscatter, and skyshine. This model was based on NBS Monograph 42.

A single annulus model is described in order to show clearly the basic premises upon which the full "circular" model is based. The development of the multiple annulus model is treated in a manner to show how each of the parameters involved is handled. An example demonstrating the use of the model is included.

3. A Square-Grid Model for Approximating Gamma Ray Intensity at a Single Detector Location: This study describes a simple and practical procedure for determining the approximate fallout gamma ray intensity at a point as a function of the geometry of the contributing planes and related shielding. The procedure described employs a "square-grid" technique for modeling the contaminated planes.

This model is shown to be reasonably accurate and easily adapted to practical situations with the help of scaled overlays for city maps to be used in conjunction with the tables and graphs developed in the research. An example analysis is carried out to illustrate the method.

4. A Point Source Model for Approximating Gamma Ray Intensity at a Single Detector Location (The Equivalent Planes Method): A method for analyzing the dose contributions from plane areas of fallout is developed; each contaminated plane is treated as a weighted point source of radiation intensity. Only the area, the location of the center, the eccentricity of the approximating rectangle, and the intervening shielding need be considered. Limits are developed for the eccentricity of an area, centered over the detector, which can be represented by a square of the same area with an error of less than ten percent in dose rate contribution. Limits are also developed for the area of off-center contaminated areas such that the product of area times the dose rate contribution per unit area is within ten percent of the true contribution from the area. A sample analysis is given.

A step by step procedure based on this model, called "The Equivalent Planes Method," is presented. A small booklet which could be used as an "Equivalent Planes Method" workbook (together with some work sheets) is included in an envelope at the back of this volume.

5. A FORTRAN Program for Decontamination Analysis: This study describes a debugged and tested FORTRAN computer program to compute the effectiveness parameters used to analyze municipal decontamination. The program was written in FORTRAN 64 to be used on large scale computers such as the CDC 3600.

6. The Nature and Scope of Command and Control System Elements Required for Conducting Effective Decontamination in Municipalities: This study serves to determine the nature and scope of command and control system elements which are required to effect practical municipal decontamination. The preattack and

postattack data requirements for decontamination are specified, and the essential components of an information system for decontamination are identified and related. The influence of direct weapons effects on the decontamination system is examined.

ABSTRACT FOR VOLUME III

Volume III contains the cost and effectiveness data for decontamination analyses of sixteen sites and facilities in San Jose, California. Costs are measured in team-hours of effort. Decontamination effectiveness is measured in terms of fractions of dose-rate remaining at specified detector locations and fractions of dose remaining for persons who perform functions requiring specified daily activity patterns at the sites and facilities chosen.

ABSTRACT FOR VOLUME IV

Volume IV contains the cost and effectiveness data for decontamination analyses of twelve sites and facilities in Detroit, Michigan. Costs are measured in team-hours of effort. Decontamination effectiveness is measured in terms of fractions of dose-rate remaining at specified detector locations and fractions of dose remaining for persons who perform functions requiring specified daily activity patterns at the sites and facilities chosen.

TABLE OF CONTENTS FOR VOLUME II

	<u>Page</u>
PREFACE	iii
ACKNOWLEDGMENTS	iv
ABSTRACT.	v
ABSTRACT FOR VOLUME I	vi
ABSTRACT FOR VOLUME II.	vii
ABSTRACT FOR VOLUME III	x
ABSTRACT FOR VOLUME IV.	xi
 I. INTRODUCTION	 1
 REFERENCES.	 3
 APPENDIX A: A Feasibility Study of the Application of Analog Computers to the Analysis of Decontamination	 A-1
B: A Circular Model for Approximating Gamma Ray Intensity at a Single Detector Location	 B-1
C: A Square-Grid Model for Approximating Gamma Ray Intensity at a Single Detector Location.	 C-1
D: A Point-Source Model and the Equivalent Planes Method for Approximating Gamma Ray Intensity at a Single Detector Location	 D-1
E: A FORTRAN Program for Decontamination Analysis	E-1
F: The Nature and Scope of Command and Control System Elements Required for Conducting Effective Decontamina- tion in Municipalities	 F-1

Radiological Recovery Requirements, Structures, and Operations Research
Volume II, Development of Analytical, Computer, and Systems Models in Support
of Decontamination Analysis

I. INTRODUCTION

This volume reports six studies performed under Office of Civil Defense Subtask 3233B, Radiological Recovery Requirements, Structures, and Operations Research. It is addressed to technical personnel concerned with the planning of postattack recovery operations as summarized and described in Volume I of this report. All of the studies presented in Volume II are concerned with the development of tools which can be used to examine the effectiveness and costs of decontamination when applied to accelerating recovery of an activity in a postattack environment.

When this work began, it seemed that large complexes comprised of several buildings could not be analyzed quickly or efficiently without modifying the analysis techniques that were previously developed for single-facility shielding analysis. Thus, to meet what then appeared to be a requirement for efficient decontamination analysis, a number of models were developed for approximating gamma ray intensity at a point due to complex contaminated plane configurations. Each of these models is discussed in a separate appendix (Appendices A through D) in this volume.

Paralleling the development of the analytical models and the analog computer model, two computer programs written in FORTRAN for the CDC 3600 were completed and debugged to perform most of the computation required to analyze decontamination operations as applied to several sites and facilities selected from San Jose and Detroit. The first of these programs (Reference 1) was developed and debugged under another contract. This program computes the plane-by-plane contributions to intensity at a specified detector location. The second of these programs computes

the effectiveness parameters of the individual decontamination analyses. This program is described in Appendix E.

Lastly, the nature and scope of the command and control system elements required to effect practical municipal decontamination are defined. The pre-attack and postattack data requirements are identified and related to the system as a whole. The influence of direct weapons effects on the decontamination system are examined. This work is described in Appendix F. The six supporting studies included in this volume are:

1. Appendix A: A Feasibility Study of the Application of Analog Computers to the Analysis of Decontamination
2. Appendix B: A Circular Model for Approximating Gamma Ray Intensity at a Single Detector Location
3. Appendix C: A Square-Grid Model for Approximating Gamma Ray Intensity at a Single Detector Location
4. Appendix D: A Point-Source Model and the Equivalent Planes Method for Approximating Gamma Ray Intensity at a Single Detector Location
5. Appendix E: A FORTRAN Program for Decontamination Analysis
6. Appendix F: The Nature and Scope of Command and Control System Elements Required for Conducting Effective Decontamination in Municipalities

REFERENCES

1. E. L. Hill, T. Johnson, and R. O. Lyday, Jr. Computer Program for Analysis of Building Protection Factors. RM-OU-205-1. Durham, North Carolina. Research Triangle Institute, Operations Research and Economics Division, 6 July 1965.

Appendix A

A Feasibility Study of the Application of Analog Computers to the Analysis of Decontamination

Note: The material in this Appendix was originally submitted to USNRDL as Research Memorandum RM-OU-214-2*.

* J. T. Ryan. A Feasibility Study of the Application of Analog Computers to the Analysis of Decontamination. RM-OU-214-2. Durham, North Carolina: Research Triangle Institute, Operations Research and Economics Division, 1 April 1965

TABLE OF CONTENTS FOR APPENDIX A

	<u>Page</u>
I. INTRODUCTION	A-1
II. DISCUSSION OF ANALOG COMPUTERS	A-3
A. General	A-3
B. Analog Computers and Decontamination Analyses	A-5
III. DESCRIPTION OF LIMITED DECONTAMINATION SIMULATION	A-7
A. Introduction	A-7
B. The Hardware Used	A-7
C. The Limited Decontamination Model	A-7
IV. SAMPLE RUNS WITH PROTOTYPE MODEL	A-15
V. AN ELABORATE MODEL	A-25
VI. A TECHNICAL DESCRIPTION OF THE ANALOG DECONTAMINATION MODELS . .	A-27
A. Calculations to be Performed	A-27
B. Range of Constants, Parameters, and Variables	A-28
C. Computer Scaling	A-30
D. Computer Diagram	A-32
E. Function Generators	A-35
F. Equipment Requirements	A-37
VII. CONCLUSIONS AND RECOMMENDATIONS	A-39
A. Conclusions	A-39
B. Future Work	A-39
REFERENCES	A-41

LIST OF TABLES

<u>Table</u>	<u>Page</u>
A-1 System Equations for Simplified Model	A-13

LIST OF FIGURES

<u>Figure</u>	<u>Page</u>
A-1 Model 3400 Desk Top Donner Analog Computer Installation . .	A-8
A-2 A Close-up of the Problem Board Set Up to Analyze a Simple Decontamination Operation	A-8
A-3 Schematic Diagram of Simplified Decontamination Operations with Four Contaminated Planes	A-9
A-4 Analog Record of Dose Rate and Total Dose as a Function of Time for Case I	A-17
A-5 Analog Record of Dose Rate and Total Dose as a Function of Time for Case II	A-18
A-6 Analog Record of Dose Rate and Total Dose as a Function of Time for Case III	A-19
A-7 Analog Record of Dose Rate and Total Dose as a Function of Time for Case IV	A-20
A-8 Analog Record of Dose Rate and Total Dose as a Function of Time for Case V	A-21
A-9 Analog Record of Dose Rate and Total Dose as a Function of Time for Case VI	A-22
A-10 Analog Record of Dose Rate and Total Dose as a Function of Time for Case VII	A-25
A-11 Functional Diagram of Calculations	A-29
A-12 Table of Flow Chart Symbols and Operations	A-33
A-13 Computer Diagram	A-34
A-14 Approximation of the Function of the Form $t^{-1.2}$ by Two Exponentials	A-36
A-15 Approximation of $t^{-1.2}$ Function	A-34

Appendix A

A Feasibility Study of the Application of Analog Computers to the Analysis of Decontamination

I. INTRODUCTION

To the author's knowledge, only digital computer programs are presently used to calculate the protection factor associated with specific detector locations. These programs, with some modifications, can be used to calculate the individual intensity contributions from each of the contributing contaminated planes. Thus, these programs can be effectively used to estimate the value of decontaminating one or more of these planes of contamination. These programs are very detailed. The inputs are an itemized description of all of the planes of contamination and of the intervening shielding.

The over-all time required to prepare such inputs is usually very long, and thus reduces the number of facilities or activities which can be considered in the analysis of decontamination for a large municipal area. This deficiency led to the investigation of an analog model that uses continuous variables for the environmental parameters as well as the parameters associated with the decontamination operations. Analog models are characteristically smaller in scope than digital models, less minute in detail, have a shorter running time, and can be more easily changed.

This study is a result of a very brief effort to determine the applicability of analog computers to the analysis of decontamination. This appendix presents a detailed, non-technical description of the analog computer study. The initial pages are devoted to a description and discussion of analog computers. The subsequent pages describe both the limited decontamination simulation fitted to the available hardware at the Research Triangle Institute and a more elaborate model which requires substantially more equipment. Sample runs are included. The final section of the appendix presents conclusions and recommendations for future work.

Section VI is a technical description of the mathematical equations and hardware components (both existing and proposed) of the decontamination models.

II. DISCUSSION OF ANALOG COMPUTERS*

A. General

The history of computers is, in fact, two histories. Most authors (References A-1 and A-2 for example) recognize that there are very basic factors which distinguish between the family of digital computers and the family of analog computers. Usually the abacus and the slide rule are used to exemplify a simple computer from each of these families respectively. For the purpose of this report, however, it is not necessary to elaborate on the philosophy or historical divergence of the two families of computers. It is only necessary to discuss the one primary factor which distinguishes between analog and digital computers--the way in which data is handled in each machine.

In the digital computer, data is comprised of discrete numbers (represented by digits, magnetic senses, bit positions--or in the case of the abacus--bead positions, etc.) whereas in the analog computer data is represented as a continuous variable (represented by wheel positions, electric voltages--or in the case of the slide rule--slide bar positions, etc.).

The general-purpose electronic analog computer is the type of computer considered in this report. In order to evaluate the features of this type of analog computer, it is helpful also to consider electronic digital computers. **
The following several paragraphs extracted from Reference A-3 very clearly present the pertinent differences between analog and digital models as they affect the analysis and conclusions presented in this report:

* Readers already familiar with analog computers should omit this section. Readers who would like to learn more about the use of analog computers are referred to Reference A-1.

** For a detailed (technical) comparison of digital and analog computers, see Reference A-2, Chapter 2.

"Digital computers are composed of a large number of multiple interconnected bistable devices. These on-off components along with transferring devices form the basis of the digital computer capability--they enable formation and storage of numbers, simple arithmetic operations, and two-valued logic operations. Any function which can be expressed or approximated as a sequence of these operations can be performed on the digital computer.

"Analog computers are not as simply composed but consist of many components with different functions or operating modes. Their capability depends on their having a large and varied collection of components to draw on. Electronic circuits provide this required variety, including summers, integrators, multipliers, function generators, switches, comparators, and many simple circuits which may be built quickly from resistors and capacitors to provide special functions.

"Mechanizing an analog computer model consists in connecting these various components together in the same way as the equations are formed or as the physical system is envisioned. The model is built in parallel; for each operation in the system there is a component in the model that performs the same operation. If there are ten multiplications in the system, then there must be ten multipliers in the model, which will all be operating at once. This is just the opposite of digital computers, which are organized in series. That is, every operation in the system is performed by one component. If there are ten multiplications in the system, then the digital model will perform one multiplication at a time in the programmed sequence.

"One consequence of parallel organization is that increases in system size or complexity bring a corresponding increase in the number of components required in the model. With series organization, an increase in system size or complexity results in a longer running time for the model.

"A second consequence of the parallel organization is that if the model is interrupted at any time during the run, all variables will be found to be at the value corresponding to the one the system would have at that time. That is to say, there is an isomorphism between time in the system and time in the model. This is not the case with series organization as in digital computer models, where the model can be interrupted only at certain specific times to be meaningful.

"Computing time on an analog computer model is usually very short. While the basic switching time of the digital computer may be one thousand to ten thousand times faster than the response time of an analog computer component, the number of operations required in the digital computer for any complicated function is so large that, in fact, the total operation may not be faster than the analog computer component. Thus, speed in performing the total operation coupled with parallel organization allows the time variable on the analog to be scaled as a fraction or multiple of real time. Running times on the analog are usually scaled to range between 10 seconds and 2 minutes. For example, an analog model of a valve which opens in 2 seconds might be scaled to have 1 second of real time equal 10 seconds of computer time, thereby slowing down the operation for each observation. A battle model in which the time of flight to target is 5 hours

might be scaled to have 1 hour of real time equal 1 second on the computer, vastly speeding up the time required for a run.

"Analog computer models require a considerably more contracted treatment of large-scale problems but provide a more tractable model. That is, large volumes of data, readily handled by digital computers, are impossible on the analog unless they can be treated in an aggregated manner; but changes can be made easily, while operating, by simply resetting a dial.

"There is considerable difference between the form of the output on the two computers. The usual output of a digital computer is a tabulation of the results. Analog output is usually in a graphic form, whether as a chart showing the variation of a number of parameters with time or as a plot of one variable against another. This graphical output is adapted very well to problems where a physical understanding of the interactions is desired, since the effect of variations can be immediately seen.

"In summary then, an analog computer model with its treatment of data and variables quite aggregated would be expected to be considerably smaller in scope than a digital computer model. Operational changes could be simply made and input data easily varied. Output would be graphical and running time short, so that results of input changes would be immediately available and easily interpreted. This is in contrast with present digital models which are detailed, longer running, less readily changed, and considerably broader in scope."

B. Analog Computers and Decontamination Analyses

Some comments augmenting and tying the above remarks to the problem of analyzing decontamination operations are appropriate here.

The "parallel organization" feature described above is particularly useful in analyzing the effects of decontaminating a number of independent contaminated surfaces. Instead of having to compute the effects of the separate operation serially, one can build the model so as to show, as a function of (scaled) real time, the effect of the sum of these decontamination operations, where they could be performed simultaneously, or sequenced in any way whatsoever.

Furthermore, different differential equations can be used to govern the efficiency of the individual decontamination operations where the parameters describing these differential equations can be varied manually at run time. This, of course, would be impossible to do with a digital computer. The ability to easily solve very complex differential equations (not easily solvable by paper

and pencil methods) is one of the chief capabilities of analog computers.

The "graphical output" feature can, of course, be performed on a digital computer with the appropriate peripheral equipment, but the ability to respond at computer running time to the information being graphed is impossible with normal digital equipment. Thus, analog computers can be a useful tool for training personnel responsible for large-scale municipal decontamination. This will be discussed in more detail later in this appendix.

XII. DESCRIPTION OF LIMITED DECONTAMINATION SIMULATION

A. Introduction

The limited decontamination analog model was developed to explore the possibilities and determine the application of analog computers to decontamination analysis. As such, this model does not provide realistic answers to decontamination problems and only roughly simulates any real situation. Very gross treatment of the details was used in order to simulate the main features of a single decontamination operation on a small sized computer.

B. The Hardware Used

The limited analog model described in this section was fitted to a basic installation of the model 3400 Desk Top Donner Analog Computer (Figure A-1). The basic model 3400 computer contains ten amplifiers, usable as summers or integrators. The Research Triangle Institute installation also includes a Donner Model 3430 Problem Board and a Donner Model 3073 Potentiometer Strip. The problem board (shown in Figure A-2) is used to interconnect components for the solution of particular problems and the potentiometers are used to adjust constant and parametric coefficients in the equations which describe particular problems. The output from the analog model is graphed using an Offner Dynograph Amplifier-Recorder Model 542. The recorder is also shown on the right in Figure A-1. A more detailed description of the actual components used in this model is contained in section VI.

C. The Limited Decontamination Model

In the limited decontamination analog, each contaminated plane which contributes to the intensity at a detector location is approximated by a point source at the centroid of the contaminated plane.

Figure A-3 is a schematic showing the relationships between a single detector and four contaminated planes.

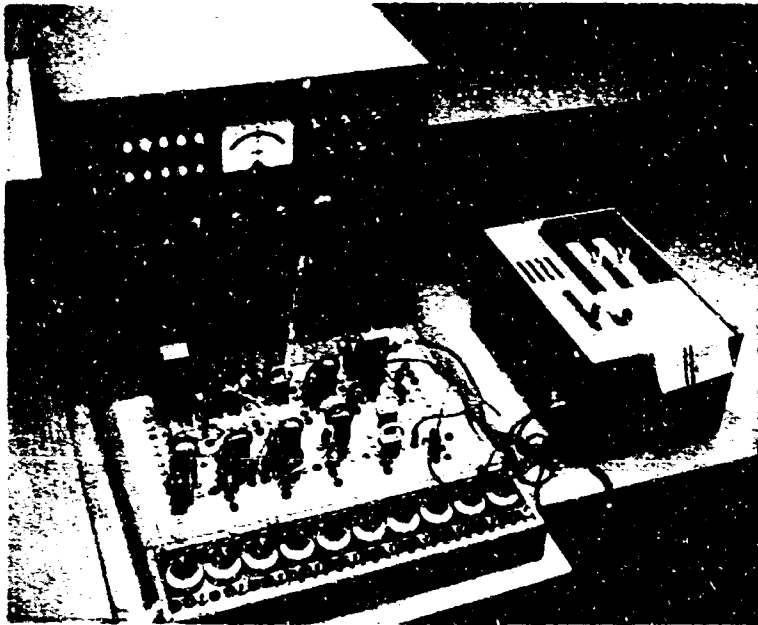


Figure A-1
Model 3400 Desk Top Donner Analog
Computer Installation

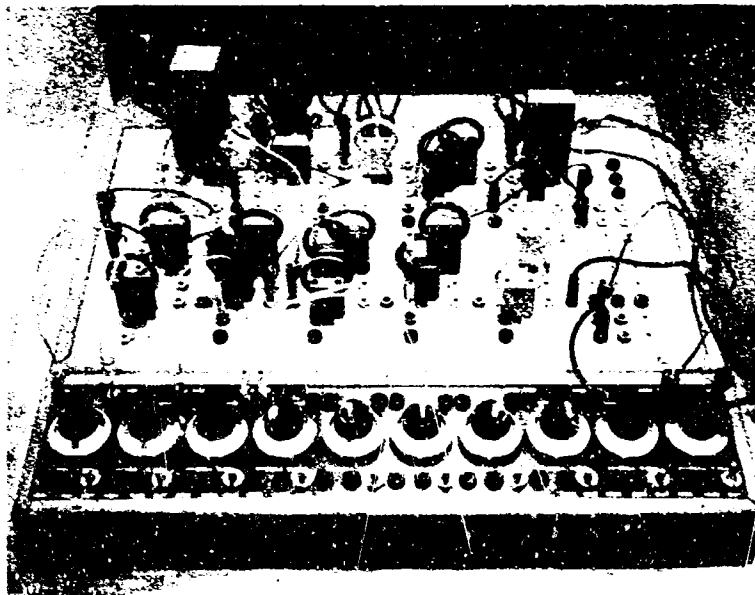


Figure A-2
A Close-up of the Problem Board
Set up to Analyze a Simple
Decontamination Operation

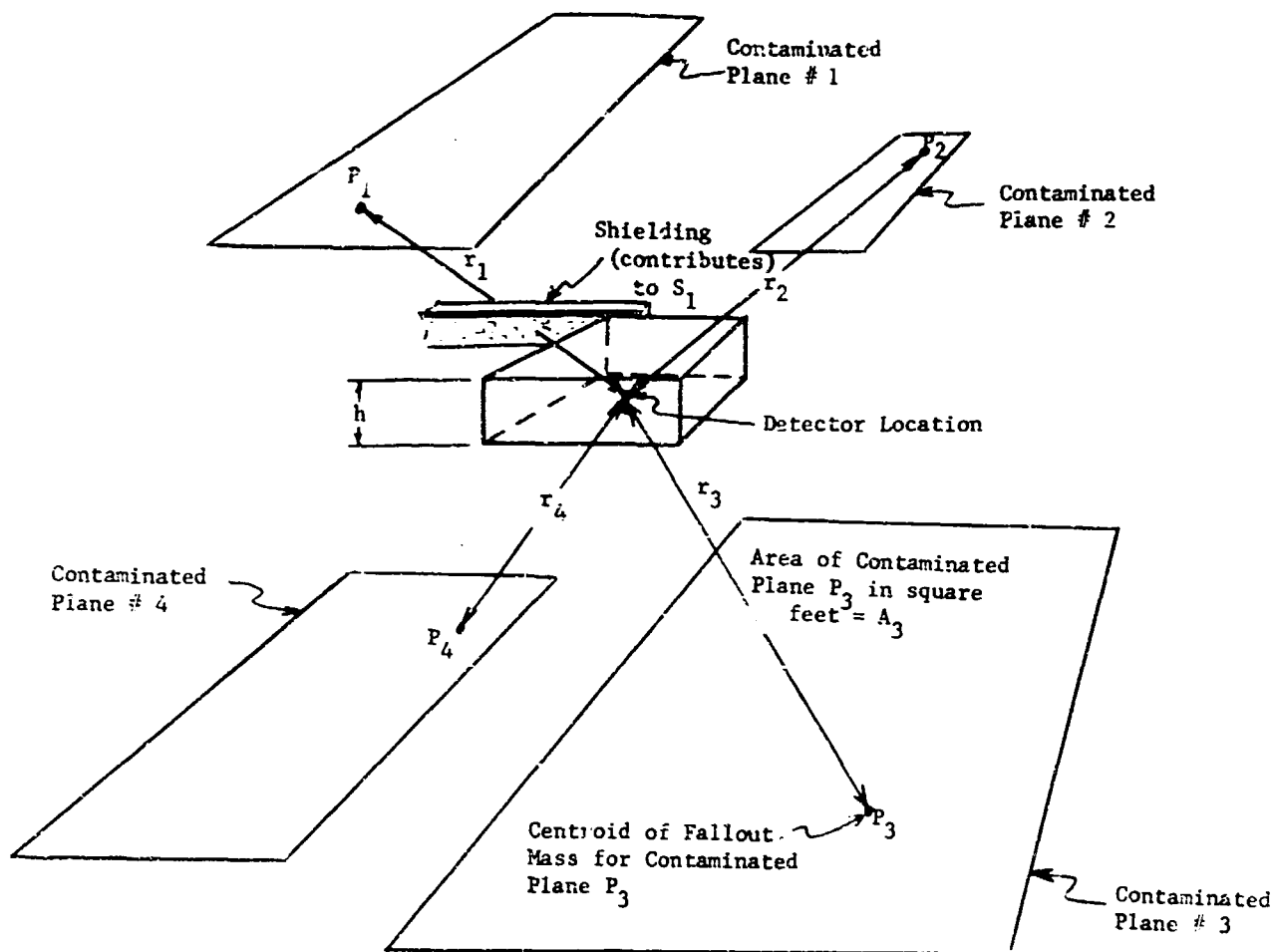


Figure A-3

Schematic Diagram of Simplified Decontamination Operations
with Four Contaminated Planes.

The contributions, C_i , to radiation intensity from ground level sources of contamination are computed using Equation A-1.

$$C_i = \frac{A_i}{r_i^2} S_i \quad (A-1)$$

where A_i = the area in square feet of the i^{th} contaminated plane,

r_i = the distance in feet from the centroid of the i^{th} contaminated plane to the detector, and

S_i = the shielding factor associated with the i^{th} contaminated plane.

Here C_i represents the fraction of the total intensity (received at the detector) which comes from the i^{th} plane. The shielding factor S_i is a dimensionless number which attenuates the contribution according to the shielding between the detector and the i^{th} plane. (Note that $0 \leq S_i \leq 1$).

The fraction of the total intensity received at the detector which comes from the roof of the building in which the detector is centrally located is found by Equation A-2*

$$C_r = \pi \ln \left(1 + \frac{r^2}{h^2} \right) S_r \quad (A-2)$$

where r = the radius of a circular roof, with an area equal to the area of the actual roof over the detector,

h = the height of the roof above the detector, and

S_r = the shielding factor associated with the roof.

Equation A-2 can also be used to determine the contribution to the intensity at an unshielded detector (out-of-doors) from the plane directly below the detector.

Here $S_r = 1$ and h is a height corresponding to the ground roughness factor.**

* See page 743 of Reference A-7 for a derivation of Equation A-2.

** See Reference A-5 for an explanation of how the ground roughness factor affects the "effective" height of the detector.

In the simplified model both $\frac{A_i}{r^2} S_i$ and $\Pi \ln \left(1 + \frac{r^2}{h^2}\right) S_i$ are treated as single constant inputs. Any variations in these individual parameters can be simulated by appropriately changing the capacitors which represent these aggregate variables before running the model.

Decontamination is governed (for each individual plane) by Equation A-3. ^{**}

$$F_i = F_i^* + (1 - F_i^*) e^{-K_i E_i} \quad (A-3)$$

where F_i = the fraction of fallout remaining on the i^{th} contaminated plane after it has been decontaminated.

F_i^* = the limiting fraction of fallout remaining on the i^{th} contaminated plane after infinite decontamination.

K_i = a constant associated with a given method and the physical nature of the i^{th} contaminated plane.

E_i = the effort (usually measured in man-hours) which is applied to the i^{th} contaminated plane.

Here, both $1 - F_i^*$ and $K_i E_i$ are treated as single variable inputs. Both of these variables can be varied by changing settings of the potentiometer which is assigned to the particular variable parameter. This can be done while the model is being run.

Table A-I is a summary of the equations used in the limited model of decontamination.

While the model is being run, the individual contributions are summed and the radiation intensity at the detector is output as a function of time. The total dose than an individual would receive at the detector location is also output as a function of time. The dose is measured over the time interval from t_1 to t_2 . This is simply given by

^{**} See Reference A-6 for a derivation of Equation A-3.

$$\text{Total Dose} = \begin{cases} 0 & \text{for } t < t_1 \\ \int_0^t H(x) x^{-1.2} dx & \text{for } t_1 \leq t \leq t_2 \\ \int_{t_1}^{t_2} H(x) x^{-1.2} dx & \text{for } t > t_2 \end{cases}$$

$H(t)$ denotes the value (represented by a voltage on the analog computer) associated with the sum of the intensity contributions from the individual planes as a function of time. For a system with a number of instantaneous decontamination operations, $H(t)$ will be a monotonically decreasing step function.

TABLE A-I.

System Equations for Simplified Model

1. Intensity contribution from the i^{th} ground level contaminated plane:

$$C_i = \frac{A_i}{r_i^2} S_i \quad \text{where}$$

A_i = the areas in square feet of i^{th} contaminated plane.

r_i = distance in feet from centroid of fallout on i^{th} contaminated plane to the detector location.

S_i = shielding factor associated i^{th} contaminated plane.

2. Intensity contribution from roof:

$$C_r = \pi \ln \left(1 + \frac{r^2}{h^2} \right) S_r \quad \text{where}$$

r = the radius of a circular roof of equal area.

h = height of roof (above detector).

S_r = shielding factor associated with roof.

3. Decontamination efficiency:

$$F_i = F_i^* + (1 - F_i^*) e^{-K_i E_i} \quad \text{where}$$

F_i = fraction of fallout remaining after decontaminating i^{th} plane.

F_i^* = fraction of fallout which cannot be removed.

K_i = constant associated with i^{th} surface and the method used to decontaminate it.

E_i = the amount of effort applied to decontaminate the i^{th} contaminated plane. (Usually measured in man-hours of effort).

For the simplified model the following parts of the above equations were set to single constant parameters;

$$1. \quad K_1^i = \frac{A_i}{r_i^2} S_i$$

$$2. \quad K_2^r = \pi \ln \left(1 + \frac{r^2}{h^2} \right) S_r$$

The following parts of the above equation were set to single variable parameters:

$$1. \quad V_1^i = 1 - F_i^*$$

$$2. \quad V_2^i = K_i E_i$$

IV. SAMPLE RUNS WITH PROTOTYPE MODEL

Several test runs were made. Seven of these runs are included here to illustrate the nature and format of the answers obtainable. The situation simulated in all seven runs was the decontamination of a single contaminated plane. For simplicity, no fallout build-up function was used. The $t^{-1.2}$ decay curve was approximated as the sum of two exponential decay curves (i.e., $t^{-1.2} \approx e^{-K_1 t} + e^{-K_2 t}$). A fuller discussion of this approximation is contained in Chapter VI.

In all of these sample runs, no attempt was made to quantitatively scale dose-rate and total dose. The time variable was also left arbitrary. Thus, two inches of horizontal distance on the graph outputs might correspond to two weeks, two hours, etc. The actual graph outputs from these seven runs are presented as Figures A-4 through A-10. Time runs from right to left on these graphs. For Figures A-4 through A-9, decontamination is assumed to take a small finite time. In Figure A-10 decontamination is instantaneous.

Figure A-4 shows the effect of decontaminating a single plane of contamination where 90% of the fallout material has been removed. Figures A-5 and A-6 show the effect of decontaminating the same plane of contamination where the decontamination efforts expended are only 75% and 50% of the effort expended in the operation simulated by the run which produced Figure 4. (Still assuming the percent of removable fallout equals 90%).

Figure A-7 shows the effect of decontaminating the same plane where only 50% of the fallout can be removed and a "full" effort (the same effort is assumed for Figure A-4) is expended. Figure A-8 shows the effect of decontaminating this plane where only 50% of "full" effort is expended.

For all of the Figures A-4 through A-8, both total dose and dose-rate are shown where total dose begins to accumulate at time t_1 and stops accumulating at time t_2 . Note that the vertical scale for total dose in Figures A-7 and A-8 is

exactly half of the scale used for total dose in Figures A-4, A-5, and A-6.

In Figure A-9, total dose begins to accumulate at t_a where no build-up function is assumed. The total dose continues to accumulate throughout the graph on Figure A-9. Here, the horizontal scale for total dose was again cut to half of that used in Figure A-8. The same fraction of removable fallout and effort expended are used in Figures A-8, A-9, and A-10.

Figure A-10 shows how the graphs would look if decontamination took place instantaneously. Otherwise Figure A-10 is the same as Figure A-9.

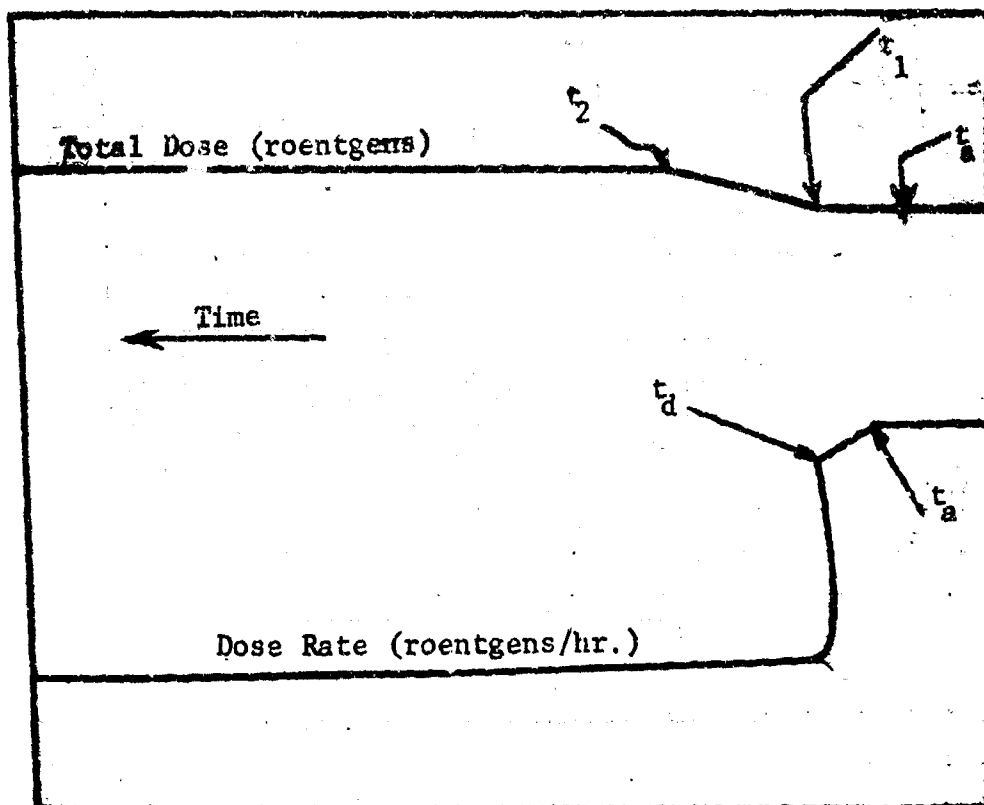


Figure A-4

Analog Record of Dose Rate and Total Dose as a Function of Time
for Case I

Legend

t_a = instantaneous time of arrival of fallout (no buildup).

t_d = time when decontamination begins.

(t_1, t_2) = interval of time for which total dose is calculated.

Thus,

$$\text{Dose} = \begin{cases} 0 & t < t_1 \\ \int_{t_1}^t H(x)x^{-1.2} dx & t_1 \leq t \leq t_2 \\ \int_{t_1}^{t_2} H(x)x^{-1.2} dx & t > t_2 \end{cases}$$

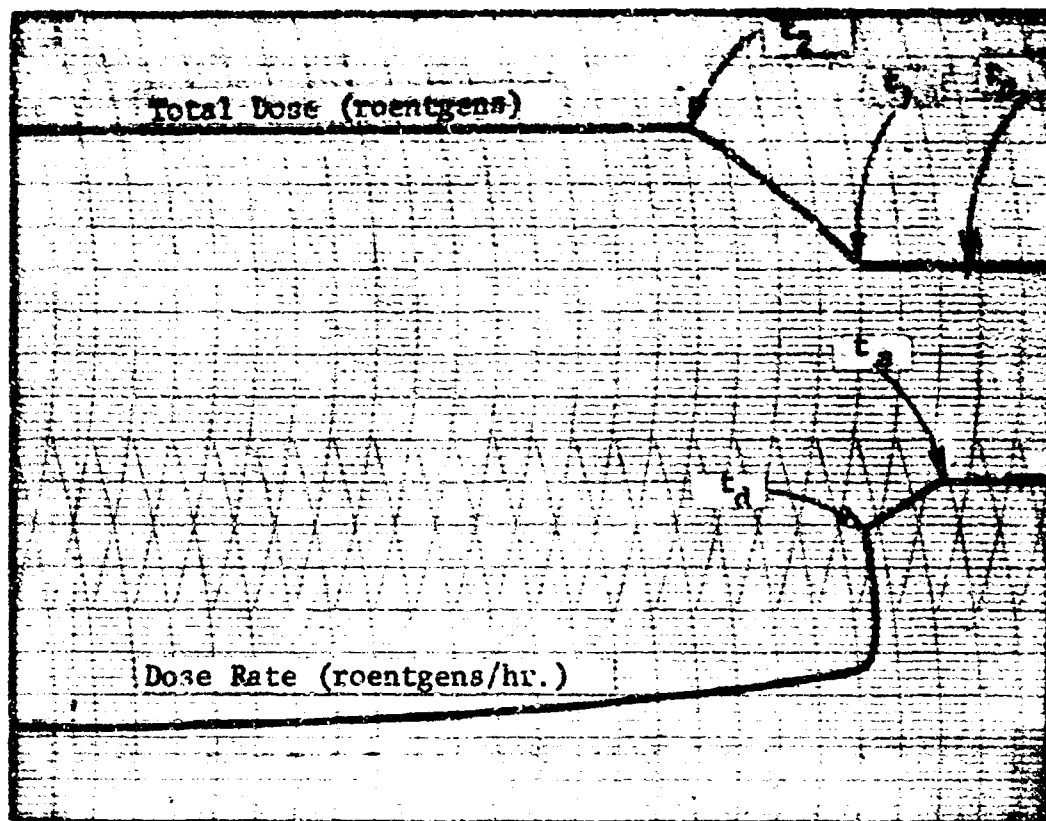


Figure A-5

Analog Record of Dose Rate and Total Dose as a Function of Time
for Case II

Legend

t_a = time of arrival of fallout (no buildup).

t_d = time when decontamination begins.

(t_1, t_2) = interval of time for which total dose is calculated.

Thus,

$$\text{Dose} = \begin{cases} 0 & t < t_1 \\ \int_{t_1}^t H(x) t^{-1.2} dx & t_1 \leq t \leq t_2 \\ \int_{t_1}^{t_2} H(x) t^{-1.2} dx & t > t_2 \end{cases}$$

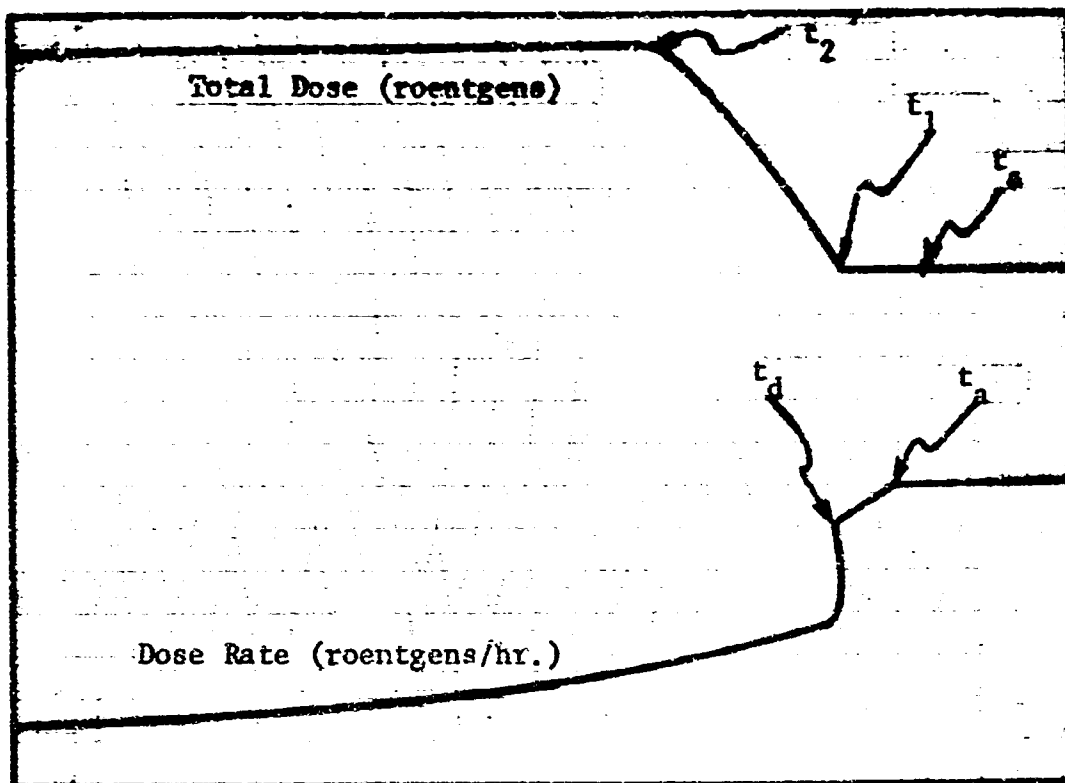


Figure A-6

Analog Record of Pose Rate and Total Dose as a Function of Time
for Case III

Legend

t_a = time of arrival of fallout (no buildup).

t_d = time when decontamination begins.

(t_1, t_2) = interval time for which total dose is calculated.

Thus,

$$\text{Dose} = \begin{cases} 0 & t < t_1 \\ \int_{t_1}^t H(x)x^{-1.2} dx & t_1 \leq t \leq t_2 \\ \int_{t_1}^{t_2} H(x)x^{-1.2} dx & t < t_2 \end{cases}$$

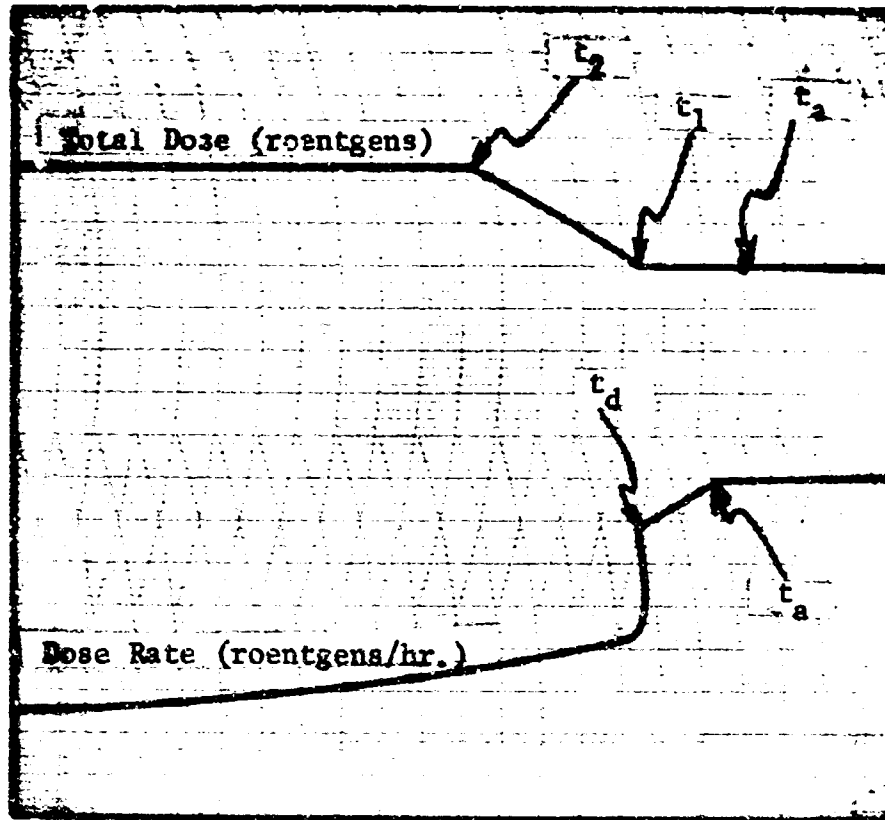


Figure A-7

Analog Record of Dose Rate and Total Dose as a Function of Time
for Case IV

Legend

t_a = time of arrival of fallout (no buildup).

t_d = time when decontamination begins.

(t_1, t_2) = interval of time for which total dose is calculated.

Thus,

$$\text{Dose} = \begin{cases} 0 & t < t_1 \\ \int_{t_1}^t H(x)x^{-1.2} dx & t_1 \leq t \leq t_2 \\ \int_{t_1}^{t_2} H(x)x^{-1.2} dx & t > t_2 \end{cases}$$

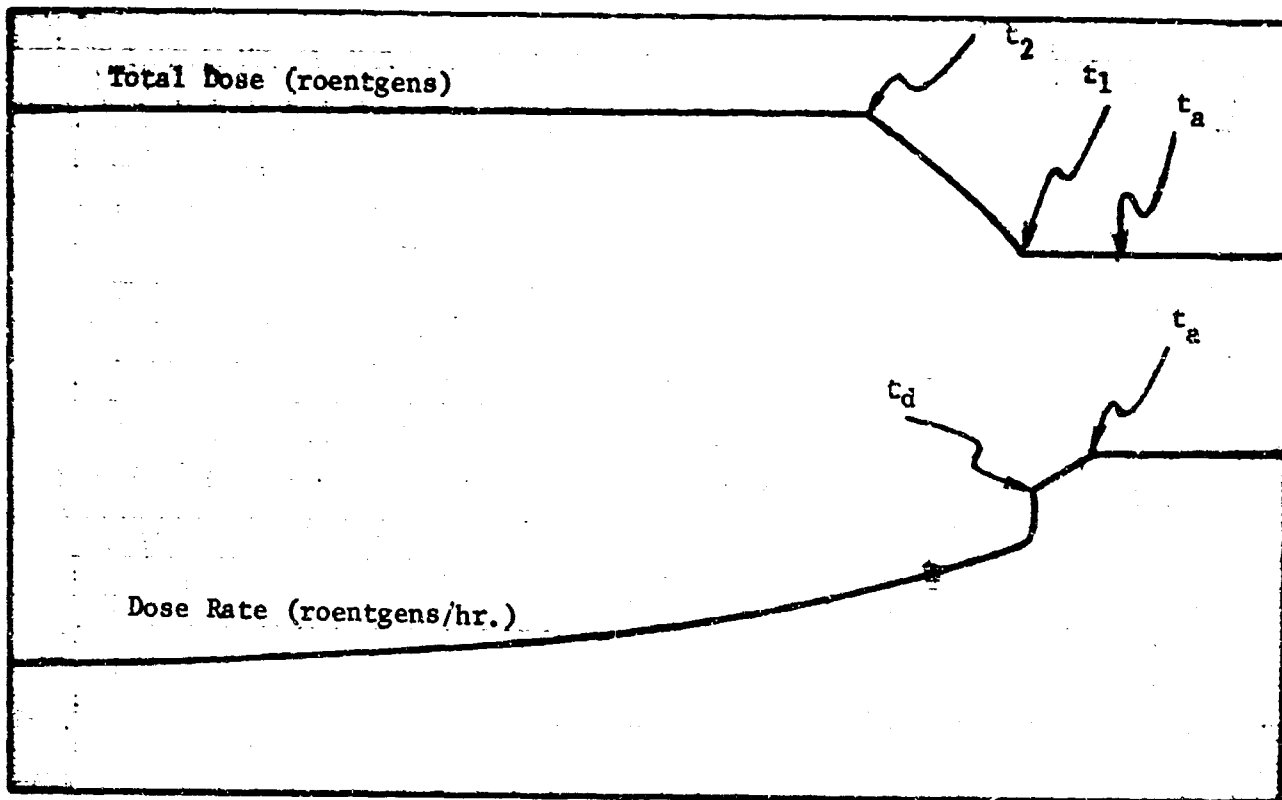


Figure A-8

Analog Record of Dose Rate and Total Dose as a Function of Time
for Case V

Legend

t_a = time of arrival of fallout (no buildup).

t_d = time when decontamination begins.

(t_1, t_2) = interval of time for which total dose is calculated.

Thus,

$$\text{Dose} = \begin{cases} 0 & t < t_1 \\ \int_{t_1}^t H(x)x^{-1.2} dx & t_1 \leq t \leq t_2 \\ \int_{t_1}^{t_2} H(x)x^{-1.2} dx & t > t_2 \end{cases}$$

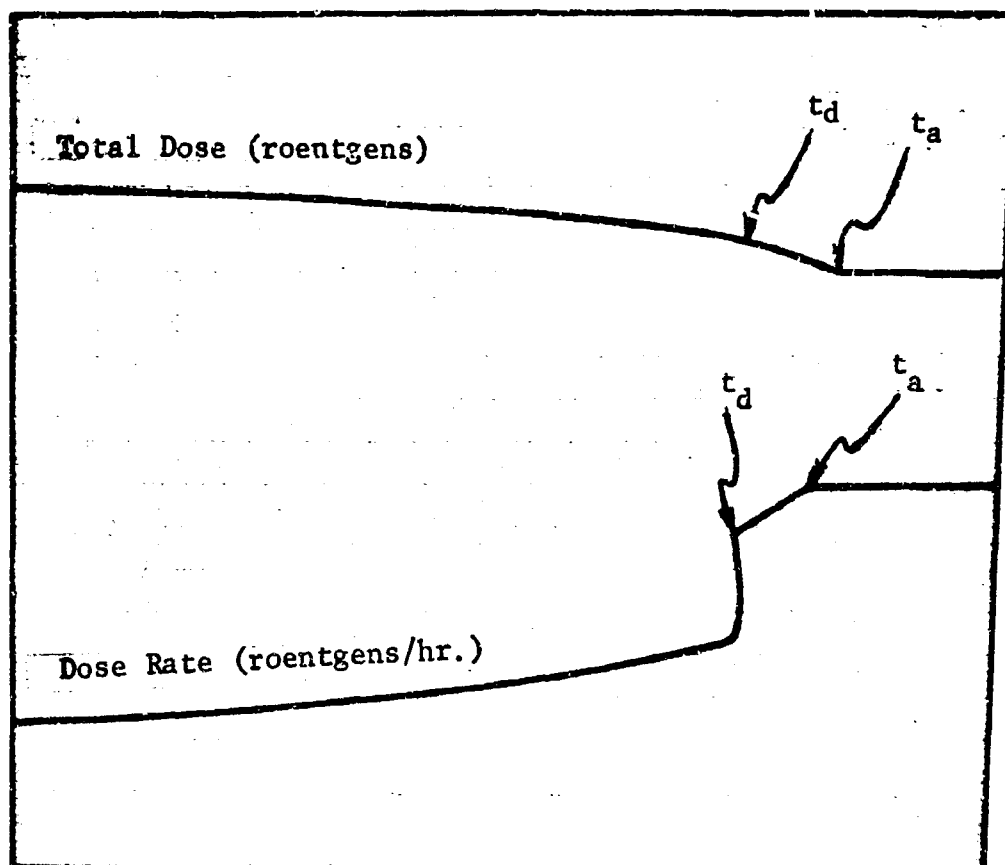


Figure A-9

Analog Record of Dose Rate and Total Dose as a Function of Time
for Case VI

Legend

t_a = time of arrival of fallout (no buildup).

t_d = time when decontamination begins.

Total dose is calculated from t_a to any time t .

Thus,

$$\text{Dose} = \begin{cases} 0 & t \leq t_a \\ \int_{t_a}^t H(x)x^{-1.2} & t_a < t < \infty \end{cases}$$

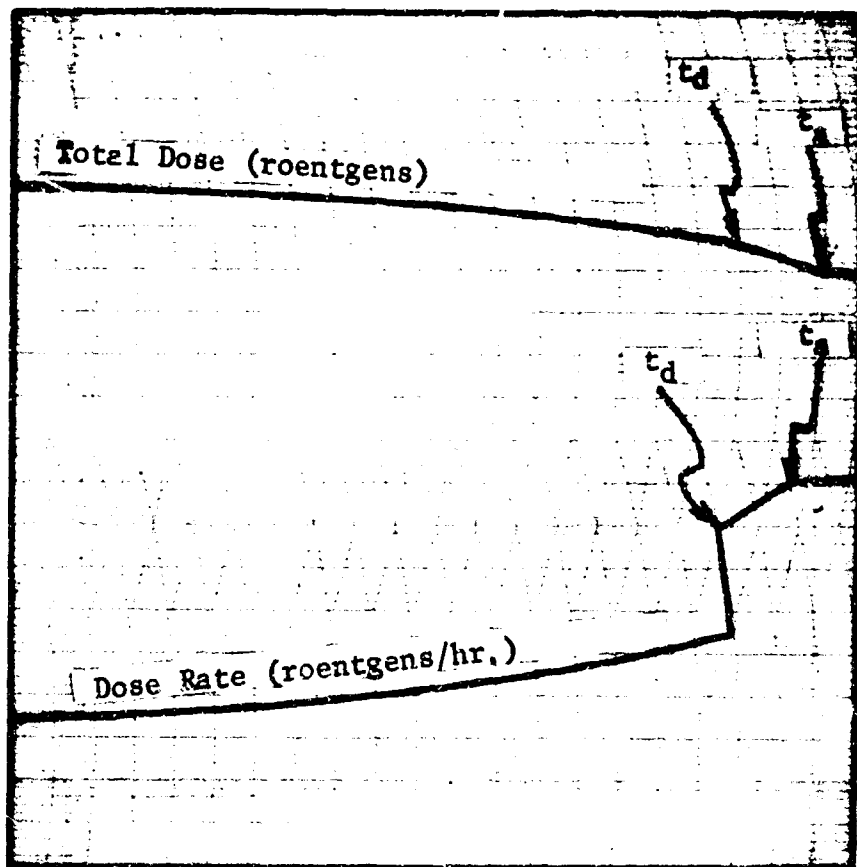


Figure A-10

Analog Record of Dose Rate and Total Dose as a Function of Time
for Case VII

Legend

t_a = time of arrival of fallout (no buildup).

t_d = time when decontamination begins.

Total dose is calculated from t_a to any time t .

Thus,

$$\text{Dose} = \begin{cases} 0 & t \leq t_a \\ \int_{t_a}^t H(x) x^{-1.2} dx & t_a < t < \infty \end{cases}$$

V. AN ELABORATE MODEL

Although quite adequate to demonstrate feasibility, the limited analog model described in Section III is not suitable for complex decontamination problems. A more elaborate model with less aggregation of variables and a capacity for handling a larger number of contaminated planes is necessary. The basic system equations, however, remain the same for the larger analog model described in this section.

As in the model already implemented and described in Section III, decontamination is measured by a "graph" of dose-rate (radiation intensity) at some detector location of interest. Total dose is measured for selected time intervals at the same point. Complex buildup functions can be used to simulate the initial stages of fallout arrival. The number of contaminated planes which can be considered for a given detector, as well as the number of detector locations, is in theory, unlimited. A practical limit on the numbers of analog components would limit the number of contaminated planes to 20 and the number of detector locations to three. By appropriately using relays and switching circuits, the total dose received by a person changing environments instantaneously (such as moving from indoors to outdoors) could be simulated.

All functions (\log , $t^{-1.2}$, etc.) can be quite accurately simulated by using suitably adapted function generators. This will improve the precision of the simulation.

Furthermore, a quick-response capability could be included to serve as an analysis and training tool. This is accomplished by using manual over-rides which permit the operator to apply decontamination efforts on the basis of graphs which portray previous decontamination efforts during the same run.

A technical description and flow diagram of the more elaborate model is included in Chapter VI.

VI. A TECHNICAL DESCRIPTION OF THE ANALOG DECONTAMINATION MODELS

A. Calculations to be Performed

The calculations to be performed by the computer are expressed in Equations A-5 and A-6:

$$R(t) = \sum_{i=1}^n \frac{A_i S_i}{r_i^2} \left[1 - u(t - t_{1i}) C_{E_i} e^{-\frac{(t - t_{1i})}{\tau_i}} C_{m_i} \right] t^{-1.2} + \pi \left(\ln \left[1 + \frac{\rho^2}{h^2} \right] \right) S_s t^{-1.2} \quad (A-5)$$

$$D(t) = \int_{t_1}^{t_2} R(t) dt = \int_0^{\infty} v(t; t_1, t_2) R(t) dt \quad (A-6)$$

where the symbols are defined as follows:

- $R(t)$ = dose rate in roentgens per hour,
- $D(t)$ = dose (normalized units) in roentgens,
- n = number of contaminated planes considered,
- A_i = area of i^{th} contaminated plane in square feet,
- r_i = distance from detector to centroid of i^{th} contaminated plane in feet,
- S_i = shielding factor for i^{th} location ($0 \leq S_i \leq 1$),
- K_i = constant for i^{th} contaminated plane and a particular decontamination method,
- E_i = effort applied to i^{th} contaminated plane in man hours/1000 sq ft,
- C_{E_i} = effort coefficient = $1 - e^{-K_i E_i}$,
- C_{m_i} = fraction of removable mass for i^{th} contaminated plane,
- τ_i = decontamination time constant,
- ρ = effective radius of surrounding contaminated plane (roof or detector surface),
- h = effective height of surrounding contaminated plane (roof or detector surface),
- S_s = shielding factor for surrounding contaminated plane (roof or detector surface),

$t_1, t_2 =$ integration limits for dose $D(t)$.

The function $u(t-t_1)$ is a unit step function which has the values:

$$\begin{aligned} u(t-t_1) &= 0 & 0 \leq t < t_1 \\ &= 1 & t_1 \leq t < \infty \end{aligned}$$

The function $v(t, t_1, t_2)$ has the values:

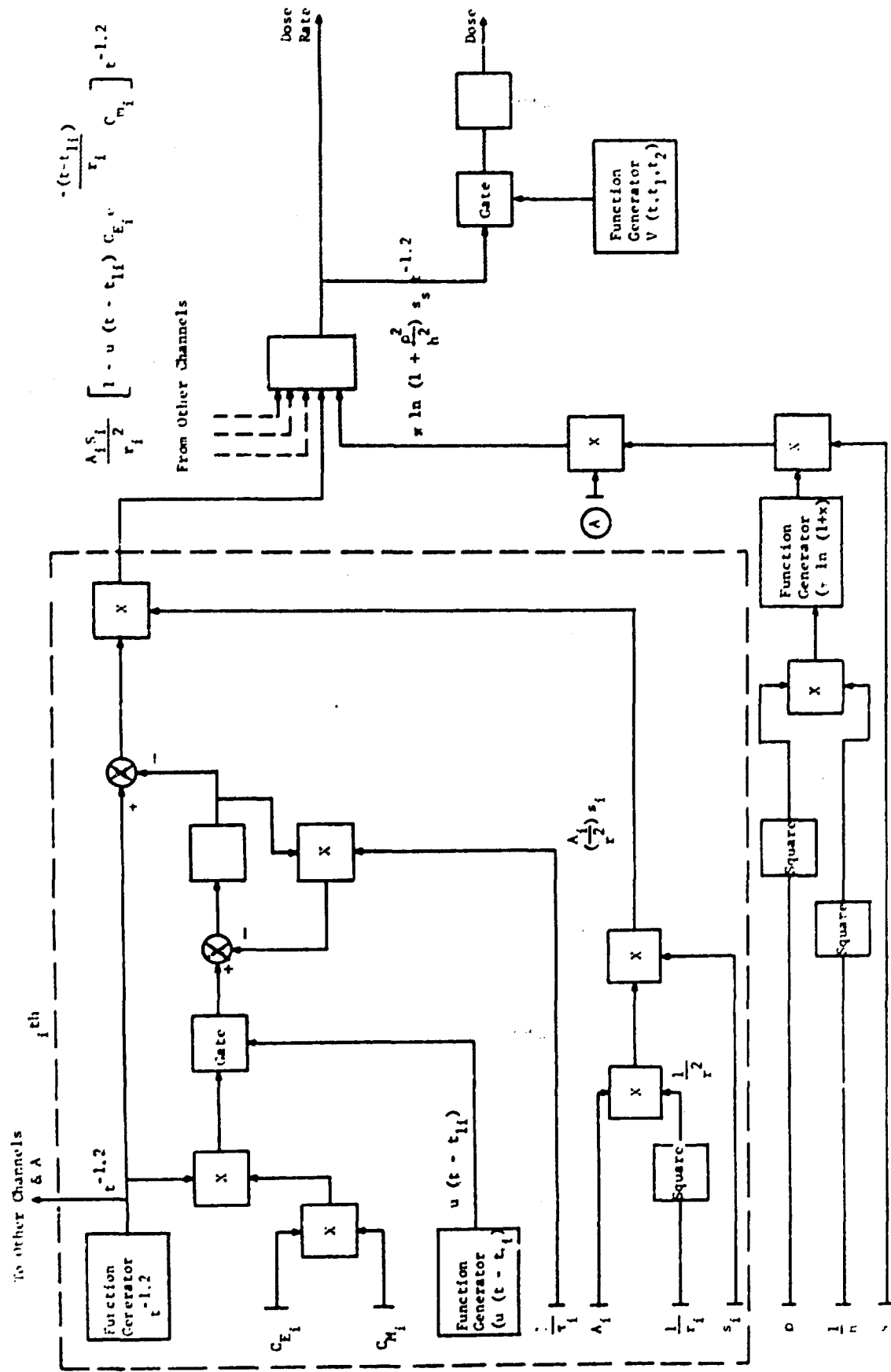
$$\begin{aligned} v(t, t_1, t_2) &= 0 & 0 \leq t < t_1 \\ &= 1 & t_1 \leq t < t_2 \\ &= 2 & t_2 \leq t < \infty \end{aligned}$$

A functional diagram showing the calculations to be performed is shown in Figure A-11. Only one of the n identical channels (each channel corresponding to a single contaminated plane) is shown. For n areas, the calculations represented within the dotted outline will be repeated n times.

B. Range of Constants, Parameters, and Variables

The units of the various quantities and the expected ranges of these quantities are listed below:

<u>SYMBOL</u>	<u>UNITS</u>	<u>RANGE</u>
$R(t)$	r/hr	-
t	hrs	24-336 (1000)
n	dimensionless	1-10
A	ft^2	100-100,000
r	ft	10-500
S	dimensionless	0-1
C_E	dimensionless	0-1
K	$\text{ft}^2/\text{man-hour}$.1-5



A-29

Figure A-11
Functional Diagram of Calculations

<u>SYMBOL</u>	<u>UNITS</u>	<u>RANGE</u>
E	man hrs/1000 ft ²	.01-1
C _m	dimensionless	0-1
τ	hr ⁻¹	10-0.1
t _{1i}	hr	10-1000
ρ	ft	10-200
h	ft	1-100
S _s	dimensionless	0-1
t ₂	hr	10-1000
t ₁	hr	10-1000
D(t)	roentgens	-

For computational purposes the dose rate R(t) and dose D(t) are measured in normalized units. To convert to roentgens per hour or roentgens, one point on the dose rate curve must be hand calculated, and the proper scale factor determined.

C. Computer Scaling

1. Choice of Time Scale

The time range of major interest is from 24 to 336 hours. For convenience, the computer time scale, t_c , may be chosen so that one hour of real time, t_r , corresponds to .5 second of computer time. Time zero on the computer will correspond to time 24 hours in real time. Thus:

$$t_c = \frac{1}{2} (t_r - 24) \text{ seconds,} \quad (\text{A-6})$$

where t_c = computer time in seconds, and

t_r = real time in hours.

2. Dose Rate Scale

At $t_r = 24$ hrs, the dose rate R(t) will be assigned the value 100 in arbitrary units. The computer scale factor for R(t) will be taken as 1 volt/unit. To convert from arbitrary units to roentgens per hour, the scale

factor is determined by hand calculation of the dose rate at $t_r = 24$ hrs.

The dose $D(t)$ will be scaled at .01 volt per arbitrary unit to prevent the integrator from overloading with long integration times.

3. Coefficient Scaling

For adjusting values of the various parameters that remain constant during a particular computer run, the computer potentiometers will be used. In order to simplify the equipment requirements, it is convenient to group certain parameters into dimensionless ratios where possible. These parameter groups will then be set into the computer as potentiometer settings. Additional coefficients are defined as follows:

$$C_{r_i} = \frac{A_i}{r_i^2} \quad \text{range} \quad .01 - 10$$

$$C_s = \pi \ln \left[1 + \frac{\rho^2}{h^2} \right] \quad \text{range} \quad 0 - 20$$

For potentiometers with dial divisions from 0 to 100, the following scale factors are assigned to the parameters that are to be set on potentiometer dials:

<u>Coefficient</u>	<u>Range</u>	<u>Scale Factor</u> (units per dial division)
C_{r_i}	.01-10	.1
C_s	0-20	.2
C_{E_i}	0-1	.01
C_{m_i}	0-1	.01
S_i	0-1	.01
S_s	0-1	.01

It should be noted that with additional equipment complexity, each value such as r_i , A_i , etc. may be entered separately as a dial setting, and the necessary multiplications and divisions accomplished by the computer.

4. Dynamic Range Requirements

In some cases, it would be desirable to simulate a time period longer than 15 days. In increasing the time period of a single computer run, difficulties may be encountered because of the small signal levels that will be present. For example, the function $t^{-1.2}$ decreases by a factor of approximately 100 between 24 hours and 1100 hours. If the computer output were initially set at 100 volts, the output at 1100 hours (550 seconds computer time) would be approximately 1 volt if no decontamination had taken place. This level is not too small; however, the signal level from each of the i channels must be considerably less than 1 volt (with 10 channels giving equal contributions, the signal level would be .1 volt). On certain computers, the noise level prevents accurate operation at these low voltage levels.

In order to avoid the inaccuracies inherent in using low signal levels, the best approach would appear to be to break the problem into time periods of interest. If the period of interest were from 10 to 20 days, the computer time would be scaled such that the problem starts at $t_r = 240$ hrs instead of 24 as discussed previously.

D. Computer Diagram

A computer diagram to perform the necessary calculations is shown in Figure A-13 where the symbols are defined in Figure A-12. A function generator generates a voltage proportional to $t^{-1.2}$. This voltage is adjusted to a value analogous to the contribution of each of the contaminated planes by the potentiometers C_{r_i} , S_{r_i} , C_g , and S_g . The voltages analogous to the radiation received from each area are summed in a summing amplifier, and the resultant voltage is recorded on a strip chart recorder.

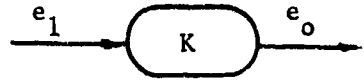
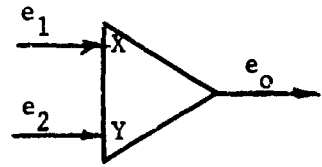
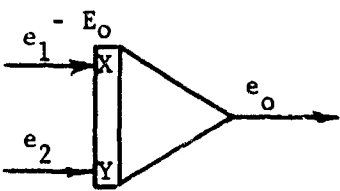
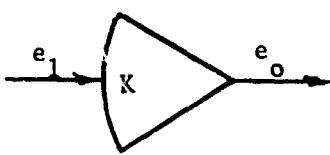
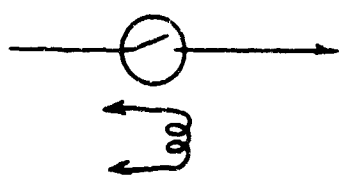
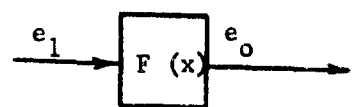
<u>Symbol</u>	<u>Name</u>	<u>Operation</u>
	Coefficient	$e_o = K e_1 \quad (0 \leq K \leq 1)$
	Summer	$e_o = x e_1 + y e_2$
	Integrator	$e_o = \int (x e_1 + y e_2) dt + E_o$
	High Gain Amplifier	$e_o = k e_1 \quad k > 10^6$
	Relay	$e_o = e_1 \quad \text{energized}$ $e_o = 0 \quad \text{unenergized}$
	Function Generator	$e_o = F(e_1)$

Figure A-12
Table of Flow Chart Symbols and Operations

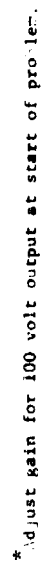


Figure A-13

Computer Diagram

To simulate decontamination of a given area, the relay Ry A₁ is closed. A time lag of the form e^{-t/τ_1} is introduced by operational amplifier #7, and the original voltage is reduced by the proper amount by subtraction in amplifier #1. The amount of voltage subtracted depends upon the effort coefficient and the percent of removable material as set on the potentiometers C_{E₁} and C_{m₁}.

To calculate the dose from the dose rate, an integrator is energized by relay Ry B. This relay remains closed for a time period $t_2 - t_1$, as set on the sequencing function generator.

Note that the computer diagram shows only one of n identical setups that must be patched into the computer.

E. Function Generators

To simulate a function varying with time as $t^{-1.2}$, several methods are available. A conventional diode function generator with a linear time function input may be used. Another method is to use an x-y plotter as a function generator, supplying a linear time function as a drive for the x axis, and reading out a voltage proportional to $t^{-1.2}$ on the y axis by means of a curve following probe. The simplest technique, however, appears to be that of approximating the $t^{-1.2}$ function by a sum of exponentially decaying functions. For example, with three exponentials, the $t^{-1.2}$ curve may be fitted by the sum at six points on the curve. The exponential functions are generated very easily on the analog computer by setting up an initial charge on a capacitor, and discharging the capacitor slowly through a resistor. Figure A-14 shows the approximation of the $t^{-1.2}$ function in the range 24-350 hrs by the sum of two exponentials as follows:

$$t^{-1.2} \approx \frac{1}{45.3} \left[.86 e^{-.0313(t-24)} + .14 e^{-.00375(t-24)} \right]$$

The computer diagram for accomplishing this approximation would appear as shown in Figure A-15 (.5 sec computer time = 1 hr real time).

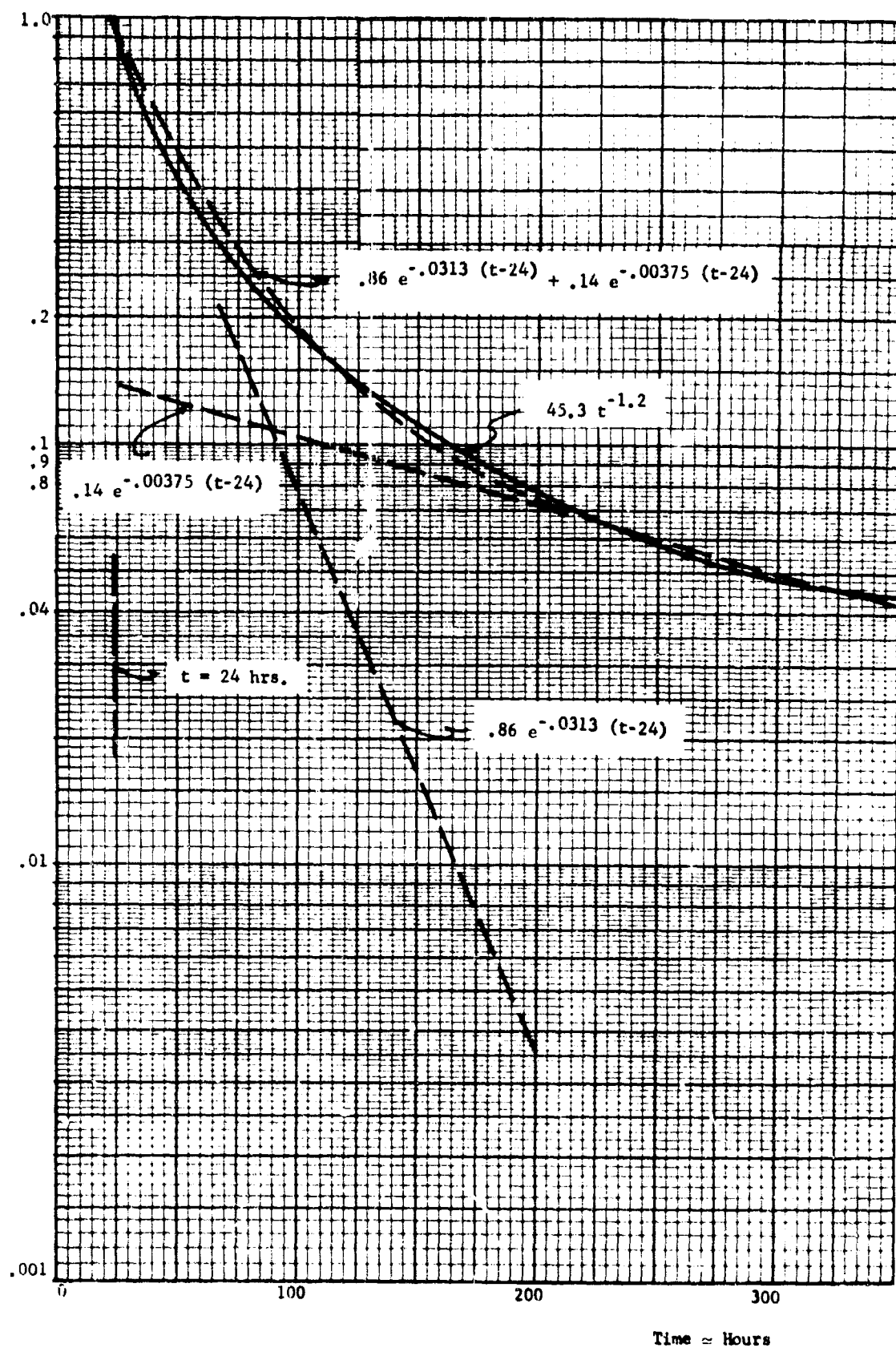


Figure A-14
Approximation of the Function of the Form $t^{-1.2}$ by Two Exponentials

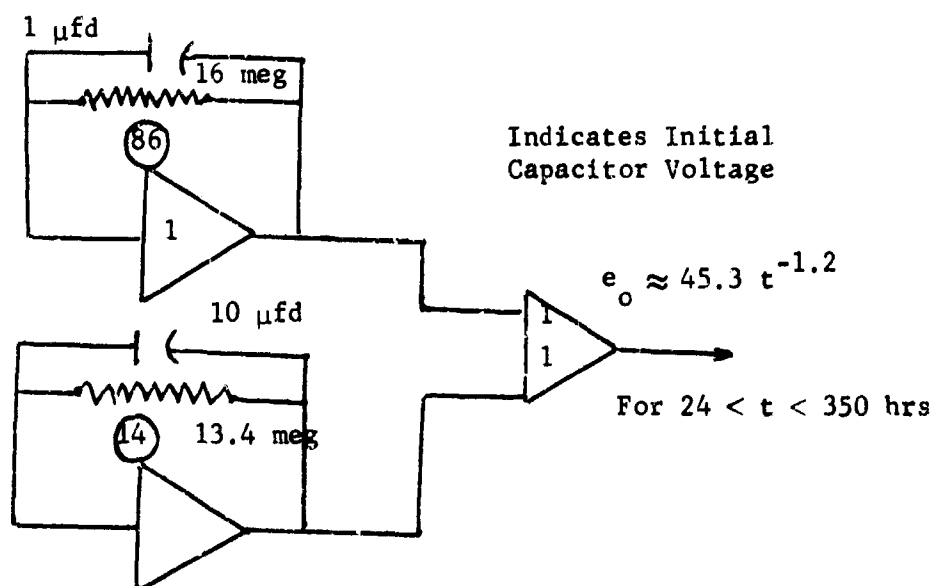


Figure A-15
Approximation of $t^{-1.2}$ Function

The functions $u(t-t_1)$ and $v(t, t_1, t_2)$ are generated by a sequencing device which may be a set of motor driven cams. Switches are closed by the cams at the desired time, and the proper relays are closed as shown in Figure A-12. Provision must be made for convenient adjustment of the times t_1 , t_1 and t_2 . For the motor driven cams, $n+1$ cams will be required.

F. Equipment Requirements

To set up a situation with 10 contaminated areas, the following analog equipment will be required:

<u>Quantity</u>	<u>Item</u>
34	Operational Amplifiers
52	Dial Setting Potentiometers
(1)	Function Generator $t^{-1.2}$
or (3)	Operational Amplifiers (for approximation of $t^{-1.2}$ function)

<u>Quantity</u>	<u>Item</u>
11	Relays
1	Sequence Function Generator (11 Channel)
1	Dual Channel Recorder

A 40 amplifier analog computer should be sufficient for the 10 area simulation.

The sequence function generator may be constructed in the laboratory if a suitable type cannot be purchased. To buy this equipment would cost about \$40,000. Total rental costs (including set-up costs) would be under \$1,000 for a one year period.

VII. CONCLUSIONS AND RECOMMENDATIONS

A. Conclusions

The basic conclusion of this study is that the analog computer provides a potentially useful and quite feasible tool for simulating and analyzing decontamination operations.

The development and implementation of this first analog model of decontamination has pinpointed the areas of difficulty and the direction in which further work appears most promising. The most difficult problem encountered was accurately approximating the $t^{-1.2}$ decay rate. This problem is considered in detail in Chapter VI; since a high-accuracy analytic function generator would be very costly (about \$1000), some form of approximation involving the sum of exponential functions of the form $K_1 e^{-K_2 t}$ is a practical compromise solution.

Even though a number of the problems associated with the simple model using only one plane of contamination were a result of complex scaling necessary to keep the range of variables within machine limits, future models, to be useful, must include even more detail and so must use even more equipment. Thus, scaling will become an increasingly difficult problem.

B. Future Work

Any future work must be undertaken in the light of the major difficulty found in using the limited analog model--the large amount of equipment required for an adequate simulation. Nonetheless it is recommended that two major directions be explored:

1. The development of a larger more detailed simulation, but still with simplified aggregation of variables where possible, and
2. The development of a quick response capability to serve as a ready analysis and training tool.

REFERENCES

- A-1. G. A. Korn and T. M. Korn. Electronic Analog Computers - 2nd Edition. New York: McGraw-Hill Book Company, 1956.
- A-2. M. G. Hartley. An Introduction to Electronic Analog Computers - Methuen's Monographs on Physical Subjects. New York: John Wiley & Sons, Inc., 1962.
- A-3. J. C. Sessler. The Application of Analog Computers to Air Battle Problems. Staff Memorandum 61-4, Technical Operations, Inc., Washington 1961 (cataloged by DDC as AD No. 261621).
- A-4. W. L. Owen, V. D. Sartor, and W. H. VanHorn. Stoneman II Test of Reclamation Performance, Vol. II: Performance Characteristics of Wet Decontamination Procedures. USNRDL-TR-335. San Francisco: United States Naval Radiological Defense Laboratory, July 1960.
- A-5. Office of Civil Defense. Shelter Design and Analysis. TR-20. Volume I, Revised Edition. Washington: Office of Civil Defense, Volume I, November 1962 and Volume 2, September 1963.
- A-6. C. F. Miller. Theory of Decontamination. Part I, USNRDL-460. San Francisco: United States Naval Radiological Defense Laboratory, July 1958.
- A-7. R. D. Evans. The Atomic Nucleus. York, Pennsylvania: McGraw Hill Book Company, 1955.

Appendix B

A Circular Model for Approximating Gamma Ray Intensity at a Detector Location

Note: The material in this Appendix was originally submitted to USNRDL as Research Memorandum RM-OU-214-3*.

W. R. Davis, M. K. Moss, and A. J. Benjamin. A Circular Model for Approximating Gamma Ray Intensity at a Given Detector Location. RM-OU-214-3. Durham, North Carolina: Research Triangle Institute, Operations Research and Economics Division, 30 April 1965.

TABLE OF CONTENTS OF APPENDIX B

TABLE OF CONTENTS	B-1
LIST OF TABLES	B-11
LIST OF FIGURES	B-11
GLOSSARY OF TERMS	B-111
 I. INTRODUCTION	 E-1
II. SINGLE ANNULUS MODEL	R-3
A. Complete Uniformly Contaminated Annulus	B-3
B. Single Annular Sector Case	B-5
C. Multiple Annular Sectors	B-7
III. MULTIPLE ANNULAR REGION MODEL	B-9
A. Complete Set of Uniformly Contaminated Annular Regions	B-9
B. Equivalent and Uniformly Contaminated Annular Sectors for a Set of Annular Regions	B-13
IV. BARRIER ATTENUATION	B-15
V. DERIVATION OF SOLID ANGLE FRACTION EXPRESSION	B-19
VI. APPROXIMATE ANALYTICAL FIT FOR $L_c(X, \omega)$ FUNCTION	B-23
VII. EXAMPLE	B-25
VIII. SUMMARY AND CONCLUSIONS	B-31
REFERENCES	B-33

LIST OF TABLES

<u>Table</u>	<u>Page</u>
B-I Calculated Values of S and A for Selected Effective Mass Thickness Values	B-24

LIST OF FIGURES

<u>Figure</u>	<u>Page</u>
B-1 Single Annulus Configuration	B-4
B-2 Geometry Factor ($L_c(X, \omega)$) Depicting Detector Response Due to a Circular Plane Gamma Radiation Source	B-6
B-3 Multiple Annular Regions Configuration Showing Uniformly Contaminated Regions of Arbitrary Height	B-10
B-4 Detector Response Due to Uniformly Contaminated Planes with Different h_{kj} Values	B-12
B-5 Two Annular Sectors of Separate Annular Regions - One Sector Shielded From the Detector	B-16
B-6 Detector Response From a Shielded Sector	B-16
B-7 Detector Geometry Associated with $L_c(X, \omega)$ and $L_c(d, \omega)$ Factors	B-17
B-8 Solid Angle Geometry	B-20
B-9 Example Illustration	B-26

GLOSSARY OF TERMS

A	=	Intercept value used in the analytical approximation of $L(X, \omega)$ functions.
d	=	Vertical height of the detector above the source plane.
D_o	=	Total detector response at a standard reference position.
D_k	=	Gamma dose rate received at a detector from the k^{th} annular region.
D_{kj}	=	Gamma dose rate received at a detector from the j^{th} annular sector of the k^{th} annulus.
D/D_o	=	Dose reduction factor.
h_{kj}	=	Height of contaminated annulus above the ground or reference plane.
$L(X)$	=	Total detector response for infinite plane isotropic source.
$L(X, \omega)$	=	Generalized expression for the geometry factor.
$L_c(X, \omega)$	=	Geometry factor describing detector response due to circular plane sources of fallout radiation.
M_j	=	Fractional area of the k^{th} annular region covered by the contaminated j^{th} annular sector.
P_k	=	Total number of sectors in the k^{th} annulus.
S	=	Slope value used in the analytical approximation of $L(X, \omega)$ functions.
ω	=	Solid angle fraction.
X	=	Effective mass thickness.
z_k	=	Height of k^{th} annular region above the detector.

A Circular Model for Approximating Gamma Ray
Intensity at a Detector Location

1. INTRODUCTION

The purpose of this appendix is to show the initial results of recent studies directed toward the development of rather simple and practical procedures for determining the gamma ray intensity at a point due to nuclear weapon induced fallout. The consensus of those involved in this research effort was that if such an approach proved feasible, it would result in a considerable reduction in both labor and computer costs for those cases where approximate results are considered adequate. In addition, the development of such an analytical tool would be of considerable value in simplifying those tasks associated with the ensuing analysis of decontamination effectiveness in municipal areas. This research is a first step in the development of several alternative approaches to a model for field analysis of fallout decontamination effectiveness.

In an effort to assure a reasonable degree of accuracy in the analytical model presented in the following discussions, such pertinent factors as gamma ray attenuation, build-up, backscatter, and skyshine, are incorporated. Another basic premise closely adhered to in connection with the development of this model is that it be built around the familiar results contained in NBS Monograph 42 (Reference B-1).

The general notational scheme presented here, together with selected elementary geometric considerations and the information contained in Reference B-1, provides the basis for what is called a "circular model". This model is utilized to furnish values of the so-called "reduction factor," D/D_0 , due to various planes of contamination at different heights with or without the inclusion of barrier shielding.

In particular, these planes of contamination are divided into annular sectors with the detector located in each instance at the origin of the polar coordinate system.

The approach taken in describing this circular model is that of developing initially the detector response for the single contaminated annulus case (Section II) following with increasingly more complex annular geometries (Section III) and terminating with a brief discussion on barrier shielding considerations (Section IV).

Each of the annular geometric configurations utilized in the analytical development of the model required the extensive use of the $L(X)$ and the $L(X,\omega)$ functions developed in Reference B-1. It was found during the course of the investigation that the $L(X,\omega)$ functions could be approximated over their range of greatest utility by simple analytical expressions (Section VI). In turn, such expressions can be quickly and easily evaluated with the aid of a desk calculator and standard mathematical tables, or efficiently stored in a computer memory without the necessity of lengthy subroutines.

The procedure for treating attenuation through barriers makes effective use of the $L(X)$ function and the $L_c(X,\omega)$ geometry factor, through judicious choices and combinations. It should be noted that considerable refinement of these procedures and associated calculations may be necessary for situations near the detector location at the origin of the coordinate system.

II. SINGLE ANNULUS MODEL

The single annulus is chosen initially since it will permit the development of the basic premises from which more complex geometries can later be described.

A. Complete Uniformly Contaminated Annulus

In order to express the detector response for the case of a single uniformly contaminated annulus (see Figure B-1), it is necessary to first define the solid angle fractions ω_{ka} and $\omega_{(k+1)a}$ subtended at the detector by the contaminated annulus.

1. Solid Angle Expressions

From Figure B-1 we define first the solid angle fraction ω_{ka} subtended by angle α_{ka} as

$$\omega_{ka} = 1 - \cos \alpha_{ka}, \text{ (See Section V for derivation of solid angle expressions)} \quad (B-1)$$

where

$$\cos \alpha_{ka} = \frac{d}{\sqrt{(ka)^2 + d^2}} \quad (B-2)$$

Similarly,

$$\omega_{(k+1)a} = 1 - \cos \alpha_{(k+1)a} \quad (B-3)$$

where

$$\cos \alpha_{(k+1)a} = \frac{d}{\sqrt{(k+1)^2 a^2 + d^2}} \quad (B-4)$$

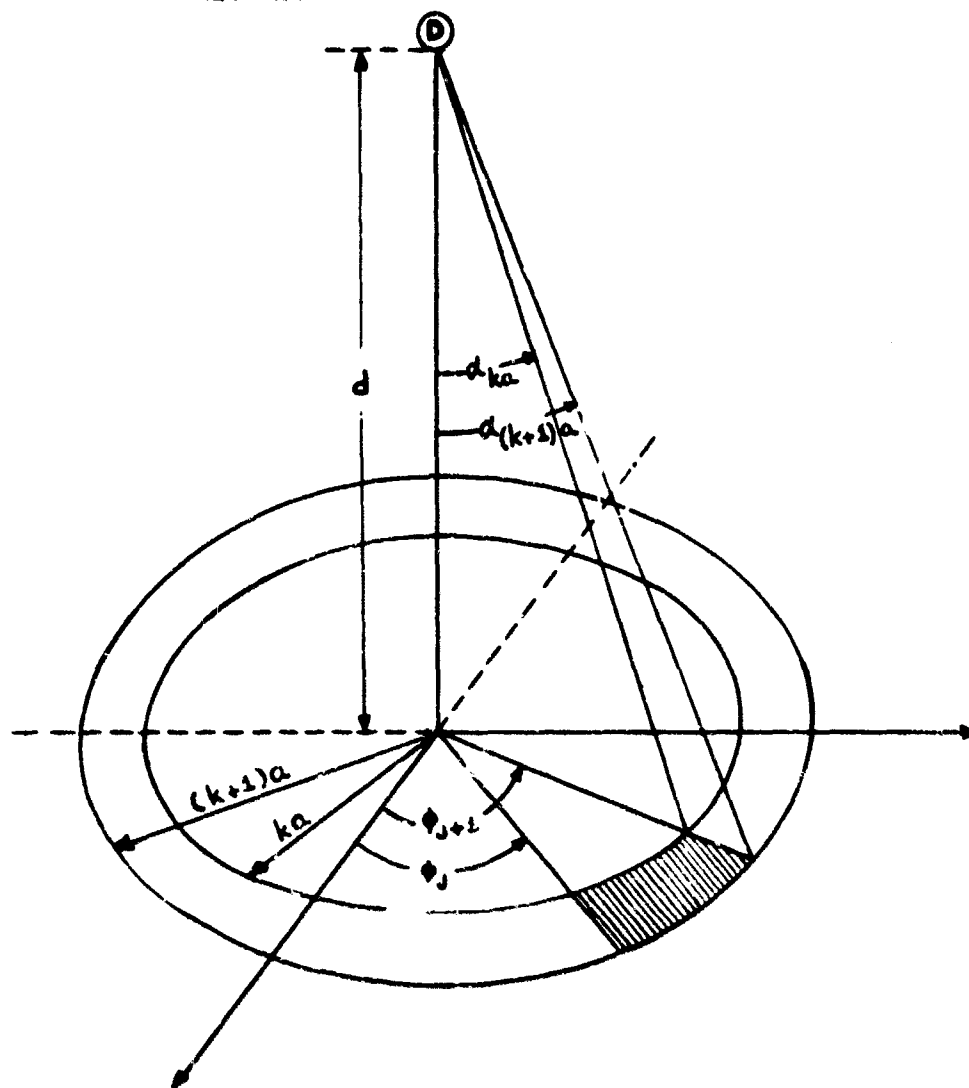


Figure 3-1
Single Annulus Configuration

2. Detector Response

The detector response for the single annulus can be computed by appropriate differencing of the geometry factor $L_c(X, \omega)$ (see Figure B-2 and Section VI) for the values of ω_{ka} and $\omega_{(k+1)a}$. This differencing can be illustrated in terms of the detector response for the uniformly contaminated annulus in Figure B-1 as follows:

$$\frac{D_k}{D_0} = L(X) \left[L_c(X, \omega_{(k+1)a}) - L_c(X, \omega_{ka}) \right] \quad (B-5)$$

where D_0 is the detector response at a standard reference position*, and D_k is the response due to the k^{th} annulus. The function $L(X)$ is graphed in Reference B-1.

It should be noted that all distances d from the detector to the contaminated plane of interest may be expressed in terms of effective mass thickness (X) for the medium between the source and detector. For the case of air (at 20°C, 76 cm Hg) as this medium, the following relationship may be written (see p. 19, Reference B-1):

$$d/X = 13.3 \text{ Ft. of air/psf.} \quad (B-6)$$

The interchangeability of d and X as the penetration variable in these analytical expressions is permissible with the use of the conversion factor indicated in Equation B-6.

B. Single Annular Sector Case

The annular sector shown in Figure B-1 represents a fraction

$$R_1 = \frac{\theta_1 + 1 - \theta_1}{2\pi} \quad (B-7)$$

* D_0 is defined here as the detector response at an unprotected position in an infinite homogeneous air medium located three feet above a hypothetical infinite plane source. This source is considered to be of the same character as the radiation fallout uniformly distributed on the contamination plane(s) being investigated.

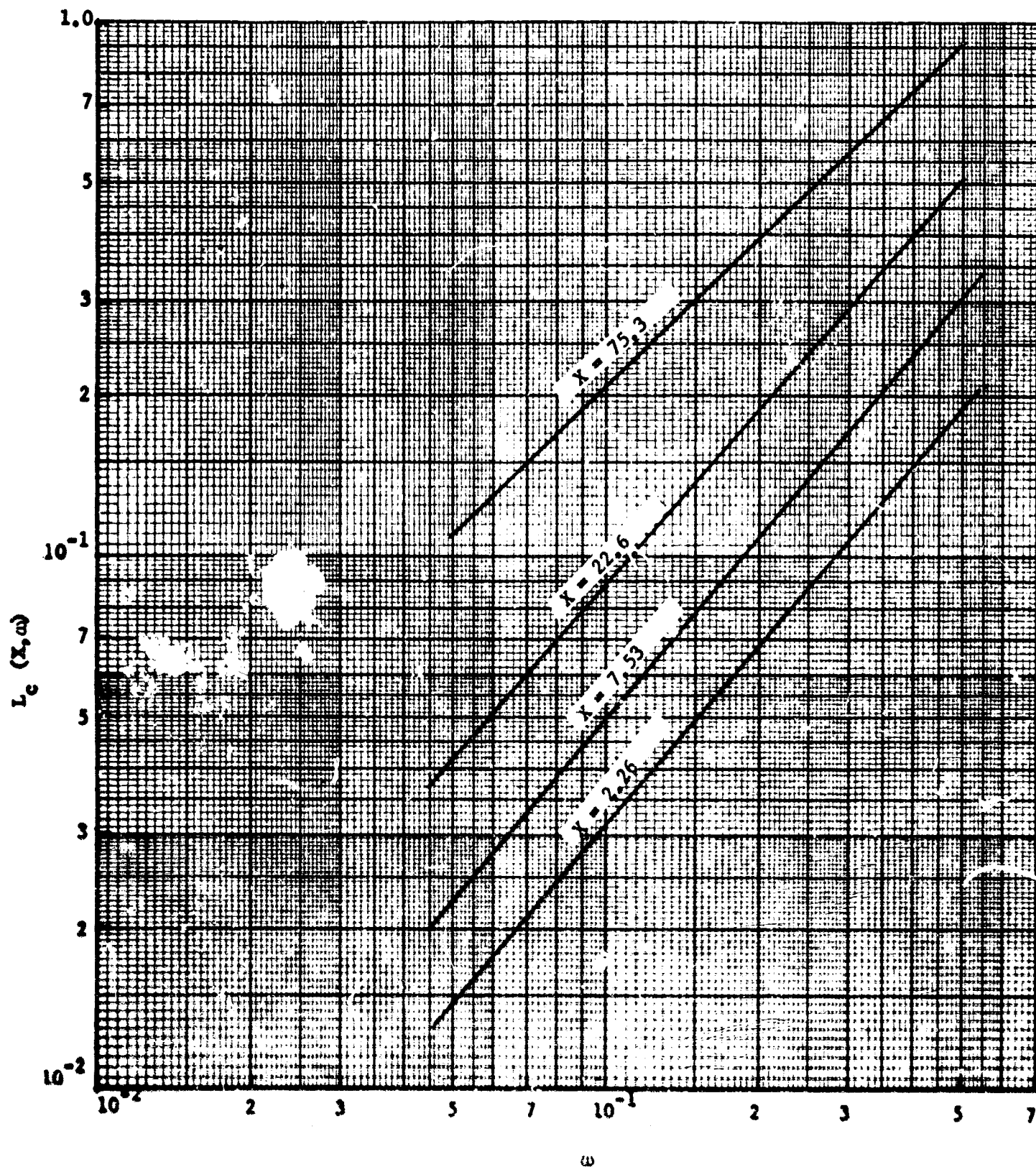


Figure B-2

Geometry Factor ($L_c(X, \omega)$) Depicting Detector Response
Due to a Circular Plane Gamma Radiation Source

of the total annulus. Consequently, the detector response due to the j^{th} annular sector in the k^{th} annulus is simply

$$\frac{D_{kj}}{D_o} = M_j L(X) \left[L_c(X, \omega_{(k+1)a}) - L_c(X, \omega_{ka}) \right] \quad (B-8)$$

C. Multiple Annular Sectors

For the case of N annular sectors comprising all the contaminated areas of the k^{th} annulus, the detector response is given as follows:

$$\frac{D_k}{D_o} = \frac{\sum_{j=1}^{j=N} D_{kj}}{D_o} = \sum_{j=1}^{j=N} M_j \left\{ L(X) \left[L_c(X, \omega_{(k+1)a}) - L_c(X, \omega_{ka}) \right] \right\} \quad (B-9)$$

where M_j (see Section II-B) represents that fraction of the annulus covered by the uniformly contaminated j^{th} annular sector.

III. MULTIPLE ANNULAR REGION MODEL

The following discussion outlines the expansion of the previously developed concepts for a single uniformly contaminated annulus to that of the more frequently encountered multiple annular region case.

The notation utilized in developing mathematical expressions for this model will relate to the physical description shown in Figure B-3. The use of the subscript, j , which refers to the (here) nonexistent annular sectors, is not required, but is retained for consistency in notation.

A. A Set of Uniformly Contaminated Annular Regions

1. Detector Response

First it is necessary to determine the detector response due to the k^{th} annular region. This quantity is given by the expression

$$\begin{aligned} \frac{D_k}{D_0} &= L(X) \left[L_c(z_k, \omega_{k+1}) - L_c(z_k, \omega_k) \right] \\ &= \left[L_c \left(\frac{d-h_{kj}}{a}, \frac{d-h_{kj}}{\sqrt{(k+1)^2 a^2 + (d-h_{kj})^2}} \right) \right. \\ &\quad \left. - L_c \left(\frac{d-h_{kj}}{ka}, \frac{d-h_{kj}}{\sqrt{(ka)^2 + (d-h_{kj})^2}} \right) \right] L(X) \end{aligned} \quad (B-10)$$

z_k is the height of the k^{th} annular region above the detector.

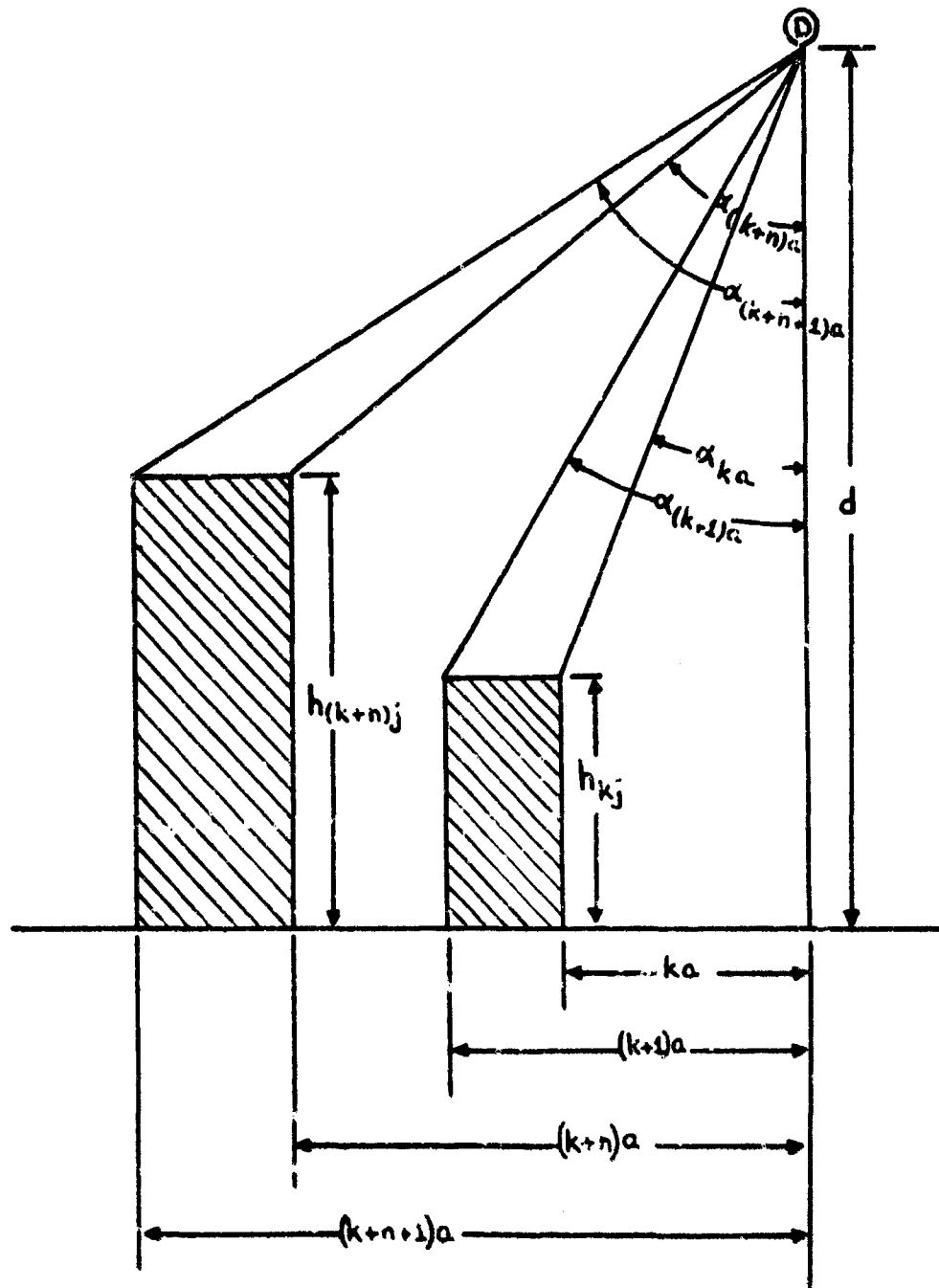


Figure B-3

Multiple Annular Regions Configuration Showing
Uniformly Contaminated Regions of Arbitrary Height

2. Contaminated Regions of Arbitrary Height

With the k^{th} annular region detector response defined, we next explore a condition which has considerable practical usage when attempting to determine detector response in urban areas where radioactive fallout can be considered uniformly distributed. It is desired to compute the detector response to N annular uniformly contaminated regions of arbitrary height.

The detector response from a set of such annular regions is given by

$$\frac{D}{D_0} = \frac{\sum_{k=1}^{k=N} D_k}{D_0} = \frac{1}{D_0} \sum_{k=1}^{k=N} \left[L_c \left(d-h_{kj}, \frac{d-h_{ki}}{\sqrt{(k+1)^2 a^2 + (d-h_{(k+1)j})^2}} \right) - L_c \left(d-h_{kj}, \frac{d-h_{ki}}{\sqrt{(ka)^2 + (d-h_{kj})^2}} \right) \right] L(X) \quad (B-11)$$

Here it is assumed that each annular region is not effectively "shadow" shielded by another. A more generalized analysis concerning mutual shielding and barrier attenuation will be given in Section IV.

As a means of illustrating the summing of the detector responses associated with equivalent and uniformly contaminated annular planes of different h_{kj} values, the following example is included.

From the information provided in Figure B-4, an expression for the total detector response can be written as follows:

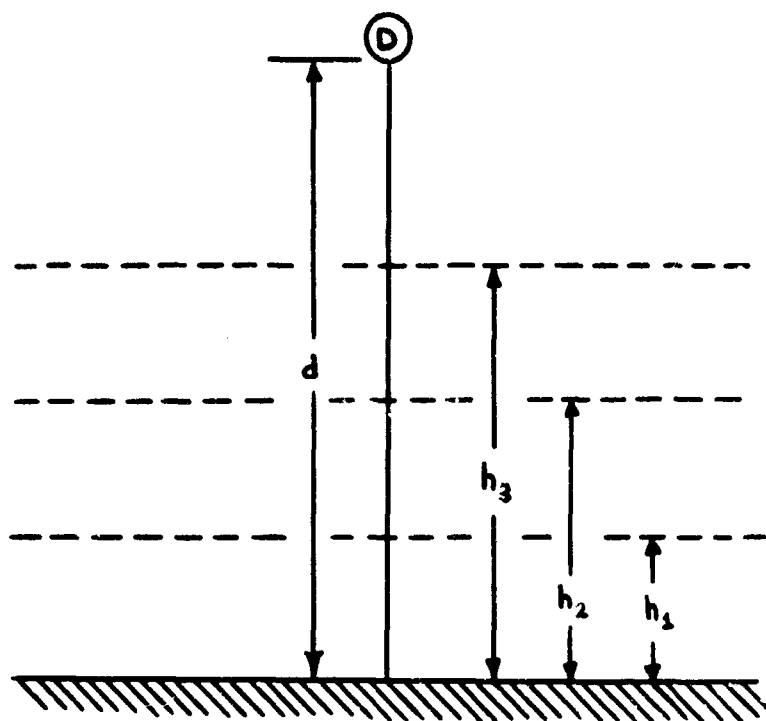


Figure B-4

Detector Response Due to Uniformly Contaminated
Planes with Different h_{jk} Values

$$\frac{D}{D_o} = \frac{\sum_{k=1}^{k=3} D_k}{D_o} = \frac{D_1 (d-h_1)}{D_{o_1} (h_1+3)} + \frac{D_2 (d-h_2)}{D_{o_2} (h_2+3)} + \frac{D_3 (d-h_3)}{D_{o_3} (h_3+3)} \quad (B-12)$$

where $D_{o_1} = D_{o_2} = D_{o_3} = D_o$.

B. Equivalent and Uniformly Contaminated Annular Sectors for a Set of Annular Regions.

The detector response which is attributed to the j^{th} annular sector of the k^{th} annular region may be defined by

$$\frac{D_{kj}}{D_o} = M_j L(X) \left[L_c \left(d-h_{kj}, \frac{d-h_{kj}}{\sqrt{(k+1)^2 a^2 + (d-h_{kj})^2}} \right) - L_c \left(d-h_{kj}, \frac{d-h_{kj}}{\sqrt{(ka)^2 + (d-h_{kj})^2}} \right) \right] \quad (B-13)$$

where M_j is again the fractional area of the k^{th} annular region covered by the contaminated j^{th} annular sector.

It is then apparent that the detector response $\frac{D_k}{D_o}$ of the k^{th} annulus is found by summing the $\frac{D_{kj}}{D_o}$ expressions as follows where we let P_k be the total number of sectors in the k^{th} annulus:

$$\frac{D_k}{D_o} = \sum_{j=1}^{j=P_k} \frac{D_{kj}}{D_o} = \sum_{j=1}^{j=P_k} M_j L(X) \left[L_c(d-h_{kj}, \omega_{(k+1)a}) - L_c(d-h_{kj}, \omega_{ka}) \right] \quad (B-14)$$

By knowing the detector response for the k^{th} annulus, it is now possible to express the detector response for any number of such annular regions by

$$D = D_0 \sum_k \frac{D_k}{D_0} = D_0 \sum_k \sum_{j=1}^{j=P_k} \frac{D_{kj}}{D_0} = D_0 \sum_k \sum_{j=1}^{j=P_k}$$

$$M_j L(X) \left[L_c(d-h_{kj}, \omega_{(k+1)a}) - L_c(d-d_{hk}, \omega_{ka}) \right] \quad (B-15)$$

IV. BARRIER ATTENUATION

One of the most common situations encountered in the analysis of contaminated regions located in core areas of large municipalities is the frequent occurrence of physical barriers between the detector and a contaminated plane of interest.

As an example of a rather simplified approach to the barrier problem, we will consider here the case of two annular sectors of separate annular regions. The heights of the respective annular sectors are assumed to be such that one is completely shielded by the other. This particular case is illustrated in Figures B-5 and B-6.

The gamma radiation dose at the detector from a shielded contaminated annular sector is essentially due to: (1) direct gamma radiation passing through the barrier; and (2) scattered gamma radiation transported by various interaction processes in air to the detector location. Here for simplicity the actual radiation dose from a shielded contaminated annular sector will be approximated by (see Figures B-6 and B-7)

$$\frac{D_{k1}}{D_0} = M_j L(X) \left[L_c(X, \omega_{(k+1)a}) - L_c(X, \omega_{ka}) \right] \quad , \quad (B-16)$$

where X is the effective distance through the barrier. This approximation will not be found to properly treat the scattered radiation contribution to the detector. The functions $L(X)$, $L_c(d, \omega)$, and $L_c(X, \omega)$ limit the detector response to a circular area of uniform gamma radiation intensity whose center is on the perpendicular from the detector to the plane and separated by either a thickness of air d or barrier thickness X (see Figure B-7). A numerical example of these considerations is given in Section VII.

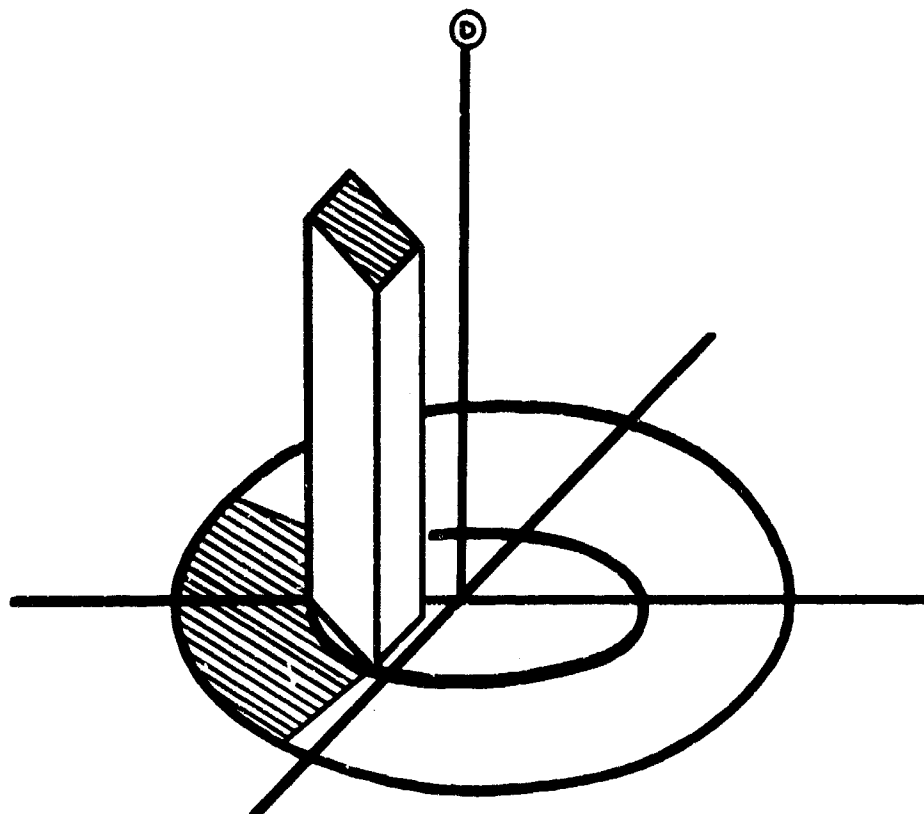


Figure B-5

Two Annular Sectors of Separate Annular Regions -
One Sector Shielded From the Detector

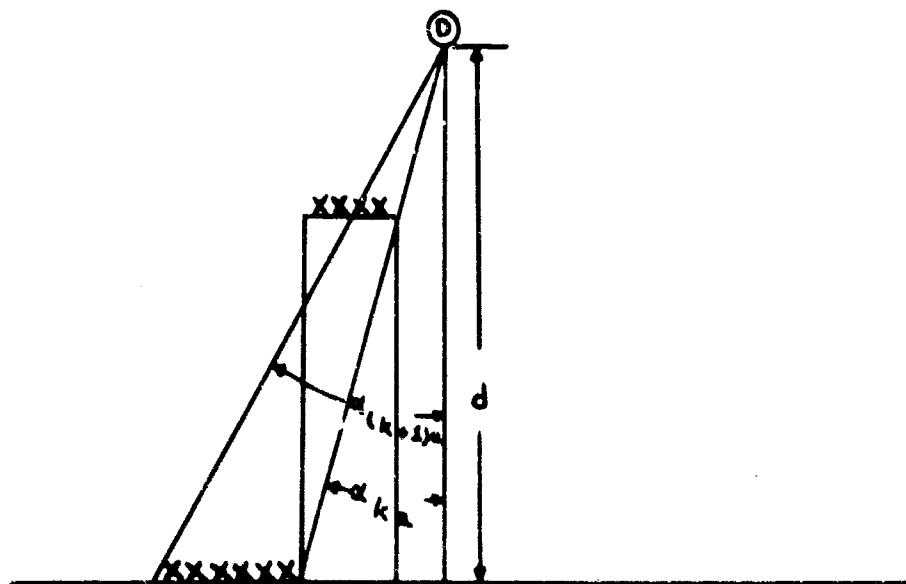


Figure B-6

Detector Response From a Shielded Sector

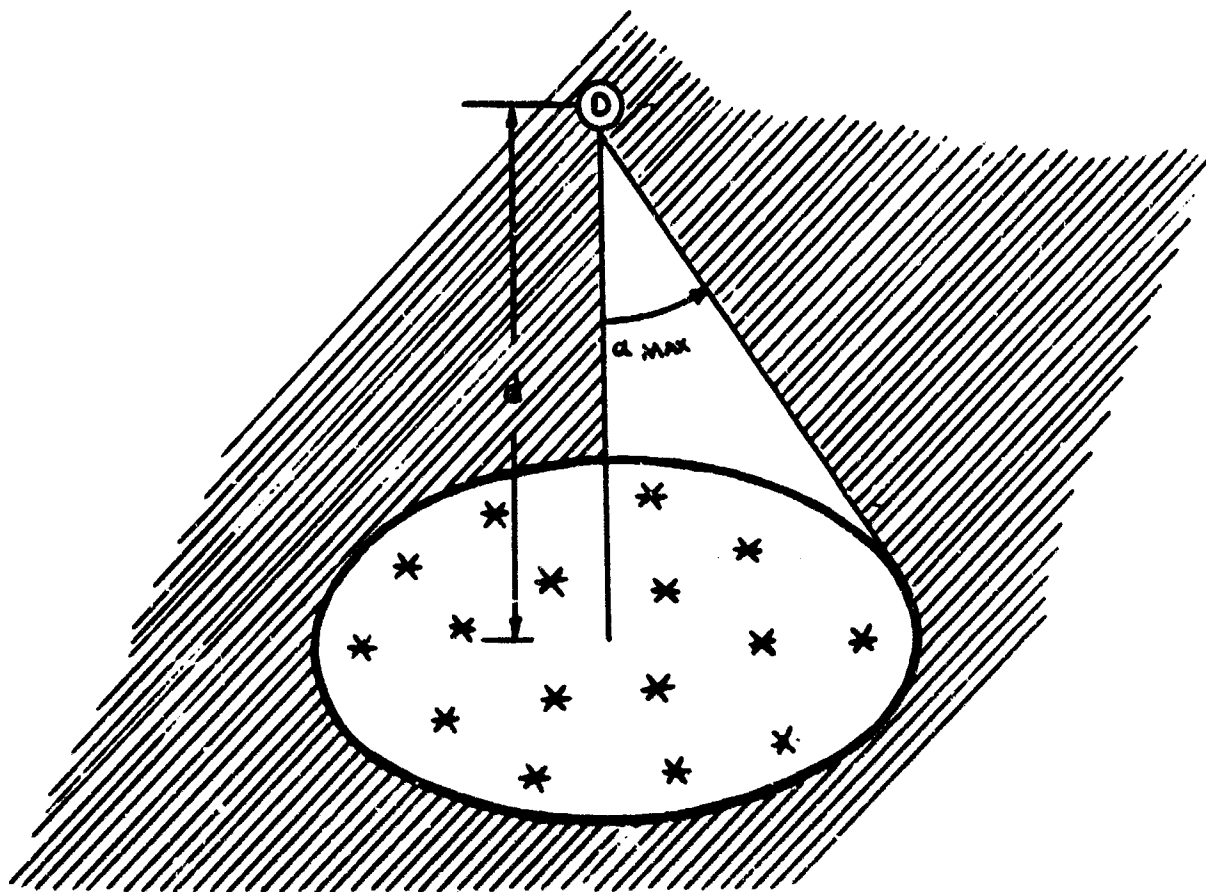


Figure B-7

Detector Geometry Associated With $L_c(X, \omega)$ and $L_c(D, \omega)$ Factors

V. DERIVATION OF SOLID ANGLE FRACTION EXPRESSION

The purpose of introducing the concept of solid angle in this memorandum is due primarily to the fact that the chosen direction for viewing the geometrical configurations associated with the circular model is not limited to that of a plane. As a result the more generalized notion of angle, i.e., solid angle, is utilized in a somewhat modified manner.

One of the most common means of envisioning a solid angle is to draw a cone from a point as the apex. Then the ratio of the area intercepted by that cone on any sphere centered at the apex to the square of the radius of the sphere is a measure of the solid angle Ω subtended by the cone. When measured in this manner the unit of solid angle is called the steradian. Since the total area of a spherical surface is $4\pi R^2$, the solid angle subtended by any surface which completely surrounds a point cannot exceed 4π steradians. It is then also apparent that the maximum solid angle subtended on one side of a plane surface is 2π steradians. On the basis of this premise, the unit of angular measurement ω adopted in this memorandum was chosen to be 2π steradians. This unit is consistent with that found in Reference B-1, where ω is designated as the "solid angle fraction" in an effort to avoid confusion in angular terminology.

By using the parameters indicated in Figure B-8, the derivation of the basic solid angle fraction expression found in Section II-A-1 of this appendix can be obtained.

With the geometry defined as illustrated above, an expression for the area intercepted on the spherical surface can be written as

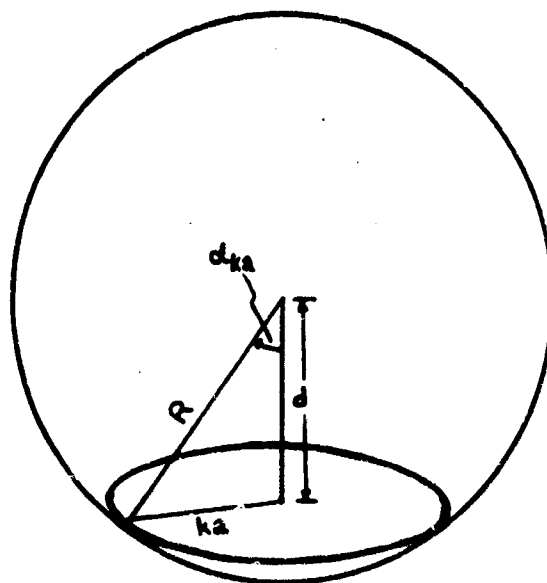


Figure B-8
Solid Angle Geometry

$$\begin{aligned}
 A &= \int_0^{\alpha_{ka}} 2\pi (R \sin \alpha) R d\alpha = -2\pi R^2 \cos \alpha \Big|_0^{\alpha_{ka}} \\
 &= 2\pi R^2 (1 - \cos \alpha_{ka}) \quad .
 \end{aligned}
 \tag{B-17}$$

From the basic definition of a solid angle, the following relationship is obtained.

$$\Omega_{ka} = \frac{A}{R^2} = 2\pi (1 - \cos \alpha_{ka}) \quad .
 \tag{B-18}$$

Since our unit of solid angle is 2π steradians, Equation B-18 must be rewritten in the following manner:

$$\frac{\Omega_{ka}}{2\pi} = 1 - \cos \alpha_{ka} = \omega_{ka} \quad ,
 \tag{B-19}$$

where ω_{ka} is the so-called "solid angle fraction."

VI. APPROXIMATE ANALYTICAL FIT FOR $L_c(X, \omega)$ FUNCTION

It was discovered during the course of developing the circular model that an analytical fit over a rather extensive range of values for the $L_c(X, \omega)$ curve found on page 41 of Reference B-1 is possible by employing an expression of the general form:

$$D/D_0 = L(X, \omega) = \omega^S e^{AX} \quad (B-20)$$

The parameter S is obtained from the previously referenced curves by applying the following familiar analytical relationship.

$$S = \frac{\ln L(X, \omega_2) - \ln L(X, \omega_1)}{\ln \omega_2 - \ln \omega_1} \quad (B-21)$$

The parameter A is then calculated by solving Equation B-20 for A as follows:

$$A = \frac{\ln L(X, \omega) - S \ln \omega}{X} \quad (B-22)$$

The best analytical fit for the $L_c(X, \omega)$ curve was achieved by obtaining the $L_c(X, \omega)$ values given on page 41 of Reference B-1 corresponding to ω_1 and ω_2 values of 0.05 and 0.2 respectively and solving for the intercept at $\omega = 0.2$ for each X value selected. The numerical results of these calculations are presented in Table B-1, and the resultant curve is available as Figure B-2 in this appendix.

It is apparent when comparing the $L(X, \omega)$ curves developed here with those appearing in Reference B-1 that the accuracy of the $L(X, \omega)$ values obtained from Equation B-20 deteriorate rapidly due to the lack of convergence as $\omega \rightarrow 0$. This is particularly true for those values of $\omega > 0.3$ and $\omega > 0.5$ associated with the $L_c(X,)$ function. It should also be noted that there are no restrictions associated with this model that would prohibit the exclusive use of exact values $L_c(X,)$ as

TABLE B-I

Calculated Values of S and A for Selected
Effective Mass Thickness Values

	$L_c (X, \omega)$	
X	S	A
2.26	1.115	-0.396
7.53	1.137	-0.0531
22.6	1.042	-0.002655
75.3	0.916	+0.00726

VII. EXAMPLE

In an effort to demonstrate the type of situations best handled by the circular model, and at the same time effectively summarize the analytical methods presented in this appendix, the following example is included.

The problem is that of determining the detector response (reduction factor) due to the contaminated annular sectors (A, B, C) in Figure B-9. For the purpose of illustration, an M_j value of 0.2 has been arbitrarily selected for each of the three planes of contamination to be investigated.

Contaminated Sector A:

First we define the solid angle fraction ω_k subtended by angle α_k by

$$\omega_k = 1 - \cos \alpha_k \quad , \quad (B-23)$$

where

$$\cos \alpha_k = \frac{d}{\sqrt{(k)^2 + (d)^2}} = \frac{100}{\sqrt{(50)^2 + (100)^2}} = 0.893 \quad . \quad (B-24)$$

Therefore, $\omega_k = 0.107$.

We can now convert the distance in air from the source plane into an effective mass thickness value by employing the conversion factor provided in Equation B-6 as follows:

$$X = \frac{100 \text{ Ft.}}{13.3 \text{ Ft. of air/psf}} \approx 7.53 \text{ psf} \quad . \quad (B-25)$$

The detector response for this case is given by the expression

$$D_A/D_0 = M_j L(X) \left[L_c(X, \omega_k) \right] \quad . \quad (B-26)$$

$d = 100 \text{ Ft.}$
 $h_k = 70 \text{ Ft.}$
 $k = 50 \text{ Ft.}$
 $k_2 = 60 \text{ Ft.}$
 $k_2 = 80 \text{ Ft.}$

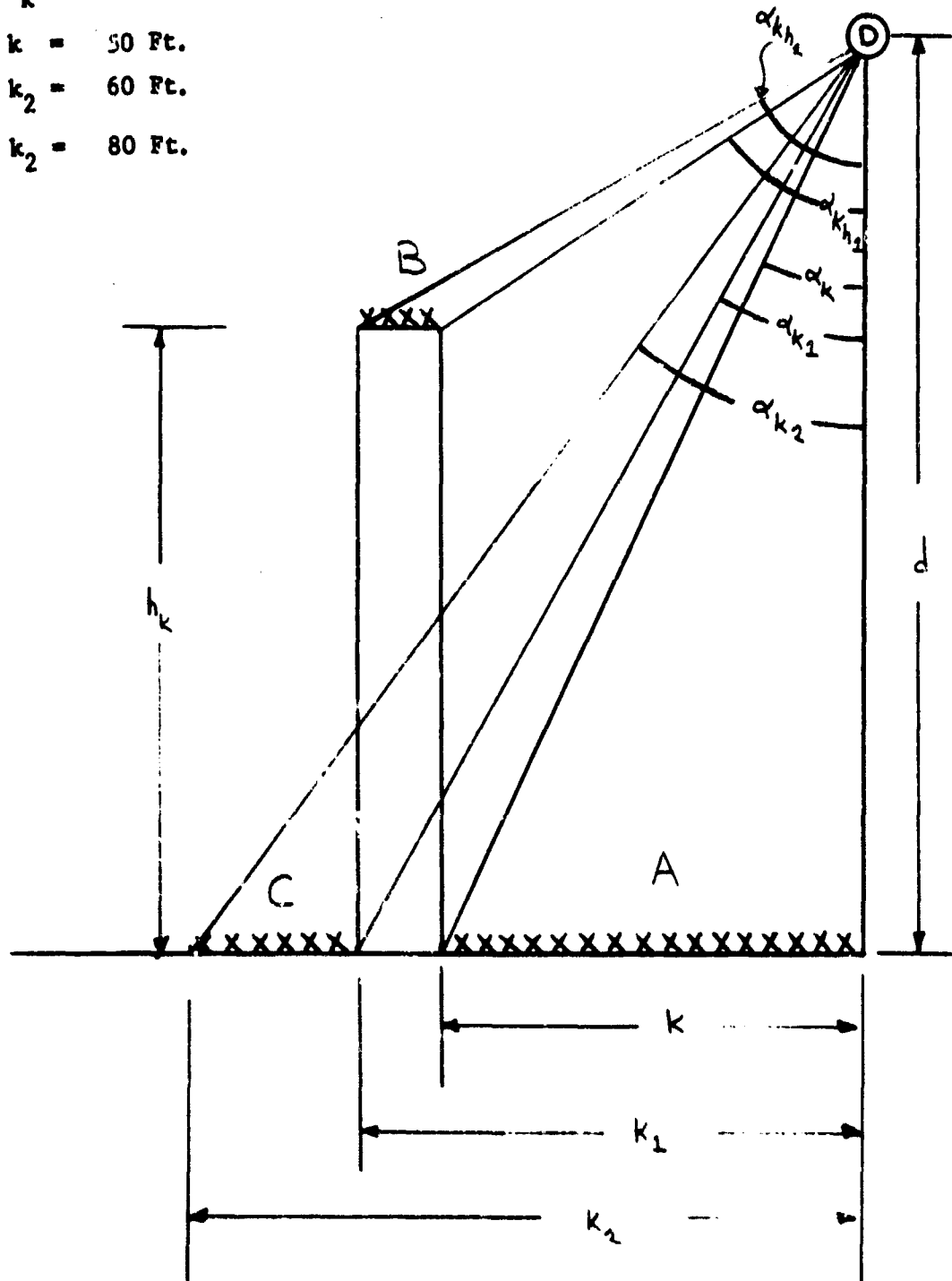


Figure B-9

Example Illustration

By substituting the values of M_j , X , and ω_k into the previous expression we obtain

$$D_A/D_O = 0.2 L (7.53) \left[L_c (7.53, 0.107) \right] \quad (E-27)$$

Obtaining the $L_c (X, \omega)$ value from Figure B-2, the detector response is found to be

$$D_A/D_O = 0.2 (0.375) (0.054) = 0.00405 \quad (B-28)$$

Contaminated Sector B:

The expression for the detector response from the j^{th} annular sector of the k^{th} contaminated annulus is derived in Section III and appears below in only a slightly modified form.

$$D_B/D_O = M_j L (X) \left[L_c \left(d-h_k, 1 - \frac{d-h_k}{\sqrt{(k_1)^2 + (d-h_k)^2}} \right) - L_c \left(d-h_k, 1 - \frac{d-h_k}{\sqrt{(k)^2 + (d-h_k)^2}} \right) \right] \quad (B-29)$$

In this case the effective mass thickness for air is

$$X = \frac{d-h_k}{13.3 \text{ Ft. of air psf}} \approx 2.26 \text{ psf} \quad (B-30)$$

With the X value and the information provided in Figure B-9, we can proceed to find the detector response in the following manner:

$$\begin{aligned}
D_B/D_O &= 0.2 L(2.26) \left[L_c \left(2.26, 1 - \frac{30}{\sqrt{(60)^2 + (30)^2}} \right) \right. \\
&\quad \left. - L_c \left(2.26, 1 - \frac{30}{\sqrt{(50)^2 + (30)^2}} \right) \right] \\
&= 0.2 L(2.26) \left[L_c(2.26, 0.554) - L_c(2.26, 0.487) \right] \quad (B-31)
\end{aligned}$$

Here the $L(X)$ and $L_c(X, \omega)$ values are obtained from page 33 and page 41 respectively of Reference B-1, since the ω values in this case approach the limits of accuracy for the approximation method described in Chapter VI. Finally,

$$D_B/D_O = 0.2 (0.57) (0.045) = 0.00513 \quad (B-32)$$

Contaminated Sector C:

In finding the detector response for Sector C, a barrier is encountered between the detector and the contaminated plane being investigated. From the discussion given in Section IV, we can express the detector response for this barrier case as follows:

$$D_C/D_O = M_j L(X) \left[L_c(X, \omega_{k2}) - L_c(X, \omega_{k1}) \right] \quad (B-33)$$

The values for ω_{k1} and ω_{k2} are found by

$$\omega_{k1} = 1 - \cos \alpha_{k1} = 1 - \frac{100}{\sqrt{(60)^2 + (100)^2}} = 0.142, \quad (B-34)$$

and

$$\omega_{k2} = 1 - \cos \alpha_{k2} = 1 - \frac{100}{\sqrt{(80)^2 + (100)^2}} = 0.220 \quad (B-35)$$

The X value chosen for the barrier is 75.3, which is equivalent to 0.523 feet of concrete. By substitution of these values into the D_c/D_o expression, we obtain

$$D_c/D_o = 0.2 L(75.3) \left[L_c(75.3, 0.22) - L_c(75.3, 0.142) \right] \quad (B-36)$$

By using the values for $L_c(X, \omega)$ in Figure B-2, the detector response for Plane C is:

$$D_c/D_o = (0.2) (0.038) \left[0.453 - 0.285 \right] = 0.00128 \quad (B-37)$$

Despite certain limitations inherent in the circular model presented here, the methods described can produce simple and practical approximate solutions to many types of problems requiring knowledge of gamma ray intensity, due to weapon-induced fallout, at a single detector location.

VIII. SUMMARY AND CONCLUSIONS

From the information provided in the previous sections, it is apparent that the circular model is somewhat restricted in application. The principal limitation is that circular or annular planes of contamination are a poor approximation to most real situations. However, it may be possible in many cases to reduce non-circular geometries of interest to circular regions of equal area. Of course, such an innovation must be approached with caution since for certain configurations the error introduced in the detector response due to radical changes in the original geometry may be quite significant. (Of course, the "Engineering Manual" azimuthal sector approach makes these approximations.) It is noted, however, that this appendix represents but one of a series of different approaches to the overall problem of quick and efficient approximations to the gamma ray intensities due to fallout radiation. Other approaches will not have the particular limitations noted here.

REFERENCES

- B-1. L. V. Spencer. Structure Shielding Against Fallout Radiation From Nuclear Weapons. NBS Monograph 42. Washington, D. C.: National Bureau of Standards. 1 June 1962.

Appendix C

A Square-Grid Model for Approximating Gamma Ray Intensity at a Single Detector Location

Note: The material in this Appendix was originally submitted to USNRDL as Research Memorandum RM-OU-214-4*.

* W. R. Davis, M. K. Moss, J. T. Ryan, and T. Johnson. A Square-Grid Model for Approximating Gamma Ray Intensity at a Given Detector Location. RM-OU-214-4. Durham, North Carolina: Research Triangle Institute, Operations Research and Economics Division, 30 April 1965.

TABLE OF CONTENTS

	<u>Page</u>
LIST OF TABLES	C-ii
LIST OF FIGURES.	C-ii
GLOSSARY OF SYMBOLS.	C-iii
I. INTRODUCTION	C-1
A. Purpose	C-1
B. Some Analysis Considerations.	C-1
C. The Model	C-2
D. Contents.	C-5
II. EXPLICIT FORMULATION OF THE SQUARE-GRID MODEL.	C-7
A. Approach.	C-7
B. Formulation of the Model.	C-9
III. APPROXIMATE ANALYTICAL FIT FOR $L_a(X,\omega)$ and $L_c(X,\omega)$ FUNCTIONS . .	C-29
IV. AN EXAMPLE	C-33
V. SUMMARY AND CONCLUSIONS.	C-37
REFERENCES	C-39

LIST OF TABLES

<u>Table</u>		<u>Page</u>
C-I	Solid Angles and Solid Angle Fractions for the 50 Foot Squares, ($z = 100$ Feet).	C-17
C-II	Solid Angles Subtended at the Detector (0,0,100') by the Square Annular Regions Centered at the Origin.	C-18
C-III	Reduction Factors at Detector (0,0,100') for Square Annular Regions Centered at the Origin-No Barriers, i.e., $X = 7.6$	C-18
C-IV	$L(X)\Delta L_{ac}$ as a Function of Barrier Thickness X	C-24
C-V	Reduction Factors for the 50 Foot Squares as a Function of Barrier Thickness X	C-24
C-VI	Calculated Values of s and A for Selected Effective Mass Thickness Values	C-32

LIST OF FIGURES

<u>Figure</u>		<u>Page</u>
C-1	Concentric Squares Configurations.	C-8
C-2	Square-Grid Labeling Scheme.	C-11
C-3	Square-Grid in n^{th} Square Annulus.	C-13
C-4	Solid Angle Fraction of 50 Foot Squares as a Function of Horizontal Distance from Detector.	C-16
C-5	Variation of $L(X)\Delta L_{ac}$ vs. X for Ring 1 = 3.	C-25
C-6	Reduction Factor D/D_0 for the Individual Square Grid Areas as a Function of the Barrier Thickness X for Ring 1 = 3	C-26
C-7	Geometry Factor ($L(X,\omega)$) Depicting Detector Response Due to a Circular Plane Gamma Radiation Source.	C-30
C-8	Geometry Factor ($L(X,\omega)$) For Detector Response to Gamma Radiation Received by a Detector from a Limited Cone of Directions	C-31
C-9	Idealized Scaled Map (to be used in conjunction with overlay - See Figure 3 and Table I).	C-34

GLOSSARY OF SYMBOLS

1. a Width of unit annulus.
2. A Intercept value of approximate $L(X, \omega)$ functions.
3. D/D_0 Dose reduction factor (D_n/D_0 is the dose reduction factor for the n^{th} annular region).
4. ϵ_i The horizontal eccentricity ratio $|y_i/x_i|$.
5. η_i The vertical eccentricity ratio $|z/x_i|$.
6. h_{ij} Height of j^{th} square in i^{th} annulus above the base reference plane.
7. $L(X)$ Total detector response for infinite plane isotropic source.
8. $L(X, \omega)$ Geometry factor.
9. $L_a(X, \omega)$ The reduction in response which occurs if an isotropic detector is replaced by a detector responding only to gamma rays incident within a particular cone of directions.
10. $L_c(X, \omega)$ The ratio of the detector response due to a concentric circular area to the response due to fallout on an entire (infinite) plane area.
11. q_i ($i = 1, 2, 3, 4$) quadrant factor =

$$\begin{cases} +1 & \text{if corner } i \text{ is in quadrant 1 or 3} \\ -1 & \text{if corner } i \text{ is in quadrant 2 or 4.} \end{cases}$$
12. s Slope of approximate $L(X, \omega)$ functions.
13. $r(\epsilon_i, \eta)$ Partial solid angle fraction.
14. X Mass thickness of barrier (or attenuation distance).
15. z Perpendicular distance from detector to plane containing the plane of contamination under analysis.
16. ω or ω Solid angle fractions.
17. $\Delta\omega$ Solid angle fraction subtended by square annular region.
18. x_i, y_i ($i=1,2,3,4$) The coordinates of the four corners of the square.
19. x_{ij}, y_{ij} The coordinates of the center of the j^{th} square in the i^{th} annulus.

A Square-Grid Model for Approximating Gamma
Ray Intensity at a Single Detector Location

I. INTRODUCTION

A. Purpose

This appendix describes the development of a simple and practical procedure for estimating fallout gamma ray intensity at a detector as a function of the geometry of the contributing planes of contamination and related shielding. The need for such a procedure arises from requirements for analyses of large municipal areas with many contaminated planes and detector locations scattered throughout the area. Conceptually, the "circular-model" procedure described in Appendix B is simple to use, but accuracy suffers when the contaminated planes and barriers do not have approximately polar symmetry about the detector location. A square-grid model can accurately approximate real situations more easily since most planes of contamination (and most buildings) are rectangular. Further, the square-grid model can be applied easily to an arbitrary detector location with the use of scaled map overlays.

B. Some Analysis Considerations

A problem encountered during the development of the square-grid model was the increased difficulty in computing the solid angles subtended at the detector by the square areas. Adjunct to this problem is the subsequent determination of the radiation at a given detector location using Spencer's L-functions (Reference C-1). A simple sector-type weighting as was used in the circular model is not possible with the square-grid model.

The solid angles subtended at a given detector location by a square area can be computed rigorously. For example, the solid angle ω subtended by any square

can be computed (Reference C-1) by the equation

$$\omega = \frac{1}{2} [q_1 \tau(\epsilon_1, \eta_1) - q_2 \tau(\epsilon_2, \eta_2) + q_3 \tau(\epsilon_3, \eta_3) - q_4 \tau(\epsilon_4, \eta_4)] \quad (C-1)$$

where:

$$q_i = \begin{cases} +1 & \text{if corner } i \text{ is in quadrant 1 or 3} \\ -1 & \text{if corner } i \text{ is in quadrant 2 or 4} \end{cases},$$

$$(x_i, y_i) = \text{coordinates of corner } i,$$

$$\epsilon_i = |y_i| / |x_i|,$$

$$\eta_i = |z| / |x_i|,$$

$$z = \text{perpendicular distance from the detector to the plane containing the plane of contamination under analysis, and directly above the origin, and}$$

$$\tau(\epsilon_i, \eta_i) = \text{solid angle of a rectangle with height } z \text{ and corners at } (x_i, y_i), (-x_i, y_i), (-x_i, -y_i), (x_i, -y_i).$$

A full discussion of Equation C-1 and the variables involved is given in Reference C-1. Unfortunately, when computing the solid angles for the situations considered in this appendix, it was found that the $\tau(\epsilon, \eta)$ curves of Reference C-1 were not sufficient for computing the solid angle ω . This is because differences must be taken between numbers of approximately the same magnitude. The $\tau(\epsilon, \eta)$ functions thus were computed from the analytic expression

$$\tau(\epsilon, \eta) = \frac{2}{\pi} \tan^{-1} \left(\frac{\epsilon}{\eta \sqrt{\epsilon^2 + \eta^2 + 1}} \right) \quad (C-2)$$

C. The Model

The general program which was followed for the development of a model for approximating fallout gamma ray intensities at a detector is now described. The

model is primarily aimed at the approximate estimation, in the field, of decontamination effectiveness. High speed computer programs are not practical in these circumstances. Of course, building and area characteristics must be known approximately. A general discussion of the model and the information required for its application is presented next.

1. General Method

The over-all approach to the square-grid model for studying the effects of decontamination of fallout radiation is based on the following criteria:

- (a) The techniques must enable local civil defense personnel in the field to calculate the effects of large-scale decontamination of municipal areas;
- (b) The approximate techniques and procedures must not require computers; i.e., graphical and tabular forms should be applicable.

As noted in Section II, the square-grid model is used to estimate the reduction factor D/D_0 for the various planes of fallout contamination - each at differing heights. The planes of contamination are divided into square-grid areas, and the detector may in principle be located at any arbitrary position, at height z . The size of the square-grid sections was chosen as 50 feet, an area which is large enough that subsequent computations are not unwieldy, but which is also sufficiently small to yield an acceptable approximation of major contaminated planes in almost any area. Consequently, any plane of contamination in this model is approximated by 50 foot square grids. An isotropic detector is assumed to be located at a height z above the center square grid. It is at this point detector that the reduction factor D/D_0 of any given contaminated plane area is computed.

Since there will in general be several planes of contamination at

varying heights, contributing to the fallout gamma radiation at a given detector location, the analysis will functionally depend to a large extent on the variable z , the detector height. By varying the detector height above the ground plane, one can generate functions which can be used for the analysis of the contributions of planes of contamination at various heights.

In this model, the z dependence of the detector response is treated separately from the other functional dependences. This is accomplished by separately considering the detector response from planes of contamination at each vertical height. The responses due to planes of contamination at all heights are then superimposed to obtain the total detector response or reduction factor D/D_0 at a given point.

The model will thus work as follows: A given plane of contamination at a particular height is approximated by 50 foot square grid areas. The detector is always vertically centered on the center of the center square in the square-grid network. The squares are numbered as discussed in Section II. When the detector response due to a given square is desired, the solid angle subtended by the square at the detector and the effective distance from the square area to the detector must be computed.

Once the solid angles are determined, the detector response due to this particular square may be determined by use of appropriate curves. Every square-grid area for the given plane of contamination may be so treated and the solid angles, weighting functions, and detector responses (reduction factors) of each of these squares may be tabulated. This procedure may be then applied to all other planes at another height, and so on. For the square-grid overlay, one then has a tabulation of the unique (in the absence of barriers) detector response for each individual square-grid area.*

*If barriers are present, one refers to specially constructed tables and curves that will be discussed in paragraph 3, Section II.

When the square-grid overlay is appropriately scaled to detailed municipal maps (for example, Sanborn Maps), then the properly scaled overlays may be placed over the maps and the contribution to the detector due to given areas of contamination may be quickly assessed. This is accomplished by noting the square-grid numbers of the areas covering the contaminated areas of interest, determining the reduction factors D_1/D_0 for each of the individual square areas from the tabulated values, and summing the resultant individual contributions.

D. Contents

Section II of this appendix presents the explicit formulation of the square-grid model including the necessary background material and mathematical expressions used. Section IV illustrates the use of the model with a concrete example. An overlay grid is constructed and applied to a hypothetical municipal area.

II. EXPLICIT FORMULATION OF THE SQUARE-GRID MODEL

A. Approach

The notation used throughout this research memorandum is similar to that used in Reference C-1. The planes of contamination are divided into 50-foot square sections (determined by a grid overlay) with the detector centered vertically over any desired grid (chosen in each instance to be the origin of a rectangular coordinate system).

The detector response due to the individual square lattice grids is then computed using the $L(X,\omega)$ functions,* provided the effective attenuation distance X and the solid angle ω are known. It should be noted here, however, that the determination of the detector responses requires special precautions since the $L(X,\omega)$ curves of Spencer are all computed for a contaminated plane which is symmetric about the detector location. This is not the case with square-grids in the square lattice model. Consider the situation depicted in Figure C-1. If one desires to know the contribution due to the square-grid in the upper right hand side of the Figure, it is first necessary to compute the $L(X,\omega)$ function for the solid angle subtended by the entire square annular region enclosed by the broken lines in Figure C-1. Then an appropriate weighting must be applied to estimate the detector response from the individual square-grid. This weighting is not as simple to compute as in the case of the circular model where a simple proportion was sufficient. The weighting scheme devised for the square-grid model is

*It was found that these functions could be approximated over their range of greatest utility by simple analytical expressions (Section III). Such expressions can be evaluated with the aid of a desk calculator and standard mathematical tables.

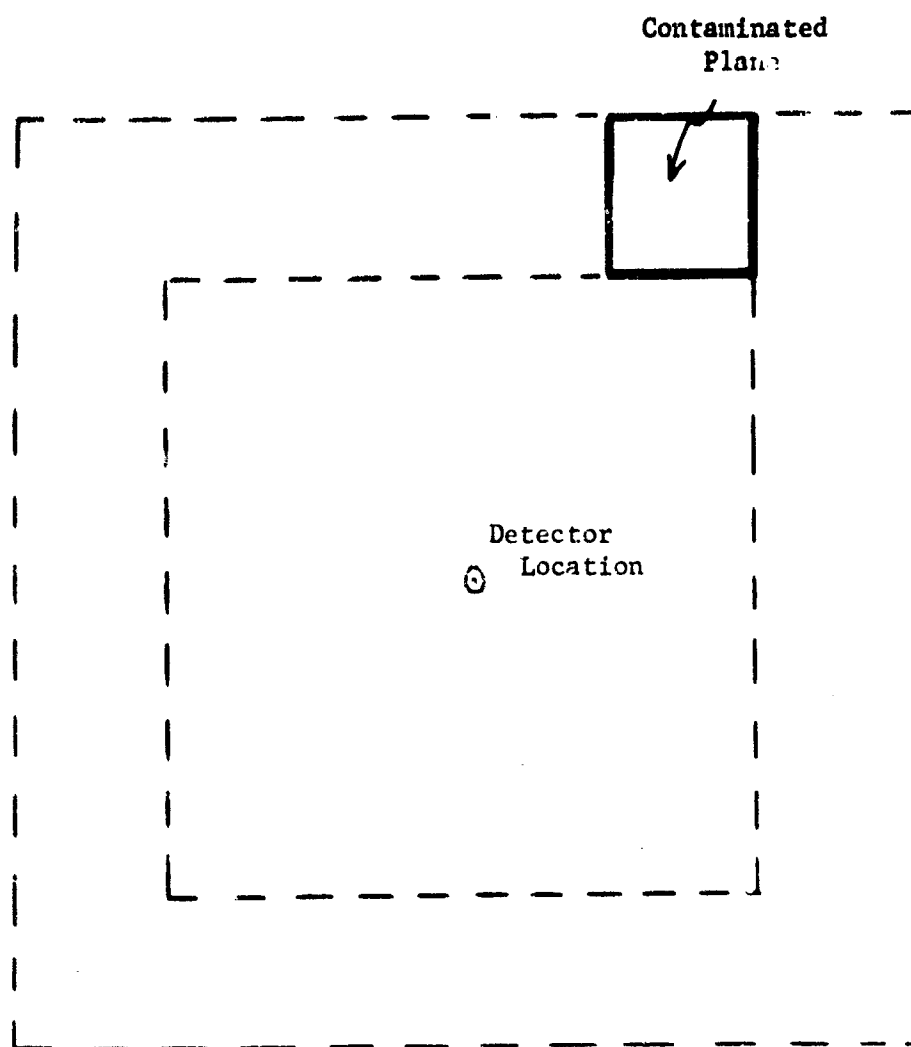


Figure C-1
Concentric Squares Configurations

discussed in Section VI-B.

B. Formulation of the Model

1. Assumptions

The basic assumptions underlying the square-grid model are:

- (a) Each 50 foot square is contaminated uniformly;
- (b) The gamma radiation dose received by the detector from a shielded contaminated square-grid is due to both direct gamma radiation passing through the barrier and air-scattered gamma radiation;
- (c) The detector response from disjoint sources is equal to the sum of the contributions from the individual sources; and
- (d) It is verified that the orientation of a square-grid with respect to the detector location need not be considered. The distance from the center of an individual 50 foot square to the detector and the distance between lattice points provide the geometric characteristics required in the computation of detector response. This property is of considerable practical importance to the construction of simple graphs and tables for determining the solid angle subtended at the detector by any lattice square as a function of distance.

2. Geometry

The square lattice or square-grid model is constructed in a manner similar to the circular model of Appendix B. The two basic differences between the circular model and the square-grid model lie in:

- (a) The procedures for computing the solid angles; and
- (b) The techniques for treating the position-dependent parameters

used to compute the individual contributions of square-grids. The lattice uses a unit-square annulus (Figure C-1); azimuthal sector contributions are used in the circular model.

Consider the labeling scheme for the unit squares of the lattice indicated in Figure C-2. In this Figure, the first number of a pair (i) in a unit square identifies the unit-square annulus. The second number (j) specifies the position of the unit square in the square annulus by indexing counter clockwise. In addition, there is a third number associated with each unit square, h_{ij} , which specifies the height of a unit square above the base reference plane.

If we let a be the width of a unit annulus, then the solid angle fractions subtended by the n^{th} square annular region is given by

$$\Delta \omega = \tau(x_n, y_n, z-h_n) - \tau(x_{n-1}, y_{n-1}, z-h_n) \quad (C-3)$$

The solid angle fraction subtended by a unit square is given by

$$\begin{aligned} \omega_{ij} = & \frac{1}{4} [q_1 \tau(x_{ij} + \frac{a}{2}, y_{ij} + \frac{a}{2}, z - h_{ij}) \\ & - q_2 \tau(x_{ij} - \frac{a}{2}, y_{ij} + \frac{a}{2}, z - h_{ij}) \\ & + q_3 \tau(x_{ij} - \frac{a}{2}, y_{ij} - \frac{a}{2}, z - h_{ij}) \\ & - q_4 \tau(x_{ij} + \frac{a}{2}, y_{ij} - \frac{a}{2}, z - h_{ij})] \end{aligned} \quad (C-4)$$

where

$$\tau(x, y, z - h) = \frac{2}{\pi} \tan^{-1} \left(\frac{|x| |y|}{(z - h) \sqrt{x^2 + y^2 + (z - h)^2}} \right) \quad (C-5)$$

$$q_i = \frac{x_i}{y_i} \left| \frac{y_i}{x_i} \right| \quad (C-6)$$

	3,10	3,9	3,8	3,7	3,6	3,5	3,4
	3,11	2,7	2,6	2,5	2,4	2,3	3,3
	3,12	2,8	1,4	1,3	1,2	2,2	3,2
	3,13	2,9	1,5	0,0	1,1	2,1	3,1
	3,14	2,10	1,6	1,7	1,8	2,16	3,24
	3,15	2,11	2,12	2,13	2,14	2,15	3,23
	3,16	3,17	3,18	3,19	3,20	3,21	3,22

Figure C-2
Square-Grid Labeling Scheme

and the coordinates $(X_{ij}, \text{ and } y_{ij})$ are the coordinates of the center of the i, j square.

The above equations are essentially those presented in Spencer's Monograph 42 (Reference C-1) on pages 68 and 69.

Differences in the $L_c(X, \omega)$ functions tabulated in Spencer's Monograph are appropriate to give the reduction factor $(\frac{D}{D_0})$ for the square annular regions described above. Of course, the proper solid angles must be substituted in their arguments.

In this section, barrier shielding of contributing source squares is not treated. This is treated separately in the next section of this report. Barriers require the use of the $L_a(X, \omega)$ function in addition to the $L_c(X, \omega)$ function. These functions may be approximated by simple functions of the form

$$L = A\omega^m \exp(BX) \quad , \quad (C-7)$$

where A is the intercept value and B is the slope of the curve (See Section III).

In order to show specifically the scheme for computing the detector response, Figure C-3 is used.

In terms of this notation and the discussion of this section, it follows that the $\frac{D}{D_0}$ of this typical square uniform annulus region is given by

$$\frac{D}{D_0} = \left[L_c(X_n, \omega_n) - L_c(X_{n-1}, \omega_{n-1}) \right] L(X) \quad . \quad (C-8)$$

Since there are $8n$ unit squares in the n^{th} square annulus ($n \geq 1$), the contribution of a typical unit square of the square annular region may be

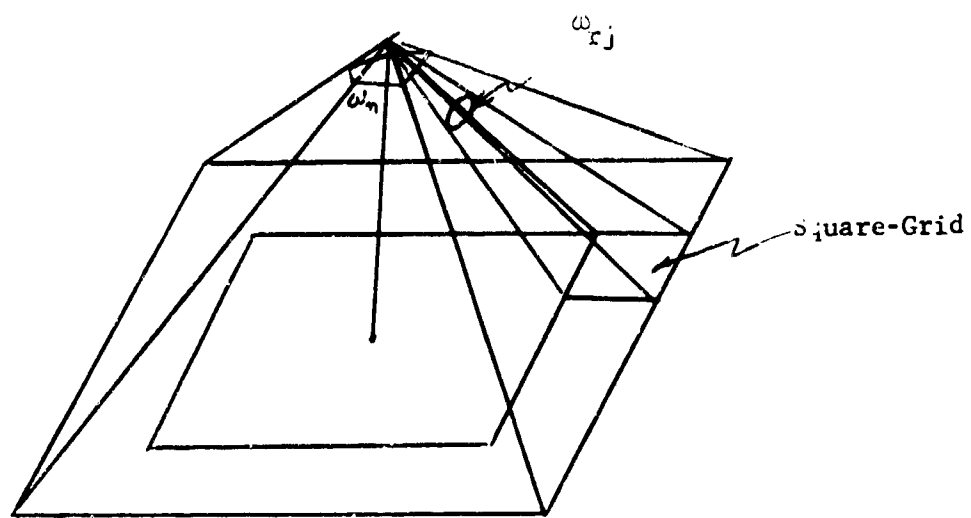


Figure C-3
Square-Grid in n^{th} Square Annulus

written in the form

$$\frac{D_{ni}}{D_o} = \frac{\omega_{ni}}{8n\omega_n} \left[L_c(X_{n,j,\omega_n}) - L_c(X_{n-1,j,\omega_{n-1}}) \right] L(X) \quad (C-9)$$

where

$$\frac{\omega_{ni}}{\omega_n} = \frac{\sum_i \omega_{ni}}{8n} = \frac{\Delta\omega_n}{8n} \quad (C-10)$$

The factor $\omega_{nj}/\sum_i \omega_{ni} = \frac{\omega_{ni}}{8n\omega_n}$ and $\omega_n = \Delta\omega_n - \omega_{n-1}$ is the weighting which corrects for the effective position of the different unit squares of a given square annular region.

It is easily seen that the contribution from each square of a given square annulus n is weighted according to the solid angle fraction it subtends. The total geometry reduction factor for the whole plane is thus given by

$$\frac{D}{D_o} = \sum_n \sum_j \frac{\omega_{ni}}{8n\omega_n} \left[L_c(X_{n,j,\omega_n}) - L_c(X_{n-1,j,\omega_{n-1}}) \right] L(X) \quad (C-11)$$

or

$$\frac{D}{D_o} = \sum_n \sum_j \frac{\omega_{ni}}{\Delta\omega_n} \left[L_c(X_{n,j,\omega_n}) - L_c(X_{n-1,j,\omega_{n-1}}) \right] L(X) \quad (C-12)$$

In order to illustrate the manner in which the square-grid model is applied, an overlay was constructed of 50 foot square-grid areas (See Figure C-2). In order to use the overlay for decontamination analysis, the reduction factor, D/D_o , for each of the 50 foot squares is required. The overlay scaled to appropriate local maps could then be quickly and effectively utilized in accessing the effects of large scale decontamination in a particular area of interest. In order to obtain the D/D_o values, the solid angle of each

individual 50 foot square must first be determined. An appropriate weight is then obtained by computing the total solid angle of the annular region in which a particular 50 foot square is located; the solid angle fraction of the individual squares may then be determined.

The individual calculations of the solid angles are quite lengthy. In keeping with the spirit of the model, an approximate but highly accurate procedure for computing the solid angles as a function of horizontal distance is derived for various detector heights. Computations of the solid angles of the 50 foot square-grids were made for appropriately spaced on-axis center distances. (The on-axis case has desirable symmetry properties which simplify the calculations.) To illustrate this construction, a detector height of 100 feet was used ($z = 100$ feet). Calculations of the solid angles subtended at the detector by the 50 foot squares were made for each of the successive on-axis square-grids. Calculations for several off-axis lattice squares were performed (e.g., $x = y = 150$ feet). It was found that the solid angles of the 50 foot squares depended (to a high degree of accuracy) only on the absolute distance of the square lattice from the detector. With z given, the dependence is a function of horizontal distance. Consequently, the curve of Figure C-4 was drawn showing the approximate solid angle of any square lattice for three detector heights. The solid angles read from Figure C-4 are given in Table C-I for $z = 100$ feet. The solid angle fractions $\omega/\Delta\omega$, used for weighting the $L(X, \omega)$ functions are also given. These solid angle fractions are computed by use of other calculations summarized in Table C-II. The reduction factors D/D_0 (no barriers) for a particular square annular region, n , at a horizontal distance (X) from the plane of contamination is then given by

$$\frac{D}{D_0} = L(X) \left[L_c(X, \omega_n) - L_c(X, \omega_{n-1}) \right]$$

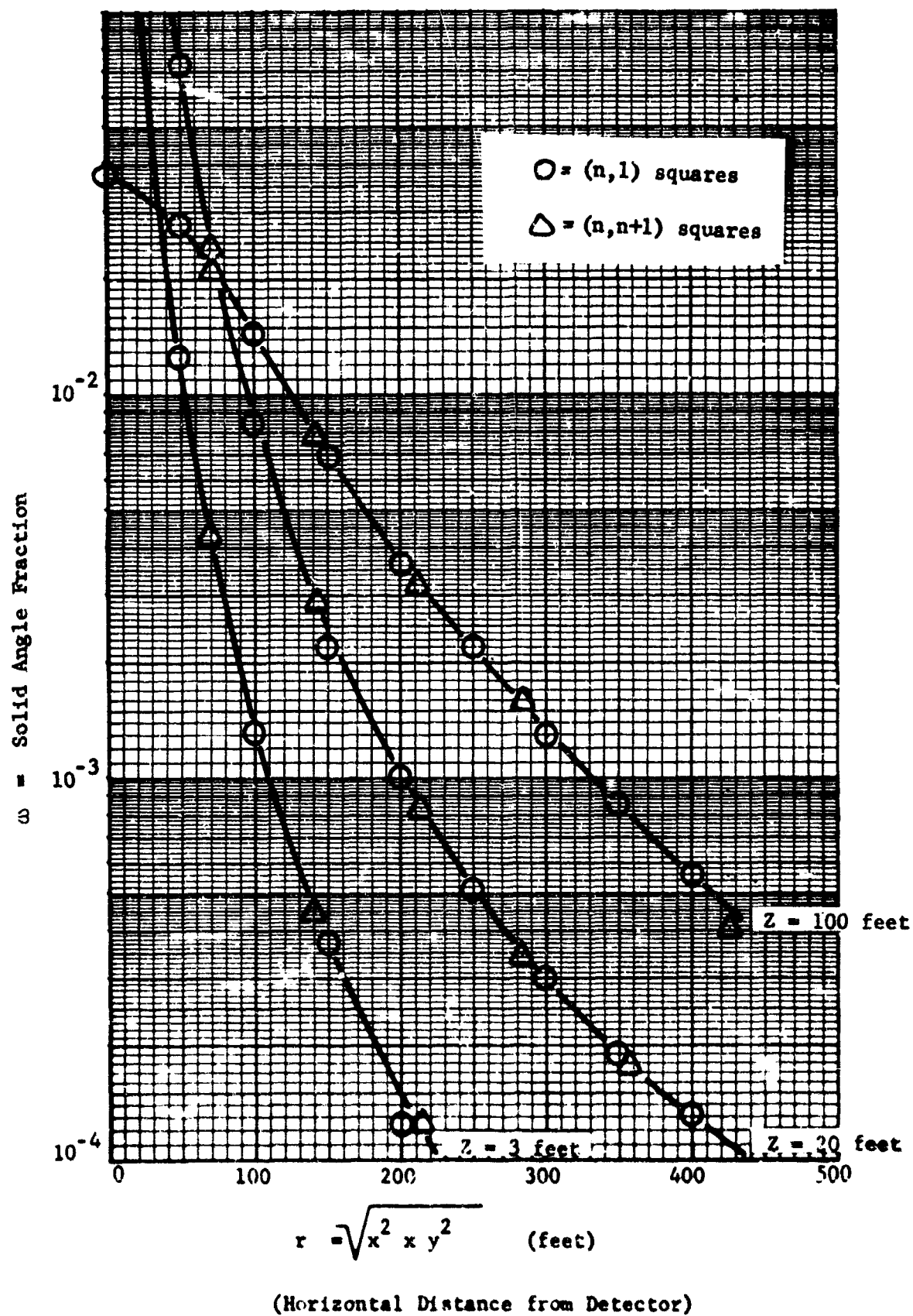


Figure C-4

Solid Angle Fraction of 50 Foot Squares as a Function of Horizontal Distance from Detector

TABLE C-1

Solid Angles and Solid Angle Fractions for
the 50 Foot Squares, (z = 100 Feet)

Lattice Number	x (ft.)	y (ft.)	ω	ω/ω_0	$\frac{\omega}{\omega_0} L(7.6) \Delta L_c(7.6, \omega_n)$
0,0	0	0	.03747	1.00	.00632
1,1	50	0	.02775	.1397	.00620
1,2	50	50	.0212	.1077	.00478
2,1	100	0	.01416	.0774	.00399
2,2	100	50	.0122	.0667	.00346
2,3	100	100	.0079	.0432	.00223
3,1	150	0	.00689	.0547	.00224
3,2	150	50	.00620	.0493	.00202
3,3	150	100	.0046	.0366	.00150
3,4	150	150	.0032	.0254	.00104
4,1	200	0	.0036	.0421	.00148
4,2	200	50	.0034	.0397	.00139
4,3	200	100	.0029	.0339	.00118
4,4	200	150	.0022	.0257	.00090
4,5	200	200	.0016	.0187	.00066
5,1	250	0	.0022	.0366	.00107
5,2	250	50	.0021	.0350	.00103
5,3	250	100	.0018	.030	.00087
5,4	250	150	.0014	.0233	.00068
5,5	250	200	.0010	.0167	.00049
5,6	250	250	.00079	.010	.00029
6,1	300	0	.00127	.0288	.00051
6,2	300	50	.00120	.0272	.00048
6,3	300	100	.00105	.0238	.00042
6,4	300	150	.0008	.0182	.000338
6,5	300	200	.00063	.0143	.000255
6,6	300	250	.00045	.0102	.000180
6,7	300	300	.00040	.0091	.000157

TABLE C-II

Solid Angles Subtended at the Detector (0,0,100')
by the Square Annular Regions Centered at the Origin

Square Annular Region	ω_n	$\Delta\omega = \omega_n - \omega_{n-1}$
n = 0	0.0375	0.0375
1	0.2344	0.1970
2	0.4175	0.1830
3	0.5436	0.1261
4	0.6292	0.0856
5	0.6892	0.0601
6	0.7333	0.0441

These reduction factors for various annular regions are given for $z = 100'$ in Table C-III. With this information, the contribution (and hence the effect of decontamination) of each of the square-grid areas shown in the overlay diagram (Figure C-2) can be tabulated. Consequently, the overlay can then be placed on a scaled city map and the direct contribution of any area can be easily determined from the tabulated contributions. A table of contributions can be prepared for any desired detector height, z . For large-scale considerations, the 50 foot square areas are small enough to be linearly divided for partial contributions with little error.

TABLE C-III

Solid Angles Subtended at the Detector (0,0,100')
by the Square Annular Regions Centered at the Origin

Square Annular Region	$D_n/D_0 = L(7.6) \Delta\omega_n(7.6, \omega_n)$
n = 0	0.0063
1	0.0444
2	0.0315
3	0.0409
4	0.0351
5	0.0291
6	0.0176

3. Barriers

An approximate treatment of barrier attenuation and scattering is now considered. Since the model is constrained to stay within the framework of the results of Spencer (Reference C-1), a formulation is developed in terms of Spencer's $L_c(X, \omega)$ and $L_s(X, \omega)$ functions (Reference C-1). Here, the detector is assumed to be located in an open area. However, this assumption does not restrict the application of the model to regions in which the detector is in an open area. If the detector is in a structure, it will be necessary to analyze the shielding by that structure. Procedures both approximate and more detailed are available for this analysis (Reference C-2).

The purpose of this section will not be to enter into the treatment of barrier problems in general. Rather, the purpose is to characterize the treatment of barriers in a manner that is consistent with the approximate character of the over-all model and which is simple enough to be practical for field applications. The formal treatment of barriers in the spirit of the above discussion is first considered.

Consider the contribution D_{nj}/D_o of the j^{th} unit square of the n^{th} square annular region to the detector located at the point $(x=0, y=0, z)$ in the absence of any barriers:

$$D_{nj}/D_o = \frac{\omega_{nj}}{\Delta_{\omega n}} \left[L_c(X_{\text{air}, n}) - L_c(X_{\text{air}, n-1}) \right] L(X) \quad (\text{C-13})$$

where X_{air} is the effective mass thickness of air between the detector and the source plane. If barriers are present which intersect the solid angle cone subtended at the detector by the n_j^{th} square, the direct and the scattered components of the radiation are affected. With intervening barriers present in the $n, n-1, \dots, n-m^{\text{th}}$ square annular regions, we have, in principle, a total mass thickness $X_{n,g}$ defined with the respect to the

n, g^{th} square and the given detector location, i.e.,

$$t_{n,g}^{X} = \sum_i a_{n,n,i} X_{n,i} + \sum_i a_{n,n-1,i} X_{n-1,i} + \dots + \sum_i a_{n,n-m,i} X_{n-m,i} +$$

$$\sum_i \sum_j (1 - a_{n,j,i}) X_{air}$$

Here the $a_{n,n-m,i}$ are weightings which are most appropriately defined by the fraction of the solid angle (defined with respect to ω_{nj}) intersected by the barrier at the n, j^{th} square. The last term of the above expression treats approximately the unobstructed fraction of the solid angle which is filled with air. It should be noted that in practice there would probably never be more than three terms, and, in general, fewer, in these sums over the mass thickness parameters of the barriers located in any square annular region.

After determining the mass factor, $t_{n,j}^{X}$, of the barriers shielding the n, j^{th} square, an expression for the relative contribution, $D_{n,j}/D_o$, may be derived. With a barrier of effective mass thickness, $t_{n,j}^{X}$ symmetrically surrounding the detector between the detector and the n^{th} annular region.

$$D_{n,j}/D_o = L(t_{n,j}^{X}) \left[L_c(t_{n,j}^{X}, \omega_n) - L_c(t_{n,j}^{X}, \omega_{n-1}) \right] \quad (C-14)$$

The fractional part $(\omega_{n,j}/\Delta \omega_n) (D_{n,j}/D_o)$ is not the desired contribution because this fraction:

- (a) includes in $\omega_{n,j}$ a scattering contribution not actually present; and
- (b) does not include the scattering around the barriers of radiation originating in $\omega_{n,j}$.

Also, differences in the $L_a(X_{n,j}, \omega_n)$ functions cannot be used in their

usual form to compute this contribution because they include a large component of scattering into $\omega_{n,j}$ from the infinite plane beyond $\omega_{n,j}$ and no contribution from the shielded area which scatters and arrives at the detector outside of $\omega_{n,j}$.

However, by defining a function in terms of the $L_a(X, \omega)$ in a manner analogous to that in which $L_c(X, \omega)$ is defined in terms of $L(X)$, we obtain a function approximating the contribution from a given area.

$$\text{Let } L_{ac}(X, \omega) = L_a(X, \omega) - \frac{L(\frac{X}{1-\omega})}{L(X)} L_a(\frac{X}{1-\omega}, \omega) .$$

This function eliminates the contribution of scattering into $\omega_{n,j}$ from the infinite portion of the plane not included in $\omega_{n,j}$. Differences of the L_{ac} , (i.e., ΔL_{ac}) include a scattering contribution into the solid angle $\Delta\omega_n$ from that portion of the source plane corresponding to the area defined by the solid angle ω_{n-1} . The ΔL_{ac} functions also include the direct contribution from the plane into $\Delta\omega_n$. However, the ΔL_{ac} does not include a contribution to the detector by radiation originating in $\omega_n - \omega_{n-1}$ which is scattered out $\omega_n - \omega_{n-1}$ and subsequently scattered back into the detector.

These are approximately compensating contributions and we will use this function to compute the approximate contribution from barrier obstructed source squares.* Clearly, for situations where most of the radiation from any given source square is unobstructed by barriers, this approximation will be adequate. When most of the source planes are obstructed by very large barriers, then (3.2) would be a better approximation. Thus, we take for the approximate contribution of the n, j^{th} square source area with effective mass

* More exact expressions could be developed for this contribution; however, it was felt that this effort would not be justified until after the potentialities of a square-grid point source model had been explored.

thickness, $t_{n,j}^X$, the expression

$$\begin{aligned} \frac{D_{n,i}}{D_o} &= \frac{\omega_{n,i}}{\Delta\omega_n} L(t_{n,j}^X) \Delta L_{ac}(t_{n,j}^X, \omega_n) \\ &= \frac{\omega_{n,i}}{\Delta\omega_n} L(t_{n,j}^X) \left[L_{ac}(t_{n,j}^X, \omega_n) - L_{ac}(t_{n,j}^X, \omega_{n-1}) \right]. \end{aligned} \quad (C-15)$$

We will show below that the values of (C-15) may be presented graphically for a large range of X . This represents a conservative approximation when most of the source squares are not obstructed by barriers.

The detector response due to a given contaminated 50 foot square area is given by the function

$$f(\omega)L(X)\Delta L_{ac}$$

where ΔL_{ac} is defined by the relation

$$\Delta L_{ac} = L_{ac}(X_1, \omega_1) - L_{ac}(X_1, \omega_{1-1})$$

with

$$L_{ac} = \frac{1}{l(X)} \left[L(X)L_a(X_1, \omega) - L\left(\frac{X}{1-\omega}\right)L_a\left(\frac{X}{1-\omega}, \omega\right) \right].$$

The quantity $f(\omega)$ is the appropriate weighting for a given square grid area and is given by $\omega/\Delta\omega$. The function $L(X)\Delta L_{ac}$ is highly dependent on the barrier mass thickness X . However, for a given annular square, (i,j) , $f(\omega)L(X)\Delta L_{ac}$ is dependent on the solid angle of the individual square only through the quantity $f(\omega)$. The quantity $f(\omega)$ varies with the position of the 50 foot lattice in a given annular square i . Consequently, the quantity $L(Y)\Delta L_{ac}$ may be computed as a function of X for any given square annulus.

Then, through the $f(\omega)$ function, the reduction factor of each of the individual 50 foot squares penetrating a barrier of any thickness S may be easily obtained. The function $L(X)\Delta L_{ac}$ as a function of X was computed for rings 0 through 6, and the results tabulated in Table C-IV. Figure C-5 also presents these data graphically. It is noted that the variation of $L(X)\Delta L_{ac}$ as a function of X is for all practical purposes a single exponential. (The variations from the straight line on the semi-logarithmic plot are well within the accuracy with which Spencer's curves $L(X)$ and $L_a(X, \omega)$ can be read.

Table C-IV gives the values of $f(\omega) = \omega/\Delta\omega$ for each of the 50 foot square-grids through ring six. Although these weighting functions for any given annular sector, i , vary from one square-grid to another, an average value of $f(\omega)$ for each ring can be obtained through the function $\Delta\omega/8i$, where $8i$ is the number of 50 foot square-grids in ring number i . The accuracy of using the average solid angle for every square-grid in an annular ring is certainly well within the general accuracy obtainable for the reduction factor in any problem in which complex barriers are present. Thus, we assign this average value to each 50 foot square-grid in a particular ring. With this assignment, the reduction factor of any square-grid through a barrier of arbitrary thickness may be computed and presented in graphical form. Table C-V presents the necessary data from which Figure C-6 is drawn. Figure C-6 thus represents the reduction factor D/D_0 for the individual square-grid areas as a function of the barrier mass thickness X .

Thus, the ease of readily superimposing the values of D/D_0 for the various square-grid areas for the case of air with no barrier is now carried completely over to the case with barrier. One needs three ingredients: the barrier mass thickness X ; the square-grid overlay; and the graphical representation of the functions $f(\omega)L(X)\Delta L_{ac}$ for the various rings, for example, Figures C-5 and C-6.

TABLE C-IV

$L(X)\Delta L_{ac}$ as a Function of Barrier Mass Thickness X

X psf	$L(X)\Delta L_{ac}(X,\omega)$						
	Ring 0	Ring 1	Ring 2	Ring 3	Ring 4	Ring 5	Ring 6
24	.00019	.0054	.0214	.02788	.02712	.01740	.00689
72	.00014	.0054	.0109	.00802	.00399	.00197	.00120
144	.00007	.00164	.00205	.000864	.00031	.00014	.00013
216	.00002	.00037	.000371	.000105	.00004	.00003	.00002
288	.00001	.00009	.000061	.0000164	.00001	$<10^{-5}$	$<10^{-5}$

TABLE C-V

Reduction Factors for the 50 Foot Squares as
a Function of Barrier Mass Thickness X

$$D_{nj}/D_o = \frac{\Delta_{nj}}{8n} L(X) L_{ac}(X,\omega)$$

psf	Ring 0	Ring 1	Ring 2	Ring 3	Ring 4	Ring 5	Ring 6
24	$7.12(-6)^*$	$1.33(-4)$	$2.44(-4)$	$1.47(-4)$	$7.25(-5)$	$2.62(-5)$	$5.31(-6)$
72	$5.25(-6)$	$1.33(-4)$	$1.24(-4)$	$4.21(-5)$	$1.07(-5)$	$2.96(-6)$	$1.10(-6)$
144	$2.52(-6)$	$4.04(-5)$	$2.34(-5)$	$4.54(-6)$	$8.30(-7)$	$2.10(-7)$	$1.19(-7)$
216	$7.50(-6)$	$9.10(-6)$	$4.23(-6)$	$5.53(-7)$	$1.07(-7)$	$4.50(-8)$	$1.83(-8)$
288	$3.75(-6)$	$2.22(-6)$	$6.95(-7)$	$8.62(-8)$	$2.68(-8)$	$<10^{-9}$	$<10^{-9}$

* $7.1(-6) = 7.1 \times 10^{-6}$

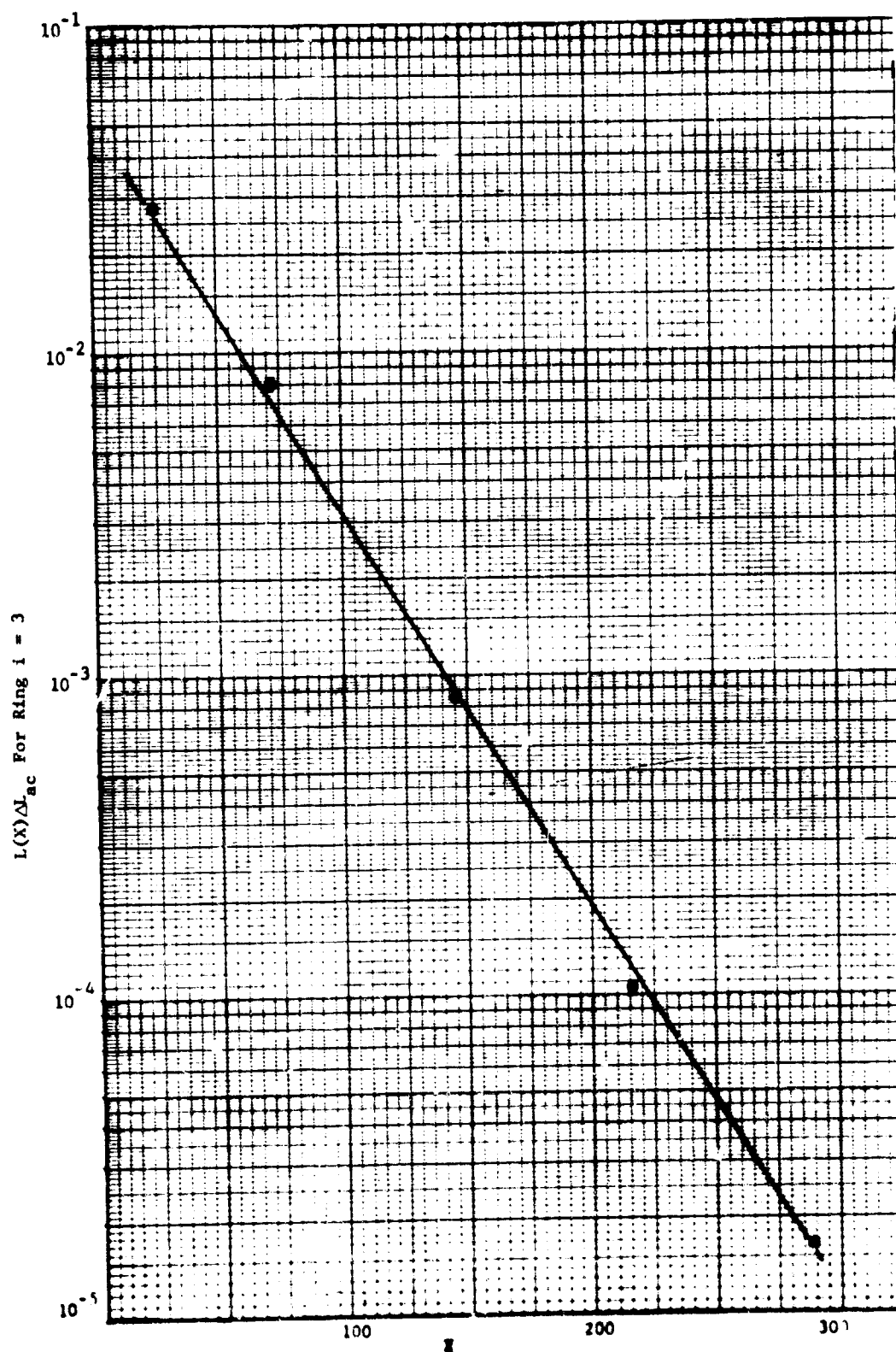


Figure C-5
 Variation of $L(X)\Delta L_{nc}$ vs. X
 For Ring $i = 3$

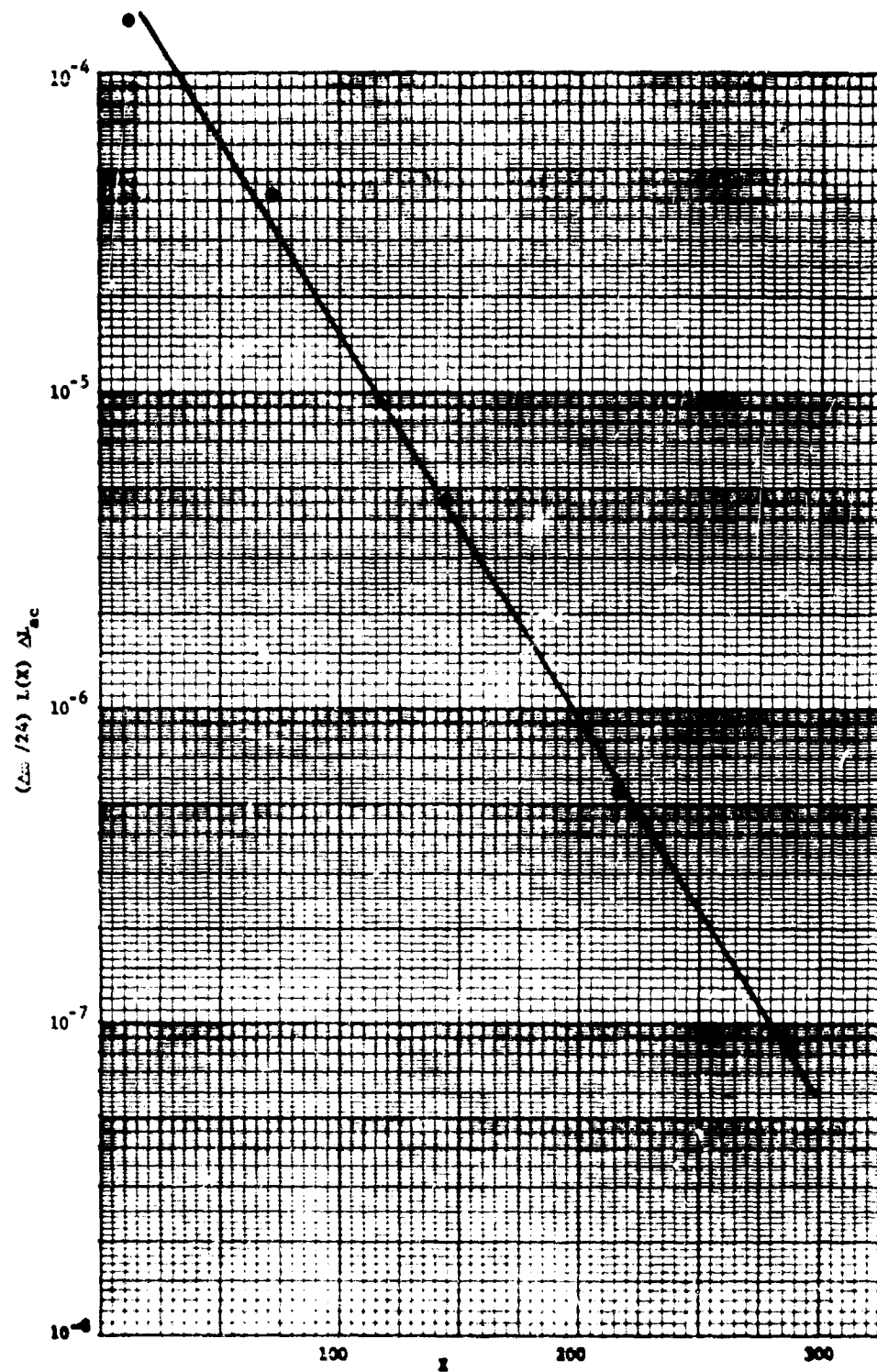


Figure C-6

Reduction Factor D/D_0 for the
Individual Square Grid Areas
as a Function of the Barrier
Mass Thickness X for Ring
 $i = 3$.

The expression (C-14) which gives the total effective mass thickness from the detector through the intervening barriers to the n,j^{th} square-grid area is in general quite difficult to evaluate. However, one can argue on physical grounds, that, for the regions of interest in the particular applications of this model, the computation of the effective mass thickness can be greatly simplified. Indeed it is possible to show theoretically that the expression (C-14) is approximately related in a rather simple manner to the effective line distance from the detector to the n,j^{th} square area for large distances and barrier detail in keeping with the approximate character of this model. Then, the total effective mass thickness $t_{n,j}^X$ can be practically estimated as follows:

- (a) Compute the line distance from the detector to the center of the n,j^{th} square radiation source area;
- (b) From considerations of the barriers (i.e., wall, floor, roof, etc., data) collected from earlier building surveys, compute the effective distance through which the radiation travels in the barriers; i.e., simply the thickness of all the walls through which the radiation travels (note: the obliqueness cancels when the area is projected to the vertical).
- (c) Add the effective thickness for each type of barrier material separately. Then use the formula for X in conjunction with the material's mass thickness table (see Reference C-1, p. 15) for each material, then sum the X 's for all the materials to obtain the total barrier mass thickness.

III. APPROXIMATE ANALYTICAL FIT FOR $L_a(X, \omega)$ AND $L_c(X, \omega)$ FUNCTIONS

It was found during the course of developing the circular model (Appendix B) that an analytical fit over a rather extensive range of values for both the $L_a(X, \omega)$ and $L_c(X, \omega)$ curves found on pages 41 and 42, respectively, of Reference C-1 is possible by employing an expression of the general form

$$D/D_0 = L(X, \omega) = \omega^s e^{AX}, \quad (C-15)$$

where s is the slope and A the Intercept for selected values of X and ω . The slope in turn is obtained by

$$s = \ln L(X, \omega_2) - \ln L(X, \omega_1), \quad (C-16)$$

while the intercept is calculated by solving Equation C-15 for A as follows:

$$A = \frac{\ln L(X, \omega) - s \ln \omega}{X}.$$

The best analytical fit for the $L_c(X, \omega)$ curves was achieved by obtaining the $L_c(X, \omega)$ values given on page 41 of Reference C-2 corresponding to ω_1 and ω_2 values of 0.05 and 0.2 respectively and solving for the intercept at $\omega = 0.2$ for each X value selected. The same procedure was followed for the $L_a(X, \omega)$ curves depicted on page 42 of Reference C-2. The slope in this case was calculated for $\omega_1 = 0.01$ and $\omega_2 = 0.1$ while the intercept was obtained at $\omega = 0.1$. The numerical results of these calculations are presented in Table C-VI, and the resultant curves are shown in Figures C-7 and C-8.

It is apparent when comparing the $L(X, \omega)$ curves developed here with those

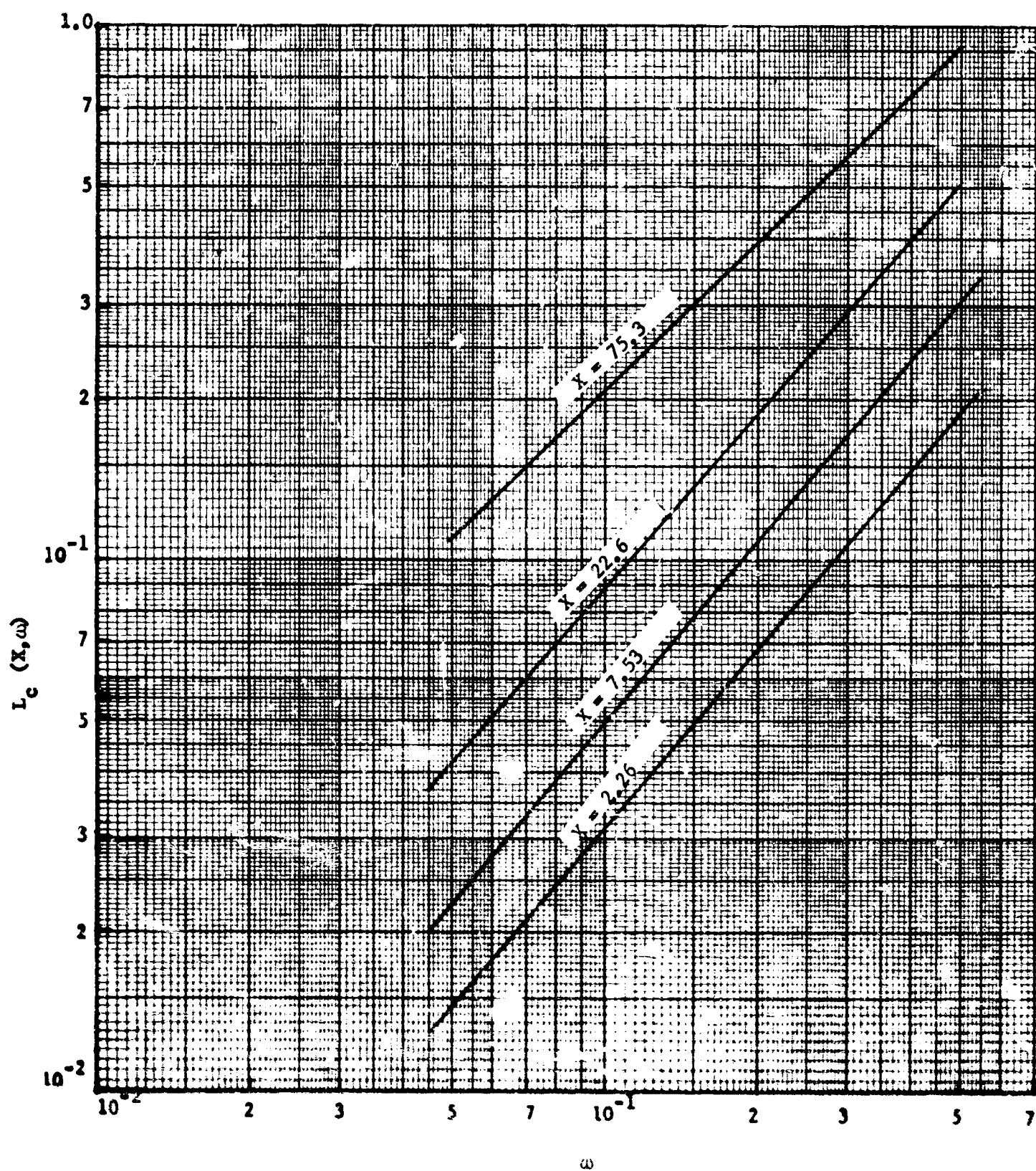


Figure C-7

Geometry Factor ($L_G(X, \omega)$) Depending, Detector Response
Due to a Circular Plane Gamma Radiation Source

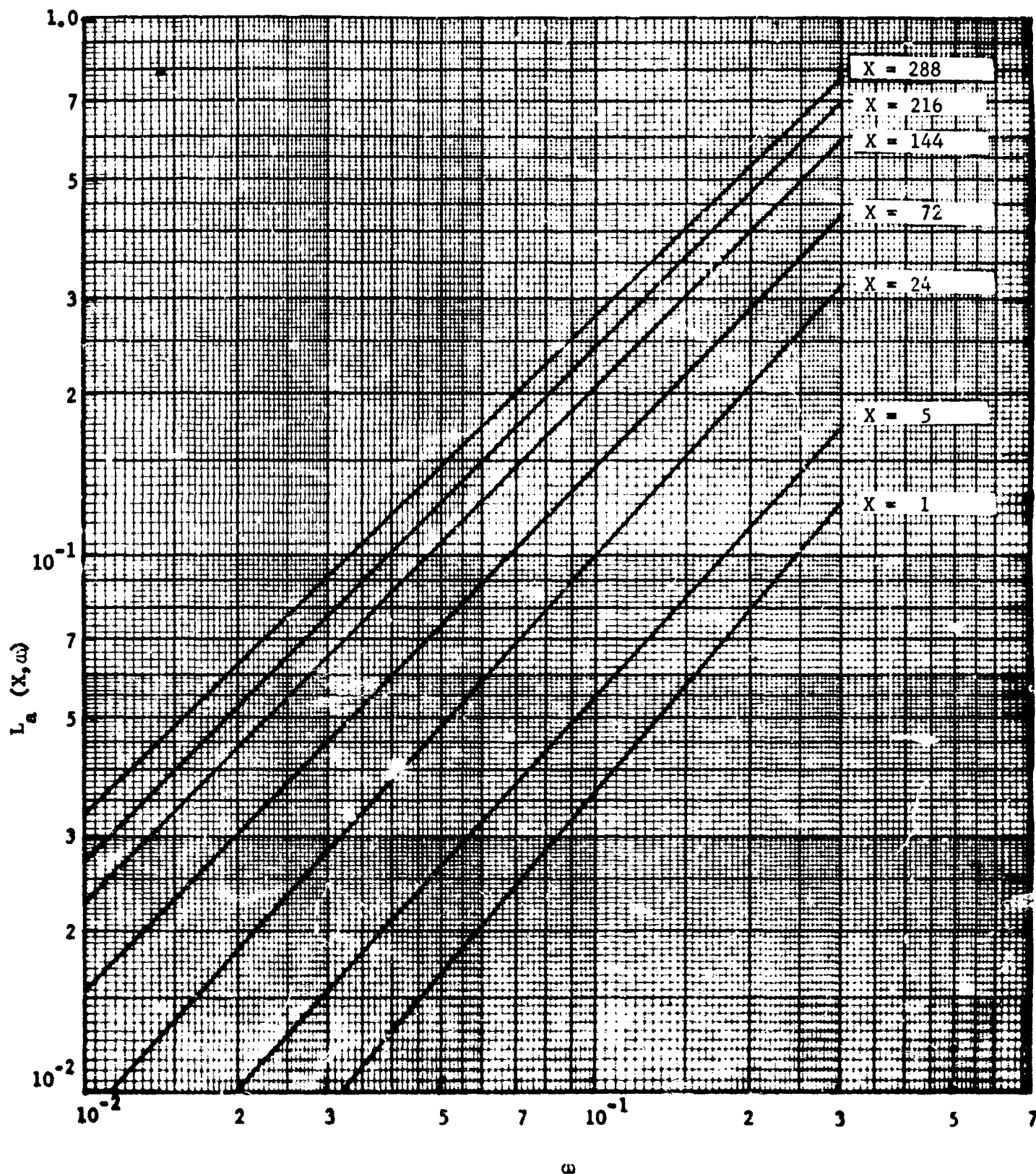


Figure C-8

Geometry Factor ($L_a(X, \omega)$) For Detector Response to Gamma Radiation

Received by a Detector From a Limited Cone of Directions

appearing in Reference C-2 that the accuracy of the $L(X, \omega)$ values deteriorate rapidly due to the lack of convergence as $\omega \rightarrow 0$. This is particularly true for those values of $\omega > 0.3$ and $\omega > 0.5$, associated with the $L_a(X, \omega)$ and $L_c(X, \omega)$ functions respectively. Despite the accuracy limitations inherent with this analytical approximation of $L(X, \omega)$ functions, there is no evidence that the approach would not produce the desired results when appropriately used in the square-grid model. It should be noted that there are no restrictions associated with this model that would prohibit the exclusive use of the exact values for $L_a(X, \omega)$ and $L_c(X, \omega)$ presented in Reference C-1.

TABLE VI

Calculated Values of s and A for
Selected Effective Mass Thickness Values

$L_a(X, \omega)$			$L_c(X, \omega)$		
X	s	A	X	s	A
1	1.125	-0.725	2.26	1.115	-0.396
5	1.055	-0.0950	7.53	1.137	-0.0531
24	1.055	-0.0952	22.6	1.042	-0.00255
72	0.975	+0.00445	75.3	0.916	+0.00726
144	0.957	+0.004355			
216	0.954	+0.00361			
288	0.930	+0.00302			

IV. AN EXAMPLE

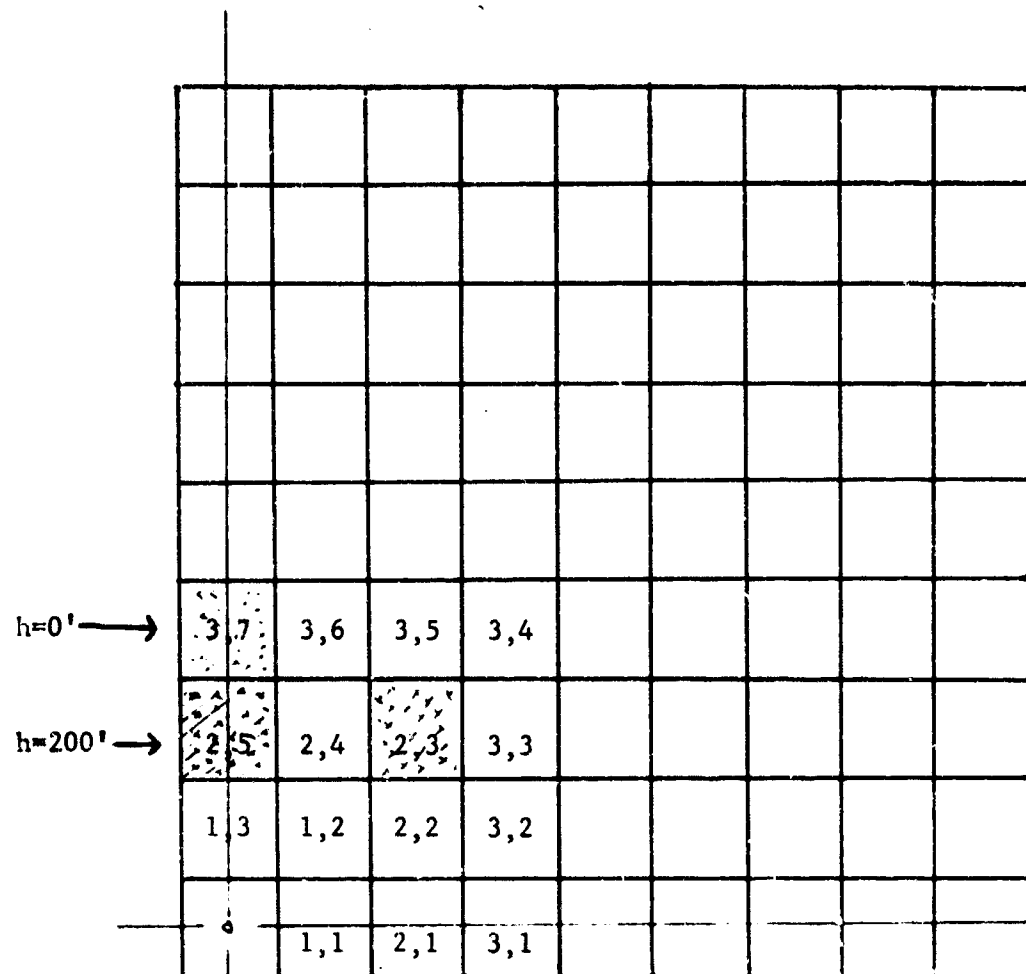
Consider the situation indicated in Figure C-9 below. We wish to explicitly demonstrate the method of calculation of the $D_{n,j}/D_o$ for several of the contributing squares of the grid. Starting with the application of the overlay, discussed in Section II-B (see Figure C-3), to the quadrant of the idealized scaled map shown in Figure C-9 for all of the contributions $D_{n,j}/D_o$ of the squares can be obtained directly from the appropriate overlay as discussed earlier. Of course, the values will only be correct when the radiating source square contributing to the detector is not appreciably obstructed by barriers. In particular, for the contribution of the 2,3 square (for a detector located 100' above the origin) the value of the function $D_{2,3}/D_o = (0.0366)L(7.6)[L_c(7.6,0.418) - L_c(7.6,0.234)] = 0.00218$ is immediately read off of the overlay.

We now assume that an equivalent thickness of 2' of concrete for the building blocking the contribution of square (3,7) has been determined. Also, we assume that an equivalent thickness of 1' of concrete for the same structure blocking the contribution of its roof, square 2,5 has been determined. Then the effective mass thicknesses of these barriers are given by (see Reference C-1, p. 15)

$$\begin{aligned} X_{3,7} &= 2(z/A)\rho\Delta = 2(0.5)(144)(2') = 288, \\ X_{2,5} &= 2(0.5)(144)(1') = 144 \end{aligned}$$

The approximate $D_{n,j}(X)/D_o$ for the source squares obstructed by barriers cannot be read from the overlay because the $L_{ac}(X,\omega)$ functions leading to this contribution are functions of the various effective barrier thicknesses X present.

An important but easy-to-apply approach has been discussed for obtaining the terms $D_{n,j}(X)/D_o$ in Section II, which employs a table and/or graph giving the



(The detector location is at (0,0,100'))

Figure C-9

Idealized Scaled Map (to be used in conjunction with Overlay - see Figure C-3 and Table C-I)

values of the obstructed contribution of each source square $D_{n,j}/D_o$ as a function of the effective mass thickness X (see Table C-V and Figure C-5). Using the graph or Table C-V to evaluate $D_{3,7}(X = 298)/D_o$ for the example of this section, we find $D_{3,7}/D_o = 8.617 \times 10^{-7}$. In terms of the discussion of Section I, the formal expressions representing the approximate barrier obstructed contributions of the source squares 3,7 and 2,3 (Detector location (0,0,100')) are given by

$$D_{3,7}/D_o = \frac{\omega_{3,7}}{\omega_3 - \omega_2} \left\{ L(288) \left[L_{ac}(288, \omega_3) - L_{ac}(288, \omega_2) \right] \right\}$$

and

$$D_{2,5}/D_o = \frac{\omega_{2,5}}{\omega_2 - \omega_1} \left\{ L(144) \left[L_{ac}(144, \omega_2) - L_{ac}(144, \omega_1) \right] \right\}.$$

Using the information on the overlay relating to these solid angles we can write

$$D_{3,7}/D_o = (0.055) \left\{ L(288) \left[L_{ac}(288, 0.544) - L_{ac}(288, 0.418) \right] \right\}$$

and

$$D_{2,5}/D_o = (0.077) \left\{ L(144) \left[L_{ac}(144, 0.418) - L_{ac}(144, 0.234) \right] \right\}.$$

Then using Spencer's tables (Reference C-1, pp. 37,42) we find:

$$\frac{D_{3,7}}{D_o} = (0.055) \left\{ (0.00024)(0.067) \right\}$$

$$\frac{D_{2,5}}{D_o} = (0.077) \left\{ (0.0063)(0.349) \right\}$$

or

$$D_{3,7}/D_o = 8.86 \times 10^{-7}$$

and

$$D_{2,5}/D_0 = 1.54 \times 10^{-4} \quad .$$

Of course, these results could also have been obtained from a table of the function L_{ac} as a function of ω with X as a parameter.

V. SUMMARY AND CONCLUSIONS

It has been shown that a square-grid overlay technique may be used to analyze the radiation dose contribution to a detector from individual planes of contamination. Once these contributions are known, the effectiveness of decontaminating any plane may easily be assessed. Data required for application of the square-grid model are:

- (a) A grid overlay with each square labeled in a coordinate scheme (a 50 foot grid size is proposed with each square labeled (i,j) where i is the square annulus containing the square (i,j) and j is the position of the square (i,j) in the annulus. The detector is vertically above the center of square $(0,0)$).
- (b) A map of the area under analysis which is of the same scale as the grid overlay.
- (c) Data on the effective mass thicknesses of structures in the area.
- (d) A set of tables giving the contribution from each square in the grid to the detector located a given distance above the plane of the grid. The tables are constructed as a function of the detector height above the plane.
- (e) A set of curves giving the effects of barrier shielding (as a function of X) on the detector response for each square in the grid.

The required tables and curves are derived for a detector height of 100 feet

and a square-grid length of 50 feet. It is shown for this case that the grid may be approximated by a function of the distance of the center of the square from the center of the (0,0) square. Changing the orientation of the square with respect to the detector produces only a very small perturbation in the value of the solid angle.

It is concluded that when detailed maps of a standard scale are available for an area (such as Sunborn maps) a square-grid overlay technique can offer a practical tool for analysis of decontamination effectiveness. It is recommended that data be derived for a useful range of detector heights (say 3', 10', 30', as well as the present 100') and that the method be applied to some real situations.

Further work in barrier effects is required. A more refined approach to the analysis of barrier effects should be sought.

REFERENCES

- C-1 Structure Shielding Against Fallout Radiation From Nuclear Weapons,
L. V. Spencer, NBS Monograph 42, U. S. Department of Commerce,
National Bureau of Standards, June 1, 1962.
- C-2 Shelter Design and Analysis, Volume I. Fallout Protection, TR-20-
(Vol. I), Office of Civil Defense.

Appendix D

A Point-Source Model and the Equivalent Planes Method for Approximating Gamma Ray Intensity at a Single Detector Location

Note: The material in this Appendix was originally submitted to USNRDL as Research Memorandums RM-OU-214-5* and RM-OU-214-7**.

* T. Johnson. A Point-Source Model for Approximating Gamma Ray Intensity at a Given Detector Location. RM-OU-214-5. Durham, North Carolina: Research Triangle Institute, Operations Research and Economics Division, 30 June 1965.

** T. Johnson. Equivalent Planes Method. RM-OU-214-7. Durham, North Carolina: Research Triangle Institute, Operations Research and Economics Division, 20 August 1965

TABLE OF CONTENTS OF APPENDIX D

	<u>Page</u>
LIST OF TABLES	D-11
LIST OF FIGURES	D-11
GLOSSARY OF TERMS	D-111
I. INTRODUCTION	D-1
A. Purpose	D-1
B. Background	D-1
C. The Model	D-1
II. DEVELOPMENT OF THE POINT-SOURCE MODEL	D-5
A. Areas Centered Opposite Detector	D-5
B. Off-center Areas	D-14
C. Shielding	D-19
III. EVALUATION OF EQUIVALENT BUILDING METHOD APERTURE CORRECTIONS . .	D-29
IV. AN EXAMPLE ANALYSIS	D-35
V. THE EQUIVALENT PLANES METHOD	D-39
VI. CONCLUSIONS AND RECOMMENDATIONS	D-41
REFERENCES	D-43

LIST OF TABLES

<u>Table</u>	<u>Page</u>
D-I Example Analysis of Configuration in Figure D-19	D-37

LIST OF FIGURES

<u>Figure</u>	<u>Page</u>
D-1 Geometry of Model	D-2
D-2 Comparison of Solid Angles for Centered Areas	D-7
D-3 Dose Rate From Source Area Centered Under Detector	D-8
D-4 Approximately Equivalent Areas - Circular Segments	D-9
D-5 Approximately Equivalent Areas - Circular Segment	D-11
D-6 Approximately Equivalent Areas - Centered Square	D-11
D-7 Maximum Eccentricity Ratios For Centered Rectangular Areas .	D-13
D-8 Dose Rate Contribution Per Unit Area	D-15
D-9 Approximations on a Convex Function	D-16
D-10 Form of $C_1(h-z , r)$ Functions	D-18
D-11 Maximum Square Area To Be Represented by a Point	D-20
D-12 Horizontal Barrier Factors For Centered Areas	D-21
D-13 Horizontal Barrier Factors for Off-Center Areas	D-24
D-14 Vertical Barrier Shielding Factors	D-26
D-15 Correction to Vertical Barriers for Apertures	D-28
D-16 Aperture Corrections	D-30
D-17 Correct Form for Aperture Corrections	D-32
D-18 Determination of Points of Equality of Condition D-18 . . .	D-33
D-19 Example Plan View	D-36

GLOSSARY OF TERMS

A_i	= area in square feet of the i^{th} contaminated area
A_p	= fraction of the vertical barrier voided by apertures
$\%A_p$	= percent of the vertical barrier voided by apertures
Centered area	= an area of contamination such that the line from the detector to the center point of the area is perpendicular to the plane of the area
$B_o(X_o, h_i - z , A_i)$	= horizontal barrier shielding factor for centered areas
$B_{ol}(X_o, h_i - z , r)$	= horizontal barrier shielding factor for off-center areas
$B_v(X_v)$	= vertical barrier shielding factor (no horizontal barrier between source and vertical barrier)
$B_v^i(X_v)$	= vertical barrier shielding factor with horizontal barriers between the source and vertical barrier
$C_i(h_i - z , r_i)$	= dose contribution per unit area
$C_d(h_i - z , A_i)$	= dose contribution from centered area
e	= eccentricity ratio, length/width
h_i	= height of the i^{th} area above reference plane
$L(X)$	= total dose from an infinite plane source of fallout
r_i	= horizontal distance from the detector to the center of the i^{th} area
ω	= solid angle fraction
X_o	= horizontal-shield equivalent mass thickness in psf
X_v	= vertical-shield equivalent mass thickness in psf
z	= height of detector above reference plane

Appendix D

A Point-Source Model for Approximating Gamma Ray Intensity at a Single Detector Location

I. INTRODUCTION

A. Purpose

This appendix presents a procedure for estimating the relative radiation dose contributions at a detector from multiple planes of contamination. The two objectives in developing this model are:

1. to provide accurate approximations to the relative dose contributions by many different planes of fallout contamination, and
2. to reduce to a minimum the charts and tables, maps, equipment, and time required to calculate the contributions to a given detector location.

B. Background

Two other models with similar objectives have been developed under this contract. Conceptually, the "circular model" (Appendix B) is simple, and it is easy to use, but accurate approximations are difficult to make when the contaminated planes under analysis are not segments of circular annuli. The "square grid model" (Appendix C) can be used to approximate accurately the more usual geometric arrangement of rectangular planes, but application requires a suitable scale map for use with overlays of the grid. This point-source model presents a scheme for approximating contaminated planes by the appropriately located point-sources of radiation. The point-source model is formulated such that accuracy limits are known. Scale maps are not required, but only certain dimensions; only a small number of concise charts are required for its application.

C. The Model

In this model the detector and source point geometry are presented in cylin-

drical geometry. Since the detector is isotropic, the geometry reduces to two distances. These are $|h-z|$, the vertical separation of the detector from the source plane, and r , the horizontal separation of the detector axis from the point representing a given contaminated area. Here h is the height of the source plane, and z is the height of the detector, both above a reference plane. Figure D-1 illustrates this geometry.

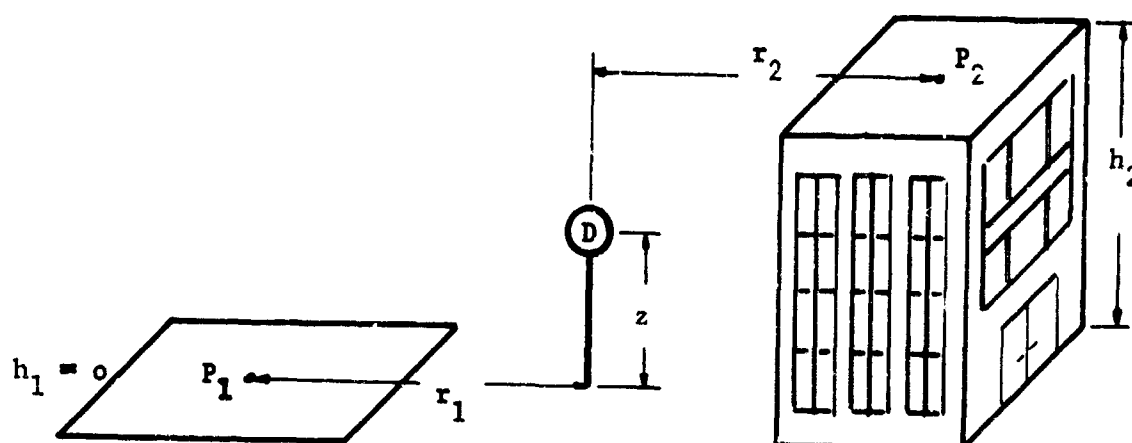


Figure D-1
Geometry of Model

The shape of the contaminated areas to be represented by a point is of concern. It is shown that for the area centered vertically below (or above) the detector, a circle or square of a given area subtends essentially the same solid angle and thus yields the same relative dose. Off-center areas are all assumed to be squares. Off-center areas which are not square should be approximated as closely as possible with squares, unless the maximum dimension meets the criterion of Figure D-11.

It has been shown (Appendix C) that the orientation of a square area within a source plane does not appreciably affect the solid angle subtended at a detector. Thus, to a good approximation the relative contribution by a contaminated area to a detector is a function only of the vertical height $|h-z|$ separating source and detector, the horizontal distance r from the center of the area to the vertical detector axis, the size of the area, and the intervening shielding.

In this paper the relative dose rate, or reduction factor delivered to the detector from a given area is developed. This relative dose rate for area i is given by the ratio D_i/D_0 where D_i is the dose rate contributed to the detector by plane i and D_0 is the total relative dose rate three feet above an infinite, uniform plane of contamination. The reduction factor RF is then given by

$$RF = \sum_{\text{all planes}} D_i/D_0$$

The relative contribution from all areas beyond those analyzed individually may be obtained by subtracting the "centered area" relative contribution, Figure D-3, from the infinite plane contribution $L(|h-z|)$ given in the right margin of Figure D-3.

A major consideration in the development of this model was the establishment of the maximum area of a square which could be accurately represented by a point-source at the center of the square. A criterion was devised and maximum areas were calculated as a function of horizontal separation for several vertical separation distances ($|h-z| = 3', 10', 20', 50', \text{ and } 100'$). The criterion establishes that for a square area less than or equal to the maximum area, the relative contribution calculated on an area basis from Spencer's curves (Reference D-1) are within 10% of the contribution calculated from the equation

$$C(A_i, |h_i-z|, r_i) = C_1(|h_i-z|, r_i)A_i \quad (D-1)$$

where $C_1 (|h_1 - z|, r_1)$ is the contribution per unit area as a function of $|h_1 - z|$ and r_1 and where A_1 is the contaminated area in square feet.

The factors for the shielding effects of barriers between the source and the detector are derived from Spencer's curves and other established sources (References D-3, D-4, & D-5). They are presented in the standard form of multiplicative adjustments of the unshielded dose from a source.

II. DEVELOPMENT OF THE POINT-SOURCE MODEL

The analysis of the effects of decontamination of multiple contaminated planes surrounding a detector usually presents unique requirements. This model seeks to provide a concise, rapid method of calculating accurately the fraction of the total fallout dose rate at a detector contributed by each contaminated area. In decontamination analyses, the detector positions of interest are usually unprotected or are in low protection factor structures. This is because decontamination is most effective in hastening the resumption of operations in poorly protected areas (Reference D-2). Shielding is treated in an approximate manner consistent with its relative importance in the model and with the requirement of conciseness. Techniques of the "Equivalent Building Method" (Reference D-5) and the "Engineering Manual" (Reference D-3) are combined.

A. Areas Centered Opposite Detector

The area immediately below or above a detector is always of interest in determining radiation doses. This area may be a major contributor to the dose in the absence of significant shielding. In any case, the difference between a centered area dose and the infinite plane dose (assuming uniform, unshielded contributions) is required as the contribution from beyond the areas which are analyzed specifically.

1. Centered Circles and Squares

In this model we wish to approximate the dose from centered areas by a function of only area and detector height. If we are to eliminate shape as a parameter, the most obvious concern is whether or not centered circles and squares of equal areas contribute equally to the detector. Assuming that the contribution from a centered circle or square is a function only of detector height and of the solid angle subtended by the area, the desired approximation of an equivalence criteria between squares and circles is that

equal solid angles are subtended by equal areas at equal relative detector heights. Comparisons of solid angle fractions subtended are given in Figure D-2. It is seen from this figure that for the range of areas and detector heights used in this model, the solid angle fraction subtended by centered circles and squares of equal area are equal within the limits of accuracy which can be used in reading dose rate contributions from graphs. Thus, the dose rate contribution from centered circular areas is taken as being equal to the dose rate contribution from centered squares of equal areas, as is the standard practice (References D-1 and D-3).

In Figure D-3 the relative dose rate contributions C_d from a contaminated circular or square area centered above or below the detector is presented as a function of area for several detector heights $|h_i - z|$. These values were derived in exactly the same manner as were Spencer's $L_c(X, \omega)$ functions where X is the equivalent mass thickness between the source and detector and ω is the solid angle fraction subtended by the source (Reference D-1). That is, letting $L(|h_i - z|)$ be the total dose rate received at a detector located $|h_i - z|$ feet above an infinite plane of fallout contamination of such intensity that $L(3') = 1$, then

$$C_d(|h_i - z|, A_i) = L(|h_i - z|) - L\left(\sqrt{|h_i - z|^2 + r_i^2}\right) \quad (D-2)$$

where

$$A_i = \text{source area}_i = \pi r_i^2 \text{ and}$$

$$\sqrt{|h_i - z|^2 + r_i^2} = |h_i - z| / (1 - \omega_i).$$

Thus, $C_d(|h_i - z|, A_i)$ corresponds to Spencer's $L(X)L_c(X, \omega)$ function. The $L(|h_i - z|)$ values given in the margin of Figure D-3 are the relative dose rates from an infinite area of fallout contamination, $A = \infty$, at a detector at height $|h_i - z|$.

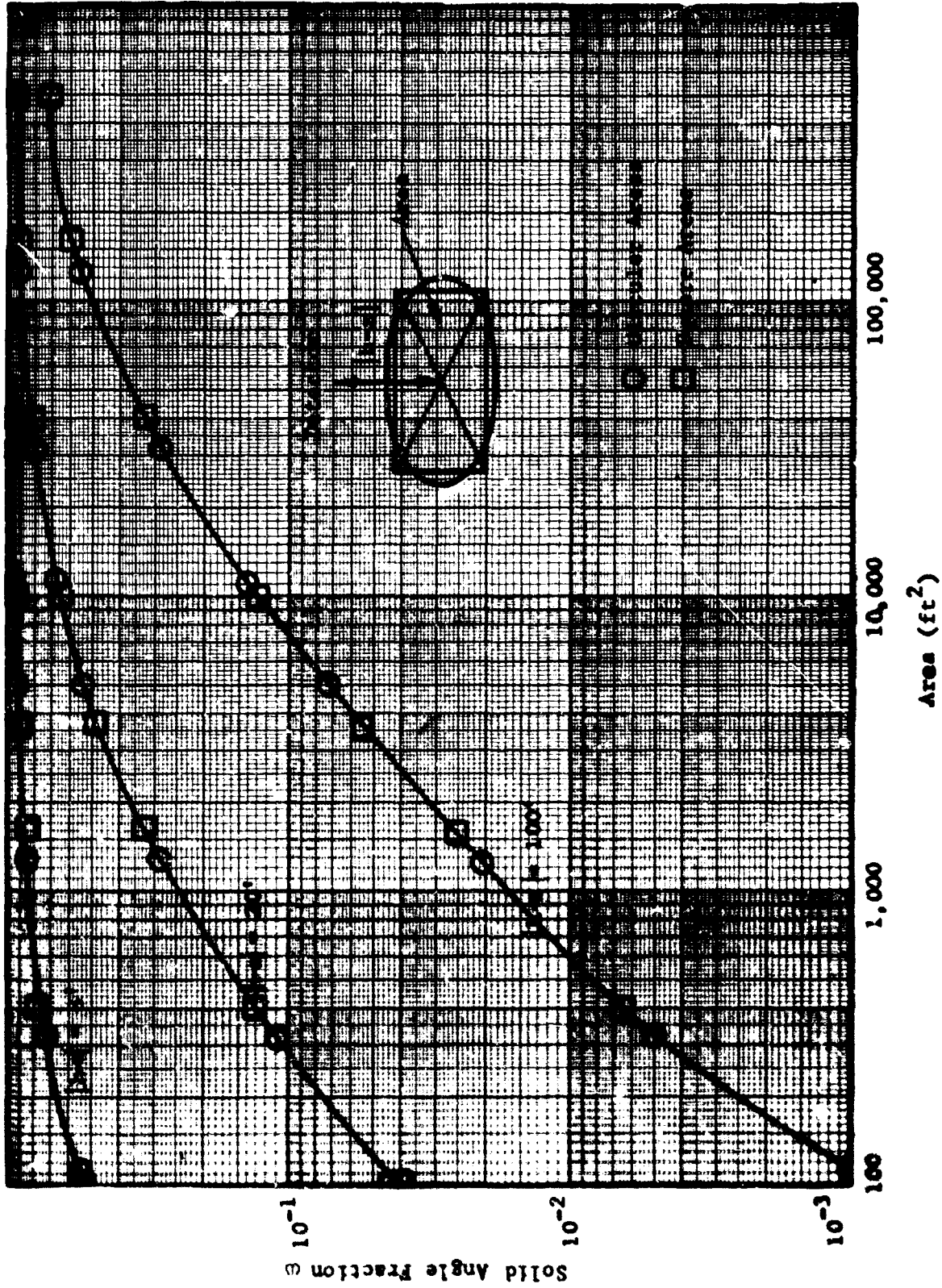


Figure D-2
Comparison of Solid Angles for Centered Areas

Dose Rates When
Area = π

L(3')	= 1.0
L(10')	= .786
L(20')	= .659
L(50')	= .495
L(100')	= .374

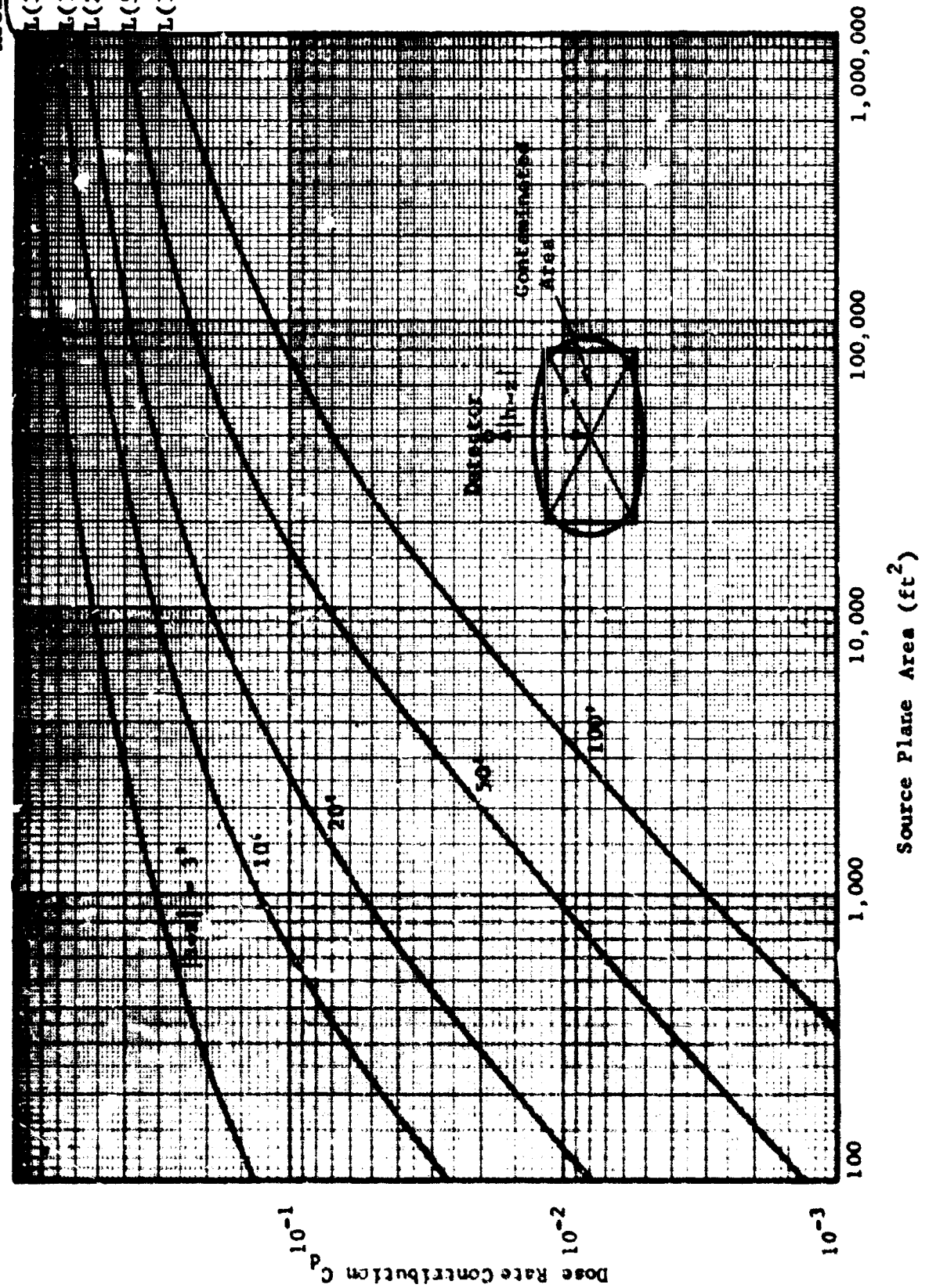


Figure D-3
Dose Rate From Source Area Centered Under Detector

2. Centered Rectangles

Areas encountered in practical situations are most often rectangular. We shall thus investigate the maximum eccentricity of a centered rectangular area such that the dose rate contribution is within a given margin of the dose rate from a centered square (or circle) of the same area.

A centered rectangular area (i.e., $L/w \neq 1$) will always contribute less dose to the detector than a centered square of the same area. Thus by approximating a centered rectangle by a centered square of the same area, one will overestimate the dose contribution from the area and consequently will overestimate the effectiveness of decontaminating the area. This means, of course, that the dose rate overestimates should be kept to a small percent of the dose rate contribution from the area. This overestimate of the relative dose rate of decontaminating the centered area will mean that the reduction of decontaminating other areas will be underestimated. We shall establish bounds on the error introduced sufficiently stringent to insure acceptable accuracy in the application of the model.

Considering the precision of other factors in the total decontamination model, an error limit of ten percent seemed acceptable. The criterion established below assures that the error in unshielded dose contribution introduced by this approximation is less than ten percent.

Consider the two geometries of Figure D-4.

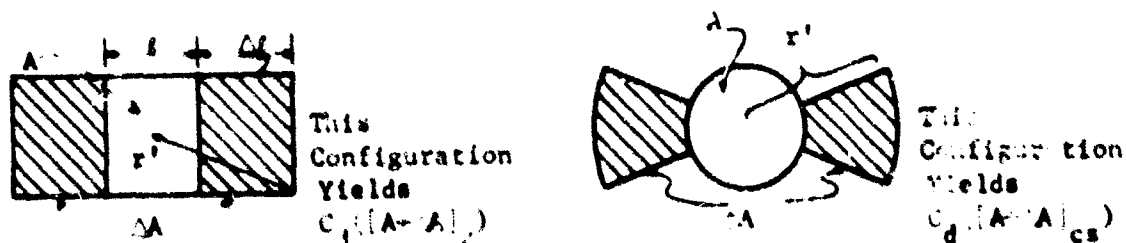


Figure D-4

Approximately Equivalent Areas - Circular Segments

We see that

$$A = \ell^2$$

$$\Delta A = \ell \Delta \ell$$

$$\Delta \ell = \Delta A / \ell$$

$$\text{and } r' = \sqrt{\left(\frac{\ell}{2} + \frac{\Delta \ell}{2}\right)^2 + \left(\frac{\ell}{2}\right)^2}$$

where

A = area of square "center" of rectangle

$A + \Delta A$ = area of rectangle

ℓ = width of rectangle

$\ell + \Delta \ell$ = length of rectangle

Thus, the eccentricity e of the rectangle is

$$e = \frac{\ell + \Delta \ell}{\ell} = 1 + \frac{\Delta A}{A} \quad (D-3)$$

We have shown (Figure D-2) that the dose from centered squares and circles of equal areas are identical within the accuracy of the graphical data. Therefore, let A_c denote the area A in a centered circular or square configuration, and let A_R denote the area A in a centered rectangular configuration. Thus, the dose rate from the area on the left in Figure D-4 is $C_d ([A + \Delta A]_R)$. Letting $A'_c = \pi r'^2$, the dose rate from the area on the right is

$$C_d([A + \Delta A]_{cs}) = C_d(A_c) + \frac{\Delta A}{A'_c - A} [C_d(A'_c) - C_d(A_c)] \quad (D-4)$$

Since the areas are equal, we make the approximation

$$C_d([A + \Delta A]_R) \approx ([A + \Delta A]_{cs}) \quad (D-5)$$

Now consider the way in which the off-center ΔA is approximated in Equation D-5. Figure D-5 depicts this approximation, and it is clear that the circular segment approximation of Equation D-5 uses areas farther from the detector and thus gives a low approximation to the dose rate from $(A + \Delta A)_R$.

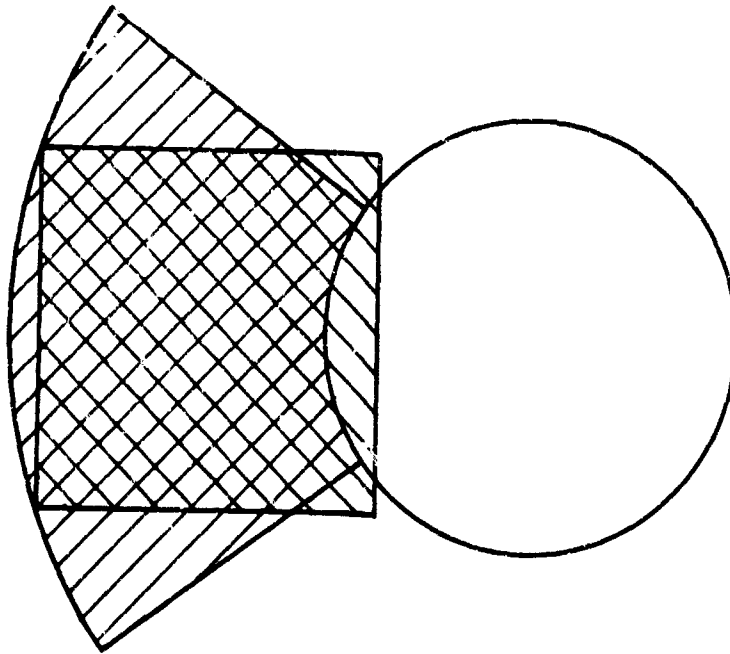
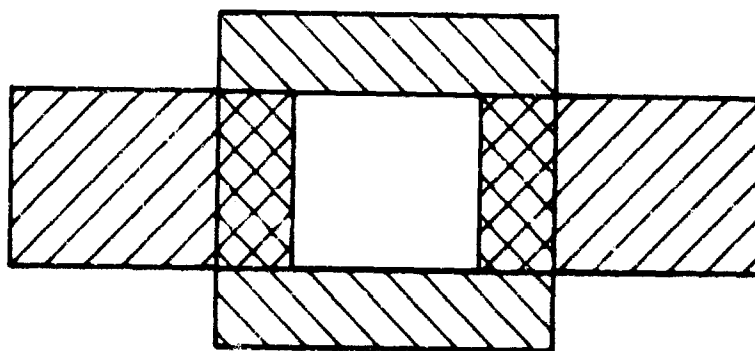


Figure D-5
Approximately Equivalent Areas - Circular Segment

Figure D-6 depicts the way in which areas are equated in the approximation

$$C_d ([A + \Delta A]_R) \cong C_d ([A + \Delta A]_c). \quad (D-6)$$



Yields $C_d ([A + \Delta A]_c)$

Figure D-6
Approximately Equivalent Areas - Centered Square

In this case it is clear that the centered square approximation, Equation D-6, uses areas closer to the detector and thus gives a high approximation to the dose rate from $(A + \Delta A)_R$. Therefore,

$$C_d ([A + \Delta A]_c) \geq C_d ([A + \Delta A]_R) \geq C_d ([A + \Delta A]_{cs})$$

and

$$\frac{C_d ([A + \Delta A]_c) - C_d ([A + \Delta A]_R)}{C_d ([A + \Delta A]_c)} \leq \frac{C_d ([A + \Delta A]_c) - C_d ([A + \Delta A]_{cs})}{C_d ([A + \Delta A]_c)}.$$

The dose from the rectangular area $C_d ([A + \Delta A]_R)$ is then within ten percent of the estimate $C_d ([A + \Delta A]_c)$ if

$$\frac{C_d ([A + \Delta A]_c) - C_d ([A + \Delta A]_{cs})}{C_d ([A + \Delta A]_c)} \leq 0.1. \quad (D-7)$$

Satisfaction of Equation D-7 is thus taken as the criterion for the maximum eccentricity of a centered rectangle of area $A + \Delta A$ to be approximated by a centered square of area $A + \Delta A$ by using the dose curves in Figure D-3.

The locus of maximum allowable eccentricity e from Equation D-3, as a function of total area, $A + \Delta A$, is derived as described below for the detector heights of 3, 10, 20, 50, and 100 feet. To obtain a point on the locus for a given height, the following steps are taken:

- (a) an area A is selected for the center square
- (b) incremental ΔA 's are added to A and the ratio of Equation D-7 is computed for each ΔA
- (c) the maximum ΔA satisfying Equation D-7 is found graphically
- (d) the maximum allowable eccentricity e_{\max} is calculated by Equation D-3 for the area $A + \Delta A$.

The e_{\max} values thus obtained are shown as functions of area $A + \Delta A$ in Figure D-7. The form of these curves is anticipated by noting that

$$\lim_{A \rightarrow \infty} \left\{ C_d ([A + \Delta A]_c) - C_d ([A + \Delta A]_{cs}) \right\} = 0.$$

To Keep Dose Rate Error $\leq 10\%$

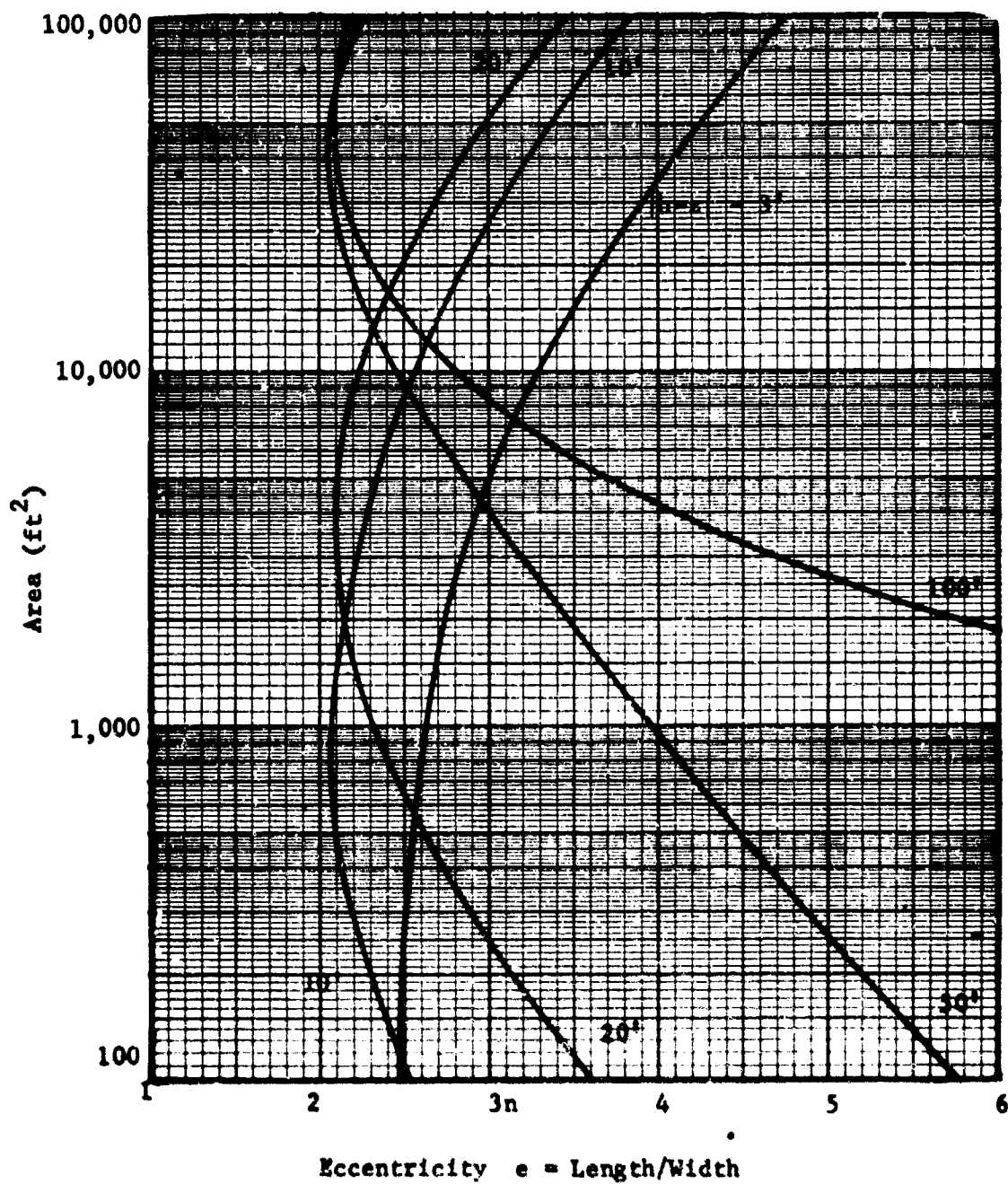


Figure D-7
Maximum Eccentricity Ratios For Centered Rectangular Areas

since as the center square area increases, the dose rate from A approaches the dose rate from the entire plane. And

$$\lim_{[A + \Delta A] \rightarrow 0} \left\{ C_d([A + \Delta A]_c) - C_d([A + \Delta A]_s) \right\} = 0 ,$$

since a zero area contributes zero dose rate regardless of the "eccentricity".

B. Off-center Areas

As implied by the title "Point-Source Model", we wish to establish a scheme to represent areas of contamination by point sources. There was no requirement to introduce point sources for centered areas in the previous section. For off-center areas we shall establish criteria by which off-center areas may be represented by an equivalent point source at the center of the area. Actually we will not use point source data. To approximate the dose contribution from the area, we will multiply the area by the contribution per unit area at the center of the area. This approach requires two sets of data for its application. First, the dose rate contribution per unit area as a function of horizontal distance from the detector is required for each detector height. Next, a set of criteria for the maximum area which can be treated in this manner must be established.

1. Dose Rate Contribution Per Unit Area

The dose rate contribution per unit area as a function of horizontal distance from the detector was calculated for each detector height using the equation

$$C_1(|h-z|, r) = \frac{C_d(|h-z|, r + \frac{\Delta r}{2}) - C_d(|h-z|, r - \frac{\Delta r}{2})}{2\pi r \Delta r} \quad (D-8)$$

where

$|h-z|$ = vertical separation of detector and source area

r = horizontal separation of detector and center of source area

$C_1(|h-z|, r)$ = contribution per unit area at center of source

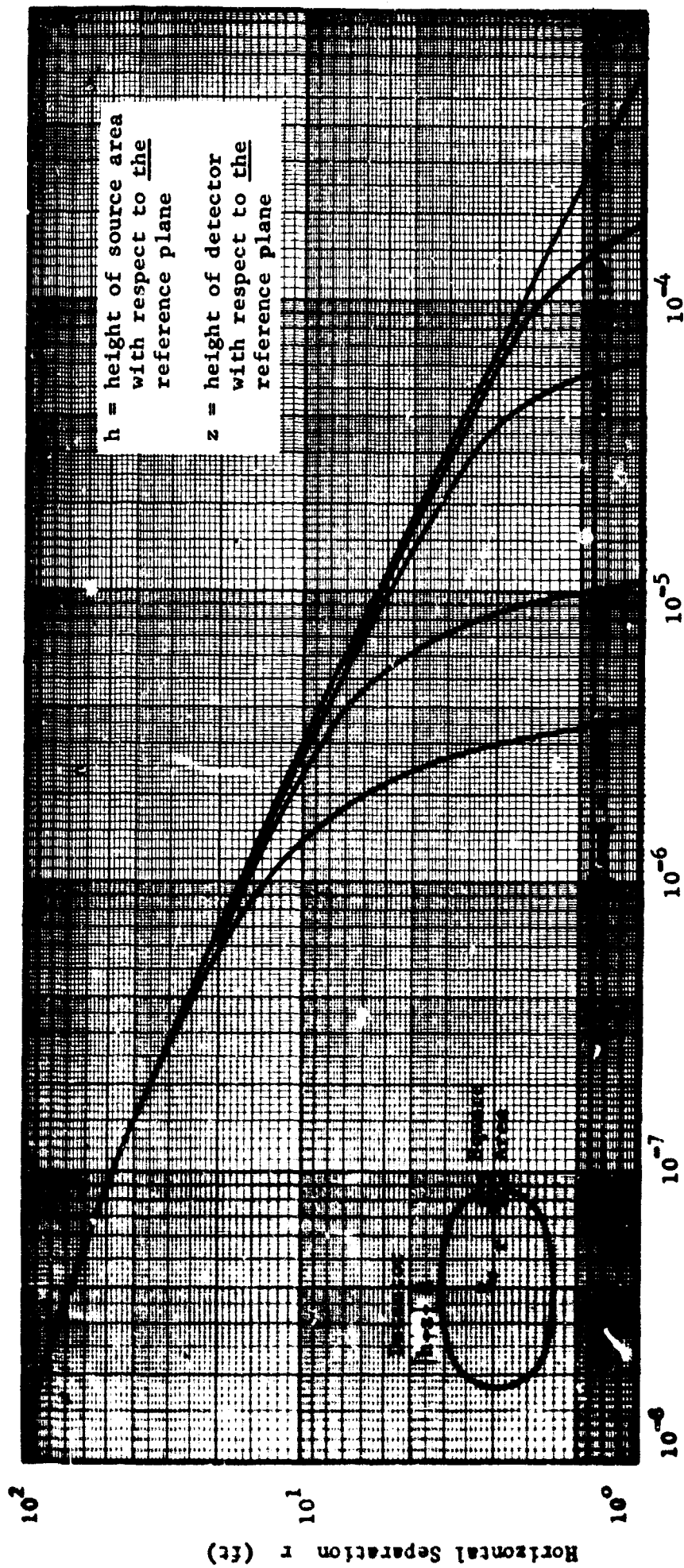


Figure D-8

Dose Rate Contribution Per Unit Area

$C_d(|h-z|, r)$ = contribution from a centered area of radius r as defined in Equation D-2, (the change of argument from A to r is only for clarity in Equation D-8)

$2\pi r \Delta r$ = area between circles of radius $r - \frac{\Delta r}{2}$ and $r + \frac{\Delta r}{2}$.

The function $C_1(|h-z|, r)$ is presented in Figure D-8 for the selected $|h-z|$ values of 3, 10, 20, 50, and 100 feet.

The differencing in Equation D-8 to obtain these values must be accomplished before the maximum allowable Δr is established. To assure the validity of these values, the increments are chosen well below values which previous work (Appendix C) and judgement indicated would be the maximum values of Δr . These judgements are confirmed by the maximum values of Δr established below.

2. Maximum Area to be Represented by a Point

Since there was obviously some limit to the validity of the point source approximation, the following limiting arguments were devised. Consider the convex function shown in Figure D-9.

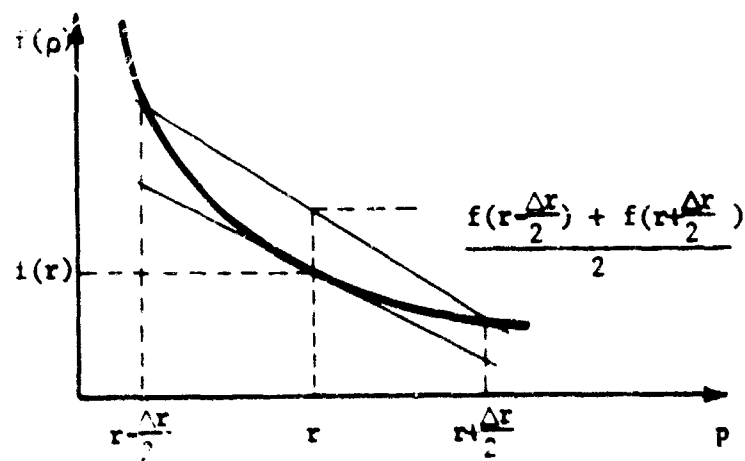


Figure D-9

Approximations on a Convex Function

Because of the convexity of the function, the tangent to $f(\rho)$ at any point touches the curve only at that point, and the chord from $(f(r)$ at $r - \frac{\Delta r}{2}$) to $(f(r)$ at $r + \frac{\Delta r}{2})$ intersects the curve only at the two end points. Thus,

$$f(r) \Delta r \leq \int_{r - \frac{\Delta r}{2}}^{r + \frac{\Delta r}{2}} f(\rho) d\rho \leq \left[\frac{f(r - \frac{\Delta r}{2}) + f(r + \frac{\Delta r}{2})}{2} \right] \Delta r$$

and

$$\int_{r - \frac{\Delta r}{2}}^{r + \frac{\Delta r}{2}} f(\rho) d\rho - f(r) \Delta r \leq \left[\frac{f(r - \frac{\Delta r}{2}) + f(r + \frac{\Delta r}{2})}{2} \right] \Delta r - f(r) \Delta r \quad (D-9)$$

which means that the error introduced in approximating the integral by $f(r)\Delta r$ is less than or equal to the difference between $f(r)$ and the average of $f(r - \frac{\Delta r}{2})$ and $f(r + \frac{\Delta r}{2})$.

The dose per unit area functions, $C_1(|h-z|, r)$ are convex over most of their range. The log-log scale of Figure D-8 obscures this fact, but the general form of each of these curves is like that in Figure D-10 when shown on linear scales. The value r_0 , such that $r > r_0$, implies $f(r)$ is convex, is less than ten feet for all of the values of $|h-z| \leq 100$ feet. The inequality (D-9) thus is used in establishing the criterion for maximum area to be represented by a point. Only the convex portions of the $C_1(|h-z|, r)$ functions are used.

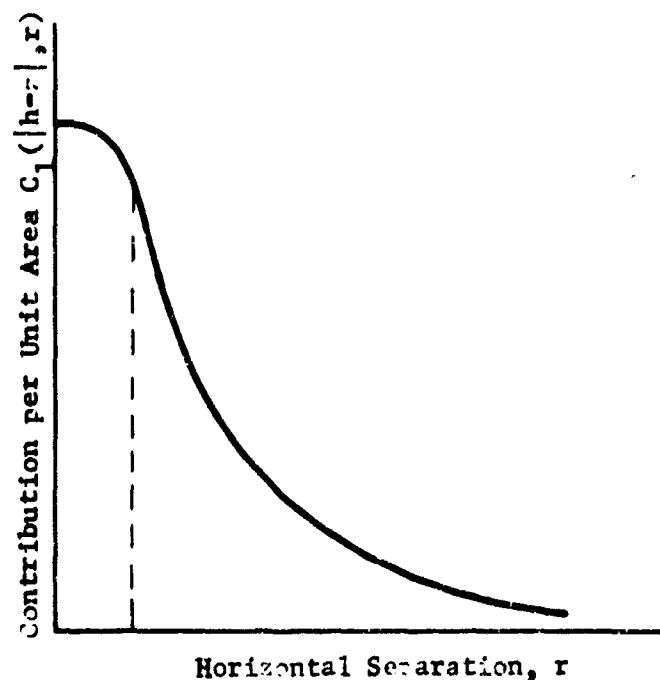


Figure D-10

Form of $C_1(|h-z|, r)$ Functions

As stated earlier, in accordance with our objective of making a slightly conservative estimate of decontamination effectiveness, we establish the criterion

$$\frac{C_1(|h-z|, r + \frac{\Delta r}{2}) + C_1(|h-z|, r - \frac{\Delta r}{2})}{2} - C_1(|h-z|, r) \leq 0.1 \quad (D-10)$$

It has been shown that the dose contribution from an off-center square area is insensitive to the orientation. Thus we set the maximum area to be represented by a point located at its center to be a square of area $A_{\max} (\Delta r_{\max})^2$, where Δr_{\max} is the maximum Δr satisfying the condition of Equation D-10, and where r is the horizontal distance to the center of the square area. For areas which are not square, the criterion should be that the maximum dimension is less than or equal to Δr_{\max} . The locus of maximum

square area to be represented by a point at the center is given in Figure D-11 for each of the detector heights 3, 10, 20, 50, and 100 feet. If the area does not meet the criterion, it should be subdivided into areas which do.

C. Shielding

In the previous sections we have considered only unshielded detectors. In this section we shall obtain conventional multiplicative factors to account for shielding. The cases considered are:

- (a) horizontal shielding between the detector and a centered area of contamination;
- (b) horizontal shielding between the detector and an off-center area of contamination; and
- (c) vertical shielding between the detector and an off-center area of contamination.

1. Centered Areas and Horizontal Barriers

The horizontal barrier shielding factor for centered areas B_o is given by the equation

$$B_o(X_o, |h-z|, A) = \frac{C_o(X_o, |h-z|, A)}{C_o(0, |h-z|, A)} = \frac{C_o(X_o, \omega)}{C_o(0, \omega)} \quad (D-11)$$

where

- X_o = shield equivalent mass thickness in psf
- $|h-z|$ = vertical separation of detector and source in feet
- A = area in square feet
- ω = solid angle fraction subtended by area A at height $|h-z|$
- $C_o(X_o,)$ = overhead contribution for the given X_o and ω (Reference D-3)

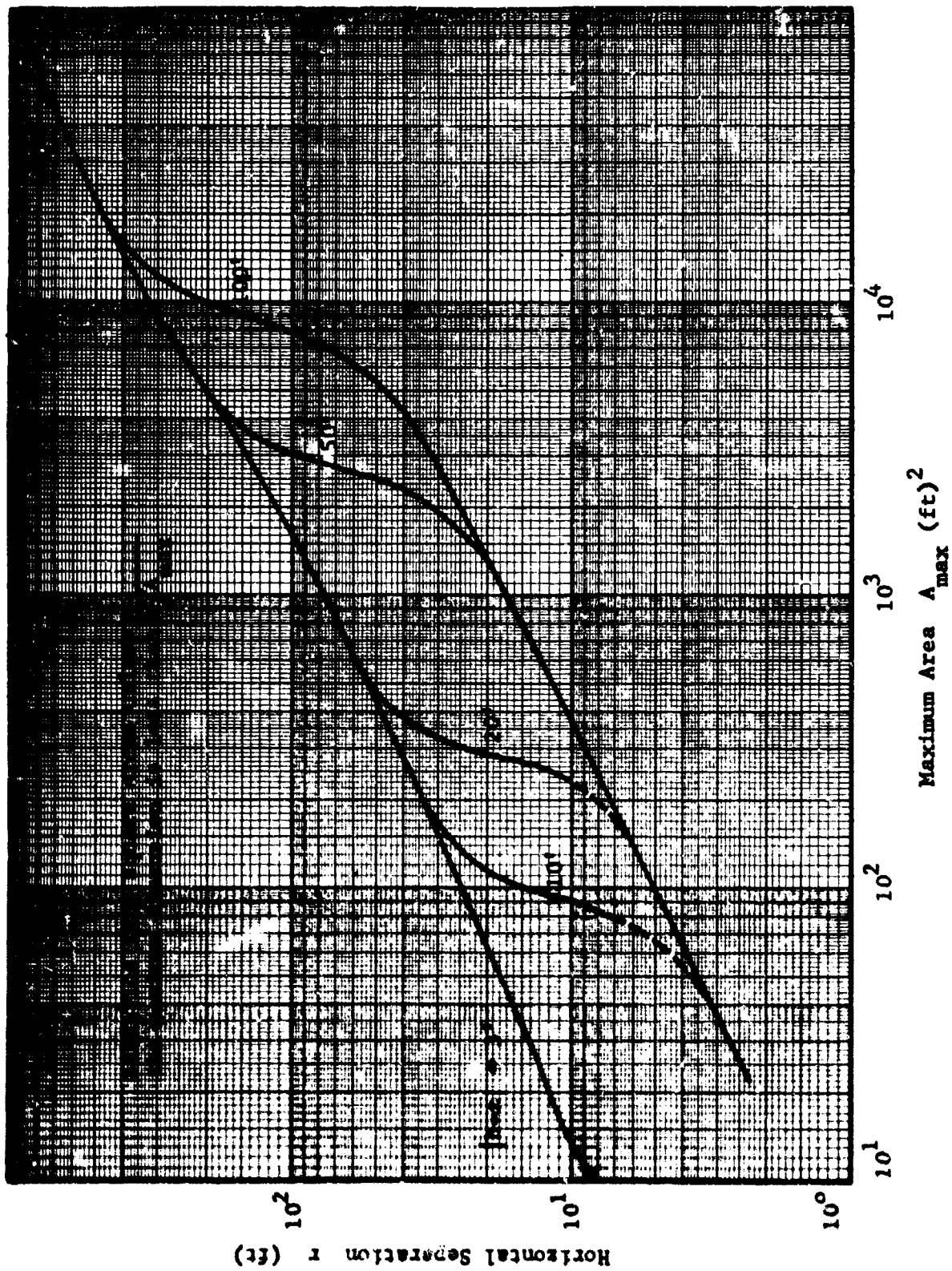


Figure D-11
Maximum Square Area To Be Represented by a Point

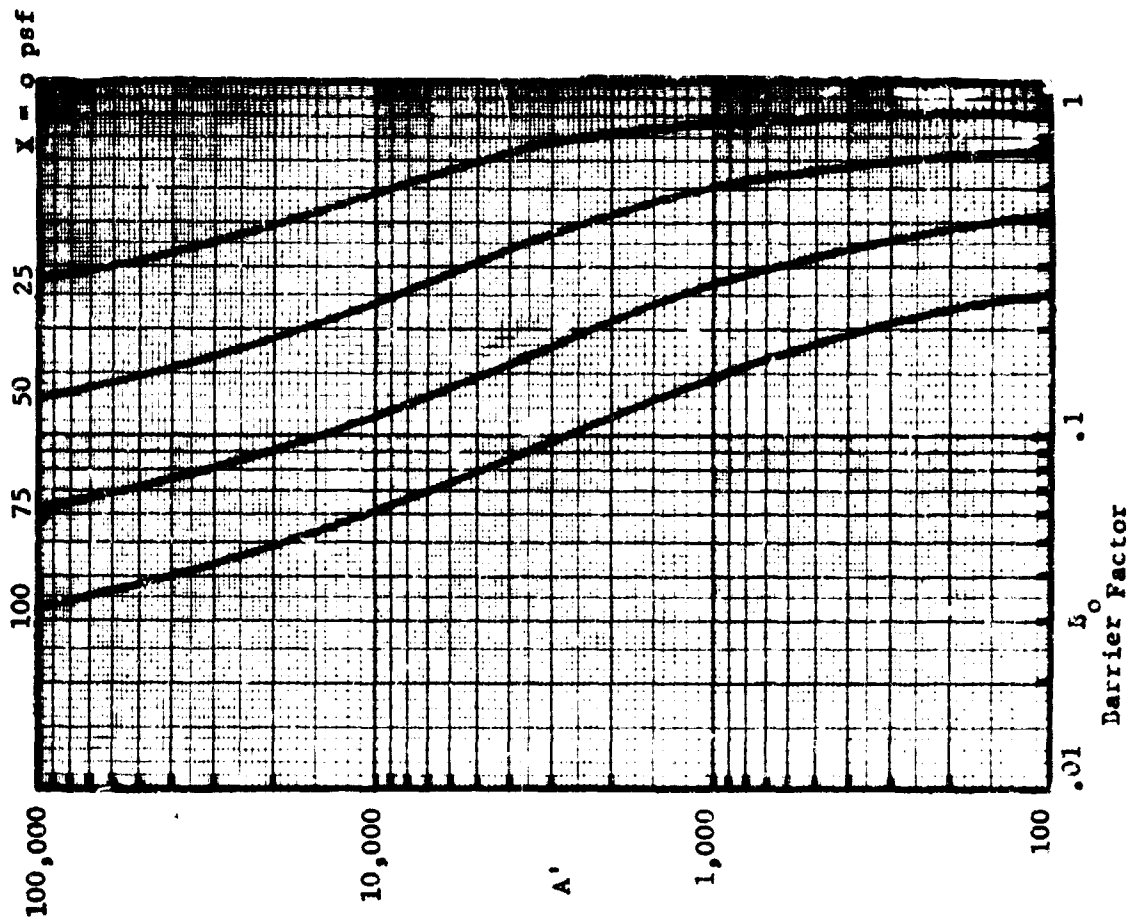
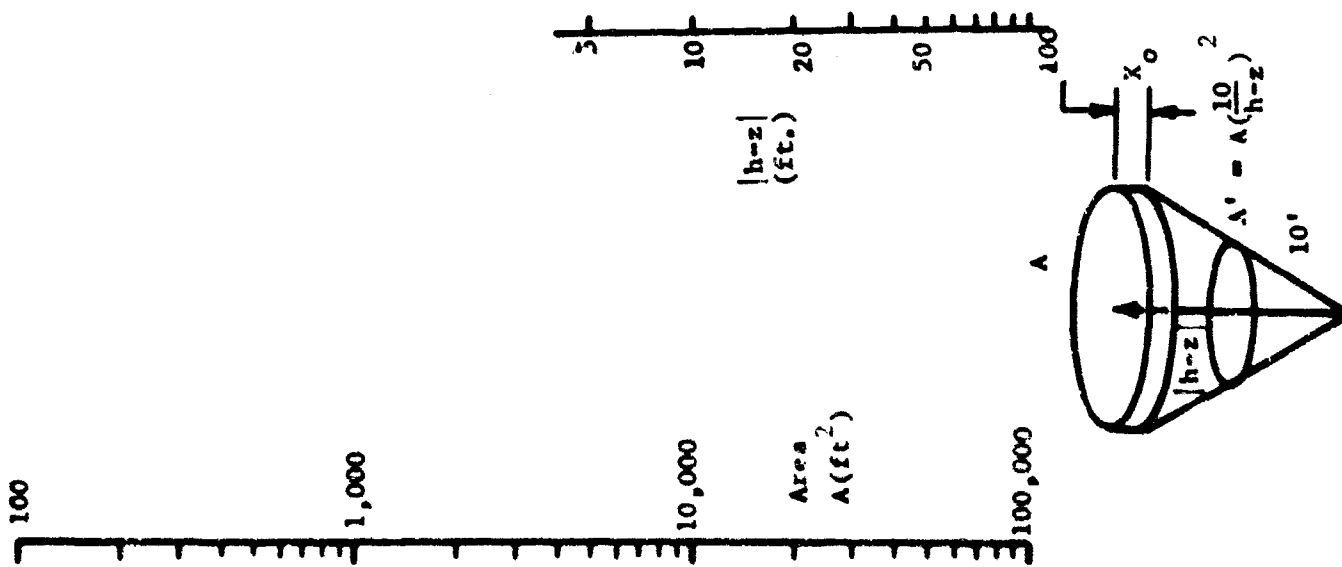


Figure D-12
Horizontal Barrier Factors For Centered Areas

Since $C_0(X_0, \omega)$ is a function only of the solid angle subtended, separate graphs are not given for each $|h-z|$ in Figure D-12. Rather, a nomogram is given in Figure D-12 for converting areas at different $|h-z|$ values to equivalent areas at $|h-z| = 10$ feet. Essentially this is the same approach as that taken in Reference D-5.

The $B_0(X_0, |h-z|, A)$ values of Figure D-12 are used in the following manner to obtain the shielded dose contribution from a centered area:

- (a) find $C_d(|h-z|, A)$ using Figure D-18
- (b) in the Figure D-12 nomogram locate the given area value on the A scale (on the left)
- (c) draw a straight line from this point A' through the given value of $|h-z|$ on the middle scale and continue to the A' scale on the right side
- (d) from the intercept of this line with the A' scale, follow a horizontal line to the curve for the correct X_0 (if X_0 falls between two curves, an interpolation should be made)
- (e) read the $B_0(X_0, |h-z|, A)$ value at the bottom
- (f) multiply $C_d(|h-z|, A)$ by $B_0(X_0, |h-z|, A)$ to obtain $C_d(X_0, |h-z|, A)$.

This would be the contribution from the centered area. Areas also shielded by vertical barriers should be treated as off-center areas.

2. Off-center Areas and Horizontal Barriers

The horizontal barrier shielding factor for off-center areas B_{01} is given by the equation

$$B_{01}(X_0, |h-z|, r) = \frac{C_0(X_0, |h-z|, \pi(r + \frac{\Delta r}{2})^2) - C_0(X_0, |h-z|, \pi(r - \frac{\Delta r}{2})^2)}{C_0(0, |h-z|, \pi(r + \frac{\Delta r}{2})^2) - C_0(0, |h-z|, \pi(r - \frac{\Delta r}{2})^2)} \quad (D-12)$$

where the terms are the same as those defined for Equation D-11, except that the area has been given by a function of the horizontal separation of source and detector.

The values of $B_0(X_0, |h-z|, r)$ are given in Figure D-13. Again, separate curves are not given for each $|h-z|$. The $C_0(X_0, |h-z|, A)$ values are functions only of the solid angle subtended by the Area A which is defined by r in Equation D-12. The nomogram thus can be used for converting radii at different $|h-z|$ values to equivalent radii at $|h-z| = 10$ feet. The B_{01} values of Figure D-13 are used in analogous manner to those of Figure D-12. That is, to obtain the shielding dose contribution from an area:

- (a) find $C_1(|h-z|, r)$ from Figure D-8 and multiply the value by the area (a square area satisfying the criteria of Figure D-11)
- (b) in the Figure D-13 nomograms, locate the given horizontal separation distance r on the r scale (on the left)
- (c) draw a straight line from this point r through the given value of $|h-z|$ on the middle scale and continue to the r' scale on the right side
- (e) read the $B_{01}(X_0, |h-z|, r)$ value at the bottom
- (f) multiply $\left[C_1(|h-z|, r) \right] A$ by $B_{01}(X_0, |h-z|, r)$. (If there are no vertical barriers, this is the contribution from that area.)

3. Vertical Barriers

As a multiplicative barrier factor for vertical barriers, we again need the ratio of the contribution with the barrier present to the contribution without the barrier. First, the case for which no horizontal barriers exist between the source and the vertical barrier is considered. The contributions through the walls are obtained from values in "The Equivalent Building Method" (Reference D-5). To obtain these contributions, we find the protection factors (PF) with no roof contribution (infinite roof weight) and we note that the PF is the reciprocal of the relative contribution through the wall. Thus we obtain

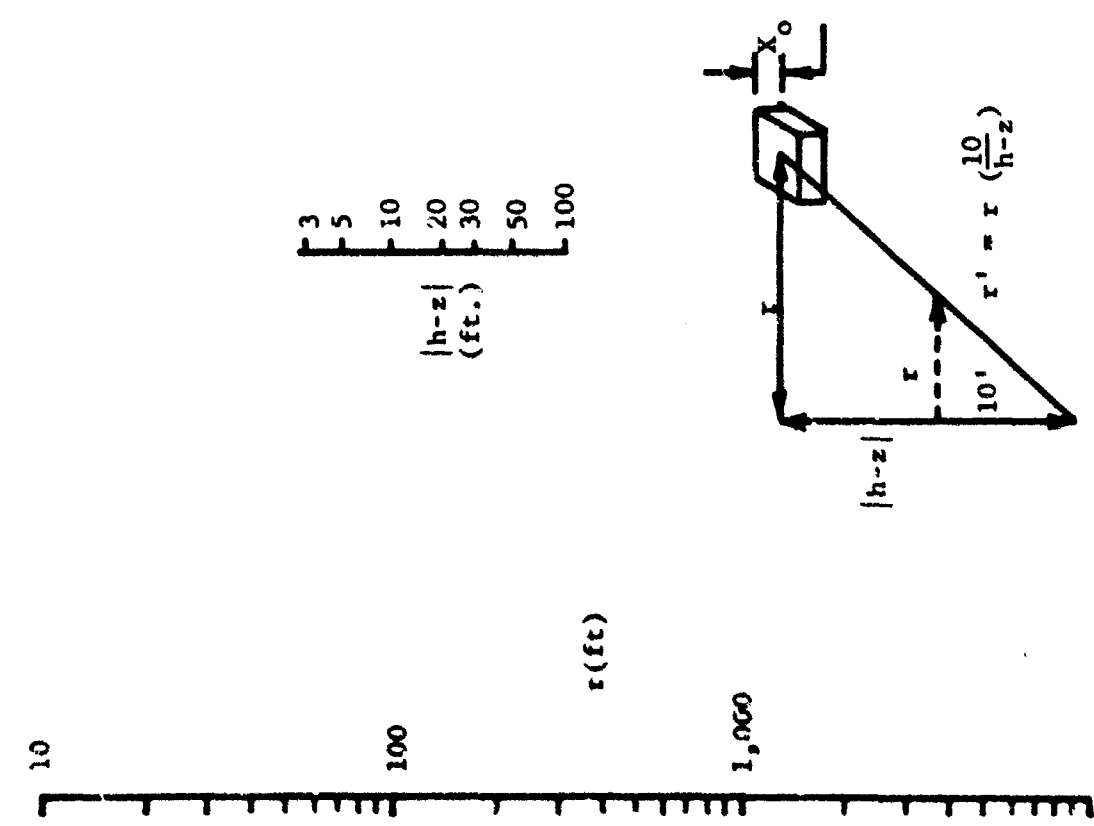
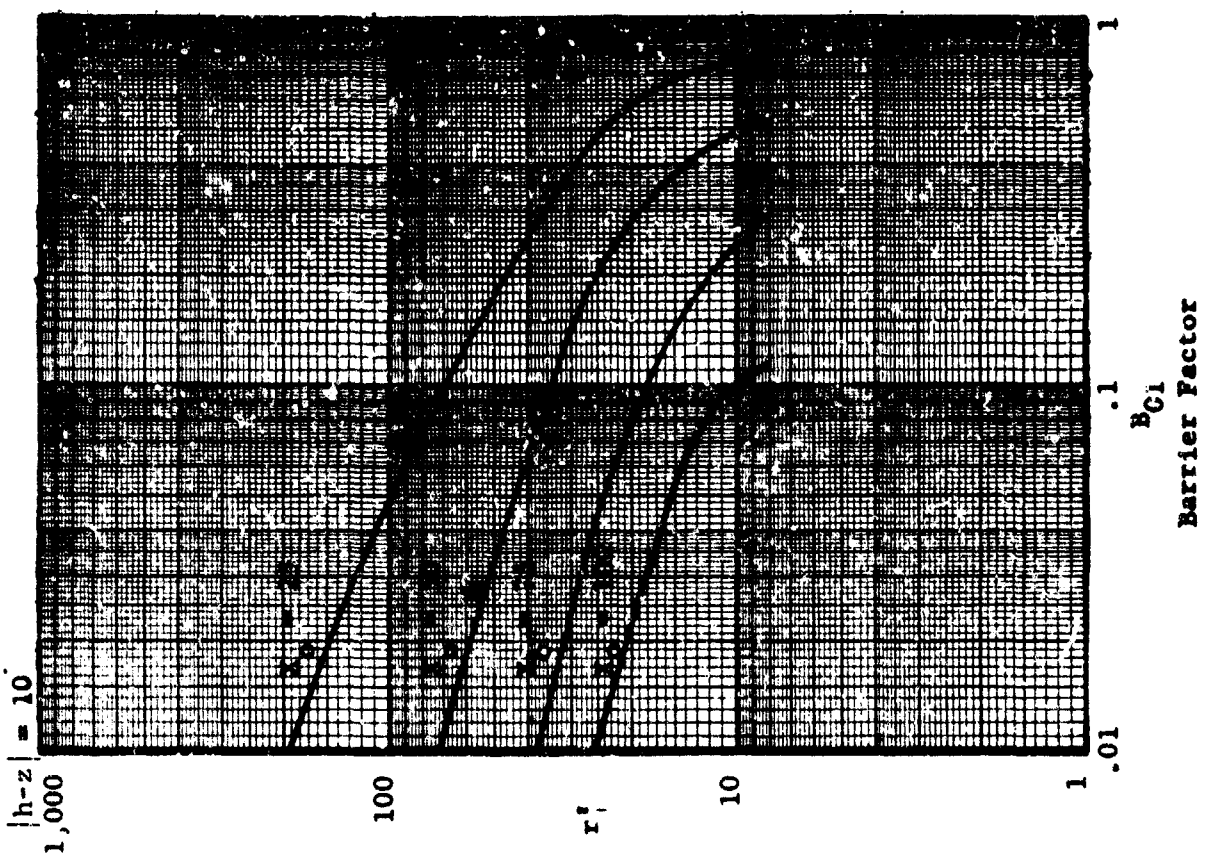


Figure D-13

Horizontal Barrier Factors for Off-Center Areas

$$B_v(X_v) = \frac{C_d(X_v, A^*)}{C_d(0, A^*)} = \frac{PF(\infty, 0, A^*)}{PF(\infty, X_v, A^*)} \quad (D-13)$$

where

$B_v(X_v)$ = vertical barrier factor with no horizontal shield
between the source and the vertical barrier

X_v = equivalent mass thickness, in psf, of the vertical barrier

A^* = $(2r^*)^2$

r^* = horizontal distance from detector to the vertical barrier.

The PF values in Reference D-5 are given for areas A^* in values ranging from 100 to 100,000 square feet. Since these numbers include wall scattering as well as direct attenuation, it is conceivable that the barrier factor $B_v(X_v)$ is also a function of the distance r^* . However, the ratio of equation D-13, when obtained for the complete range of areas A^* given in Reference D-5, shows no appreciable difference between the values obtained for the different areas. That is, the variance introduced by reading the graphs of Reference D-5 was greater than the differences in the values for different areas. Thus, a single curve of $B_v(X_v)$ is given in Figure D-14.

If a horizontal barrier exists between the source and the vertical barrier, the curve derived from Reference D-3 for this configuration will be used. This curve is reproduced in Figure D-14 as $B'_v(X_v)$.

If there are apertures in a vertical barrier, corrections to the mass thickness of the solid portion should be made before using Figure D-14. In the configuration with an intervening horizontal barrier, the mass thickness of the solid wall should be multiplied by the fraction of the wall not voided by apertures. Thus,

$$X_v = (1 - A_p) X \quad (D-14)$$

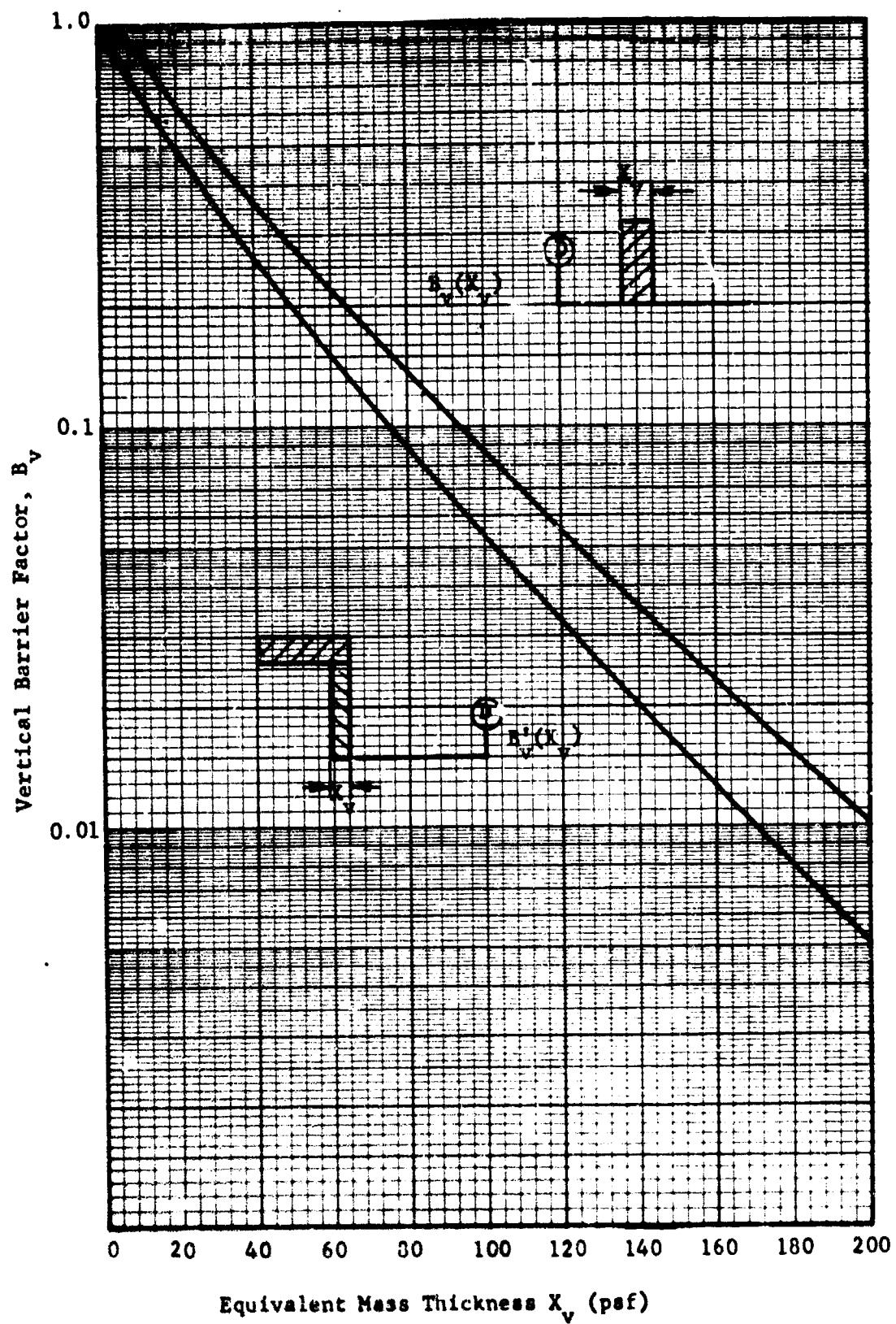


Figure D-14

Vertical Barrier Shielding Factors

where

A_p = fraction of wall voided by apertures

X = mass thickness of solid portion of wall

In the configuration with no intervening horizontal barriers, correction curves for apertures are presented in Reference D-5. However, a consideration of their basis indicates that the correction curves of Reference D-5 deviate somewhat from the form which they should possess (see Chapter III). Because of this deviation, and since the corrections do not differ greatly for different areas A^* , a single "consensus" set of correction curves will be used in this model. Figure D-15 presents the aperture corrections to be applied in this configuration with no intervening horizontal barrier. To use these correction curves, compute the percent of the vertical barrier occupied by apertures $\% A_p$, and determine the mass thickness of the solid portion of the barrier X . For these values of $\% A_p$ and X , read from Figure D-15 the value of X_v to be used in Figure D-14 to obtain $B_v(X_v)$.

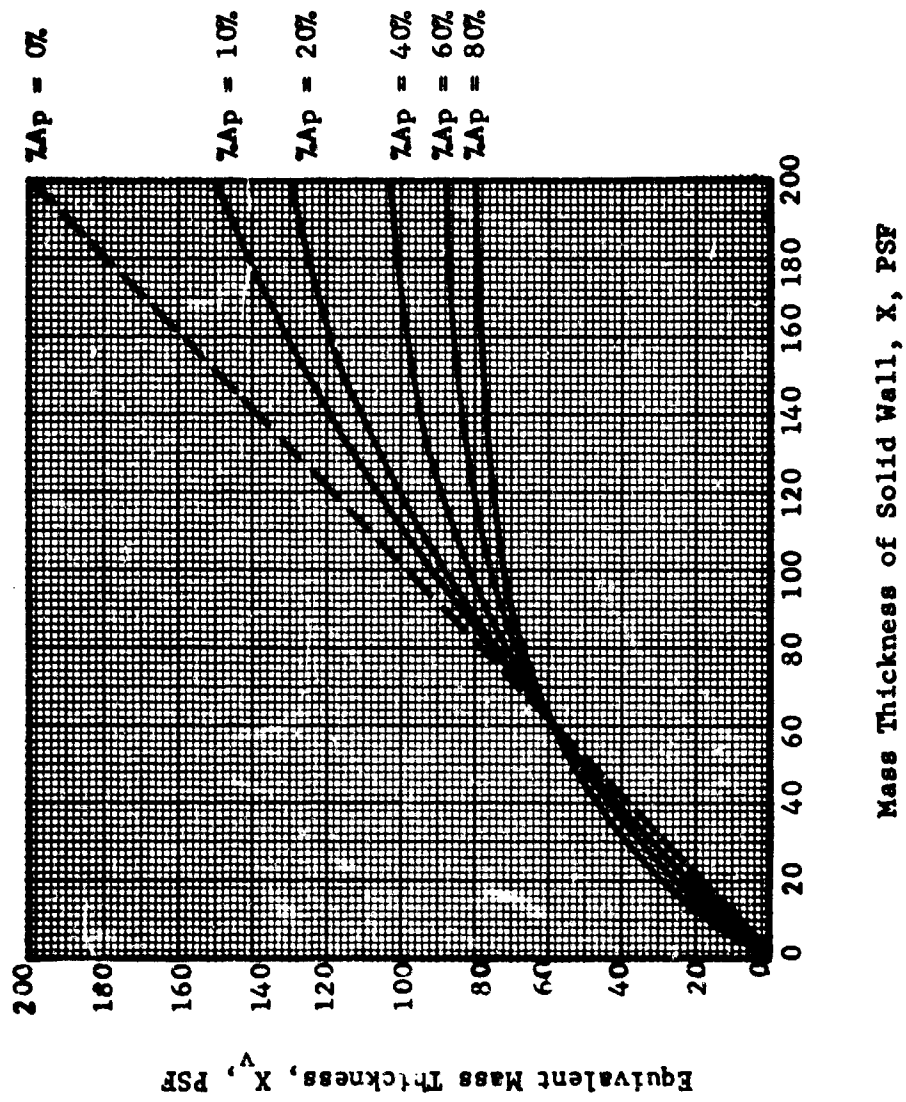


Figure D-15
Correction to Vertical Barriers for Apertures

III. EVALUATION OF EQUIVALENT BUILDING METHOD APERTURE CORRECTIONS

Shelter Design and Analysis Volume II presents the Equivalent Building Method of Fallout Radiation Shielding Analysis Design. The Equivalent Building Method is based on the approximation of reducing a complex shielding situation to an equivalent simple, solid-wall, single-story structure problem. For above the ground, the basic structure assumed in TR-20, Volume II is a solid-wall, single-story, square building. The wall height is 13 feet with the detector 3 feet above the floor. The aperture sill heights are 3 feet, the detector height. Basic structure areas of 100, 1,000, 10,000, and 100,000 square feet are used. For each of these areas a family of curves which relate the protection factor to wall mass thickness, with roof mass thickness as a parameter, is given. When a structure varies from the basic case, an equivalent mass thickness is found from given curves such that a standard structure with this wall weight has the same protection factor as the structure under study. In particular, corrections for apertures are made using Figure 10 of TR-20, Volume II, reproduced here as Figure D-16.

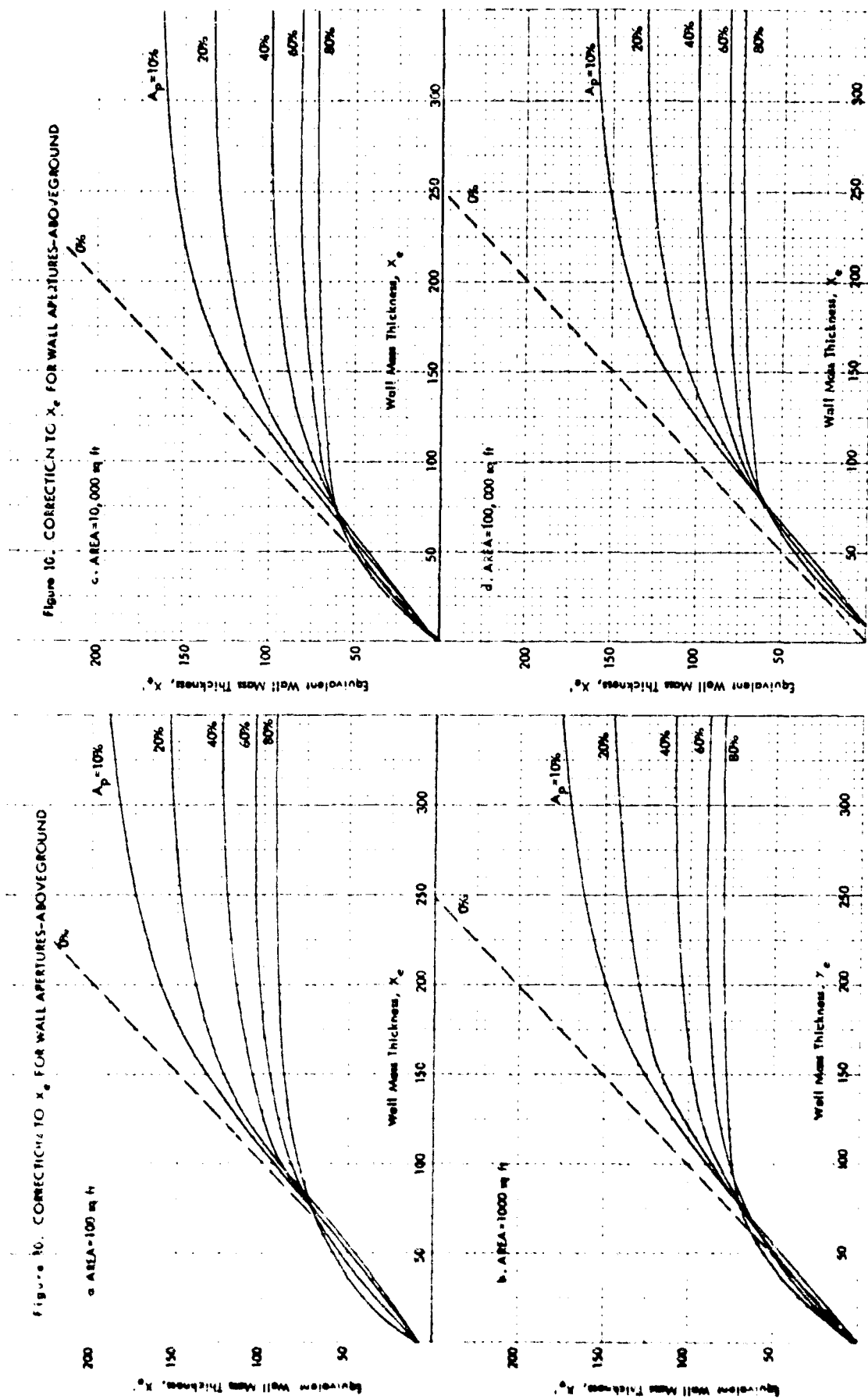
The purpose of this appendix is to examine the peculiarities exhibited by these curves at mass thicknesses less than 100 psf. In Figure D-16, A_p is the fraction of the wall taken by apertures; so let A_p be the fraction of wall above the detector taken by apertures, and let all apertures be above detector height. Only the ground contribution C_g is affected by apertures in the exterior walls; therefore, equivalent wall mass thickness is found by equating ground contributions

$$C_g(A_p, X_e) = C_g(0, X'_e)$$

Since

$$\frac{\partial C_g(0, X_e)}{\partial X_e} < 0$$

(Figures 1 through 4 of References D-3 and D-5)



(Source: Figure 10 of TR-20, Volume II - Reference (1))

Figure D-16
Aperture Corrections

$$C_g(A_p', X_e) \leq C_g(0, X_e) \iff X_e' \geq X_e. \quad (D-15)$$

Using the method of the Engineering Manual (TR-20, Volume I), we have

$$\begin{aligned} C_g(A_p', X_e) = & \left\{ [G_d(\omega_L) + (1-A_p') G_a(\omega_u)] [1-S_w(X_e)] \right. \\ & + [(1-A_p') G_s(\omega_u) + G_s(\omega_L)] S_w(X_e) E \left. \right\} B_e(X_e, H) \\ & + A_p' G_a(\omega_u). \end{aligned} \quad (D-16)$$

Given $A_p' \leq 1$, and $A_p'' \leq 1$, then by equation D-16

$C_g(A_p'', X_e) \leq C_g(A_p', X_e)$ is equivalent to

$$\begin{aligned} & \left\{ -A_p'' G_a(\omega_u) [1-S_w] - A_p'' G_s(\omega_u) S_w E \right\} B_e + A_p'' G_a(\omega_u) \leq \\ & \left\{ -A_p' G_a(\omega_u) [1-S_w] - A_p' G_s(\omega_u) S_w E \right\} B_e + A_p' G_a(\omega_u) \end{aligned}$$

or

$$\begin{aligned} & \frac{A_p''}{A_p'} \left\{ G_a(\omega_u) [1-B_e + S_w B_e] - G_s(\omega_u) S_w E B_e \right\} \geq \\ & G_a(\omega_u) [1 - B_e + S_w B_e] - G_s(\omega_u) S_w E B_e. \end{aligned} \quad (D-17)$$

If

$A_p' = 0$, then by equation D-17, $C_g(A_p'', X_e) \leq C_g(0, X_e)$ if and only if

$$0 \geq G_a(\omega_u) \left[1 - B_e + S_w B_e \right] - G_s(\omega_u) S_w E B_e$$

$$\text{or} \quad \frac{G_s(\omega_u)}{G_a(\omega_u)} \geq \frac{1 - B_e + S_w B_e}{S_w E B_e}, \quad X_e \neq 0. \quad (D-18)$$

Now, for any $A_p' \leq A_p''$, satisfaction of condition D-18 implies satisfaction of condition D-17. Thus, with $A_p'' \geq A_p'$, if all apertures are above the detector, then

$$X_e'' \geq X_e' \iff C_g(A_p'', X_e) \leq C_g(0, X_e) \iff C_g(A_p'', X_e) \leq C_g(A_p', X_e) \\ \iff C_g(0, X_e'') \leq C_g(0, X_e') \iff X_e'' \geq X_e'.$$

For a given area, then X_e' plotted to X_e with A_p' as a parameter has the form of Figure D-17.

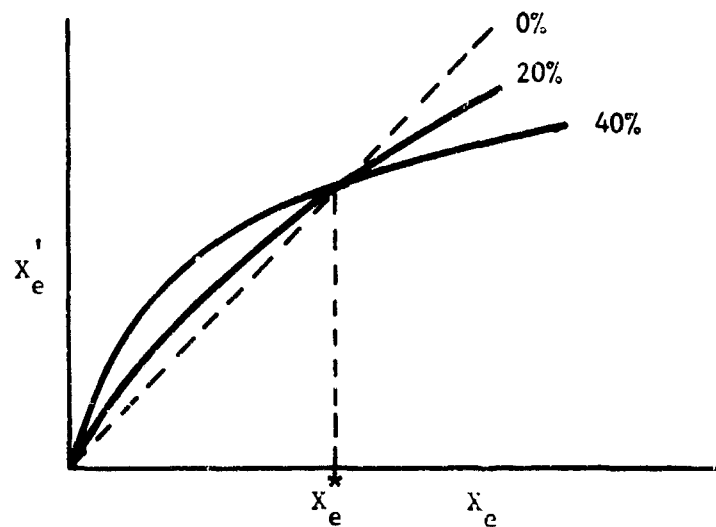
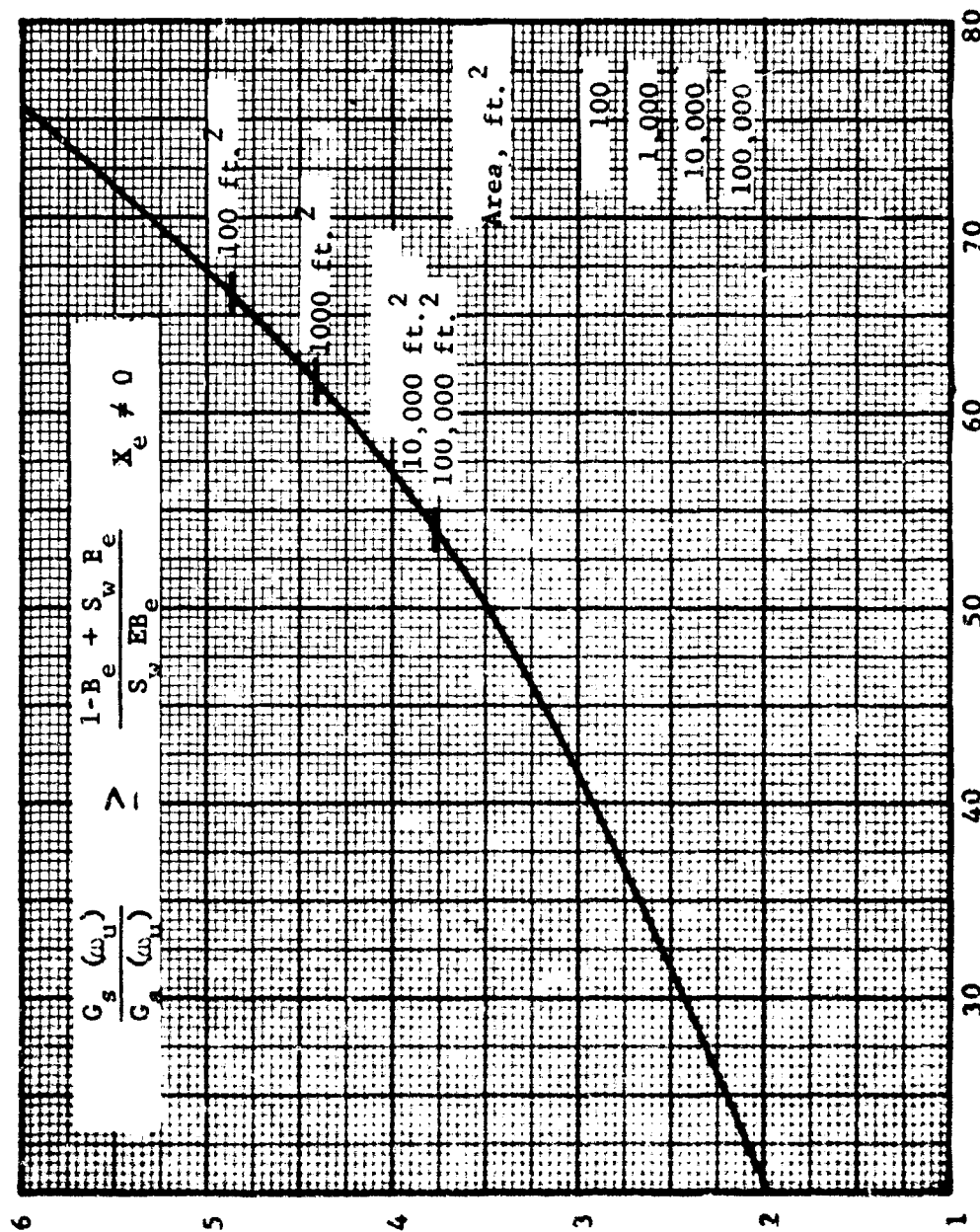


Figure D-17

Correct Form for Aperture Corrections

The crossover point, X_e^* , is given by the equality of condition D-18. In condition D-18, for a given eccentricity ratio, the right side is independent of area and the left side is independent of X_e . The crossover point may then be found as in Figure D-18.



$G_s(\omega_u)/G_a(\omega_u)$

4.87
4.44
3.80
3.78

Figure D-18
Determination of Points of Equality of Condition D-18

IV. AN EXAMPLE ANALYSIS

The application of the point source model is illustrated by a simple, but fairly realistic example. Consider the decontamination situation of Figure D-19. In this example the detector is located three feet above an open area (a parking lot or park, say) which covers a city block. Area I includes the parking lot and the adjoining streets. Area II is the flat roof of a building one block long, 75 feet wide, and 15 feet high. Area III is another parking lot separated from the detector by the building.

The detailed analysis of these three areas is shown in Table D-I. First, the centered area is analyzed; the analysis is very simple in this example since the eccentricity meets the criterion and there is no shielding. If this area does not meet the eccentricity criterion, it should be subdivided and the off-center subdivisions should be treated as other off-center areas.

Since Areas II and III are quite elongated and the areas do not meet the criterion of Figure D-11, they are subdivided into areas which are nearly square (in this case exactly square) and which meet the area criterion in Figure D-11. The data for Area II with $|h-z| = 12$ feet is interpolated between the 10 and 20 foot curves. Note that the horizontal barrier factor B_0 is off-scale on Figure D-12 and thus is carried as an inequality. Note also that the aperture correction for vertical barriers is given by $X_v = (1 - \frac{ZAp}{100}) X$ for Area II where a horizontal barrier exists between the vertical barrier and the source, and is given by Figure D-15 for Area III where there is no horizontal barrier.

In the application of the point-source model, a tabulation sheet such as Table D-I will be found very useful.

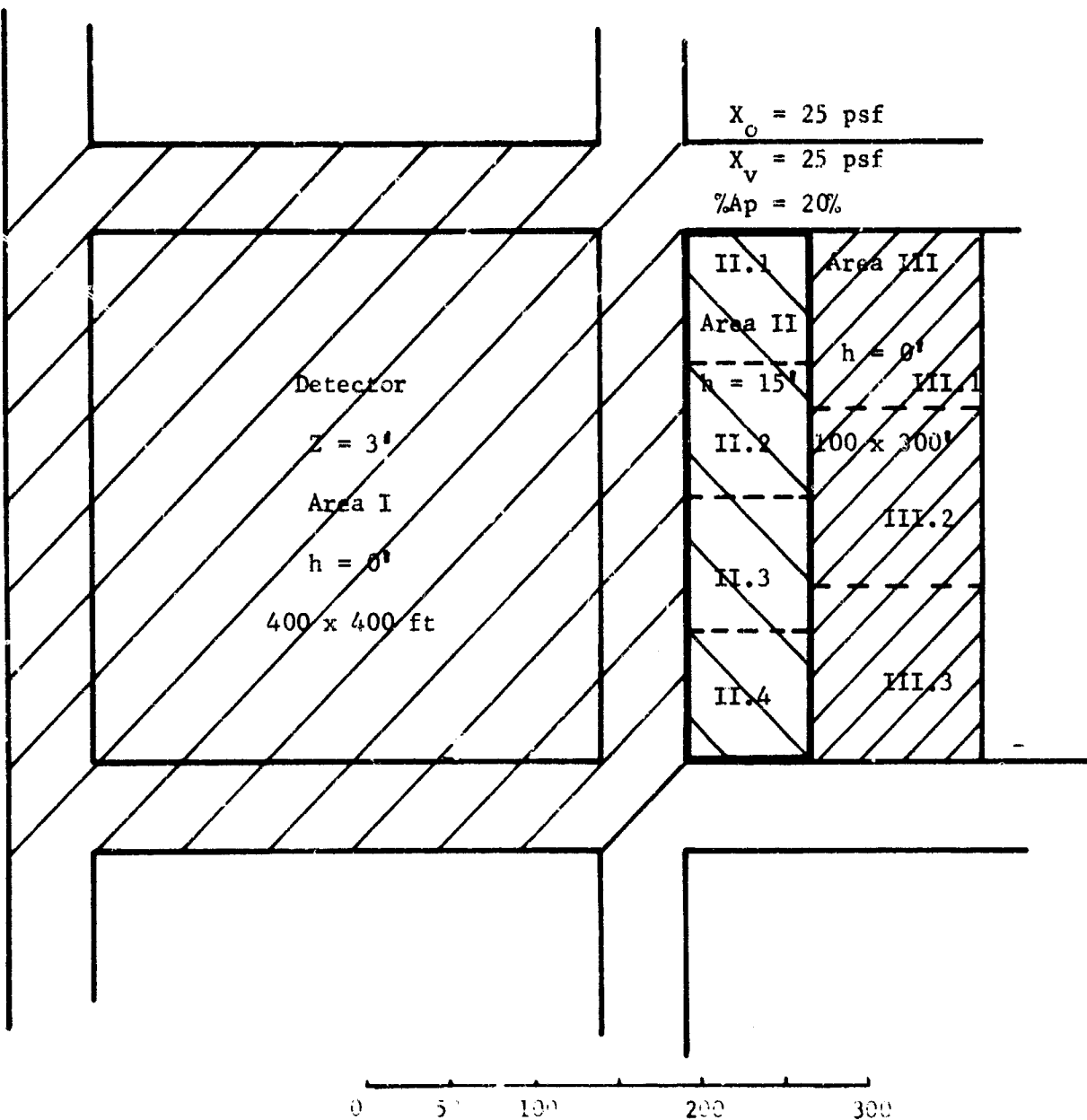


Figure D-19
Example Plan View

Example Analysis

Region	$ h-z $	Area	$E=L/W$	$E \leq E_{\max}$ Chart 3 $A \leq A_{\max}$ Chart 11	Sub-Area No.	Sub-Area	r	Sub-Area $\leq A_{\max}$ Chart 11	$C_1 (h-z r)$ Chart 8	$C_d (h-z , A)$ or $AC_1 (h-z , r)$ Chart 3	Horizontal Barrier X_0 (psf)	B_0 or B_{01} Chart 1
I	3'	16,000	1	Yes	I.1	16,000	-	-	-	5.70 (-1)*	0	
I	12'	22,500	4.0	No	II.1	5625	265	Yes	3.6 (-7)	2.025 (-3)	25	
					II.2	5625	240	Yes	4.5 (-7)	2.53 (-3)	25	
					II.3	5625	240	Yes	4.5 (-7)	2.53 (-3)	25	
					II.4	5625	265	Yes	3.6 (-7)	2.025 (-3)	25	
I	33'	30,000	3.0	No	III.1	10,000	340	Yes	2.0 (-7)	2.0 (-3)	0	
					III.2	10,000	340	Yes	2.25 (-7)	2.25 (-3)	0	
					III.3	10,000	340	Yes	2.0 (-7)	2.0 (-3)	0	

* $5.70(-1) = 5.70 \times 10^{-1}$

TABLE D-1

Example Analysis of Configuration in Figure D-19

Horizontal Barrier X_0 (psf)	$E_0(X_0, h-z , A)$ or $B_{01}(X_0, h-z , r)$ Chart 12 or Chart 13	$C_d \times B_0$, or $AC_1 \times B_{01}$	Vert. Barrier X (psf)	% Ap	Aperture Correction $X_v = (1 - \frac{Z_{ap}}{100})X$ or Chart 15	$B'_v(X_v)$ or $B_v(X_v)$ Chart 14	Contribution $C_d \times B_0 \times B'_v$, $AC_1 \times B_{01} \times B_v$ or $AC_1 \times B_v$	Total Contribution of Sub-Areas in Each area = C_{ij}
0	1.0	5.70(-1)	0	0	0	1.0	5.70 (-1)	5.7 (-1)
25	< .01	< 2.0 (-5)	25	20	20	.49	< 1.0 (-5)	
25	< .01	< 2.5 (-5)	25	20	20	.49	< 1.25 (-5)	
25	< .01	< 2.5 (-5)	25	20	20	.49	< 1.25 (-5)	
25	< .01	< 2.0 (-5)	25	20	20	.49	< 1.0 (-5)	< 4.5 (-5)
0	1.0	2.0 (-3)	50	20	51	.275	5.5 (-4)	
0	1.0	2.25(-3)	50	20	51	.275	6.2 (-4)	
0	1.0	2.0 (-3)	50	20	51	.275	5.5 (-4)	1.72(-3)

B

V. THE EQUIVALENT PLANES METHOD

The Equivalent Planes Method is based on the analyses of the previous sections. The keys to the method are two limiting criteria. The first gives limits on the length-to-width ratio (eccentricity) of an area centered above or below the detector such that the dose contribution is within ten percent of the approximating dose from a centered square of the same area. The other criterion gives limits on the area of an off-center square such that the dose contribution is within ten percent of the approximation given by the product of the area times the dose contribution per unit area from the center of the square.

Shielding factors are presented for above ground detectors which are separated from source areas by relatively light shields. These data should be most applicable to decontamination studies. The dose contributions calculated are suitable for inclusion in formulas for decontamination analysis.

A concise manual, giving a step-by-step procedure for applying the Equivalent Planes Method, is included at the end of this volume. Several data tabulation sheets to be used with the manual are also included.

VI. CONCLUSIONS AND RECOMMENDATIONS

It is concluded that the point-source model can be a useful and realistic method of analyzing fallout radiation contributions for decontamination studies. The real keys to the method are the limiting criteria given in Figures D-7 and D-11. The first criterion, Figure D-7, gives limits on the length-to-width ratio (eccentricity) of an area centered above or below the detector such that the dose contribution is within ten percent of the approximating dose from a centered square of the same area. The other criterion, Figure D-11, gives limits on the area of an off-center square such that the dose contribution is within ten percent of the approximation given by the product of the area times the dose per unit area at the center of the square. These criteria are based on unshielded areas. In future studies it would be desirable to investigate these criteria for shielded areas.

Shielding factors employed in this model are obtained from well-known sources (References D-1, D-2, D-4 and D-5). The approach taken is based on the premise that above ground detectors which are separated from source areas by relatively light shields are of primary interest in decontamination studies. If applications indicate that basement areas and heavier shields are of more interest, the model can readily be extended. Probably it will be found necessary to generate data for X_0 values between zero and 25 psf to fill in Figure D-13 since many "curtain" walls and light roofs have mass thicknesses in this range. The data are not available from Reference D-3, so they will have to be generated directly from Spencer's data, Reference D-1.

REFERENCES

- D-1 L. V. Spencer, Structure Shielding Against Fallout Radiation from Nuclear Weapons, NBS Monograph 42, Washington, D. C.: National Bureau of Standards, 1 June 1962.
- D-2 J. T. Ryan, J. D. Douglass, Jr., and H. E. Campbell, Radiological Recovery Concepts, Requirements and Structures, R-OU-156, Durham, North Carolina: Operations Research and Economics Division, Research Triangle Institute, 16 October 1964.
- D-3 Shelter Design and Analysis, Volume I, Fallout Protection, TR-20-(Vol. I): Department of Defense, Office of Civil Defense, (undated).
- D-4 Protection Factor Estimator, TM-64-11: Department of Defense, Office of Civil Defense, May 1964.
- D-5 Shelter Design and Analysis, Volume II, Equivalent Building Method, TR-20-(Vol. II): Department of Defense, Office of Civil Defense, September 1963.

Appendix E

A FORTRAN Program for Decontamination Analysis

Note: The material in this Appendix was originally submitted to USNRDL as Research Memorandum RM-OU-214-10.*

* C. Dillard and J. Ryan. A FORTRAN Program for Decontamination Analysis. RM-OU 214-10. Durham, North Carolina: Research Triangle Institute, Operations Research and Economics Division, 31 August 1965.

TABLE OF CONTENTS OF APPENDIX E

	<u>Page</u>
TABLE OF CONTENTS.	E- i
I. INTRODUCTION.	E- 1
A. General.	E- 1
B. Contents	E- 1
II. THE COMPUTER PROGRAM.	E-3
A. Introduction	E- 3
B. Data Input Format.	E-4
C. Printed Output Format.	E-7
D. Detailed Flow Charts of Computer Program	E-10
E. Card Listing of Sample Input Deck.	E-25

Appendix E

A FORTRAN Program for Decontamination Analysis

I. INTRODUCTION

A. General

This appendix describes a computer program written in FORTRAN to compute the effectiveness parameters used to analyze municipal decontamination. The program was written in FORTRAN 64 to be used on large scale computers such as the CDC 3600. The program has been debugged and tested and has been used under OCD work unit 3233B.

For a given level of decontamination the program is capable of determining both the reductions in dose-rate at specified detector locations and the reductions in total dose for persons spending prescribed amounts of time at specified detector locations. Other parameters used in the analysis of municipal decontamination, such as the PF's at the detector locations and the equivalent PF's* associated with the activities (without decontamination), are also computed.

B. Contents

Section II of this Appendix is a description of the computer program and includes:

1. a list of the equations which are computed
2. the data input formats
3. the printed output formats

* The basic equation defining the equivalent protection factor is:

$$EPF = \frac{1}{f_1/P_1 + f_2/P_2 + \dots + f_n/P_n}$$

where f_i is the fraction of time spent with protection P_i .

4. the detailed flow charts
5. a card listing of the program with a set of sample inputs
6. a sample output of the program.

II. THE COMPUTER PROGRAM

A. Introduction

The CDC 3600 FORTRAN program computes the values of the following: the protection factor (PF) at each location, the equivalent protection factor (EPF) for each activity pattern, the fraction (CF) of the total intensity prior to decontamination at a given detector due to a particular contaminated plane, the intensity reduction factor (RN) for each decontamination strategy at each detector location, and the activity dose reduction factor (RN_A) for each combination of activity and decontamination strategy at all detector locations.

Calculations are made from the following input data: Contributions (C) to intensity at each detector location from each plane of contamination, the fraction (f) of time that an individual spends at each detector location performing each particular activity, the mass reduction factor (f) for each decontamination strategy, and the key (S) to associate the appropriate value of F with each composite decontamination strategy for each plane.

The program is designed to accept a maximum of twelve each: detector locations, planes of contamination, activity patterns, composite decontamination strategies; and twenty mass reduction factor values.

The equations used to compute the above parameters are the following:

$$PF_j = \frac{1}{\sum_{i=1}^p C_{ij}} \quad (E\ 1)$$

$$EPF_k = \frac{1}{\sum_{j=1}^d \left(\frac{f_{kj}}{PF_j} \right)} \quad (E-2)$$

$$CF_{ij} = \frac{C_{ij}}{\sum_{i=1}^p C_{ij}} \quad (E\ 3)$$

$$RN_{jh} = \sum_{i=1}^d (CF_{ij}) (Fs_{hi}) \quad (E-4)$$

$$RNA_{kh} = \frac{\sum_{j=1}^d \left(\frac{f_{kj}}{PF_j} \right) (RN_{jh})}{\sum_{j=1}^d \frac{f_{kj}}{PF_j}} \quad (E-5)$$

where:

j identifies the detector location; d, the number of detector locations

j = 1, 2, ..., d (d maximum = 20)

i identifies the plane of contamination; p, the number of planes of contamination

i = 1, 2, ..., p (p maximum = 12)

k identifies the activity pattern; a, the number of activity patterns

k = 1, 2, ..., a (a maximum = 20)

ℓ identifies the decontamination strategy; s, the number of decontamination

strategies. ℓ = 1, 2, ..., s (s maximum = 20)

h identifies the composite decontamination strategy; c, the number of composite

decontamination strategies. h = 1, 2, ..., c (c maximum = 100)

C_{ij} identifies the contribution to intensity at j detector location from ith plane of contamination

f_{kj} identifies the fraction of time spent at detector location j performing the activity denoted by k

F_{ℓ} identifies the mass reduction factor (fraction of fallout remaining) for decontamination strategy ℓ

S_{hi} identifies which strategy ℓ is used to decontaminate plane i for composite strategy h

B. Data Input Format

The first input card, identified by a 2 in card column one, specifies the

number of values to be entered for each variable subscript in integer form (XX) as shown below:

cc 1	cc 2,3	cc 4,5	cc 6,7	cc 8,9	cc 10,11
<u>2</u>	<u>XX</u>	<u>XX</u>	<u>XX</u>	<u>XX</u>	<u>XX</u>
I d e n t	d	p	a	s	c

Each value for each of the input variables C_{ij} and f_{kj} is entered on a separate card and entered in sequence by row ($A_{1,1}, A_{1,2}, A_{1,3}, \dots, A_{1,n}; A_{2,1}, A_{2,2}, A_{2,3}, \dots, A_{2,n}; A_{m,1}, A_{m,2}, A_{m,3}, \dots, A_{m,n}$).

cc 1	cc 2-10	cc 1	cc 2-5
<u>3</u>	<u>XXXXXXXXXX</u>	<u>4</u>	<u>X . X X</u>
I d e n t	C_{ij} (Real Number)	I d e n t	f_{kj} (Real Number)

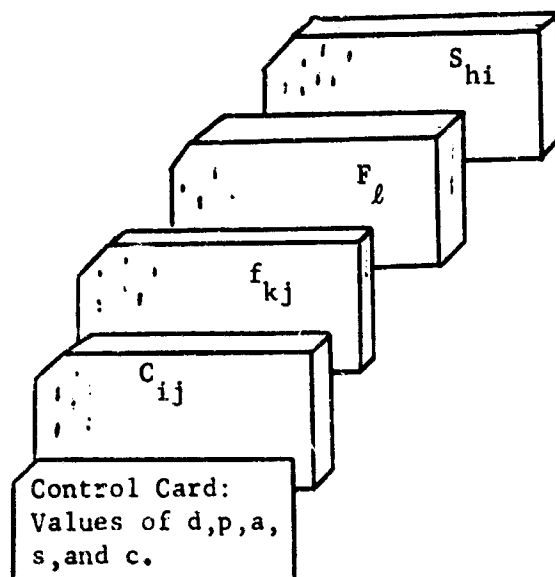
The values for input variables F_ℓ (up to twenty) are entered from a single card. The first value, which serves also as the identification number, in card columns 1-4 must always be 1.00.

cc 1-4	cc 5-8	cc 9-12	cc 13-16	cc 17-20	cc 21-24	cc 25-28	cc 29-32	cc 33-36	cc 37-40	cc 41-44	cc 45-48
1.00 F ₁	X.XX F ₂	X.XX F ₃	X.XX F ₄	X.XX F ₅	X.XX F ₆	X.XX F ₇	X.XX F ₈	X.XX F ₉	X.XX F ₁₀	X.XX F ₁₁	X.XX F ₁₂

The values for input variable S_{hi} (up to twelve planes) are entered by row, each row completed in one card which is numbered in sequence:

5	XXX	XX	XX	XX	XX	XX	XX	XX	XX	XX	XX	XX	XX
I _{dent}	Serial No.	S _{h,1}	S _{h,2}	S _{h,3}	S _{h,4}	S _{h,5}	S _{h,6}	S _{h,7}	S _{h,8}	S _{h,9}	S _{h,10}	S _{h,11}	S _{h,12}

Data cards are to be entered in the following sequence:



C. Printed Output Format

D = XX, P = XX, A = XX, S = XX, C = XX

Values of C(J,I)--

Detector Location	PLANE NUMBER				p
	1	2	3		
No. 1	.XXXXXXXX	.XXXXXXXX	.XXXXXXXXXXXXXXXX
No. 2	.XXXXXXXX	.XXXXXXXX	.XXXXXXXXXXXXXXXX
No. 3	.XXXXXXXX	.XXXXXXXX	.XXXXXXXXXXXXXXXX

No. d	.XXXXXXXX	.XXXXXXXX	.XXXXXXXXXXXXXXXX

Values of FR(J,K)--

Detector Location	ACTIVITY PATTERN NUMBER				a
	1	2	3		
No. 1	X.XX	X.XX	X.XX	. . .	X.XX
No. 2	X.XX	X.XX	X.XX	. . .	X.XX
No. 3	X.XX	X.XX	X.XX	. . .	X.XX

No. d	X.XX	X.XX	X.XX	. . .	X.XX

Values of S(H,I)--

X.XX X.XX X.XX . . . X.XX

Values of S(H,I)--

Composite Strategy	PLANE NUMBER				p
	1	2	3		
No. 1	XX	XX	XX	. . .	XX
No. 2	XX	XX	XX	. . .	XX
No. 3	XX	XX	XX	. . .	XX

No. c	XX	XX	XX	. . .	XX

PF(J) =

Detector
Location

No. 1 XXXX.XX

No. 2 XXXX.XX

. . .

No. d XXXX.XX

EPF(K) =

Activity
Pattern

No. 1 XXXX.XX

No. 2 XXXX.XX

. . .

No. a XXXX.XX

CF(J,I) =

Detector Location	PLANE NUMBER					p
	1	2	3	4		
No. 1	X.XX	X.XX	X.XX	X.XX	. . .	X.XX
No. 2	X.XX	X.XX	X.XX	X.XX	. . .	X.XX
No. 3	X.XX	X.XX	X.XX	X.XX	. . .	X.XX

No. d	X.XX	X.XX	X.XX	X.XX	. . .	X.XX
Check by summing CF(I,J) on each J. Should equal 1.						
	X.XX	X.XX	X.XX	X.XX		X.XX

RN(H,J) =

Composite Strategy	DETECTOR LOCATION NUMBER					d
	1	2	3	4		
No. 1	X.XX	X.XX	X.XX	X.XX	. . .	X.XX
No. 2	X.XX	X.XX	X.XX	X.XX	. . .	X.XX
No. 3	X.XX	X.XX	X.XX	X.XX	. . .	X.XX

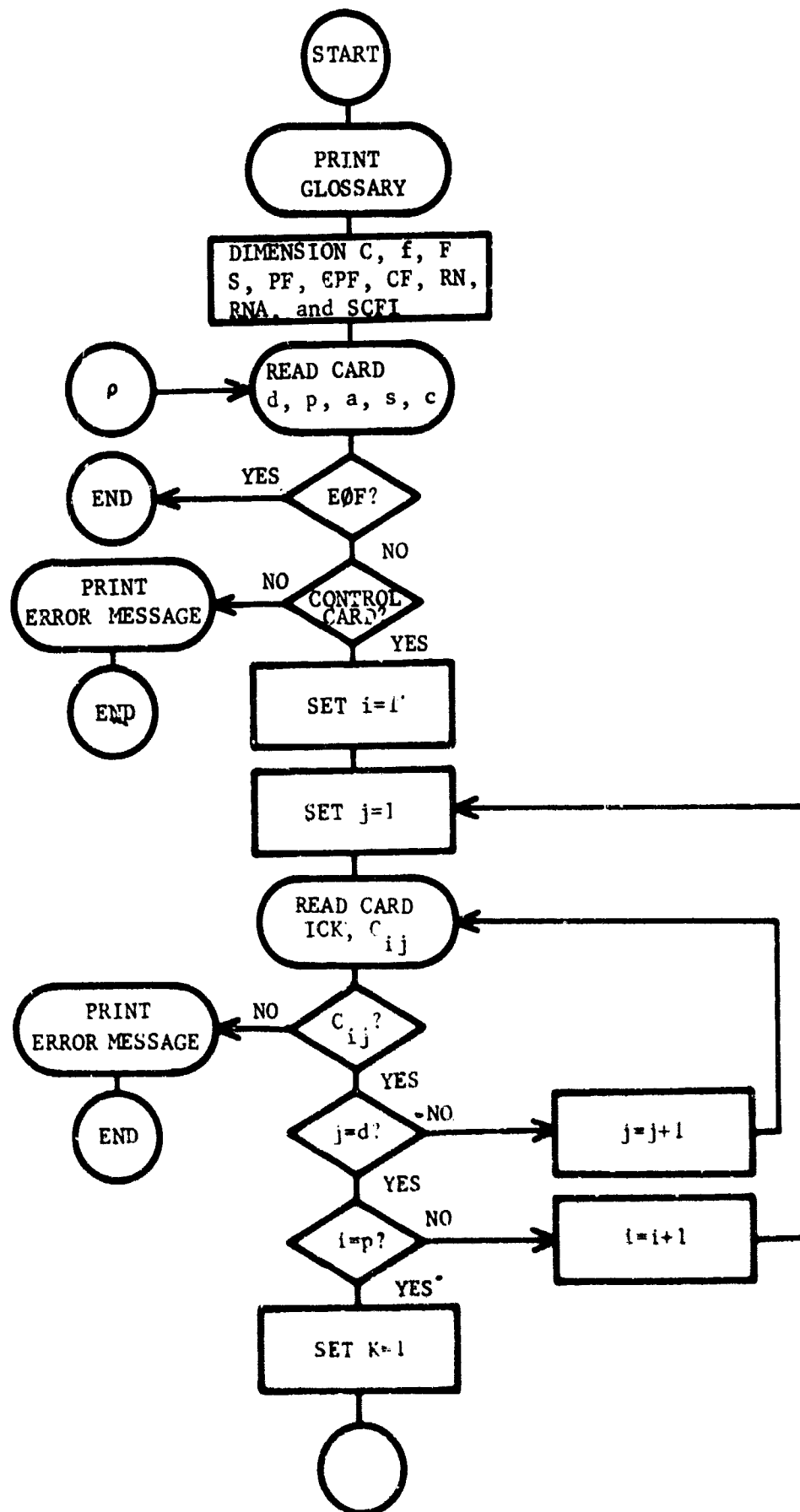
No. c	X.XX	X.XX	X.XX	X.XX	. . .	X.XX

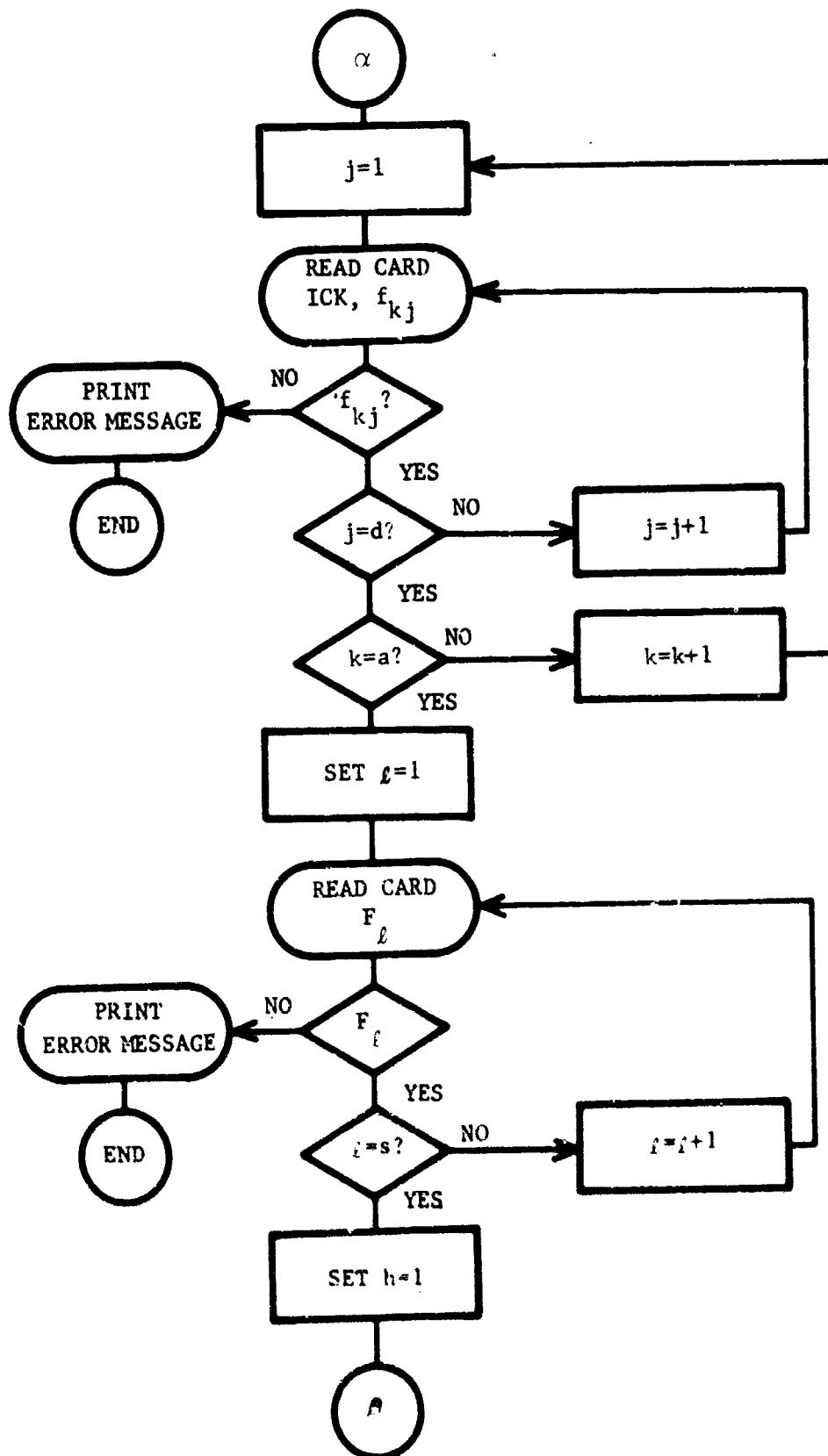
RNA(H,K) =

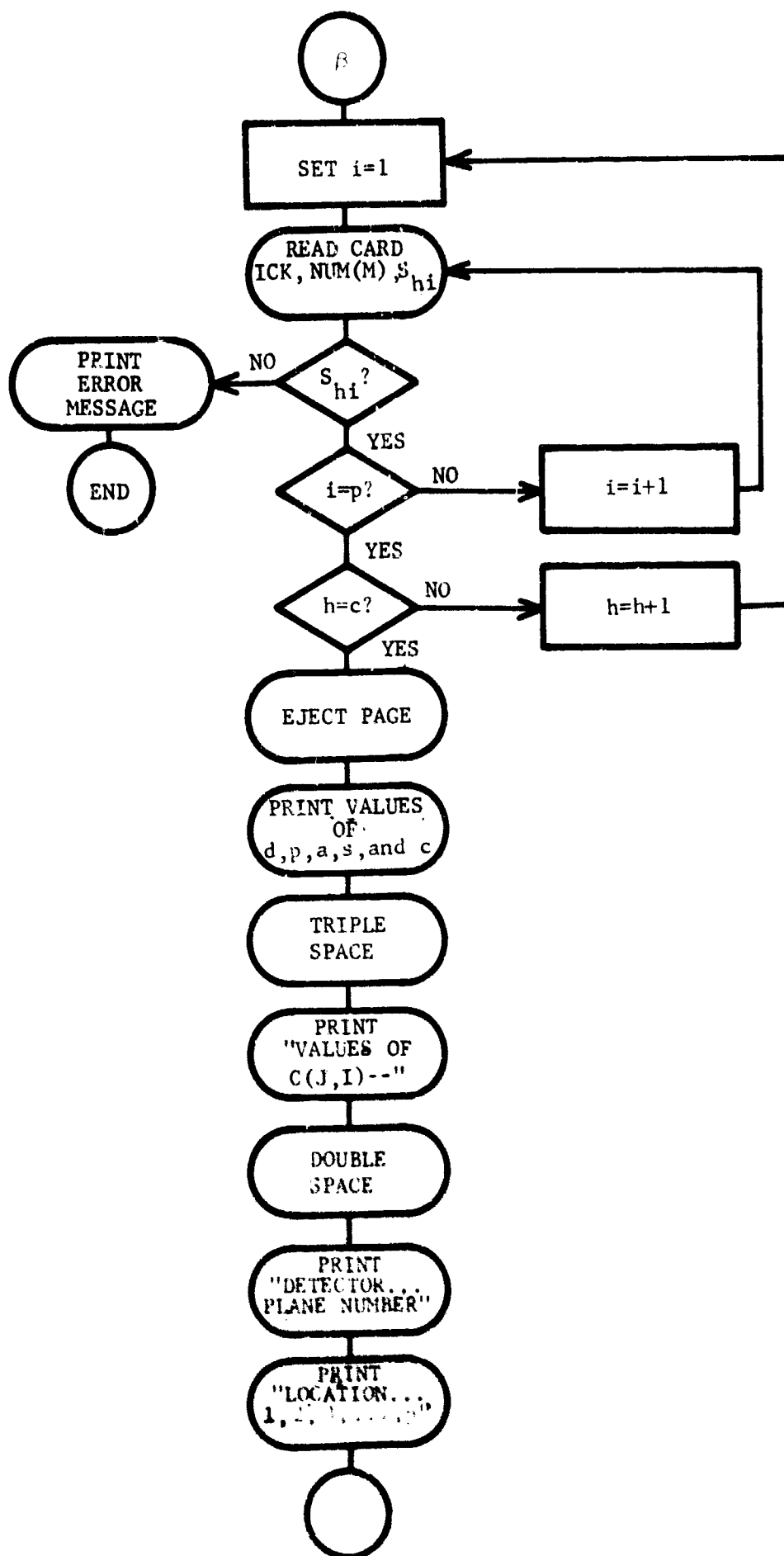
Composite Strategy	ACTIVITY PATTERN NUMBER				a
	1	2	3	4	
No. 1	X.XX	X.XX	X.XX	X.XX	. . . X.XX
No. 2	X.XX	X.XX	X.XX	X.XX	. . . X.XX
No. 3	X.XX	X.XX	X.XX	X.XX	. . . X.XX

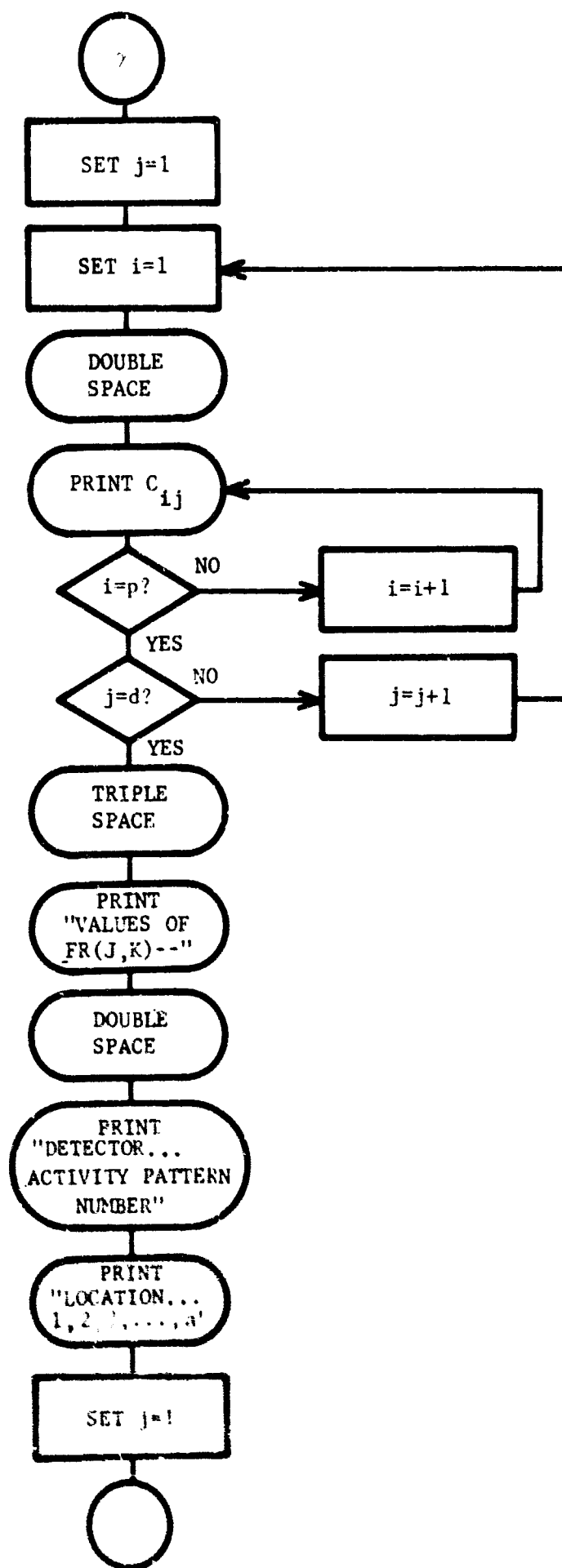
No. c	X.XX	X.XX	X.XX	X.XX	. . . X.XX

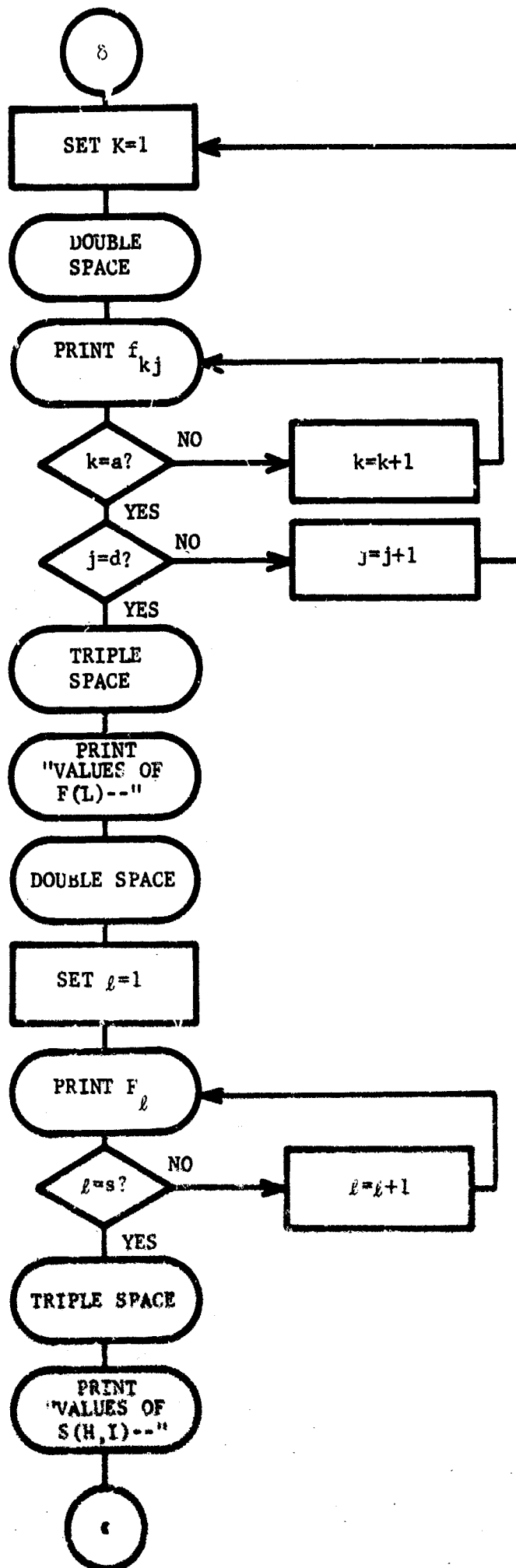
D. Detailed Flow Charts of Computer Program

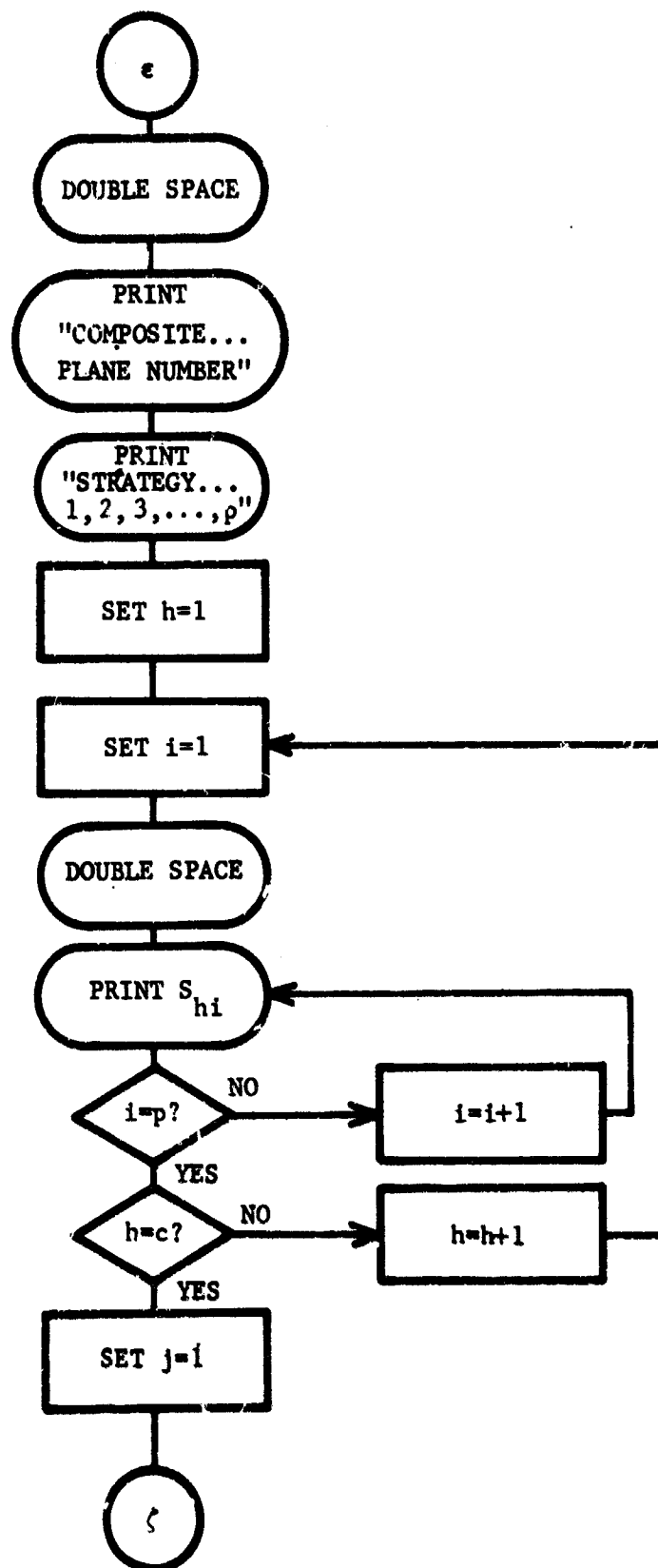


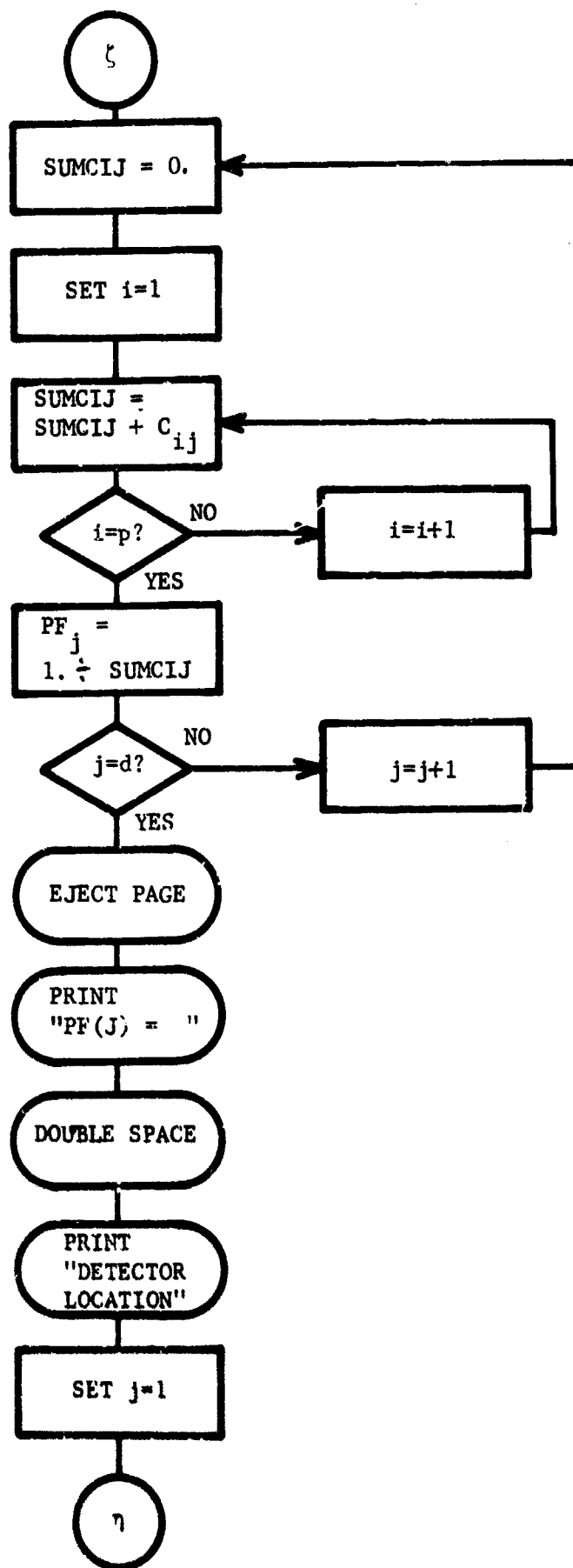


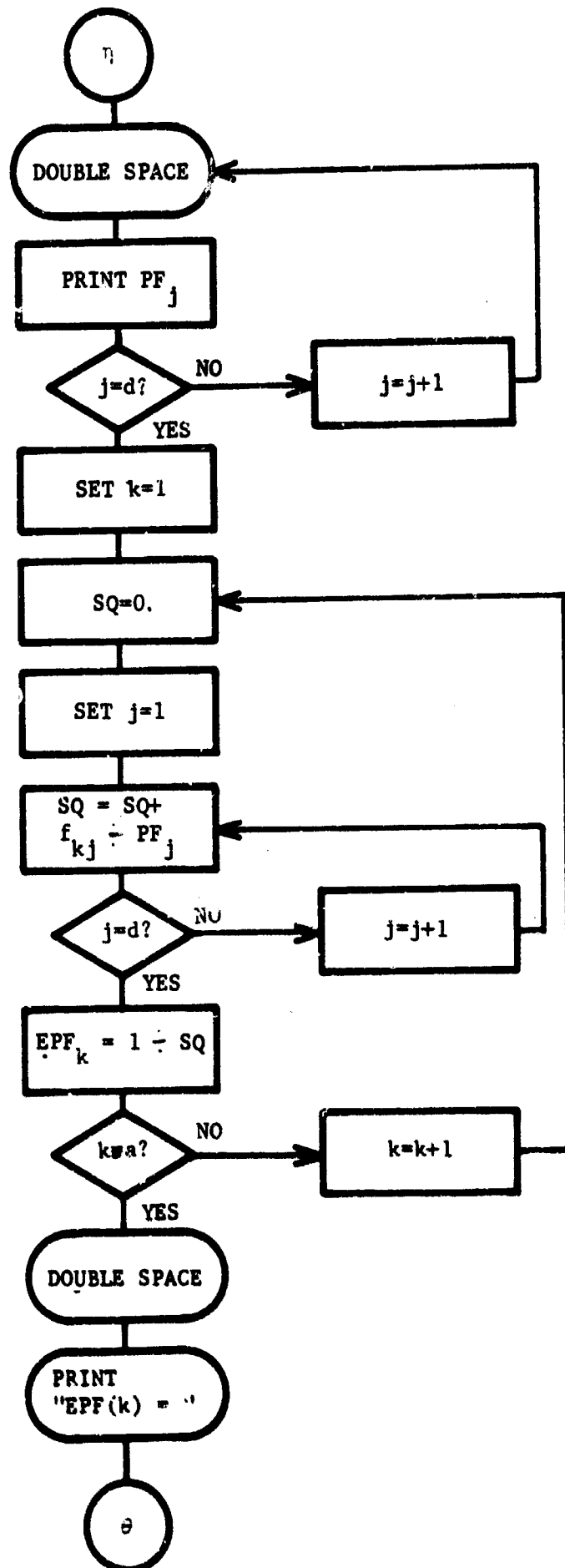


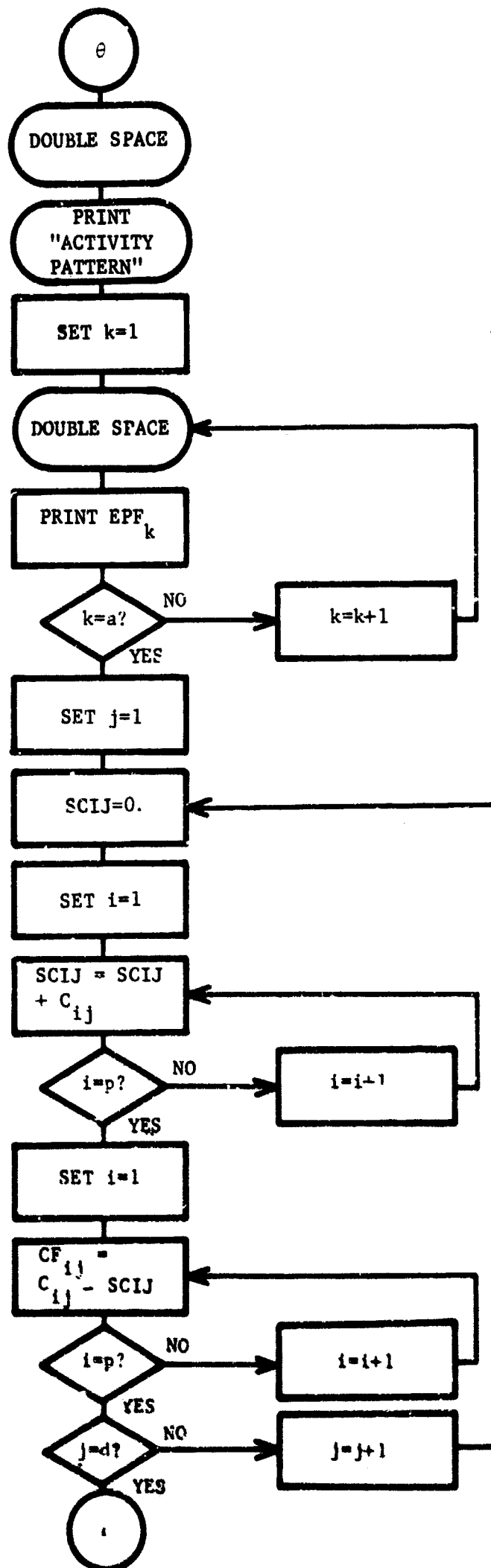


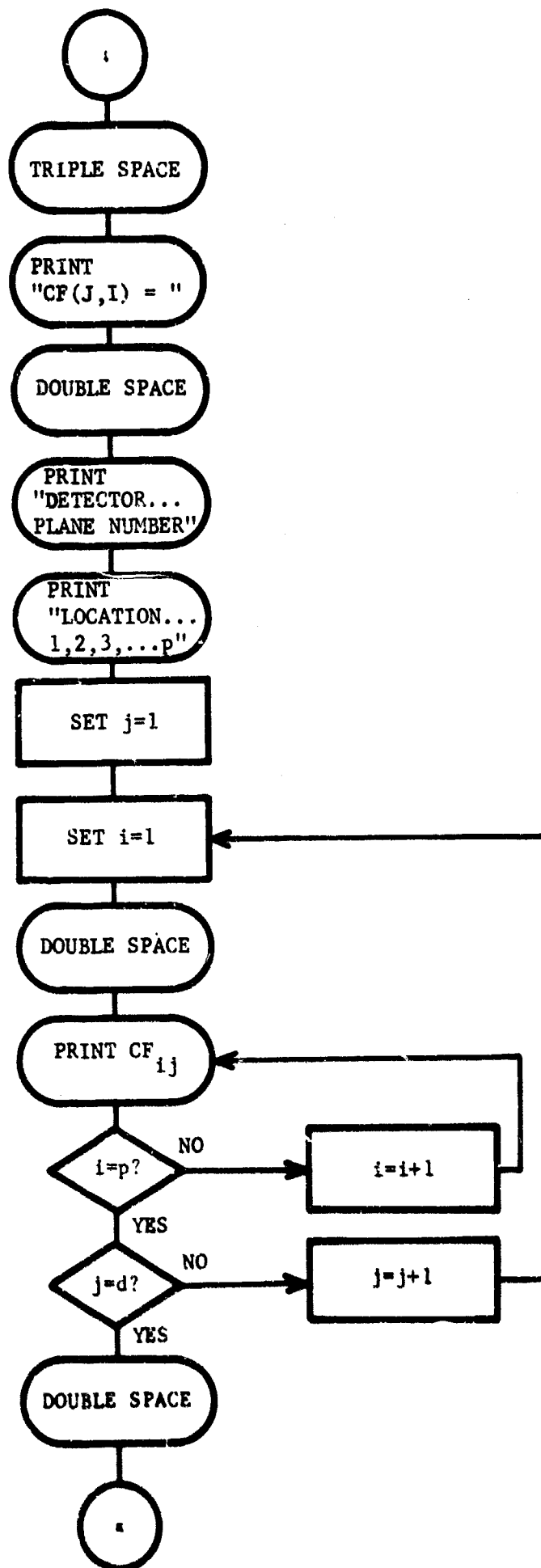


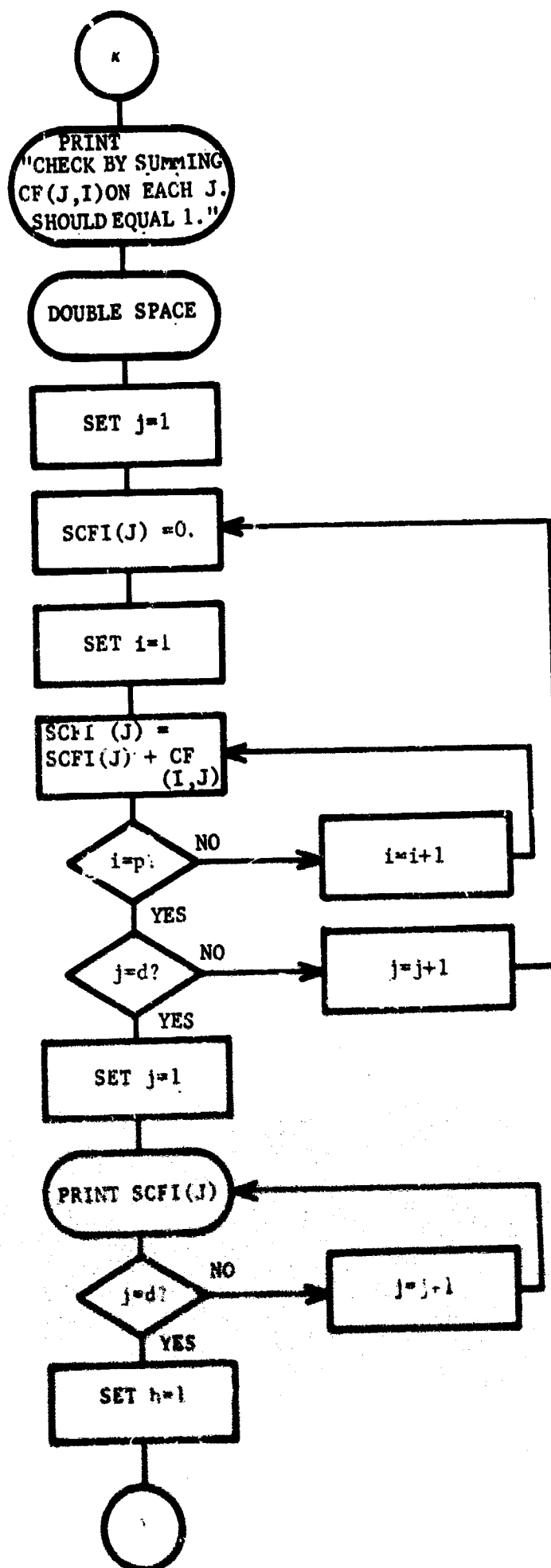


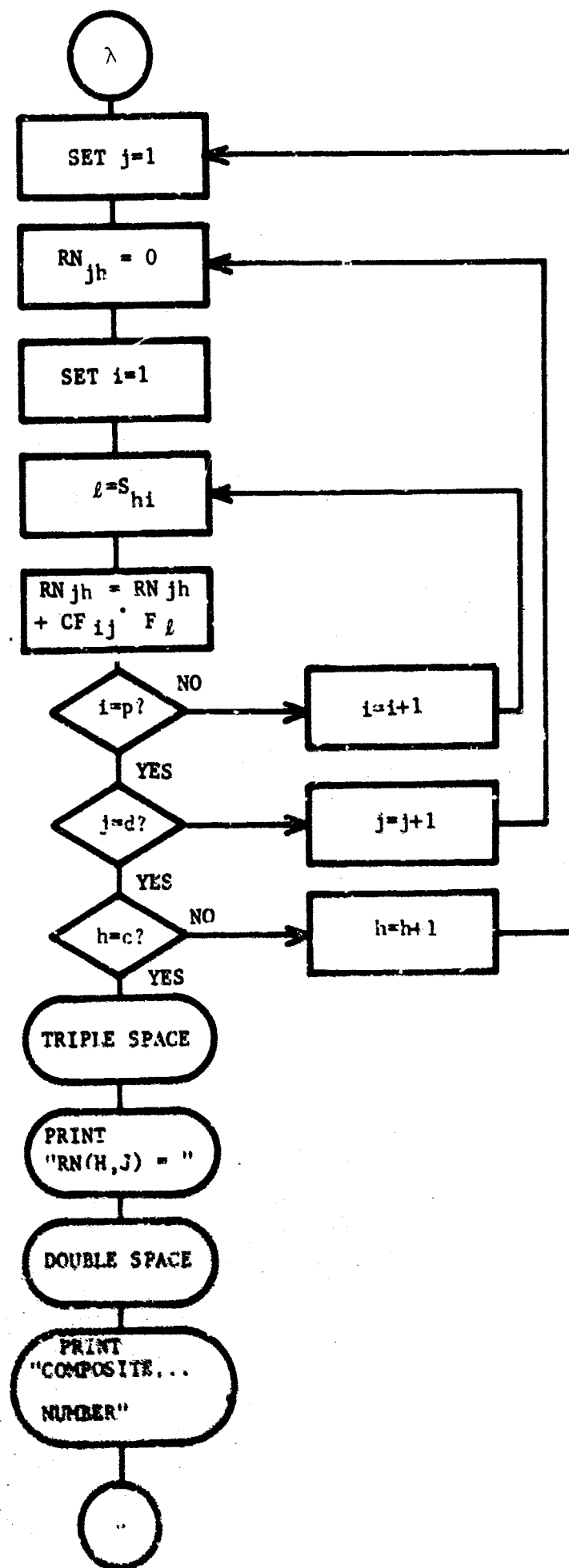


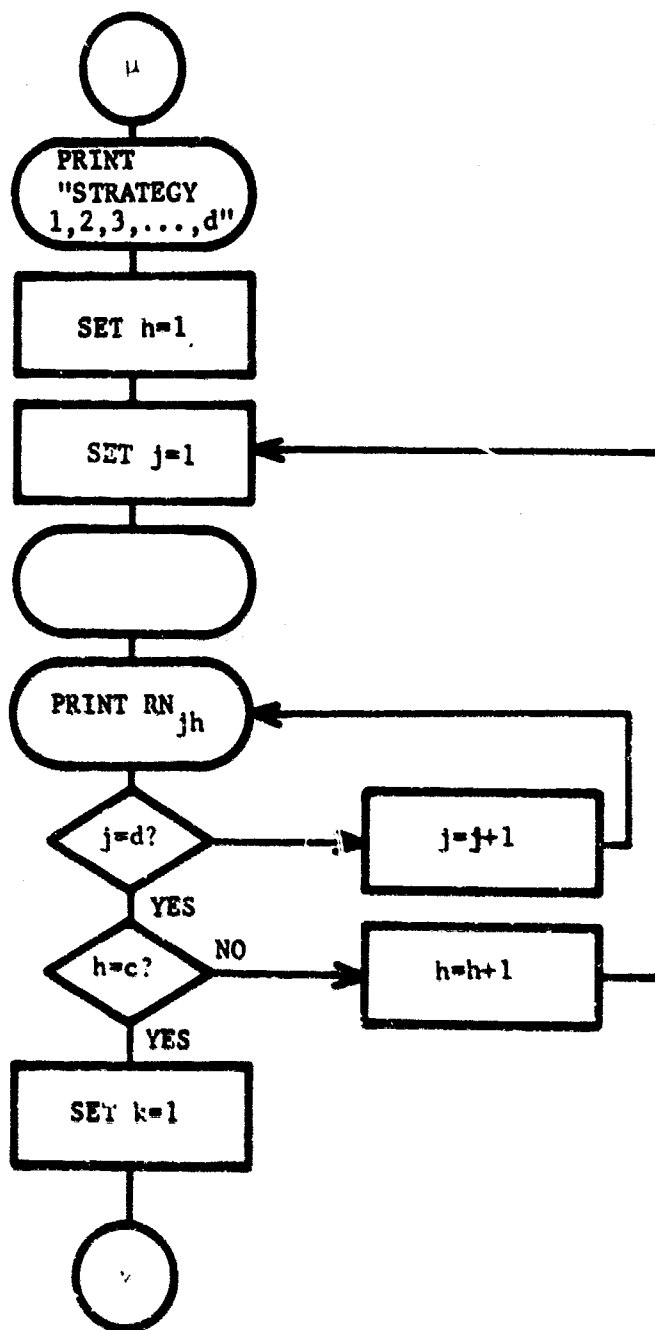


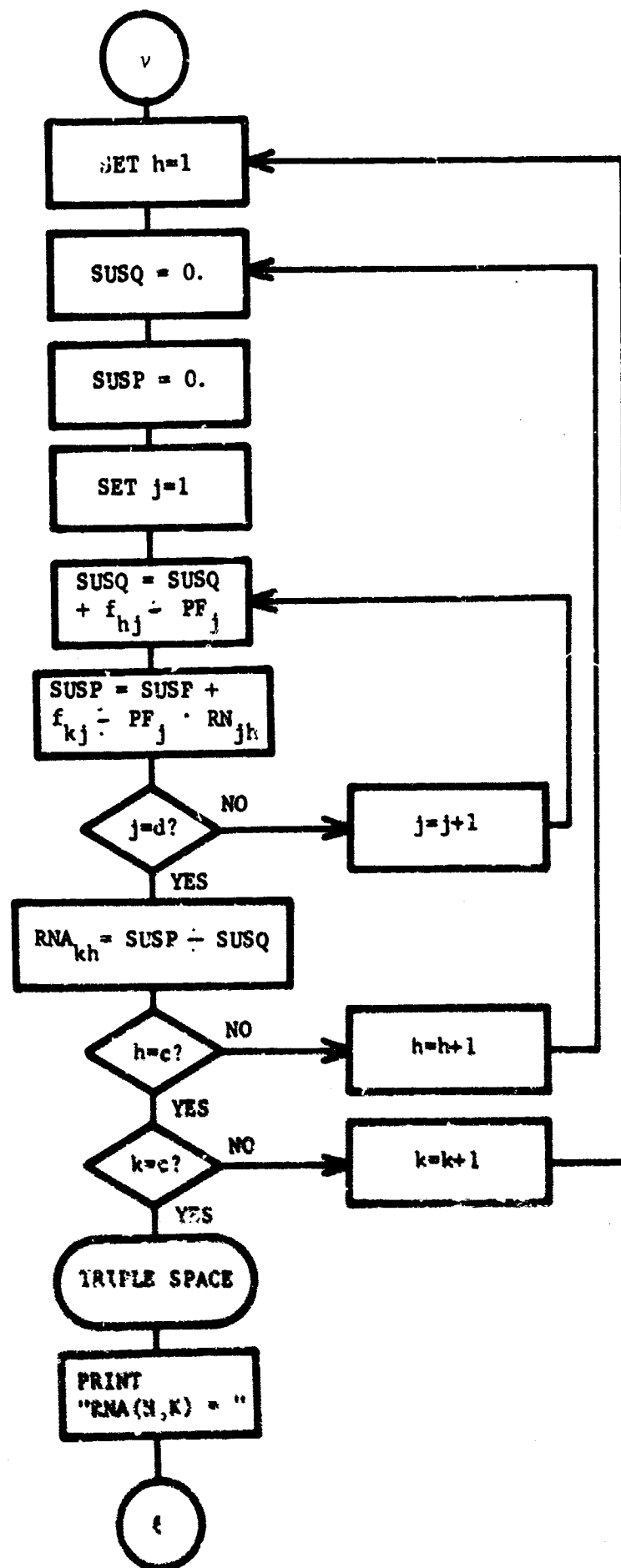


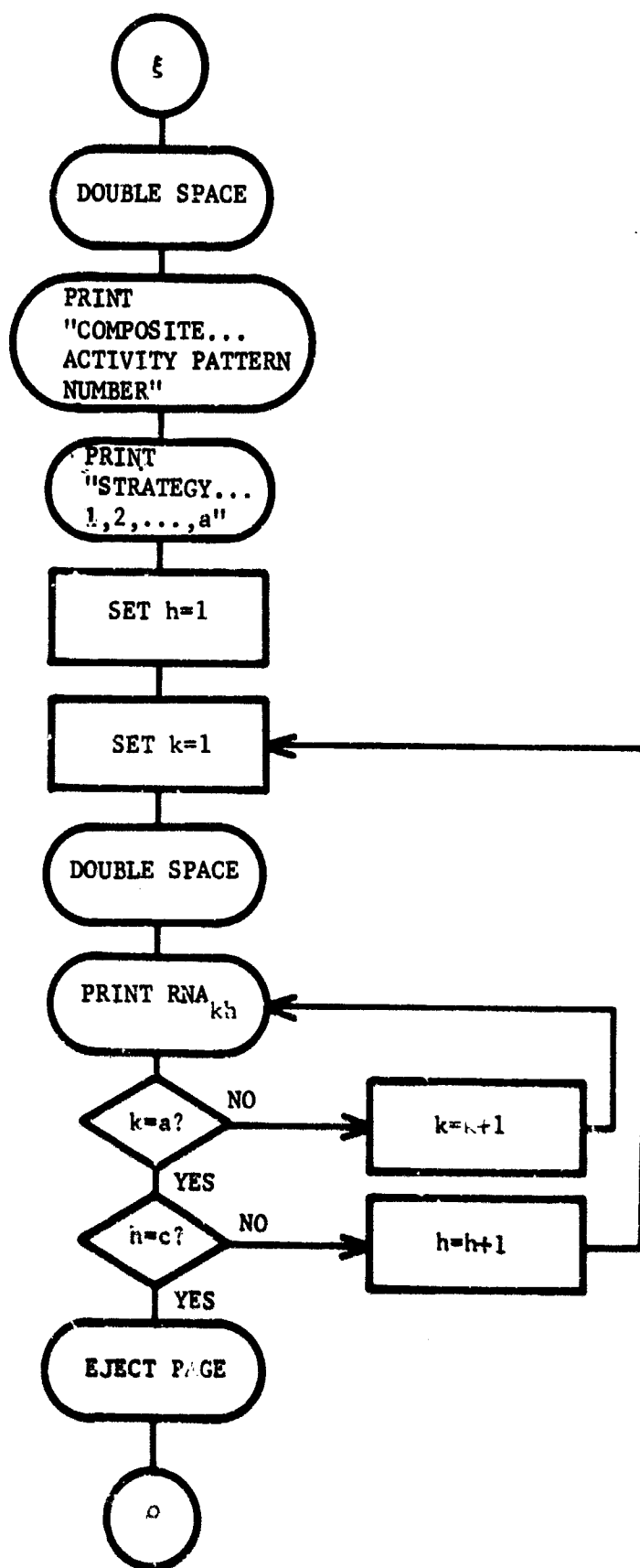












E. Card Listing of Sample Input Deck

```

SEQUENCE,339
JOB,12345,JRYAN
FTN,L,X
PROGRAM JRYAN
DIMENSION C(10,20),FR(20,20),F(20),LS(10,10),PF(20),EPF(20),CF(20
1,10),RN(100,20),RNA(100,20),SCFI(20),NUM(100)
PRINT 1000
1000 FORMAT(50X16H C L O S S A R Y)
PRINT 1001
1001 FORMAT(*0C(I,J) DENOTES CONTRIBUTIONS TO INTENSITY AT JTH DETECTOR
1 LOCATION FROM ITH PLANE OF CONTAMINATION*)
PRINT 1002
1002 FORMAT(*0FR(K,J)DENOTES THE FRACTION OF TIME SPENT AT DETECTOR J P
2PERFORMING THE ACTIVITY DENOTED BY K*)
PRINT 1003
1003 FORMAT(*0F(L) DENOTES THE MASS REDUCTION FACTOR (FRACTION OF FALLU
3UT REMAINING) FOR DECONTAMINATION STRATEGY L*)
PRINT 1004
1004 FORMAT(*0S(H,I) DENOTES WHICH STRATEGY L IS USED TO DECONTAMINATE
4 PLANE I FOR COMPOSITE STRATEGY H*)
PRINT 1005
1005 FORMAT(*0PF(J) DENOTES THE PROTECTION FACTOR AT EACH DETECTOR LOC
5ATION*)
PRINT 1006
1006 FORMAT(*0EPF(K) DENOTES THE EQUIVALENT PROTECTION FACTOR FOR EACH
6ACTIVITY PATTERN*)
PRINT 1007
1007 FORMAT(*0CF(J,I) DENOTES THE FRACTION OF THE TOTAL INTENSITY PRIL
7 TO DECONTAMINATION AT A GIVEN DETECTOR*)
PRINT 1008
1008 FORMAT(* DUE TO A PARTICULAR CONTAMINATED PLANE*)
PRINT 1009
1009 FORMAT(*0RN(H,J) DENOTES THE INTENSITY REDUCTION FACTOR FOR EACH
8DECONTAMINATION STRATEGY AT EACH DETECTOR LOCATION*)
PRINT 1010
1010 FORMAT(*0RNA(H,K) DENOTES THE ACTIVITY DOSE REDUCTION FACTOR FOR
9ACH COMBINATION OF ACTIVITY AND DECONTAMINATION*)
PRINT 1011
1011 FORMAT(* STRATEGY AT EACH DETECTOR LOCATION*)
99 READ 1,ICK,ID,IP,IA,IS,IC
1 FORMAT(11,5I2)
IF(EOF,60)41,42
42 IF(ICK-2)61,43,61
43 DO 10 I=1,IP
DO 10 J=1,ID
READ 2,ICK,C(I,J)
2 FORMAT(11,F9.8)
IF(ICK-3)62,10,62
10 CONTINUE
DO 20 K=1,IA
DO 20 J=1,ID
READ 3,ICK,FR(K,J)
3 FORMAT(11,F4.2)
IF(ICK-4)63,20,63

```

```

20 CONTINUE
  READ 4,(F(L),L=1,IS)
  4 FORMAT(20F4.2)
  IF(F(1)-1.)64,30,64
30 DO 40 M=1,IC
  READ 5,ICK,NUM(M),(LS(M,I),I=1,IP)
  IF(ICK-5)65,40,65
40 CONTINUE
  PRINT 21,ID,IP,IA,IS,IC
  21 FORMAT(4HID =,13,3X,3HP =,13,3X,3HA =,13,3X,3HS =,13,3X,3HC =,13/)
  PRINT 22
  22 FORMAT(/#0VALUES OF C(I,J)---*)
  PRINT 220
  220 FORMAT(9HODETECTOR,53X,22HP L A N E N U M B E R)
  PRINT 221,(I,I=1,IP)
  221 FORMAT(16H LOCATION ,13,10111)
  DO 222 J=1,ID
  222 PRINT 11,J,(C(I,J),I=1,IP)
  11 FORMAT(4HONO.,15,2X,11F11.8)
  PRINT 23
  23 FORMAT(/#0VALUES OF FR(J,K)---*)
  PRINT 230
  230 FORMAT(9HODETECTOR,42X,43H A C T I V I T Y P A T T E R N N U M B E R)
  PRINT 231,(I,I=1,IA)
  231 FORMAT(11H LOCATION ,2016)
  DO 232 J=1,ID
  232 PRINT 12,J,(FR(K,J),K=1,IA)
  12 FORMAT(4HONO.,15,3X,20F6.2)
  PRINT 24
  24 FORMAT(/#0VALUES OF F(L)---*/)
  PRINT 13,(F(L),L=1,IS)
  13 FORMAT(12X,20F5.2)
  PRINT 25
  25 FORMAT(/#0VALUES OF S(H,I)---*)
  PRINT 250
  250 FORMAT(10HOCOMPOSITE,52X,22HP L A N E N U M B E R)
  PRINT 251,(I,I=1,IP)
  251 FORMAT(12H STRATEGY ,1216)
  DO 252 M=1,IC
  252 PRINT 14,NUM(M),(LS(M,I),I=1,IP)
  14 FORMAT(4HONO.,15,3X,1216)
  DO 50 J=1,ID
  SUMCIJ=0.
  DO 50 I=1,IP
  50 SUMCIJ=SUMCIJ+C(I,J)
  60 PF(J)=1./SUMCIJ
  PRINT 15
  15 FORMAT(*1PF(J) *)
  PRINT 150
  150 FORMAT(9HODETECTOR,79H LOCATION)
  PRINT 151,(J,PF(J),J=1,ID)
  151 FORMAT(4HONO.,15,F9.2)
  DO 60 K=1,IA

```

```

      SQ=0.
      DO 70 J=1,ID
170  SQ=SQ+FR(K,J)/PF(J)
      EPF(K)=1./SQ
      PRINT 16
16  FORMAT(*0EPF(K) =*)
      PRINT 160
160  FORMAT(9H0ACTIVITY,/8H PATTERN)
      PRINT 161,(K,EPF(K),K=1,IA)
161  FORMAT(4H0NO.,I5,F9.2)
      DO 110 J=1,ID
      SCIJ=0
      DO 100 I=1,IP
100  SCIJ=SCIJ+C(I,J)
      DO 110 I=1,IP
110  CF(I,J)=C(I,J)/SCIJ
      PRINT 17
17  FORMAT(/*0CF(J,I) = *)
      PRINT 220
      PRINT 231,(I,I=1,IP)
      DO 120 J=1,ID
120  PRINT 12,J,(CF(I,J),I=1,IP)
      PRINT 9
9  FORMAT(*0 CHECK BY SUMMING CF(J,I) ON EACH J. SHOULD EQUAL 1./)
      DO 130 J=1,ID
      SCFI(J)=0
      DO 130 I=1,IP
130  SCFI(J)=SCFI(J)+CF(I,J)
      PRINT 13,(SCFI(J),J=1,ID)
      DO 140 M=1,IC
      DO 140 J=1,ID
      RN(J,M)=0.
      DO 140 I=1,IP
      L=LS(M,I)
140  RN(J,M)=RN(J,M)+CF(I,J)*F(L)
      PRINT 18
18  FORMAT(/*0RN(H,J) =*)
      PRINT 130
180  FORMAT(10H0COMPOSITE,38X,45HD E T E C T O R L O C A T I O N N U
      1M B E R)
      PRINT 254,(J,J=1,ID)
      DO 253 M=1,IC
253  PRINT 12,NUM(M),(RN(J,M),J=1,ID)
      DO 310 K=1,IA
      DO 310 M=1,IC
      SUSQ=0.
      SUSP=0.
      DO 300 J=1,ID
      SUSQ=SUSQ+FR(K,J)/PF(J)
300  SUSP=SUSP+FR(K,J)/PF(J)*RN(J,M)
310  RNA(K,M)=SUSP/SUSQ
      PRINT 19
19  FORMAT(/*0RNA(H,K) = *)
      PRINT 190

```

```

190 FORMAT(10HCOMPOSITE,38X,43HACTIVITY PATTERN,10X,
13 E R)
PRINT 254,(K,K=1,1A)
DO 191 M=1,1C
191 PRINT 12,NUM(M),(RNA(K,M),K=1,1A)
PRINT 98
58 FORMAT(1H1)
GO TO 99
61 PRINT 71
71 FORMAT(*0INCORRECT DATA CARD--NOT VALUES OF SUBSCRIPTS.*)
GO TO 41
62 PRINT 72
72 FORMAT(*0INCORRECT DATA CARD--NOT VALUE OF C(I,J).*)
GO TO 41
63 PRINT 73
73 FORMAT(*0INCORRECT DATA CARD--NOT VALUE OF FR(K,J).*)
GO TO 41
64 PRINT 74
74 FORMAT(*0INCORRECT DATA CARD--NOT VALUES OF F(L).*)
GO TO 41
65 PRINT 75
75 FORMAT(*0INCORRECT DATA CARD--NOT VALUES OF S(H,I).*)
GO TO 41
5 FORMAT(11,13,1212)
254 FORMAT(11H STRATEGY ,1216)
41 CONTINUE
END
SCOPE
!LOAD
!RUN,3,2000,1
20404050606
3.299
3.386
3.024
3.002
3.101
3.031
3.209
3.005
3.729
3.206
3.182
3.001
3.071
3.377
3.085
3.002
40.06
40.07
40.20
40.67
40.07
40.17
40.09

```

40.67
40.28
40.02
40.03
40.67
40.13
40.05
40.15
40.67
40.19
40.08
40.06
40.67
1.000.020.030.090.100.13
00101050102
00203030401
00301010401
00401030601
00504020101
00601010505
1115

F. Sample Output

PROGRAM NAMES									
1 02473 JHYAN	14402	1 02050 IOS.	00423	1 01040 QSDERROR	00202	1 01562 QSDENTRY	00004		
1 00213 TOP.	01347	1 57760 ALLOC.	00733	1 57513 RSTAR	00245	1 57445 STM.	00036		
1 57411 TSM.		1 57350 QSDIFLOC	00033	1 55141 IOM.	02215				

PROGRAM EXTENS.
NONE

LAMELED COMMON
NONE

NUMBERED COMMON
NONE

ENTRY POINTS									
0 00074 SENTRY	1 75334 JHYAN	1 01566 QSDENTRY	1 02367 TMEND.						
1 01562 QSDICT.	1 57365 QSDIFLOC	1 57415 TSM.	1 57441 STM.						
1 02361 QSDINCL.	1 02050 IOM.	1 02373 IOM.	1 02070 IOS.						
1 02242 QSDCHAIN	1 02123 QSDHIST.	1 02364 QSDHIST.	1 02216 TOP.						
1 01040 QSDERROR	1 01793 QSDERSET	1 01563 EXIT	1 57513 RSTAR						
1 57001 QSDCHECK	1 57010 QSDCLOSE	1 57577 QSDSELEN	1 00110 ALLOC.						
1 57760 QSDJHYAN	1 00072 QSDJHYAN	1 00101 QSDRETURN.	1 00102 QSDALLOCIN.						
1 55145 IOM.	1 55141 QSDBUF.	1 57361 QSDIFLOC	1 56755 QSD.						
1 57213 QSDPCVT.									

EXECUTION STARTED AT 1417 -02

G L O S S A R Y

$C(I,J)$ DENOTES CONTRIBUTIONS TO INTENSITY AT JTH DETECTOR LOCATION FROM ITH PLANE OF CONTAMINATION
 $F(K,J)$ DENOTES THE FRACTION OF TIME SPENT AT DETECTOR J PERFORMING THE ACTIVITY DENOTED BY K
 $F(L)$ DENOTES THE MASS REDUCTION FACTOR (FRACTION OF FALLOUT REMAINING) FOR DECONTAMINATION STRATEGY L
 $S(H,I)$ DENOTES WHICH STRATEGY L IS USED TO DECONTAMINATE PLANE I FOR COMPOSITE STRATEGY H
 $PF(J)$ DENOTES THE PROTECTION FACTOR AT EACH DETECTOR LOCATION
 $EPF(K)$ DENOTES THE EQUIVALENT PROTECTION FACTOR FOR EACH ACTIVITY PATTERN
 $CF(J,I)$ DENOTES THE FRACTION OF THE TOTAL INTENSITY PRIOR TO DECONTAMINATION AT A GIVEN DETECTOR DUE TO A PARTICULAR CONTAMINATED PLANE
 $RN(H,J)$ DENOTES THE INTENSITY REDUCTION FACTOR FOR EACH DECONTAMINATION STRATEGY AT EACH DETECTOR LOCATION
 $RNA(H,K)$ DENOTES THE ACTIVITY DOSE REDUCTION FACTOR FOR EACH COMBINATION OF ACTIVITY AND DECONTAMINATION STRATEGY AT EACH DETECTOR LOCATION

D = 4 P = 4 A = 5 S = 6 C = 6

VALUES OF C(I,J)--

DETECTOR LOCATION		1	2	3	4	PLANE NUMBER
NO, 1		0.29900000	0.10100000	0.52900000	0.07100000	
NO, 2		0.38600000	0.03100000	0.70600000	0.37700000	
NO, 3		0.02400000	0.20900000	0.18200000	0.08900000	
NO, 4		0.00200000	0.00500000	0.00100000	0.00200000	

VALUES OF FR(J,K)--

DETECTOR LOCATION		1	2	3	4	5	ACTIVITY PATTERN NUMBER
NO, 1		0.06	0.07	0.20	0.13	0.19	
NO, 2		0.07	0.17	0.02	0.05	0.08	
NO, 3		0.20	0.09	0.03	0.15	0.06	
NO, 4		0.67	0.67	0.67	0.67	0.67	

VALUES OF F(L)--

1.00 0.02 0.03 0.09 0.10 0.13

VALUES OF S(M,I)--

COMPOSITE STRATEGY		1	2	3	4	PLANE NUMBER
NO, 1		1	5	1	2	
NO, 2		3	3	4	1	
NO, 3		1	1	4	1	
NO, 4		1	3	6	1	
NO, 5		4	2	1	1	
NO, 6		1	1	5	5	

PF(J) =

DETECTOR
LOCATION

NO.	1	1.00
NO.	2	1.00
NO.	3	2.00
NO.	4	100.00

EPF(K) =

ACTIVITY
PATTERN

NO.	1	4.22
NO.	2	3.43
NO.	3	3.11
NO.	4	3.82
NO.	5	3.26

CF(J,I) =

DETECTOR
LOCATION

	1	2	3	4
NO. 1	0.30	0.10	0.53	0.07
NO. 2	0.39	0.03	0.21	0.30
NO. 3	0.05	0.42	0.36	0.17
NO. 4	0.20	0.50	0.10	0.20

PLANE NUMBER

CHECK BY SUMMING CF(J,I) ON EACH J. SHOULD EQUAL 1,

1.00	1.00	1.00	1.00
------	------	------	------

HN(M,J) =

COMPOSITE
STRATEGY

	1	2	3	4
NO. 1	0.04	0.60	0.46	0.35
NO. 2	0.13	0.41	0.22	0.23
NO. 3	0.52	0.01	0.67	0.91
NO. 4	0.44	0.70	0.20	0.43
NO. 5	0.63	0.62	0.75	0.33
NO. 6	0.40	0.40	0.52	0.73

DETECTOR LOCATION NUMBER

HNA(M,K)=

COMPOSITE
STRATEGY

ACTIVITY PATTERN NUMBER

		1	2	3	4	5
NO,	1	0.59	0.63	0.80	0.67	0.73
NO,	2	0.25	0.31	0.15	0.21	0.21
NO,	3	0.66	0.72	0.55	0.63	0.62
NO,	4	0.48	0.62	0.46	0.46	0.52
NO,	5	0.58	0.60	0.62	0.60	0.61
NO,	6	0.50	0.48	0.47	0.49	0.48

Appendix F

The Nature and Scope of Command and Control System Elements
Required for Conducting Effective Decontamination
Analysis

Note: The material in this Appendix was originally submitted to USNRDL as Research Memorandum RM-OU-214-9*.

* J. T. Ryan. The Nature and Scope of Command and Control System Elements Required for Conducting Effective Decontamination in Municipalities. RM-OU-214-9. Durham, North Carolina: Research Triangle Institute, Operations Research and Economics Division, 30 July 1965.

TABLE OF CONTENTS FOR APPENDIX F

	<u>Page</u>
TABLE OF CONTENTS.	F-i
LIST OF TABLES	F-ii
LIST OF FIGURES.	F-ii
I. INTRODUCTION	F-1
A. Purpose	F-1
B. Summary	F-1
II. GENERAL CHARACTERISTICS OF COMMAND AND CONTROL SYSTEMS	F-3
A. Introduction.	F-3
B. The Purpose of Command and Control Systems.	F-3
C. The Basic Components of Command and Control Systems	F-3
D. Some Examples of Command and Control Systems.	F-12
III. A COMMAND AND CONTROL SYSTEM FOR MUNICIPAL DECONTAMINATION	F-13
A. General	F-13
B. Environmental Aspects of Municipal Decontamination.	F-13
C. Goals of Municipal Decontamination.	F-16
D. Municipal Decontamination System Performance Criteria	F-17
E. Elements of a Decontamination System.	F-18
F. Decontamination System Elements	F-22
IV. AN INFORMATION SYSTEM (SUBSYSTEM) FOR DECONTAMINATION.	F-29
A. Introduction.	F-29
B. Information Input Requirements for Conducting Decontamination	F-29
C. Information Utility Criteria.	F-30
D. Means for Obtaining, Storing, and Disseminating the Information	F-32
E. Summary	F-32
V. CONCLUSIONS AND RECOMMENDATIONS.	F-33
A. Conclusions	F-33
B. Recommendations	F-33
REFERENCES	F-35

LIST OF TABLES

<u>Table</u>	<u>Page</u>
F-I Decontamination Subsystem Functions	F-25

LIST OF FIGURES

<u>Figure</u>	<u>Page</u>
F-1 Functional Diagram of Command and Control System.	F-5
F-2 Structure of Information Acquired by Sensor Subsystem	F-7
F-3 The Decision Subsystem as a Transformation.	F-9
F-4 Functional Characteristics of On-line Control Subsystem	F-11
F-5 Time Phases of Radiological Defense	F-14
F-6 Schematic Diagram Showing the Relation of Decontamination to the Postattack Emergency Operating System	F-19
F-7 Supporting Data Base for the Decontamination of a Facility or Activity.	F-23
F-8 Illustration of Functional Relationships Among Decontamination System Activities	F-27

Appendix F

The Nature and Scope of Command and Control System Elements Required for Conducting Effective Decontamination in Municipalities

I. INTRODUCTION

A. Purpose

The purpose of this study is to determine the nature and scope of the command and control system elements which are required to effect practical decontamination. Emphasis is placed on decontamination within municipalities. Such a study is necessary in order to answer a number of questions basic to decontamination analysis. The five questions on which this study focuses are:

1. What are the preattack and postattack data required to effect decontamination operations?
2. What are the essential components of the information system needed to effect decontamination operations?
3. How should trained and untrained personnel and decontamination equipment be prepositioned, organized, and controlled?
4. How can a decontamination system in a municipality be evaluated?
5. How can a decontamination system in a municipality be most effectively modeled to provide a ready vehicle for system analysis?

Of course, all of these questions are asked for various levels of decontamination capabilities, requirements, and attack environments. As implied by the questions above, a subsidiary purpose of this study is to develop a procedure for analyzing a decontamination system in a municipality.

B. Summary

This appendix first describes elements and purposes of command and control

systems in general. The various components of a decontamination system in a municipality are then identified and embedded in the general command and control system framework. It is shown that a command and control system for decontamination operations must provide both for decisions on whether or not to undertake a mission and for manpower and decontamination resource commitment and allocation decisions. These decision functions require an elaborate information subsystem consisting of organized data files containing prestored (preattack) data and postattack assessments (including system feedback).

The detailed characteristics of the individual components in each of the essential subsystems of a decontamination command and control system are studied. The interrelationships among the individual subsystem components are identified and displayed.

In order to determine the command and control system elements required to accomplish practical decontamination missions in a municipality, the environment and the system goals are reviewed and analyzed. Basic system evaluation criteria are also discussed and the essential decontamination system evaluation criteria are identified.

Recommendations and guides leading to the design of a basic command and control system for municipal decontamination are indicated.

II. GENERAL CHARACTERISTICS OF COMMAND AND CONTROL SYSTEMS

A. Introduction

Most persons who are concerned with business, government, or military operations are also acquainted with the basic characteristics of command and control systems. However, a review of the elements and purposes of command and control systems is useful in providing a framework into which the components of a decontamination system can be embedded.

Further, since the technology of command and control systems is advancing rapidly, the terms which define the basic components of such systems are changing day by day. Thus, it is necessary to define precisely the terms and expressions used in this appendix to define the system components and system goals.

The succeeding parts of this explanatory section are:

Section II-B The Purpose of Command and Control Systems

Section II-C The Basic Components of Command and Control Systems

Section II-D Some Examples of Command and Control Systems

B. The Purpose of Command and Control Systems

The purpose of any command and control system is to: (1) determine for a given operation or set of operations, what must be done, who (or what) does it, and when, where, and how they do it; and (2) direct the activities which accomplish it.

Obviously from the above, it is seen that a command and control system must have the capacity both to initiate and to monitor activities. As operations or sets of operations become more complex, systematized command and control mechanisms become more necessary.

C. The Basic Components of Command and Control Systems

Most command and control systems are composed of a set of basic elements called

subsystems. The expressions used to identify these subsystems as well as their defining characteristics are presented here along the lines indicated in Reference F-1.

The following subsystems are common to all command and control systems:

1. Sensor subsystem;
2. Effector subsystem;
3. External communication subsystem;
4. Internal communication subsystem;
5. Information subsystem;
6. Decision subsystem;
7. On-line control subsystem; and
8. Off-line control subsystem.

The command and control center is composed only of the internal communication subsystem, the information subsystem, the decision subsystem, and the on-line control subsystem. Figure F-1 shows the functional relationships among the basic subsystems of a command and control system.

1. Sensor Subsystem

The basic purpose of the sensor subsystem is to acquire information inputs. This information input material is classified into three categories:

- a. observed information inputs;
- b. derived information inputs; and
- c. command information inputs.

Unfortunately, sensor subsystems also acquire material which is not information input at all. This non-information input or "noise" represents irrelevant or erroneous material.

Observed information inputs can be such things as visual observations, verbal communications, radar scope readings, radiological dosimeter readings, or on-site damage computations. Derived information inputs are data which result from deductive processes. It may be the product of either experimental

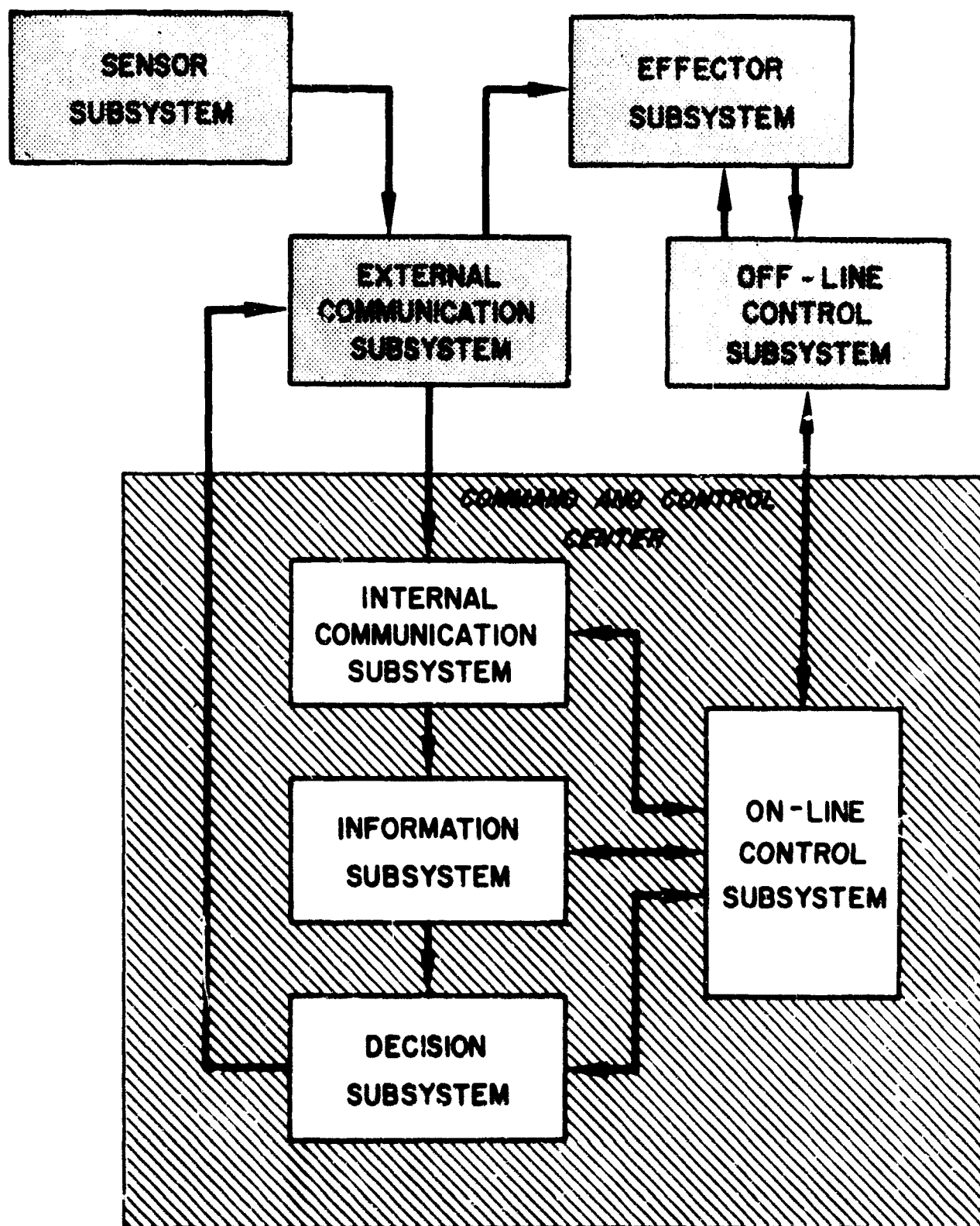


Figure F-1 Functional Diagram of Command and Control System

or theoretical research, for example. This is usually prestored data and thus the external sensors which acquire such information inputs may be inactive during most of the time that the system is operating. Command information inputs are in the form of directives which enter the system from external sources. Decisions made outside of the command and control system but affecting the operation of the system are a form of command information input. Figure F-2 shows the structure of information inputs which are acquired by the sensor subsystem.

2. Effector Subsystem

The purpose of the effector subsystem is to carry out the directives of the decision subsystem. This may consist of simply disseminating information or at the other extreme carrying out the over-all system missions. The effectors are thus controlled by the output commands and decisions of the command and control center. The effectors' task is to apply the energy committed for some external action. An example of an effector would be an offensive aircraft directed to attack a target as prescribed in the command and control center.

3. External Communications Subsystem

The external communications subsystem is the network of paths which carries material (information inputs, information, etc.) to and from the functional blocks tied to this subsystem in Figure F-1. These paths can consist of radio communications, telephone links, verbal information transmission, etc. Often an external sensor or effector can also be a part of the external communications subsystem as well as the sensor or effector subsystem. The organization and other systems variables involved in this subsystem depend largely on the characteristics of the particular command and control system of which it is a part.

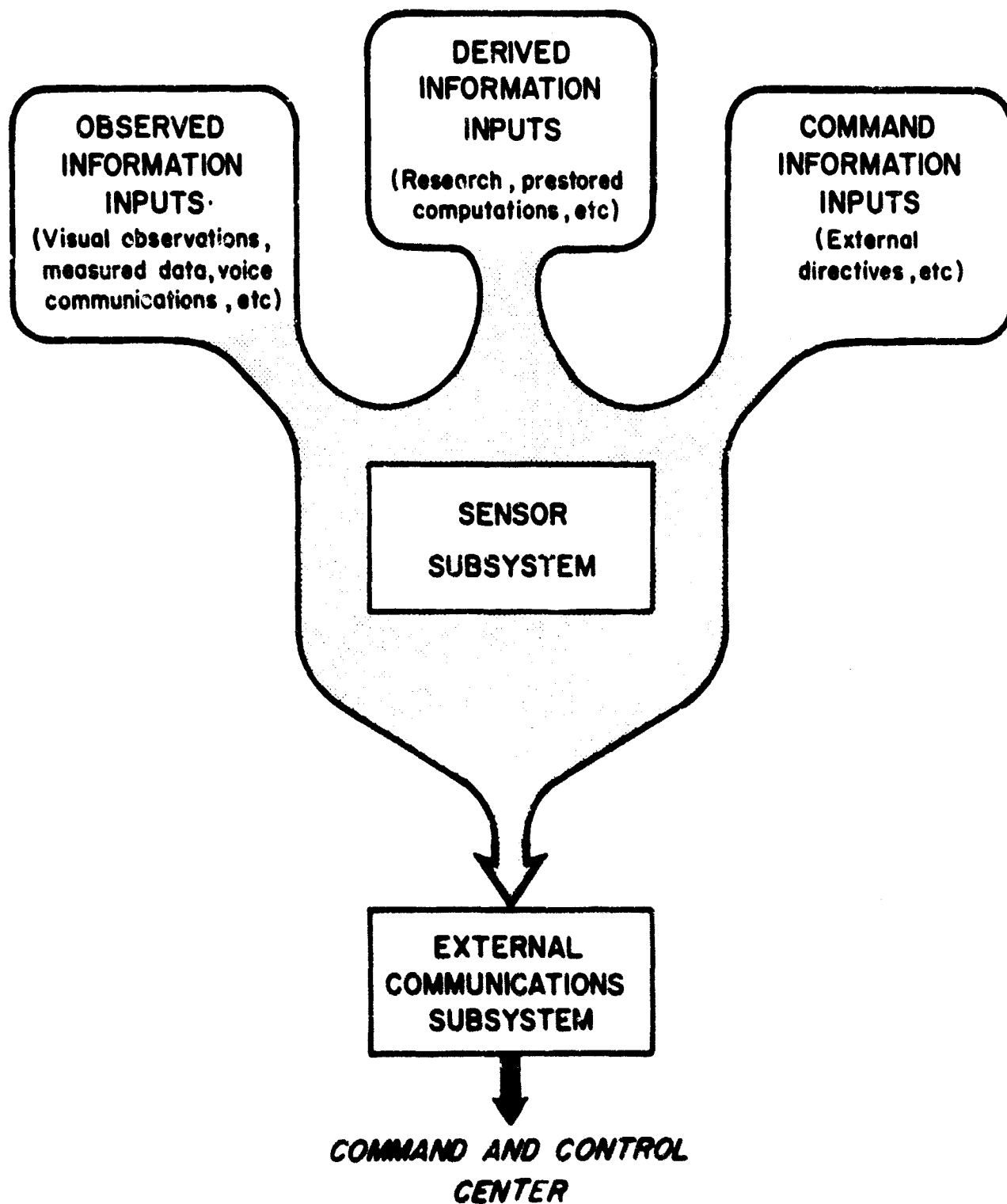


Figure F-2 Structure of Information Acquired by Sensor Subsystem

4. Internal Communications Subsystem

The internal communications subsystem is similar to the external communications subsystem except that it is entirely contained in the command and control center. Figure F-1 shows its functional relationship to the system as a whole.

5. Information Subsystem

The information subsystem is the part of the command and control center which handles, stores, transforms, or displays the information which is transmitted to the command and control center. It consists of all of the people, machines, reports, and files within the command and control center which are employed to perform this function.

6. Decision Subsystem

The decision subsystem (illustrated in Figure F-3) might also be called the command subsystem. It is the component of the command and control system which transforms information into decisions. These decisions are usually translated into commands to perform an activity, or commit resources to perform prescribed actions during a prescribed time interval. Figure F-3 illustrates how the decision subsystem transforms information into decisions and commands.

7. On-line Control Subsystem

Ideally, the on-line control subsystem (illustrated in Figure F-4) controls all information transmission and monitors all actions performed by the command and control system. In practice, the on-line control mechanism only attempts to perform these tasks in most real situations. Many activities are performed by the effectors by their own volition because there is not enough time for the decision subsystem to outline a course of action. For example, a Polaris submarine under attack presumably would either attack its adversary or take evasive action immediately without communicating through a higher echelon decision

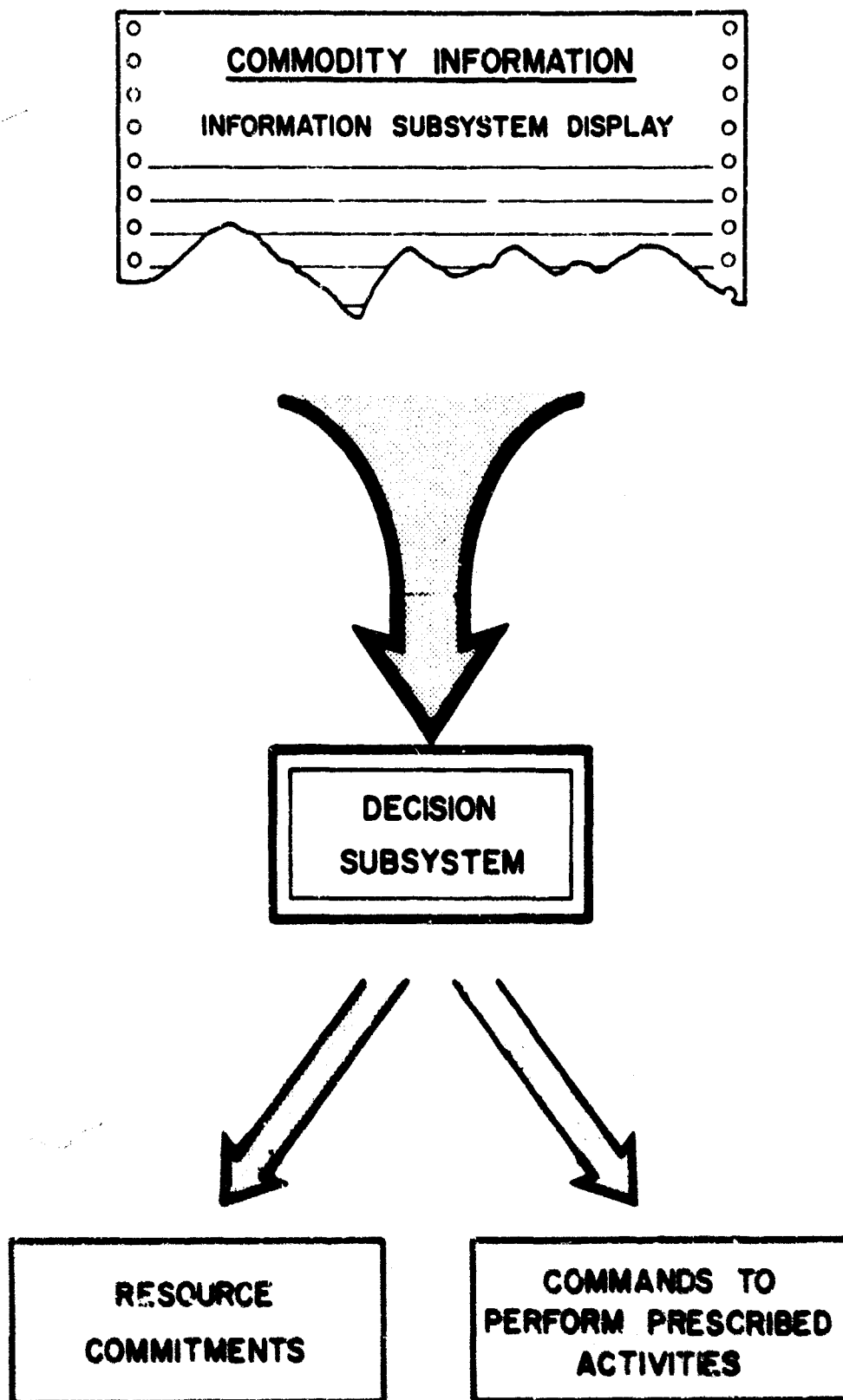


Figure F-3 The Decision Subsystem as a Transformation

subsystem.

A very important aspect of such on-line control is the regulation of system accuracy and/or response time. This means that the on-line control subsystem attempts to control delays and errors in the transmission and transformation of information in the command and control system. This role of the on-line control subsystem makes it the most important element in the system. Unfortunately, it is also the most difficult to identify precisely in most physical systems. In the above Polaris example, the effector subsystem performed a function which, for at least one situation, identified the effector as a part of the on-line control system. Usually those machines, people, etc., which perform on-line monitoring and control functions from within the command and control center are considered to comprise the on-line control subsystem. Figure F-4 shows schematically how the on-line control subsystem performs in the system environment.

8. Off-line Control Subsystem

The off-line control subsystem monitors and controls processes which affect the system but are not performed on-line. That is, they are either performed before the system is operational or are performed outside of the control of the on-line control subsystem. One important function of the off-line control subsystem is to collect and process statistics and research for future augmentation of the static variables of the system. On the basis of the observed statistics and research, the off-line control subsystem makes recommendations to the on-line control subsystem for possible future control of the dynamic variables. Basic research performed long in advance of an operational system must be controlled. It is the purpose of the off-line control subsystem to control this research. Thus, most often, some segments of the off-line control subsystem are the first operational parts of a command and control system.

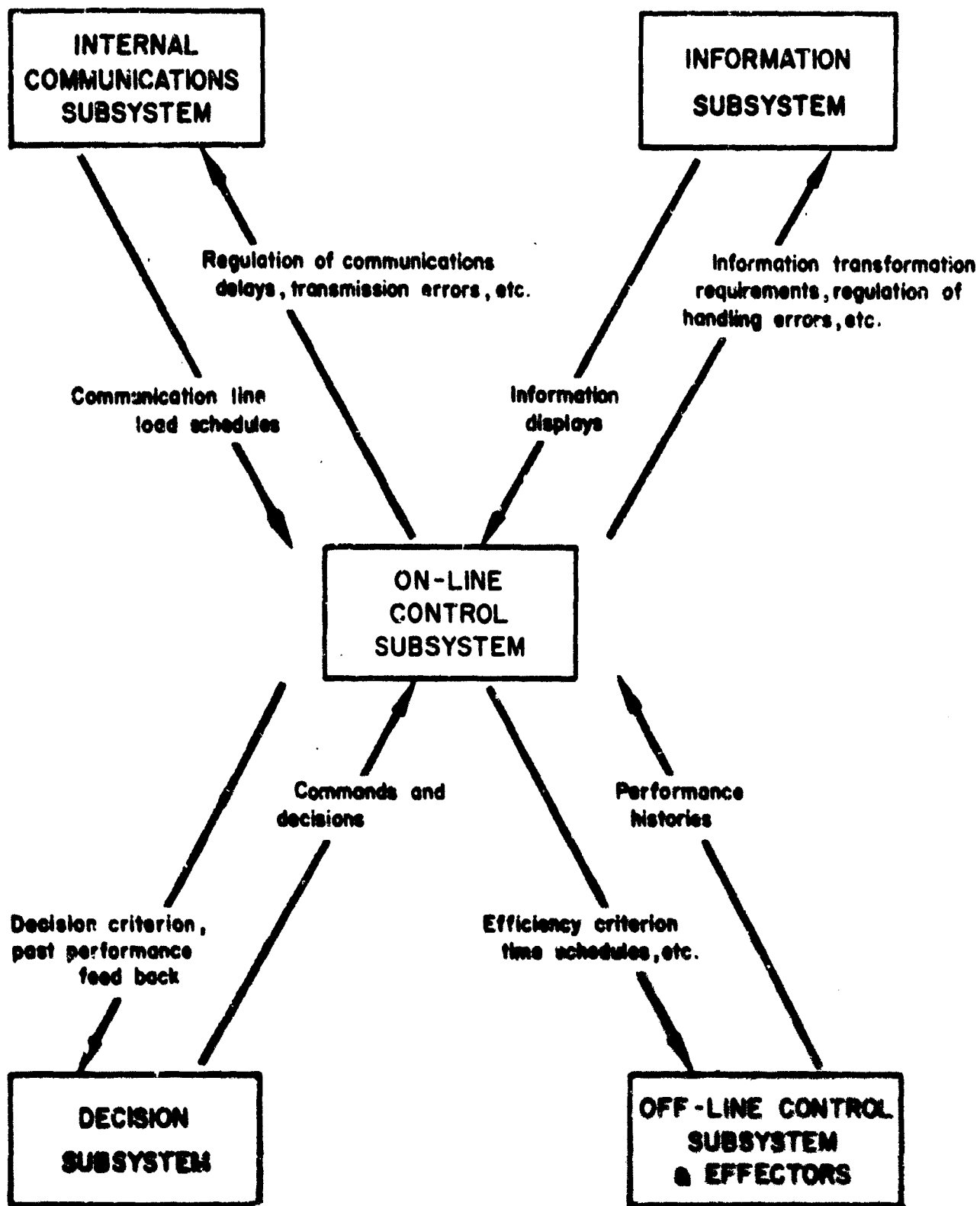


Figure F-4 Functional Characteristics of On-line Control Subsystem

D. Some Examples of Command and Control Systems

Some of the Air Force's "L" Systems are excellent examples of military command and control systems. A few are summarized below (See Reference F-2 for these and additional examples):

412L - Air Weapons Control System

An overseas theater tactical air weapons control and warning system.

416L - SAGE Air Defense System

A semi-automatic area air weapons control and warning system including the Back Up Interceptor Control (BUIC) for detecting, identifying, tracking, and providing interceptor weapon direction against air-breathing threats to the United States and Canada.

474L - Ballistic Missile Early Warning System

A system to provide early warning of a mass ballistic missile attack on the North American continent from the North.

481L - Postattack Command and Control System

A system to enable the Commander-in-Chief, Strategic Air Command, to control his forces in the event that a nuclear attack destroys or seriously degrades his normal facilities.

Many of these as well as other of the "L" Systems are subsystems of higher echelon command and control systems. 474L (BMEWS), described above, is also a sensor subsystem of higher echelon systems.

III. A COMMAND AND CONTROL SYSTEM FOR MUNICIPAL DECONTAMINATION

A. General

The previous section defined the characteristics of subsystem interrelationships common to all command and control systems. It is the purpose of this section to identify the basic system elements required by municipal decontamination and to embed these elements into the general command and control systems framework of the previous section. In order to accomplish this, the following steps are taken in this section:

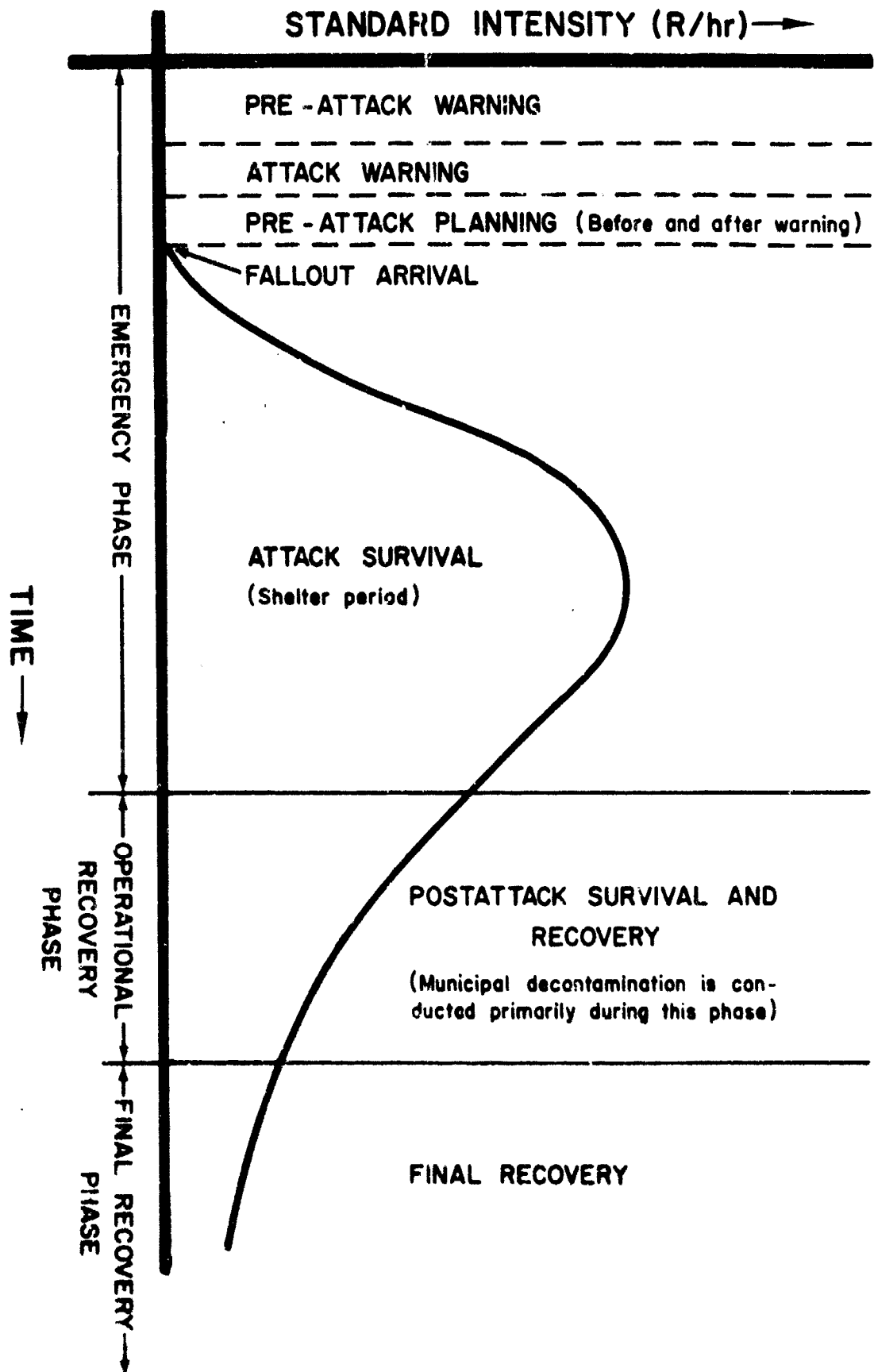
1. Analyze the environment, within which municipal decontamination is expected to operate.
2. Identify the goals of municipal decontamination.
3. Prescribe the decontamination system performance requirements.
4. Identify and relate the elements of a decontamination system.
5. Relate the elements identified in 4 above to the general command and control system framework defined in Section II.

B. Environmental Aspects of Municipal Decontamination

Municipal decontamination by itself is only a part of the broader system of postattack radiological defense. The time during which a radiological defense system operates can be logically divided into three time phases: the emergency phase, the operational recovery phase, and the final recovery phase (Reference F-3). The underlying reason for dividing radiological defense into three time phases is the change due to fallout decay.

Figure -5 shows that the emergency phase begins with a preattack warning--an event highly probable during times of international crisis--if it occurs, or attack warning otherwise. It may last for several days, weeks, or months depending on the warning obtained (combined with the population discipline attained for such an event) and the attack parameters. The decision-makers during this phase utilize preattack

Figure F-5 Time Phases of Radiological Defense



planning, before and after warning, the extent and effectiveness of which is determined by the amount of preattack warning given. This is a function of intelligence indicators.

The objective of radiological countermeasures during this phase is survival, for it is during this period that the fallout arrives, accumulates, attains some maximum intensity, and then begins to decay. It has been shown that the optimal or primary radiological countermeasure during this period is enshelterment. The central requirement of the system during this period is to provide a sufficient number of adequate shelters so located as to minimize casualties. The potential effectiveness of the system during this period is determined by the degree of protection afforded, space availability and accessibility, and warning time.

The operational recovery phase follows the emergency phase and encompasses the operations prerequisite to:

1. Sustaining life in a hostile environment; and
2. The recovery of essential postattack activities and/or facilities.

From Figure F-5 it is seen that the transition to the operational recovery phase takes place when limited egress from shelters is feasible.

The final recovery phase begins when radiation intensity decays to an insignificant level and primary considerations can be focused on functional restoration of the target area as nearly as possible to its preattack condition.

Municipal decontamination will be activated primarily during the operational recovery phase. The following environmental conditions will then prevail:

1. Fallout deposition, generally, will be complete.
2. Fallout radiation will still be a hazard in some areas. Most of the civilian population will be sheltered during much of the time that decontamination is being performed.
3. There may be damage in the area from direct weapons effects (blasts, thermal, EMP, etc.).

4. The entire Civil Defense System will be very active, i.e., communications lines, logistics supplies and equipment, etc. will be very busy.

This last item is perhaps the most important condition affecting the environment of municipal decontamination systems. It is a factor over which the decision-maker has some control. As is pointed out in Reference F-3, the decision-maker has little or no control over most environmental factors.

Reference F-3 also points out that the environment is an important factor limiting the range of decisions which can be made in the postattack period. Because of the wide variation of damage, yielding a wide variety of physical environments (in which municipal decontamination might operate), the decision subsystem of any proposed decontamination system must be extremely flexible and capable of making very complex decisions. Further, it should be capable of making decisions based on varying amounts of reliable (and unreliable) information. This will subsequently be discussed in some detail.

C. Goals of Municipal Decontamination

The primary goals of decontamination within a municipality (in a very broad sense) are:

1. Continued survival within the municipality,
2. Accelerated municipal recovery, and
3. Assistance in the recovery of a region (not necessarily containing the municipality where the decontamination system is operating).

Since the three goals listed above are also primary goals of the overall radiological defense system, any decontamination system must be closely coordinated with other radiological defense systems. This implies the existence of an overall radiological defense command and control system. Although it is not the purpose of this report to elaborate on the overall system, it should be recognized that much of the command information input to the decontamination command and control system will be output from such a higher echelon decision subsystem.

D. Municipal Decontamination System Performance Criteria

In light of the existence of a higher echelon command and control system, the question might be asked: "Why a command and control system for decontamination?" There are two basic reasons for proposing a separate system to command and control decontamination operations in a municipality:

1. The specific decisions involved with effecting decontamination operations in a municipality are in themselves complex enough to warrant a "decontamination-level" decision subsystem.
2. The information requirements for effecting useful decontamination decisions are in themselves very involved and require a separate "decontamination-level" information subsystem. This is not to say that a decontamination information subsystem would not borrow components from, or overlap with, parts of other radiological defense information subsystems, e.g., RADEF.

Later in this appendix, the information input and decision structure requirements for effecting decontamination will be identified and will substantiate the above reasoning for a separate decontamination command and control system.

The basic criteria upon which to judge a decontamination system are:

1. To what extent does the system increase the effectiveness of decontamination in achieving the goals and requirements prescribed by higher echelon decision subsystems?
2. How effectively does the system reduce on-line decontamination costs (in manpower, crew doses, expenditures of fuel, water, etc.) for specified levels of performance?
3. How effectively does the system reduce off-line decontamination costs (research funds required, training of personnel, procurement of equipment, etc.) for specified levels of performance.

This last criterion is separated from the second, in that it can be treated as a static goal of the system (i.e., one which is evaluated by off-line simulation

and/or analysis of on-line system performance). The first two are dynamic goals (i.e., those evaluated by on-line performance and which can be controlled on-line).

E. Elements of a Decontamination System

The purpose of this section is to identify the functional decontamination decision elements as well as to determine the data base and information flow required by these elements. These data and information flow may be internal to the decontamination system (between subsystems) or external to the system (to and from higher echelon or parallel systems). The higher echelon command and control system with regard to decontamination is the Postattack Civil Defense Emergency Operating System. Parallel systems would include systems to control such functions as rescue, law and order, engineering, welfare, firefighting, medical, etc. Certain other subsystems of the Emergency Operating System would provide sensor information inputs for the decontamination system. These include RADEF, damage assessments, NUDETS, etc. Figure F-6 illustrates schematically the information flow between the various command and control systems related to decontamination.

The subsystems of the decontamination system must provide the basis for commanding and controlling all of the activities and decisions which comprise decontamination. Thus, a first step towards identifying the elements of a decontamination command and control system is to list all of the important activities and decisions which are required to perform effective decontamination. In order to determine whether or not to decontaminate a given facility or activity and thence to schedule the operation, the following steps must be taken:

1. Determine that the facility or activity is essential to sustaining life or accelerating recovery. This may involve no more than being told by the higher echelon decision subsystem that a given facility or activity is essential.
2. Determine that the given facility or activity is presently denied by fallout or will be when you want it.

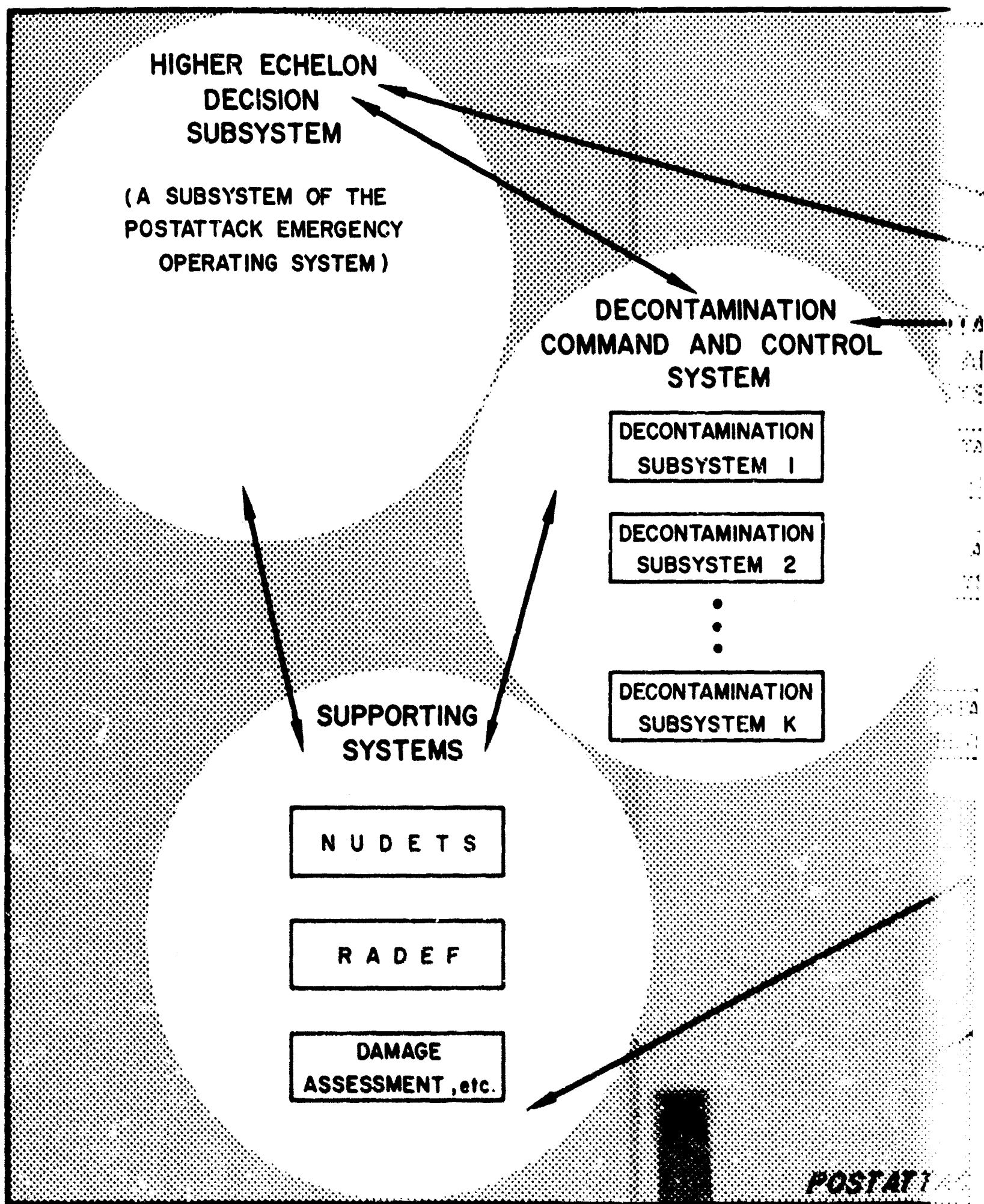


Figure F-6 Schematic Diagram Showing the Relation of Decontamination to the Postattack Emergency Operating System

AMINATION
AND CONTROL
STEM

AMINATION
STEM 1

AMINATION
STEM 2

•
•
•

AMINATION
STEM K

PARALLEL
SYSTEMS

RESCUE

LAW AND
ORDER

MEDICAL

ENGINEERING
(PUBLIC WORK)

FIREFIGHTING

WELFARE

8

POSTATTACK EMERGENCY OPERATING SYSTEM

3. Determine that decontamination can reduce the fallout denial time of this facility or activity to or below the minimum desired.
4. Determine that equipment and supplies (water, etc.) are available to decontaminate around this facility or activity.
5. Determine that sufficient manpower (taking dose histories into account) is available to decontaminate this facility or activity.
6. Determine that the facility or activity can be decontaminated to a specified level of effectiveness without overexposing the decontamination crews.
7. Determine that direct weapons effects or congestion will not impede the decontamination equipment in reaching the facility or activity.
8. Decide to decontaminate the given facility or activity.
9. Commit resources and schedule the decontamination of the given facility or activity.
10. Initiate and conduct the decontamination operation.
11. Monitor and control the decontamination operation.
12. Determine whether additional resources are required and available to complete the decontamination of the facility or activity.
13. Commit additional resources to decontaminate the facility or activity if needed.
14. Determine that the decontamination operation is completed.

Each of these activities triggers a response within the system. Thus, none of these activities can be omitted in the analysis without reflecting a gap in the required data base and organizational structure. Each activity demands a supporting data base, some resources, and some organizational (command and control) structure. This organizational structure should provide for both information channels and decision structures.

Figure F-7 shows the supporting structure and data base for conducting the decontamination of a given facility or activity. Each of the important activities

involved with such an operation is delineated and the data base for each activity specified. Clearly the required information channels comprise a complex network and imply the necessity for a well organized information subsystem.

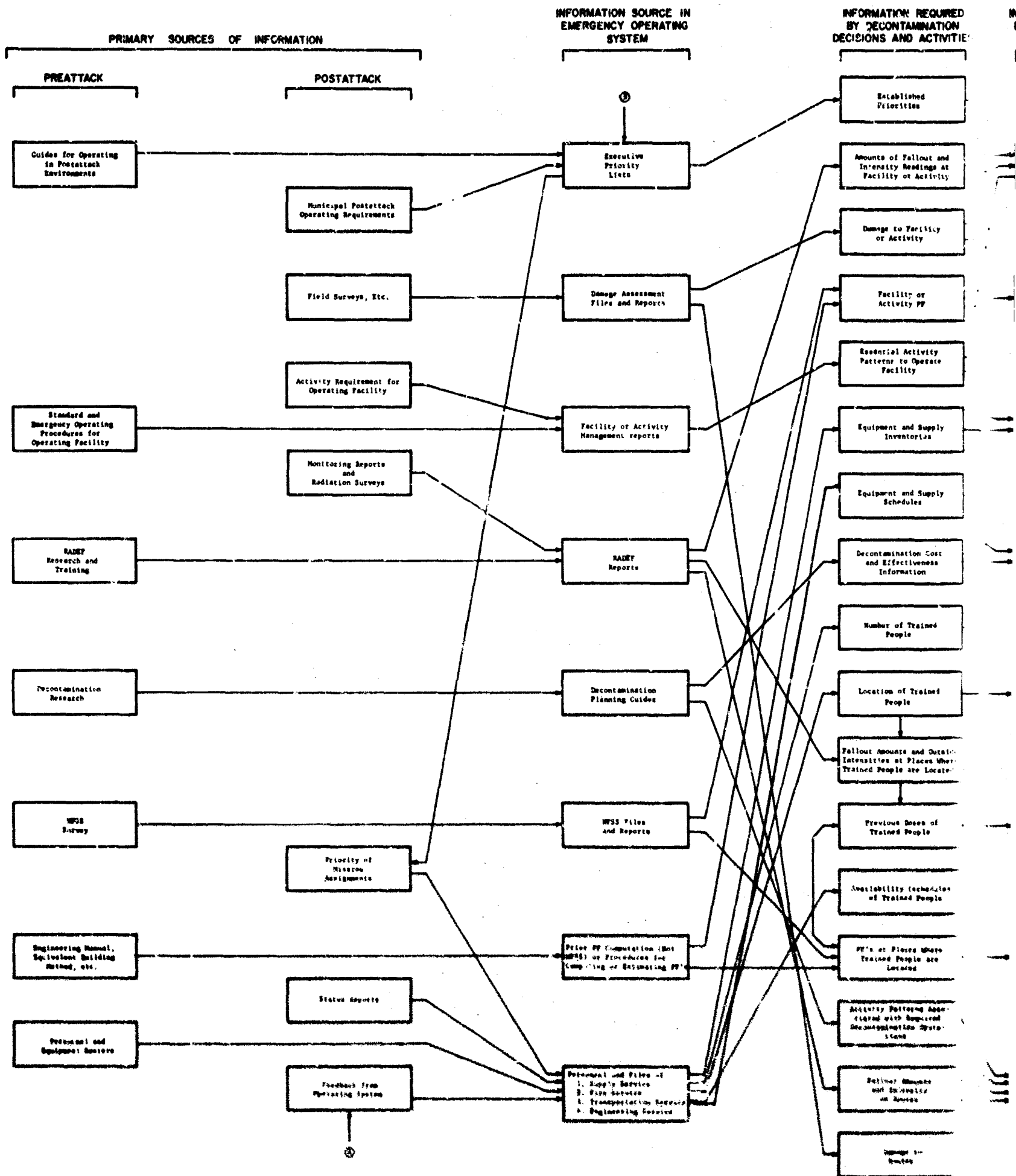
Close examination of Figure F-7 reveals the necessity for other subsystems similar to those described in Section II of this report. For instance, an on-line control system will be required to monitor and control the decontamination operations and also to direct and insure that information is forwarded to the proper functional elements of the decontamination system. The parallelism between required decontamination system elements and classical command and control subsystems is considered next.

F. Decontamination System Elements

The purpose here is to identify the command and control system elements required to conduct effective municipal decontamination. The interrelationships between the functional elements are discussed and displayed.

In Section II of this report, each of the necessary subsystems of any command and control system are identified and defined. The basic supporting data base as well as the activities and decisions necessary to conducting postattack decontamination are illustrated in Figure F-7. It is now necessary to relate these necessary decontamination system activities to the command and control framework described in Section II. Table F-I lists some of the basic decontamination functions performed by each of the command and control subsystems. Figure F-8 illustrates the functional relationships among these decontamination activities. It is seen that some of these functions are also parallel systems to decontamination. Radiological monitoring, for instance, would be required for almost all of the parallel systems shown in Figure F-6.

What is possible to note from Table F-I and Figures F-7 and F-8, however, is that the system required to conduct effective decontamination does have all of the characteristics of a full scale command and control system. All of the usual sub-systems of command and control systems are needed in some fashion to perform municipal decontamination.



A

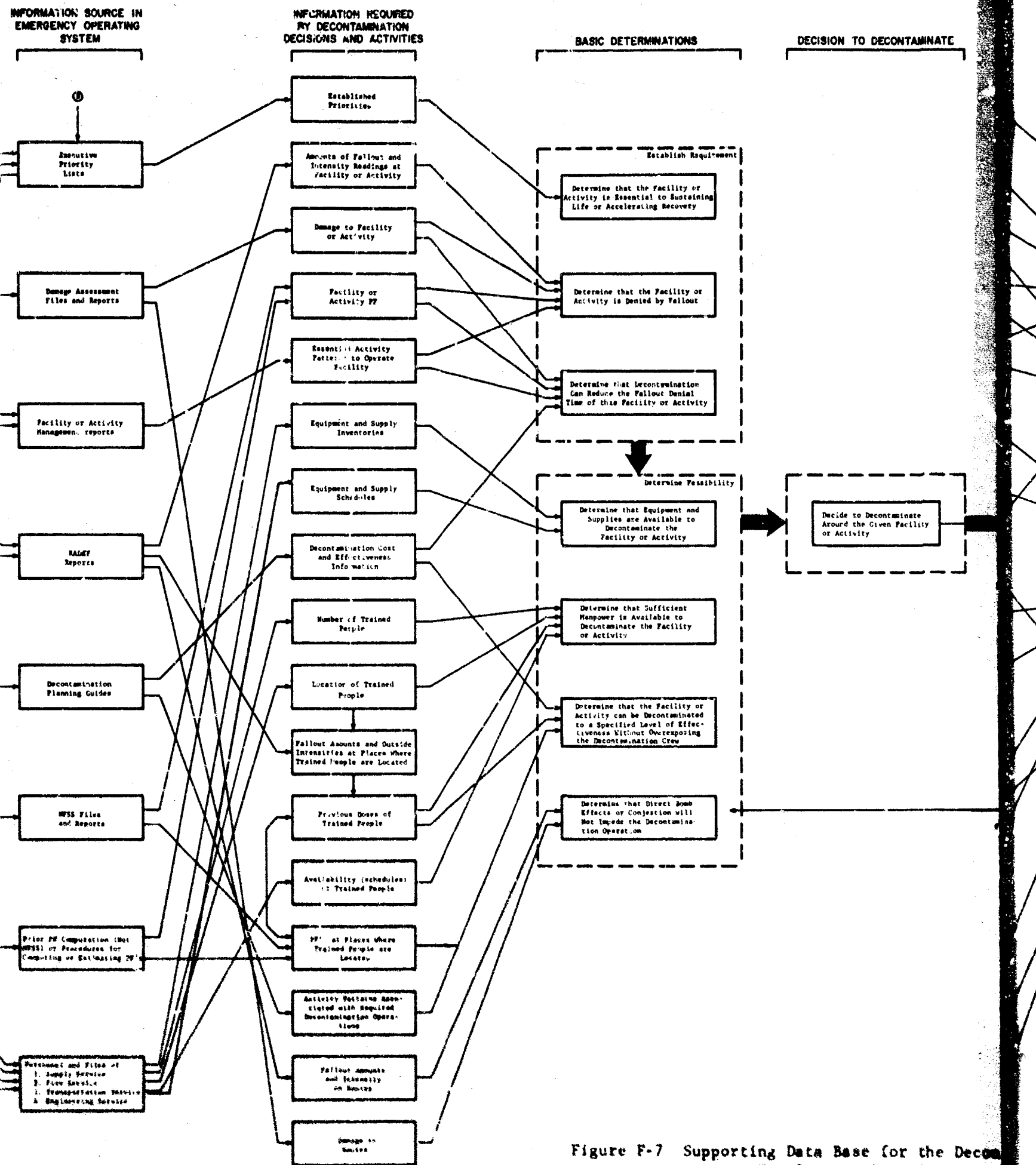


Figure F-7 Supporting Data Base for the Decon Facility or Activity

B

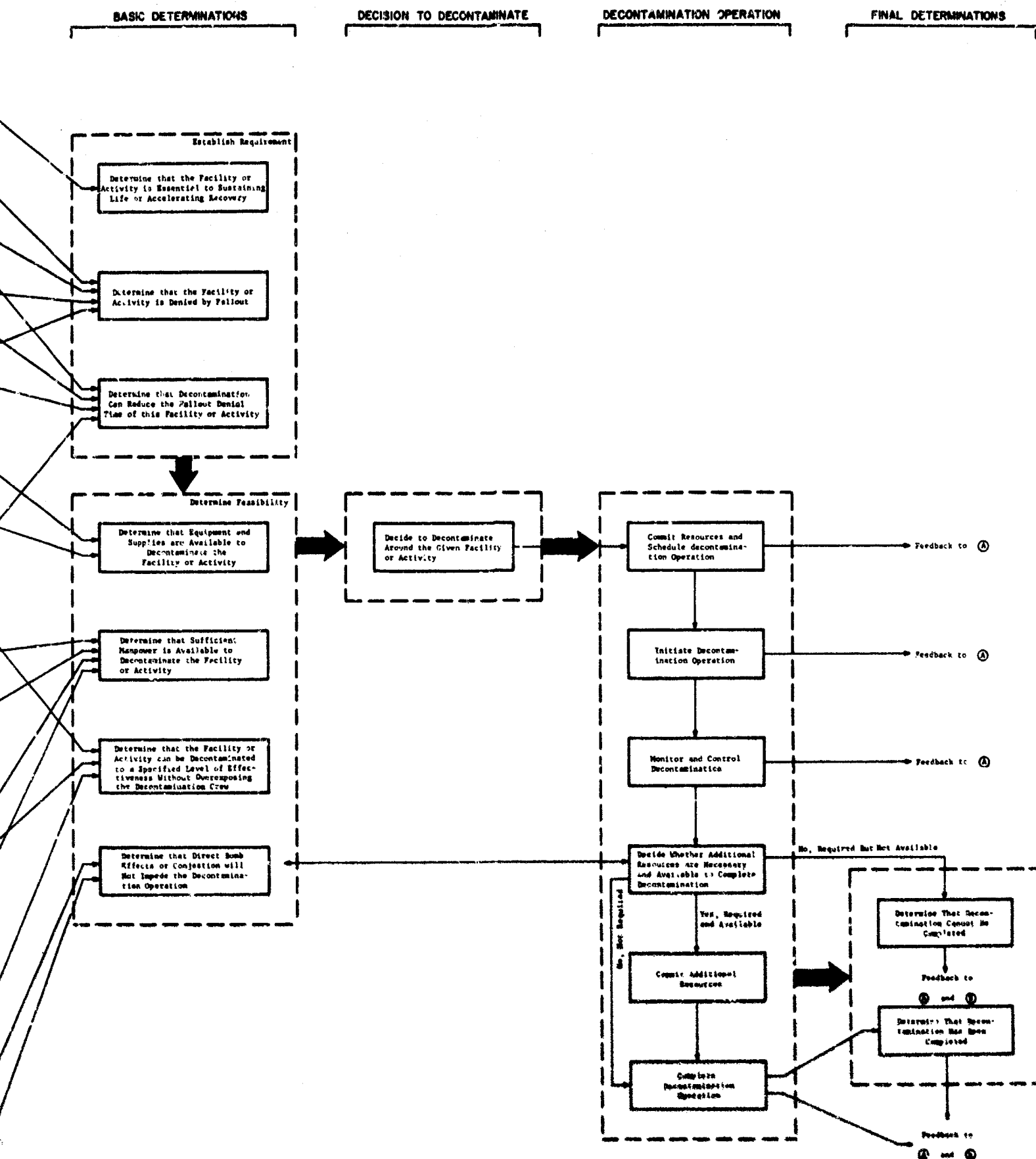


Figure F-7 Supporting Data Base for the Decontamination of a Facility or Activity

C

TABLE F- I

Decontamination Subsystem Functions

Sensor Subsystem

1. Radiological monitoring.
2. Field Surveys, etc.

Effector Subsystem

1. Move decontamination equipment to sites.
2. Perform decontamination.

External Communications Subsystem

1. Transmit data and information to and from radiological monitors, field inspection teams, etc., and decontamination crews to the Emergency Operating Center (EOC).

Internal Communications Subsystem

1. Transmit data and information within the EOC.

Information Subsystem

1. Store and catalog decontamination planning guides and other related (prestored) materials.
2. Display environmental information (RADEF, etc.) within the EOC.
3. Process data inputs and information coming in from the external sensors into a usable form for persons with information needs.
4. Provide information to decision subsystem on request.

Decision Subsystem

1. Decide when, what, and how to decontaminate.
2. Decide when to commit resources and which resources to commit.
3. Decide whether additional information is required to make a decontamination decision.

On-line Control Subsystem

1. Monitor and control decontamination.
2. Commit resources to decontamination tasks.
3. Control information flow, assign tasks to radiological monitors and field inspection teams. This included regulating response times and information accuracy.

Off-line Control Subsystem

1. Monitor and control decontamination research.
2. Preposition and inventory decontamination personnel, equipment, and supplies.
3. Organize decontamination subsystems within the EOC.

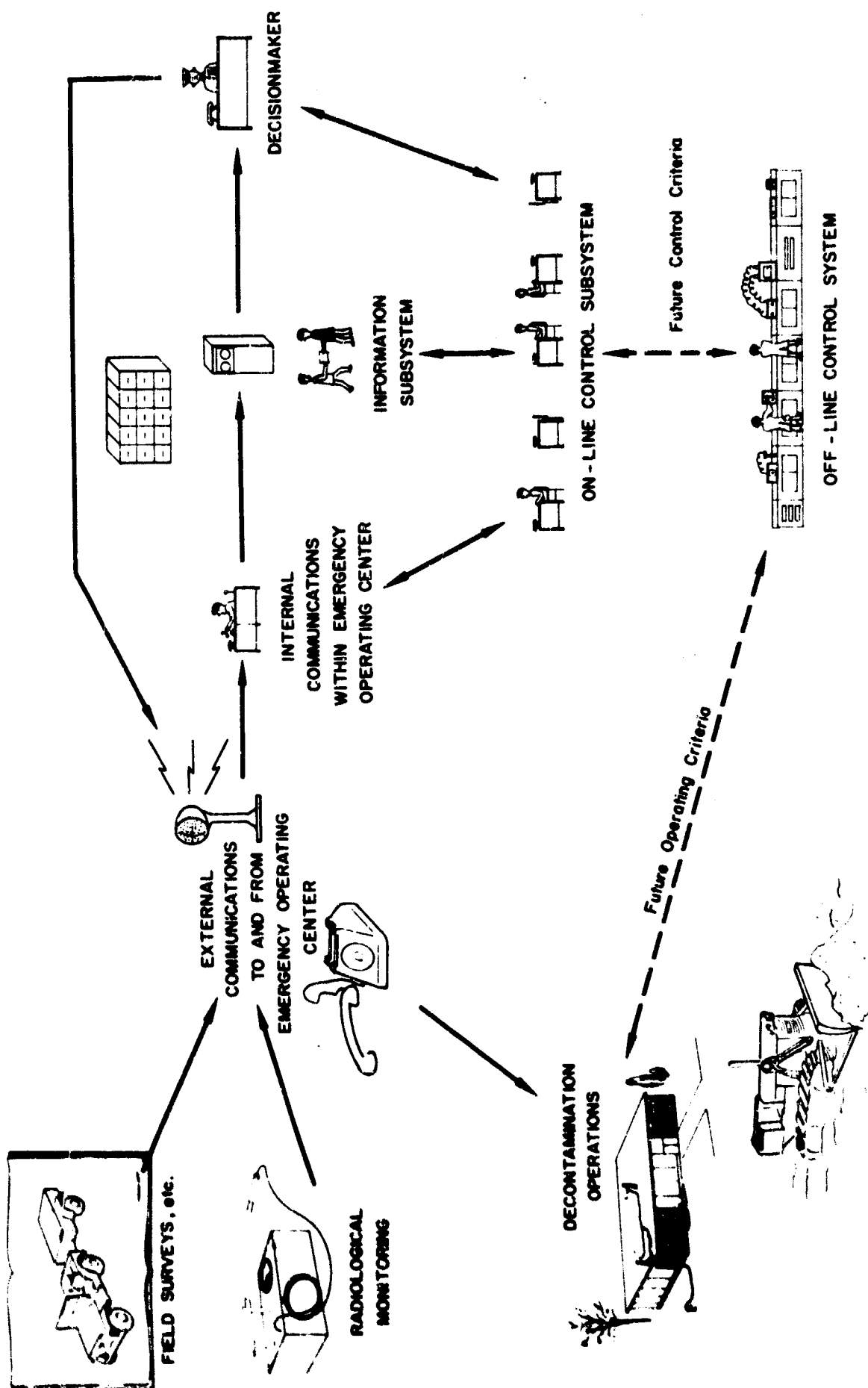


Figure F-8 Illustration of Functional Relationships Among Decontamination System Activities

IV. AN INFORMATION SYSTEM (SUBSYSTEM) FOR DECONTAMINATION

A. Introduction

Figure F-7 in the last section depicts a very complex information-flow network required in the decision whether or not to conduct a particular decontamination operation. Certainly some control over the collecting, storing, and disseminating of all of these data is necessary. It is the purpose of this section to indicate the basis upon which an information subsystem for decontamination could be designed. The steps taken towards this end are along the lines suggested in Chapter 3 of Reference F-3:

1. The information input requirements are discussed.
2. The information format including the criteria upon which to judge the usefulness of the information are discussed.
3. The means for obtaining, storing and disseminating the required information are identified.

The last two steps required in designing an information system (identifying alternative systems and choosing a best one) are not taken up in this report.

B. Information Input Requirements for Conducting Decontamination

Most of the information inputs shown in Figure F-7 are not required for every decontamination decision. For instance if no blast damage has occurred in the city where decontamination is being performed, specific blast-damage information inputs would be unnecessary. If a higher echelon decisions subsystem commands that a facility be decontaminated, the information inputs required to determine that the job is necessary are no longer relevant to the decision. Thus, there are different information input requirements depending on the environment and the kind of decontamination decision being made. The environment includes not only the attack damage but the overall decontamination resource situation and the population dispersal. (This last item is a function of the attack warning time of day of attack. pre-

conditioning and training, etc.) Clearly the problem of identifying all of the pre-attack and postattack data requirements for effecting municipal decontamination for all situations would be a mammoth undertaking. Whether or not such an effort would be fruitful is in itself a difficult question. This report will simply list some of the basic requirements which appear to be a necessary input to most decontamination decisions. They are:

1. Fallout information - This includes both amounts of fallout (mass) and the dose-rates where the fallout is deposited.
2. The location of essential facilities and the urgency of their recovery - This information may be in the form of a command from a higher echelon decision subsystem or prestored information in the EOC.
3. Decontamination resource inventories and schedules - This information should be kept up to date in the EOC.
4. Planning guides for conducting decontamination - This information is pre-stored in the EOC.

These basic information requirements are presented in a general manner only; any additional refinement would require a complete situation analysis including a description of the environment and the kind of decontamination decision being made.

C. Information Utility Criteria

As stated in Reference F-3, the basic criteria upon which to judge information are:

1. Timeliness;
2. Pertinence;
3. Reliability; and
4. Comprehensibility

1. Timeliness

The value of radiation information particularly is very dependent on when it is received. This is because of the decay rate of the fallout intensity.

Radiation reports during the build-up phase and shortly thereafter are not essential for future decontamination. This information, in fact, is best kept out of the decontamination information subsystem. It simply clutters the system. Radiation information, to be useful, must be reasonably up to date and reflect the amount of fallout or intensity. As the decay progresses it becomes less and less important that the information be processed quickly. Of course, late reports might delay a decision to decontaminate an essential facility.

Prestored data should be organized so that the decision-maker can obtain information from his files as he needs it.

2. Pertinence

The information should be organized and disseminated in a manner to minimize the amount of unnecessary information being provided to the decontamination decision-maker. Prestored information (decontamination planning guides, etc.) should be concise and to the point. As is pointed out in Reference F-3, "Extraneous material not only wastes the time of those who must use it, it may also lead to incorrect decisions by obscuring the most important considerations."

3. Reliability

Information should be accurate. Reference F-3 points out that accuracy is influenced by the quality of the information inputs as well as the ability of the system to transmit and transform data without making errors.

Unfortunately, this criterion is particularly difficult to meet for decontamination decisions. Radiological monitoring devices are quite variable in their accuracy of intensity measurements. Indeed, winds or redistributed fallout cause information inputs to reflect incorrectly the status of the radiological environment. Because of this uncontrollable reliability, decontamination decisions will have to be made despite some inaccuracy in information inputs.

4. Comprehensibility

Information inputs from external sensors must be collected (time, location, etc.) and presented in a comprehensible manner. Prestored data must be clear and written or presented in a manner readable by the user, e.g., decontamination planning guides should be readable to the local decision-maker in the EOC.

D. Means for Obtaining, Storing, and Disseminating the Information

Radiation information can be obtained from radiation monitors. This information can be measured with instruments or visually observed. It may be forwarded to the EOC via telephone, radio, or hand-carried. Such information can be posted and kept up to date on display boards, map books, or typed and hand-written reports. Field survey data can be handled in the same manner.

Prestored data are obtained by preattack data acquisition and research. The kinds of prestored data obtained are determined by careful preattack assessment of postattack data needs. They can be stored as printed reports, maps, etc., or if retrieval machinery is available, they could be stored on punched cards, magnetic tapes, drums, discs, etc.

E. Summary

It is not the purpose in this appendix to prescribe precisely an information subsystem for decontamination. Whether or not a separate information subsystem for decontamination as opposed to, say, firefighting is needed is not answered in this appendix. The answer to this question depends largely on the organizational structure and system design of whatever higher echelon systems are developed (e.g., Emergency Operating Systems).

This appendix simply indicates a basis for designing a decontamination information system.

V. CONCLUSIONS AND RECOMMENDATIONS

A. Conclusions

Some command and control structure will be necessary to conduct effective municipal decontamination. Whether or not a separate decontamination command and control system is necessary is not determined in this report--nor will it be determined without a far more extensive research effort. The decisions and activities related to decontamination do, however, require an elaborate information subsystem consisting of organized data files containing prestored (NFSS data, decontamination planning guides, etc.) data and postattack assessments (including system feedback). A good argument for a decontamination information subsystem could be presented on the basis of the complex network of information flow shown in Figure F-7.

B. Recommendations

It is recommended that decontamination be considered in the development and design of any Postattack Emergency Operating System to be operational at the municipal or community level. It is further recommended that the systems requirements for conducting decontamination be analyzed more thoroughly and the necessary system functions and minimal organizational structure for conducting effective municipal decontamination be more precisely identified.

REFERENCES

- F-1. R. C. Kiene, A. R. Butz, and L. B. Winrich. Command and Control Systems Analysis. (Final Report). RADC-TDR-62-612. Prepared for Rome Air Development Center. Griffiss Air Force Base, New York: Honeywell Military Products Group, Research Department, December 1962.
- F-2. F. V. Schell, M. Kolker, C. Abt, and M. S. Gordon. United States Capabilities for Command and Control. BR-2249. Prepared for Directorate for Arms Control, Office of the Assistant Secretary of Defense, International Security Affairs. Bedford, Massachusetts: Strategic Studies Department, Raytheon Company, January 1963.
- F-3. E. R. Brooks, G. H. Otto, D. H. Fishman, and J. E. Walker. Analysis of a Civil Defense Information System. Final Report R-OU-134. Durham, North Carolina: Research Triangle Institute, Operations Research and Economics Division, December 14, 1964.

UNCLASSIFIED

Security Classification

DOCUMENT CONTROL DATA - R&D

(Security classification of title, body of abstract and indexing annotation must be entered when the overall report is classified)

1. ORIGINATING ACTIVITY (Corporate author)

Research Triangle Institute
Post Office Box 490
Durham, North Carolina 27702

2a. REPORT SECURITY CLASSIFICATION

UNCLASSIFIED

2b. GROUP

3. REPORT TITLE

Radiological Recovery Requirements, Structures, and Operations Research -
Volume II - Development of Analytical, Computer, and Systems Models in
Support of Decontamination Analyses

4. DESCRIPTIVE NOTES (Type of report and inclusive dates)

Volume II of a 4-volume final report: 19 February 1965 - 6 June 1966

5. AUTHOR(S) (Last name, first name, initial)

Ryan, Joseph P.
Johnson, Thomas

6. REPORT DATE

6 June 1966

7a. TOTAL NO. OF PAGES

228

7b. NO. OF REFS

19

8a. CONTRACT OR GRANT NO.

N228(62479)-68153

9a. ORIGINATOR'S REPORT NUMBER(S)

R-OU-214

b. PROJECT NO.

OCD Work Unit No. 3233B

9b. OTHER REPORT NO(S) (Any other numbers that may be assigned this report)

Volume II

10. AVAILABILITY/LIMITATION NOTICES

Distribution of this document is unlimited.

11. SUPPLEMENTARY NOTES

None

12. SPONSORING MILITARY ACTIVITY

Office of Civil Defense
Department of the Army
Washington, D. C. 20310

13. ABSTRACT

This is Volume II of four separately bound volumes that report the research completed in fulfillment of Office of Civil Defense Work Unit No. 3233B, "Radiological Recovery Requirements, Structures, and Operations Research." This describes six supporting studies all previously reported to the Office of Civil Defense in research memoranda. Volume I describes the general aspects of the investigations and presents the conclusions and recommendations.

DD FORM 1473

UNCLASSIFIED

Security Classification

14. KEY WORDS	LINK A		LINK B		LINK C	
	ROLE	WT	ROLE	WT	ROLE	WT
Operations Research	10	4				
Decontamination					8	4
Recovery					2	4
Radioactive Fallout			9	3		
Postattack Operation					10	3
Contamination			5	3		
Radiological Contamination			5	3		
Radiation Hazards			1	3		
Dose Rate			6	2		
Cleaning					10	2
Structures	9	2				
Protection Factor	6	1				
Civil Defense System					0	1

INSTRUCTIONS

1. **ORIGINATING ACTIVITY:** Enter the name and address of the contractor, subcontractor, grantee, Department of Defense activity or other organization (*corporate author*) issuing the report.

2a. **REPORT SECURITY CLASSIFICATION:** Enter the overall security classification of the report. Indicate whether "Restricted Data" is included. Marking is to be in accordance with appropriate security regulations.

2b. **GROUP:** Automatic downgrading is specified in DoD Directive 5200.10 and Armed Forces Industrial Manual. Enter the group number. Also, when applicable, show that optional markings have been used for Group 3 and Group 4 as authorized.

3. **REPORT TITLE:** Enter the complete report title in all capital letters. Titles in all cases should be unclassified. If a meaningful title cannot be selected without classification, show title classification in all capitals in parenthesis immediately following the title.

4. **DESCRIPTIVE NOTES:** If appropriate, enter the type of report, e.g., interim, progress, summary, annual, or final. Give the inclusive dates when a specific reporting period is covered.

5. **AUTHOR(S):** Enter the name(s) of author(s) as shown on or in the report. Enter last name, first name, middle initial. If military, show rank and branch of service. The name of the principal author is an absolute minimum requirement.

6. **REPORT DATE:** Enter the date of the report as day, month, year, or month, year. If more than one date appears on the report, use date of publication.

7a. **TOTAL NUMBER OF PAGES:** The total page count should follow normal pagination procedures, i.e., enter the number of pages containing information.

7b. **NUMBER OF REFERENCES:** Enter the total number of references cited in the report.

8a. **CONTRACT OR GRANT NUMBER:** If appropriate, enter the applicable number of the contract or grant under which the report was written.

8b, 8c, & 8d. **PROJECT NUMBER:** Enter the appropriate military department identification, such as project number, subproject number, system numbers, task number, etc.

9a. **ORIGINATOR'S REPORT NUMBER(S):** Enter the official report number by which the document will be identified and controlled by the originating activity. This number must be unique to this report.

9b. **OTHER REPORT NUMBER(S):** If the report has been assigned any other report numbers (*either by the originator or by the sponsor*), also enter this number(s).

10. **AVAILABILITY/LIMITATION NOTICES:** Enter any limitations on further dissemination of the report, other than those imposed by security classification, using standard statements such as:

- (1) "Qualified requesters may obtain copies of this report from DDC."
- (2) "Foreign announcement and dissemination of this report by DDC is not authorized."
- (3) "U. S. Government agencies may obtain copies of this report directly from DDC. Other qualified DDC users shall request through _____."
- (4) "U. S. military agencies may obtain copies of this report directly from DDC. Other qualified users shall request through _____."
- (5) "All distribution of this report is controlled. Qualified DDC users shall request through _____."

If the report has been furnished to the Office of Technical Services, Department of Commerce, for sale to the public, indicate this fact and enter the price, if known.

11. **SUPPLEMENTARY NOTES:** Use for additional explanatory notes.

12. **SPONSORING MILITARY ACTIVITY:** Enter the name of the departmental project office or laboratory sponsoring (paying for) the research and development. Include address.

13. **ABSTRACT:** Enter an abstract giving a brief and factual summary of the document indicative of the report, even though it may also appear elsewhere in the body of the technical report. If additional space is required, a continuation sheet shall be attached.

It is highly desirable that the abstract of classified reports be unclassified. Each paragraph of the abstract shall end with an indication of the military security classification of the information in the paragraph, represented as (S), (C), or (U).

There is no limitation on the length of the abstract. However, the suggested length is from 150 to 225 words.

14. **KEY WORDS:** Key words are technically meaningful terms or short phrases that characterize a report and may be used as index entries for cataloging the report. Key words must be selected so that no security classification is required. Identifiers, such as equipment model designation, trade name, military project code name, geographic location, may be used as key words but will be followed by an indication of technical context. The assignment of links, rules, and weight is optional.